

AD-A135 738

MULTIVARIABLE FLIGHTCONTROL DESIGN WITH UNCERTAIN
PARAMETERS(U) WEIZMANN INST OF SCIENCE REHOVOTH
(ISRAEL) DEPT OF APPLIED MA. I HOROWITZ ET AL. SEP 82

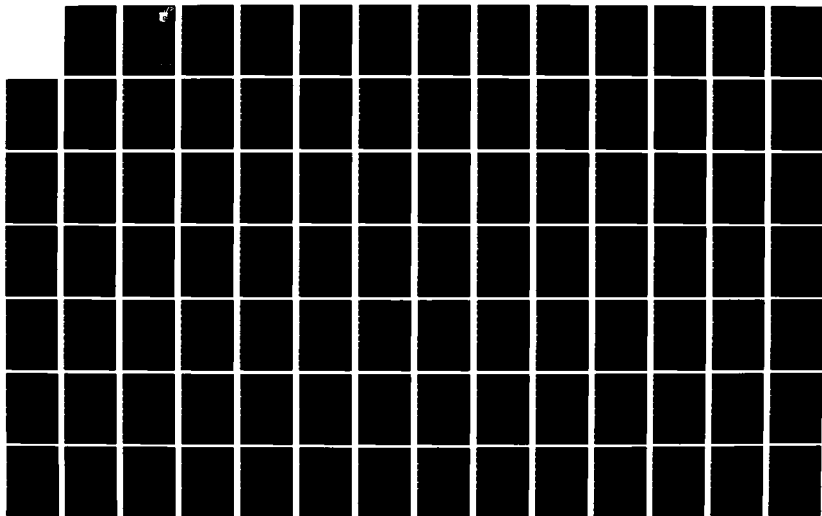
1/4

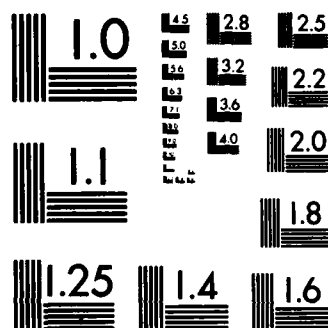
UNCLASSIFIED

AFNAL-TR-83-3036 AFOSR-80-0213

F/G 1/3

NL





MICROCOPY RESOLUTION TEST CHART
NATIONAL BUREAU OF STANDARDS-1963-A

AD-A135738

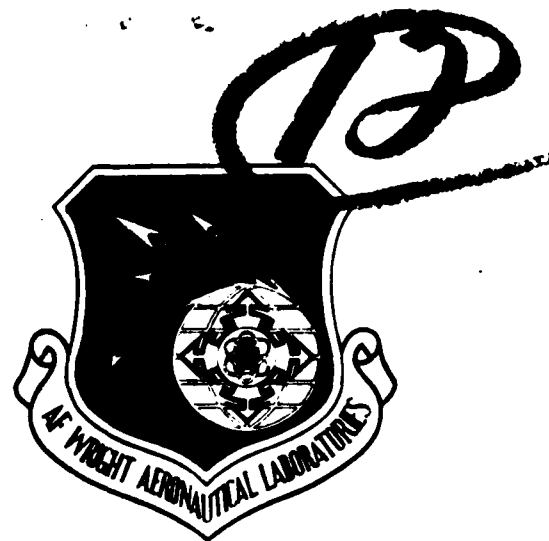
AFWAL-TR-83-3036

MULTIVARIABLE FLIGHT CONTROL DESIGN
WITH UNCERTAIN PARAMETERS

Isaac Horowitz
T. Kopelman

Department of Applied Mathematics
The Weizmann Institute of Science
Rehovot, Israel

University of Colorado
Department of Electrical Engineering
Boulder, Colorado



SEPTEMBER 1982

Final Report for Period 1 June 1981 - 31 August 1982

DTIC FILE COPY

Performed under Grant to
FLIGHT DYNAMICS LABORATORY
AIR FORCE WRIGHT AERONAUTICAL LABORATORIES
AIR FORCE SYSTEMS COMMAND
WRIGHT-PATTERSON AIR FORCE BASE, OH 45433

DISTRIBUTION STATEMENT A

Approved for public release;
Distribution Unlimited

DTIC
ELECTE
S DEC 14 1983 D
D

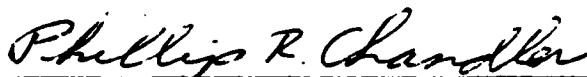
83 12 13 051

NOTICE

When Government drawings, specifications, or other data are used for any purpose other than in connection with a definitely related Government procurement operation, the United States Government thereby incurs no responsibility nor any obligation whatsoever; and the fact that the government may have formulated, furnished, or in any way supplied the said drawings, specifications, or other data, is not to be regarded by implication or otherwise as in any manner licensing the holder or any other person or corporation, or conveying any rights or permission to manufacture use, or sell any patented invention that may in any way be related thereto.

This report has been reviewed by the Office of Public Affairs (ASD/PA) and is releasable to the National Technical Information Service (NTIS). At NTIS, it will be available to the general public, including foreign nations.

This technical report has been reviewed and is approved for publication.




PHILLIP R. CHANDLER
Project Engineer



EVARD H. FLINN, Chief
Control Systems Development Branch
Flight Control Division

FOR THE COMMANDER



JAMES D. LANG
Colonel, USAF
Chief, Flight Control Division

"If your address has changed, if you wish to be removed from our mailing list, or if the addressee is no longer employed by your organization please notify AFWAL/FIGL, W-PAFB, OH 45433 to help us maintain a current mailing list".

Copies of this report should not be returned unless return is required by security considerations, contractual obligations, or notice on a specific document.

REPORT DOCUMENTATION PAGE		READ INSTRUCTIONS BEFORE COMPLETING FORM
1. REPORT NUMBER AFWAL-TR-83-3036	2. GOVT ACCESSION NO. AD A135738	3. RECIPIENT'S CATALOG NUMBER
4. TITLE (and Subtitle) MULTIVARIABLE FLIGHT CONTROL DESIGN WITH UNCERTAIN PARAMETERS		5. TYPE OF REPORT & PERIOD COVERED Final Scientific Report June 1, 1981-Aug. 31, 1982
		6. PERFORMING ORG. REPORT NUMBER N/A
7. AUTHOR(s) I. Horowitz, Z. Kopelman, O. Yaniv, L. Neumann, B. Golubev		8. CONTRACT OR GRANT NUMBER(s) AFOSR-80-0213, 82-063
9. PERFORMING ORGANIZATION NAME AND ADDRESS Weizmann Institute of Science, Dept. of Applied Mathematics, Rehovot, Israel and University of Colorado, Dept. of Elec. Eng., Boulder, CO 80309		10. PROGRAM ELEMENT, PROJECT, TASK AREA & WORK UNIT NUMBERS P.E. 61102F 2304N316/25
11. CONTROLLING OFFICE NAME AND ADDRESS Air Force Flight Dynamics Laboratory Wright Patterson AFB Ohio 45433		12. REPORT DATE August 1982
		13. NUMBER OF PAGES 309
14. MONITORING AGENCY NAME & ADDRESS (if different from Controlling Office)		15. SECURITY CLASS. (of this report) Unclassified
		15a. DECLASSIFICATION, DOWNGRADING SCHEDULE
16. DISTRIBUTION STATEMENT (of this Report) Approved for public release; distribution unlimited.		
17. DISTRIBUTION STATEMENT (of the abstract entered in Block 20, if different from Report)		
18. SUPPLEMENTARY NOTES		
19. KEY WORDS (Continue on reverse side if necessary and identify by block number) Flight Control, Multiple Input-Output Systems, Nonlinear Systems, Adaptive Systems, Parameter Uncertainty		
20. ABSTRACT (Continue on reverse side if necessary and identify by block number) A new synthesis technique for highly uncertain linear time-invariant multiple input-output (MIO) feedback systems, is applied to the flight control problem. The uncertainty is due to a fixed design having to satisfy the performance specifications over a range of flight conditions. The aircraft used is a Fighter CCV-YF16. The design specifications differ with mode, so a separate design is made for each of the modes considered: Direct Side Force (A), Vertical Translation (B), Lateral Translation (C), and Fuselage		

UNCLASSIFIED

SECURITY CLASSIFICATION OF THIS PAGE(When Data Entered)

Yaw Pointing (β_1). The first and third are 3x3, the second is 2x2, while the fourth is a mixture of 2x2 and 3x3.

The outstanding feature of the synthesis technique is the replacement of the uncertain MIO system by a number of uncertain single input, single output (SIO) single-loop systems, with disturbances. The solutions of these SIO problems are guaranteed to solve the MIO problem. In this synthesis technique one proceeds systematically step by step from the system specifications, to the derivation of the system compensation functions. The design steps are given in considerable detail, to enable the reader to learn and apply the technique to his own problems. Simulations are presented for all the designs, and which nicely satisfy the assigned performance specifications.

The tradeoffs between complexity of compensation and loop bandwidth economy are studied and presented. Performance under severe limiting and rate limiting is included for the A_y mode, and is highly satisfactory. Incorporation of scheduling and prediagonalization are also presented. A digital compensation design is included for the vertical translation mode.

Much of the same design technique is applicable to exact design for uncertain nonlinear MIO plants. The 2x2 vertical translation β_2 mode and 3x3 lateral translation β_2 mode were combined, using a 5x5 nonlinear plant model, with the same specifications as for the separate modes. In this nonlinear design technique a preliminary step converts the nonlinear MIO problem into an equivalent linear MIO invariant problem; the equivalence being exact with respect to the class of inputs under consideration. When this preliminary step was executed, the resulting equivalent linear problem was found to be very similar to the original two linear ones. Hence, the same compensation functions result - which was thoroughly verified by simulation.

UNCLASSIFIED

SECURITY CLASSIFICATION OF THIS PAGE(When Data Entered)

FOREWORD

This work was done at three institutions: Weizmann Institute of Science under Air Force Office of Research Grant AFOSR-80-0213 in 1981, Yale University where the Principal Investigator was on sabbatical 1981-82, and University of Colorado 1982 under AFOSR 82-063. The effort was performed under the direction of Air Force Aeronautical Laboratories, Air Force Flight Dynamics Laboratory, Flight Control Division, Control Systems Development Branch, Control Techniques Group, Wright Patterson Air Force Base, Ohio 45433. Phillip R. Chandler was project engineer/manager on the project. Isaac Horowitz, Cohen Professor of Applied Mathematics at Weizmann Institute and Professor, Dept. of Electrical Engineering, University of Colorado was Principal Investigator of this effort. Contributing personnel were Zvi Kopelman, Oded Yaniv, Linda Neumann and B. Golubev. The work covered by the report was performed between January 1981 and August 1982.

Accession For	
NTIS GRA&I	<input checked="" type="checkbox"/>
DTIC TAB	<input type="checkbox"/>
Unannounced	<input type="checkbox"/>
Justification	
By _____	
Distribution/	
Availability Codes	
Dist	Avail and/or Special
A/1	



MULTIVARIABLE FLIGHT CONTROL DESIGN WITH UNCERTAIN PARAMETERS

Table of Contents

List of Symbols and Abbreviations	viii
List of Tables	xi
Figures Titles	xii
CHAPTER ONE	
1. A SYNTHESIS TECHNIQUE FOR UNCERTAIN MULTIPLE INPUT-OUTPUT FEEDBACK SYSTEMS	1
1.1 Introduction	1
1.2 Summary of MIO synthesis technique	3
1.2.1 Derivation of Table 1.1	5
1.2.2 Optimization and trade-off	8
1.3 Necessary conditions for use of MIO synthesis technique	10
1.3.1 A high-frequency condition	10
1.4 A shortcoming and use of nondiagonal G	14
1.5 Summary	15
CHAPTER TWO	
2. DESIGN FOR DIRECT SIDE FORCE MODE	17
2.1 Plant equations	17
2.2 Flight conditions	19
2.3 Design procedure	26
2.4 Design of third (A_y) loop	30
2.5 Simulation results, Design 1	32
2.6 Responses under amplitude and rate limiting	33
2.7 Design Two	34
2.8 A design with scheduling	34
2.9 Nondiagonal G	37
2.10 Trade-off between speed of response and rate limiting	41
Appendix 2.1, Compensation functions for various designs	42
Figures	45

CHAPTER THREE

3. VERTICAL TRANSLATION MODE (α_2)	89
3.1 Plant equations	89
3.2 Flight conditions	94
3.3 Transfer functions	99
3.4 Problem statement and response specifications	99
3.5 Bounds and design of $L_{20}(j\omega)$	100
3.6 Design of G_1, F_1	102
3.7 Simulation results	104
Appendix 3.1, Transfer functions for 25 flight conditions	105
Figures	155

CHAPTER FOUR

4. DESIGN OF LATERAL TRANSLATION (β_2) MODE	166
4.1 Problem statement	166
4.2 Plant equations	166
4.3 Design of L_3	170
4.4 Design of L_2	171
4.5 Design of G_1	172
4.6 Simulation of design	173
4.7 Use of digital compensation	174
Figures	175

CHAPTER FIVE

5. DESIGN BASED ON NONLINEAR MULTIPLE INPUT-OUTPUT PLANT MODEL	193
5.1 Nonlinear MIO Design Technique	199
5.1.1 The barrel analogy	200
5.2 The Nonlinear Plant	200
5.3 The Nonlinear Plant Input-Output Sets	203
Figures	206

CHAPTER SIX

6. FUSELAGE YAW POINTING MODE (β_1)

6.1 Specifications	222
6.1.1 Compability of specifications with inherent capabilities	222
6.1.2 Specification on T_{ij}	223
6.2 Design	224
6.2.1 Design graphs	224
6.2.2 Compensation functions	225
6.2.3 Simulation results	225

Figures

227

CHAPTER SEVEN

7. DISCUSSION AND CONCLUSIONS	267
-------------------------------	-----

REFERENCES

269b

Appendix 1. IMPROVED DESIGN TECHNIQUE FOR UNCERTAIN MULTIPLE INPUT-OUTPUT FEEDBACK SYSTEMS

Abstract	270
----------	-----

Abbreviations	271
---------------	-----

1. Introduction	272
-----------------	-----

2. The 2x2 System	273
-------------------	-----

2.1 Reduced overdesign	276
------------------------	-----

3. 3x3 Design Equations	276
-------------------------	-----

4. nxn System, $n > 3$	278
------------------------	-----

5. Conditions for Existence of a Solution	280
---	-----

5.1 Conditions for arbitrarily small sensitivity in single-loop design	281
---	-----

5.2 Application of 5.1 to New Design Technique	282
--	-----

5.3 Inherent Constraints	284
--------------------------	-----

6. Nondiagonal G	287
------------------	-----

7. Conclusions	288
----------------	-----

References	290
------------	-----

Figures	291
---------	-----

List of Symbols and Abbreviations

a_{uv}	lower bound on $ T_{uv}(j\omega) $
A_n	normal acceleration (ft/sec ² or g's)
A_y	sideforce (ft/sec ² or g's)
b	span (ft.)
b_{uv}	upper bound on $ T_{uv}(j\omega) $
B	a matrix (p. 18)
$B(\omega)$	bounds on a function
BNIC	basically noninteracting
c	a row matrix (p. 18)
C_{ij}	aerodynamic coefficients
C	a matrix (p. 18)
db	decibels ($20 \log_{10}$)
D	a matrix (p. 18)
$F=[f_{ij}]$	prefilter matrix
g	gravity acceleration 9.8 m/sec ²
$G=[g_{ij}]$	feedback compensation matrix
I_i, I_{jk}	moment of inertia (slug ft ²)
lti	linear time invariant
$L=[L_{uv}]$	loop transmission matrix
L_{uvo}	nominal loop transmission function
m	mass in slugs
mio	multiple input, multiple output
mp	minimum-phase
M	mach number
M_i	aerodynamic coefficients (longitudinal)

nmp	nonminimum-phase
$P=[p_{ij}]$	matrix of constrained part, plant
$P=\{p\}$	set of plant matrices
q	dynamic pressure lb/ft ²
q_{ij}	Q_{ij}^{-1}
$Q=[Q_{ij}]$	derived from $P^{-1}=[1/Q_{ij}]$
QQ	see p. 93
$r = \dot{\psi}$	yaw rate
S	wing surface area (ft ²)
s	complex variable $s = \sigma + j\omega$
$T=[T_{ij}]$	matrix of closed-loop transfer functions
u	horizontal velocity
v	side velocity (ft/sec), $\int A_y dt$
v_z	vertical velocity = $\int A_n dt$
w	vertical velocity
X_i	aerodynamic coefficients (longitudinal)
Z_i	aerodynamic coefficients (longitudinal)

Greek

α	angle of attack
β	sideslip angle
δ_i	control surface
δ_a	aileron
δ_c	canard
δ_e	elevator
δ_f	flap
δ_r	rudder
θ	pitch angle
Φ	a matrix (p. 18)
ϕ	roll angle
ψ	yaw
ρ	air density
ω	radians per sec
ω_n	design parameter

Other

\succ	more demanding (p. 9)
\sim	equally demanding (p. 9)

List of Tables

	<u>Page</u>
1.1 Constraints on the equivalent single-loop structures (BNIC case, diagonal G)	6
2.2 Fighter CCV, Trimmed Aero Data (Lateral)	21
2.3 Transfer functions Q_{uv}^{-1} for 10 flight conditions	23
3.1 Fighter CCV Trimmed Aero Data (Longitudinal)	95
3.2 Calculation of bounds on $L_{20}(j\omega)$	101
4.1 Elements of Q_{ij}	168

Figures titles

Chapter 1

- Fig. 1.1 A 3×3 multiple input-output feedback structure $\underline{y} = T \underline{r}$,
 $T = (I + PG)^{-1} PGF$. 16
- Fig. 1.2 Nine single-loop structures equivalent to Fig. 1.1.
 $P^{-1} = [1/Q_{ij}]$; $-d_{uv} = \sum_i \frac{b_{iv}}{|Q_{ui}|}$, $i \neq u$ 16

Chapter 2

- Fig. 2.1 Templates of Q_{11} at $\omega = 1, 4, 8, 100$ 45-6
- 2.2 Templates of Q_{22} at $\omega = 3, 8, 100$ 47
- 2.3 Templates of Q_{33} at $\omega = 0, 16, 100$ 48
- 2.4 Simulation data, A_y mode response; .9M, 30,000 ft CG,
 35% MAC (supplied by contractor) 48
- 2.5. Tolerances on $|T_{33}(j\omega)|$.
- 2.6a Bode plots (asymptotic) of $|Q_{11}/Q_{12}|$ 49
- 2.6b Bode plots (asymptotic) of $|Q_{11}/Q_{13}|$ 49
- 2.7 Bounds on L_{10} in Nichols Chart, Design 1. (• indicate $L_{10}(j\omega)$ values). 50
- 2.8 Bode plots of L_{10} , Q_{110} . Design 1. 51
- 2.9 Bounds on L_{20} in Nichols Chart, Design 1 (x are $L_{20}(j\omega)$ values). 52
- 2.10 Bode plots of L_{20} , Q_{220} : Design 1 (asymptotes) 53
- 2.11 Some templates of $-\psi(j\omega)$ ($T_p(-\psi)$) and bounds on L_{30} in
 Nichols Chart. 54
- 2.12 Bode plots of L_{30} , Q_{330} : Design 1. 55
- 2.13 Comparison of G_1 , $G_3(j\omega)$ of various designs. 56
- 2.14 Comparison of $G_2(j\omega)$ of various designs. 57

Fig. 2.15a-c	Computer Simulation of Design 1. Responses of β , ϕ (deg.), A_y (g) due to 1g step command of A_y .	58
2.16a-c	Computer simulation of Design 1. Responses of control surfaces δ_r , δ_a , δ_c (degrees) due to 1g step command of A_y .	58
2.17a-c	Design 1, Control surface rates (deg./sec). A_y command = 1g step.	58
2.18a-c	Control surface responses (degrees) due to very large A_y command, causing saturation; Design 1.	59
2.19a-c	Control surface rates due to very large A_y command, causing saturation; Design 1.	59
2.20a-c	Lateral outputs (β , ϕ , A_y) due to large A_y commands, causing saturation; Design 1.	59
2.21a-c	Bode plots of L_{10} , L_{20} , L_{30} : Design 2.	60-2
2.22	Computer simulation: Design 2.	63
2.23	Templates of Q_{11n} , scheduled design	64
2.24	Templates of Q_{22n} , scheduled design	64-5
2.25	Templates of Q_{33n} , scheduled design	65
2.26a	Bounds on L_{10} , scheduled design (x gives $L_{10}(j\omega)$).	66
2.26b	Bounds on L_{20} and $L_{20}(j\omega)$ values, scheduled design.	67
2.26c	Bounds on L_{30} and templates of $-\psi$, scheduled design.	68
2.27a	Bode plots L_{10} , scheduled design	69
2.27b	Bode plots L_{20} , scheduled design.	70
2.27c	Bode plots L_{30} , scheduled design	71
2.28	Scheduled design, simulation results	72
(a)	$\beta(t)$, $\phi(t)$, $A_y(t)$	
(b)	δ_r , δ_a , δ_c	
(c)	$\dot{\delta}_r$, $\dot{\delta}_a$, $\dot{\delta}_c$	

2.29a,b	Template of the new Q_{11n}, Q_{22n} , for nondiagonal compensation design.	73-
2.30a	Bounds on L_{10} in nondiagonal compensation design.	75
2.30b	Bounds on L_{20} in nondiagonal compensation design.	76
2.31a	Bode plot of L_{10} in nondiagonal compensation design.	77
2.31b	Bode plot of L_{20} in nondiagonal compensation design.	78
2.32a-c	Simulation results for nondiagonal G design:	79-
	(a) β , ϕ , A_y (b) δ_r , δ_a , δ_c	
	(c) $\dot{\delta}_r$, $\dot{\delta}_a$, $\dot{\delta}_c$ (commanded A_y values are given in brackets in Fig. 2.32a).	
2.33	Simulation results for Design 1 with $F_3 = F_{3b}$	82-
2.34	Simulation results for Design 1 with $F_3 = F_{3b}$	84-

Chapter 3

Fig. 3.1	System structure for longitudinal pitch-pointing mode (a1)	155
3.2a,b	Bode sketch of $b_{11}(\omega)$; α_2 mode response.	155-
3.3	Asymptotic plots of $ Q_{21}(j\omega) $, Cases 1a-5a.	157
3.4	Asymptotic plots of $ Q_{22}(j\omega) $, Cases 1a-5a.	158
3.5	Bounds on $L_{20}(j\omega)$ and final design.	158
3.6	Some templates of $Q_{22}(j\omega)$	159
3.7	Bode plot of $L_{20}(j\omega)$	159
3.8	Bode plot of $ G_2(j\omega) $	160
3.9	Some templates of $Q_{11}^*(j\omega)$	160-1
3.10	Bode plot of nominal, $Q_{110}^*(j\omega)$	162
3.11	Bode plot of $L_{110}^*(j\omega)$	163

3.12	Locus of templates of $L_1^* = G_1 Q_{11}^*(j\omega)$	164
3.13	Simulation results	165
3.14	Simulation results for "faster" filter, $F_1 = \frac{1}{\left(\frac{s}{1.4} + 1\right)}$	165

Chapter 4

Fig. 4.1	System structure for lateral translation (β_2) mode	175
4.2	Bode plot of $b_{11}(\omega)$	175
4.3	Bounds on $ G_3(j\omega) $ for part of frequency range	176
4.4	Bounds on L_{30} in Nichols Chart and $L_{30}(j\omega)$.	177
4.5	Some templates of $Q_{33}(j\omega)$	178
4.6	Bounds on $ G_2(j\omega) $ and on $ L_{20}(j\omega) $ for part of frequency range.	178
4.7	Some templates of $Q_{22}(j\omega)$	179
4.8	Bounds on $L_{20}(j\omega)$ and $L_{20}(j\omega)$ designed	180
4.9	Some templates of $Q_{11}^*(j\omega)$	181
4.10	Bounds on $T_{11}(j\omega)$ which were used	181
4.11	Bounds on $L_{10}^*(j\omega)$ and $L_{10}(j\omega)$	182
4.12	Simulation results, $F_{1a} = 0.3/(s+.3)$	183-7
4.13	Simulation results, $F_{1b} = 0.5/(s+.5)$	188-192
4.14	Simulation results with digital compensation, $T = 0.02$ seconds, $F = F_{1a}^*$ Expanded time scale in last two figures	193-198

Chapter 5

5.1a	Flap (δ_f) input (cf Fig. 3.13) Cases: A-5, B-4, C-1, D-3, E-2	206
5.1b	Elevon (δ_e) input (cf Fig. 3.13) Cases: A-1, B-4, C-2, D-5, E-3	207

5.2a	Pitch (θ) output (cf Fig. 3.13)	208
5.2b	Vertical velocity (v_z) output (cf Fig. 3.13)	209
5.3a	Lateral velocity (v) (cf Fig. 4.12) Cases: A-1, B-4, C-2, D-3, E-5	210
5.3b	Yaw angle (ψ) (cf Fig. 4.12)	211
5.3c	Roll angle (ϕ) (cf Fig. 4.12)	212
5.4a	Lateral velocity (cf Fig. 4.12) Cases: A-6, B-9, C-7, D-8, E-10	213
5.4b	Roll angle (cf Fig. 4.12)	214
5.4c	Yaw angle (cf Fig. 4.12)	215
5.5a	Canard input (δ_c) (cf Fig. 4.12) Cases: A-1, B-4, C-2, D-3, E-5.	216
5.5b	Rudder input (δ_r) (cf Fig. 4.12)	217
5.5c	Aileron input (δ_a) (cf Fig. 4.12)	218
5.6a	Canard input (cf Fig. 4.12) Cases: A-6, B-9, C-7, D-8, E-10	219
5.6b	Rudder input (cf Fig. 4.12)	220
5.6c	Aileron input (cf Fig. 4.12)	221

Chapter 6

6.1a,b	Specifications 2x2 system	227
6.1c,d	Specifications 3x3 system	227
6.2a	Tolerances on $ T_{11}(j\omega) $	228
6.2b	Tolerances on $ T_{22}(j\omega) $	228
6.3a,b	Plant templates (a) $Q_{11}(2 \times 2)$, (b) $Q_{11}(3 \times 3)$	229
6.3c	$Q_{22}(3 \times 3)$ templates	230
6.3d	$Q_{33}(3 \times 3)$ templates	231
6.4a	Bounds on L_{10} , 3×3 , and $L_{10}(3 \times 3)$	232a
6.4b	Bounds on L_{10} , 2×2 ; $L_{10}(2 \times 2)$ and $L_{10}(3 \times 3)$. G_1 dictated by 2×2 bounds.	232b
6.4c	Bounds on G_2 due to 2×2 and 3×3 ; 2×2 dominates at low ω , 3×3 at large ω .	233a
6.4d	$L_{20}(2 \times 2)$ and $L_{20}(3 \times 3)$	233b

6.4e	Bounds on $L_{30}(j\omega)$; $L_{30}(j\omega)$	234
6.5a,b	Roll and sideslip responses ($\phi_c = 90^\circ$ at $t=0$, 2×2 ; $\beta_c = 5^\circ$ at $t=1.8$, 3×3).	235
6.5c	Lateral acceleration response, ($\phi_c = 90^\circ$, $t=0$; $\beta_c = 5^\circ$, $t=1.8$)	236
6.6a	Aileron response ($\phi_c = 90^\circ$, $t=0$; $\beta_c = 5^\circ$, $t=1.8$)	236
6.6b,c	Rudder and canard responses ($\phi_c = 90^\circ$, $t=0$; $\beta_c = 5^\circ$, $t=1.8$)	237
6.7a,b	Aileron and rudder rates ($\phi_c = 90^\circ$, $t=0$; $\beta_c = 5^\circ$, $t=1.8$)	238
6.7c	Canard rate ($\phi_c = 90^\circ$, $t=0$; $\beta_c = 5^\circ$, $t=1.8$)	239
6.8a	Roll response, 3×3 ($\phi_c = 90^\circ$, $t=0$; $t=1.8$, sinusoid $\omega = 12.5$ rps, amplitude 15°)	239
6.8b,c	Sideslip and lateral acceleration, 3×3 ($\phi_c = 90^\circ$, $t=0$; $t=1.8$, sinusoid $\omega = 12.5$ rps, amplitude 15°)	240
6.9a,b	Aileron and rudder responses, 3×3 ($\phi_c = 90^\circ$, $t=0$; $t=1.8$, sinusoid $\omega = 12.5$ rps, amplitude 15°)	241
6.9c	Canard response 3×3 ($\phi_c = 90^\circ$, $t=0$; $t=1.8$, sinusoid $\omega = 12.5$ rps, amplitude 15°)	242
6.10a,b	Aileron and rudder rates, 3×3 ($\phi_c = 90^\circ$, $t=0$; $t=1.8$, sinusoid $\omega = 12.5$ rps, amplitude 15°)	243
6.10c	Canard rate, 3×3 ($\phi_c = 90^\circ$, $t=0$; $t=1.8$, sinusoid $\omega = 12.5$ rps, amplitude 15°)	244
6.11a	Roll response 3×3 ($\phi_c = 90^\circ$, $t=0$, $t=1.8$, sinusoid $\omega = 12.5$ rps, amplitude 15°)	244
6.11b,c	Sideslip and lateral acceleration responses ($\phi_c = 90^\circ$, $t=0$; $t=1.8$, sinusoid $\omega = 4$ rps, amplitude 15°)	245
6.12a,b	Aileron and rudder responses 3×3 ($\phi_c = 90^\circ$, $t=0$, $t=1.8$, sinusoid $\omega = 4$ rps, amplitude 15°)	246

6.12c	Canard response 3x3 ($\phi_c=90^\circ$, $t=0$, $t=1.8$, sinusoid $\omega = 4$ rps, amplitude 15°)	247
6.13a	Aileron rate 3x3 ($\phi_c=90^\circ$, $t=0$, $t=1.8$, sinusoid $\omega = 4$ rps, amplitude 15°)	247
6.13b,c	Rudder and canard rates 3x3 ($\phi_c=90^\circ$, $t=0$, $t=1.8$, sinusoid $\omega = 4$ rps, amplitude 15°)	248
6.14a-i	Responses due to sideslip command β_c : 2.5° step at $t=0$, sinusoid at $t=1.0$, amplitude 1.5° , frequency 12.5 rps.	
(a)	roll	249
(b)	sideslip	250
(c)	acceleration	251
(d)	ailerons	252
(e)	rudder	253
(f)	canards	254
(g)	aileron rate	255
(h)	rudder rate	256
(i)	canard rate	257
6.15a-i	Responses due to sideslip command β_c ; 2.5° step at $t=0$, sinusoid at $t=1.0$, amplitude 1.5° , frequency 4 rps.	
(a)	roll	258
(b)	sideslip	259
(c)	acceleration	260
(d)	ailerons	261
(e)	rudder	262
(f)	canards	263
(g)	aileron rate	264
(h)	rudder rate	265
(i)	canard rate	266

CHAPTER 1

A SYNTHESIS TECHNIQUE FOR UNCERTAIN MULTIPLE INPUT-OUTPUT FEEDBACK SYSTEMS

1.1 Introduction.

The flight control problem is basically a multiple input-output (mio) feedback problem with an uncertain plant. In this report, the lateral and longitudinal systems are treated separately. The lateral system is taken as three by three with rudder, ailerons and canard as the plant control input variables. The output variables vary with the mode, for example sideslip (β), roll (ϕ) and side force (A_y) in one case. The longitudinal system has elevator and flap as the plant inputs and the outputs are usually normal acceleration (A_n) and pitch (θ). In this work the linearized plant equations are used, so different flight conditions give different coefficients in the linear equations, thereby giving a set of plants $P = \{P\}$. The fact that P is only known to be a member of a set P (but it is not known which member), constitutes uncertainty. Of course much of this uncertainty could be removed by "scheduling", but in any realistic control system, there always remains some uncertainty. Nevertheless one is interested in a feedback design which does not use scheduling, even if only as an option. Also, it is desirable to know the trade-off between the extent of scheduling and the resulting economy achieved in other system factors. Hence, it is important to have a synthesis technique for uncertain mio systems, which is flexible enough to include scheduling of any desired extent.

The difficulty inherent in developing a synthesis theory for uncertain mio systems, can be appreciated by considering the 3×3 output-feedback structure in Fig. 1.1, with 3×3 matrices:
 $P = [p_{ij}]$ of plant; $G = [g_{ij}]$, $F = [f_{ij}]$ of compensation functions.
 We even let $G = [g_i]$ be diagonal and consider only the transfer function T_{11} relating output (1) to input (1):

$$\begin{aligned} T_{11} = & (p_{11} f_{11} g_1 + p_{12} f_{21} g_2 + p_{13} f_{31} g_3) [(1 + p_{22} g_2)(1 + p_{33} g_3) \\ & - p_{23} p_{32} g_2 g_3] - (p_{21} f_{11} g_1 + p_{22} f_{21} g_2 + p_{23} f_{31} g_3) \\ & + [p_{12} g_2 (1 + p_{33} g_3) - p_{32} p_{13} g_2 g_3] + \\ & \frac{(p_{31} f_{11} g_1 + p_{32} f_{21} g_2 + p_{33} f_{31} g_3) [p_{23} p_{12} g_2 g_3 - p_{13} g_3 (1 + p_{22} g_2)]}{(1 + p_{11} g_1) [(1 + p_{22} g_2)(1 + p_{33} g_3) - p_{23} p_{32} g_2 g_3]} \\ & - p_{12} g_1 [p_{12} g_2 (1 + p_{33} g_3) - p_{32} p_{13} g_2 g_3] + p_{13} g_1 [p_{12} p_{23} g_2 g_3 - p_{13} g_3 (1 + p_{22} g_2)] \end{aligned}$$

(1.1a)

There are nine such T_{ij} functions, each one as complicated as this. Note that the variables normally refer to Laplace transforms or transfer functions. Functions of time will be explicitly expressed, e.g. $f(t)$.

Suppose that there is significant uncertainty in the functions p_{ij} , for example $p_{ij} = (A_{ij}s + B_{ij}) / (E_{ij}s^2 + J_{ij}s + F_{ij})$, with intervals of uncertainty, for (1j) = (11) say $A_{11} \in [1, 2]$, $B_{11} \in [2, 4]$, $E_{11} \in [1, 2.5]$, $J_{11} \in [-1, 3]$, $F_{11} \in [-2, 1]$, or each may be a function of other parameters with large uncertain intervals (as in the flight control problem). The problem seems hopeless, unless one is thoroughly familiar with the system, with

considerable cut and try experience so that he has a good initial starting point.

A synthesis technique has been developed [1-4] which considerably reduces the complexity of the above problem. Since it has been presented in detail in the references, it is only summarized in the next sections.

1.2 Summary of MIO synthesis technique

Fig. 1.2 applies for a 3×3 system and consists of nine single-loop structures. Note that in the first row the elements inside the loops are $G_1(s)$, $Q_{11}(s)$ the same for each of the three structures. But the disturbances $d_{1i}(s)$ are different. Also, the prefilters F_{1i} are different. This situation is repeated for each of the three rows. The F_{uv} are the elements of the F matrix in Fig. 1.1, while the G_i are the diagonal elements of the G matrix, which for the moment is taken as a diagonal matrix (see Sec. 1.4). The Q_{uv} in Fig. 1. are the inverses of the elements of the P^{-1} matrix, $P^{-1} = [1/Q_{uv}]$ where P is the plant matrix. Because of the plant parameter uncertainty, there is a set $P = \{P\}$ of plant matrices, which generates a set of Q matrices. Since $y = P\delta$ in Fig. 1.1, $\delta = P^{-1}y$, so $\delta_1 = y_1/Q_{11} + y_2/Q_{12} + y_3/Q_{13}$, $\delta_2 = y_1/Q_{21} + y_2/Q_{22} + y_3/Q_{23}$ etc. The following is a physical interpretation of (for example) Q_{12} : Adjust the inputs δ_1 , δ_2 , δ_3 so that $y_1 = y_3 = 0$. Then the resulting ratio of transforms $y_2/\delta_1(s)$ is equal to Q_{12} , $y_2/\delta_2 = Q_{22}$, $y_3/\delta_3 = Q_{32}$. In practice, one simply inverts P in order to obtain the Q_{uv} .

The elements b_{uv} in Fig. 1.2 are real positive functions of

frequency ω , obtained as follows. The 3×3 system in Fig. 1.1 has nine closed-loop transfer functions

$$T_{uv}(s) = \frac{y_u(s)}{r_v(s)} \quad (1.1)$$

In many problems, for $u \neq v$ one wants T_{uv} to be small, ideally zero, which is certainly possible at one combination of plant parameter values. But if there is uncertainty, this cannot in general be achieved for all $P \in \mathcal{P}$, so one sets a lower bound which can be a function of ω

$$|T_{uv}(j\omega)| \leq b_{uv}(\omega), \quad u \neq v \quad (1.2)$$

to be achieved for all $P \in \mathcal{P}$. Such a system is called "basically noninteracting" BNIC. In this report the designs are all desired to be BNIC. Usually one wants some sensible response for the diagonal elements $T_{uu}(s)$ in Fig. 1.1, so in minimum-phase systems [3], specifications on $|T_{uu}(j\omega)|$ suffice of the form

$$a_{uu}(\omega) \leq |T_{uu}(j\omega)| \leq b_{uu}(\omega) \quad (1.3)$$

See Chapter 2 for examples of b_{uv} , a_{uu} of (1.2, 1.3). Thus, the disturbances d_{uv} in Fig. 1.2 are derived from the Q_{ui} of the plant and the specifications b_{im} on the closed-loop response functions.

The problem in Fig. 1.2, is to choose the G_i , F_{ij} so as to satisfy the specifications on the T_{ij} of Fig. 1.1; for example choose F_{11} , G_1 so that y_{11} satisfies the specification (1.3) with $u = 1$. Choose F_{12} , G_1 so that y_{12} satisfies (1.2) with $u = 1$, $v = 2$, etc. The output y_{12} in Fig. 1.2, is the sum of two components: one due to the unit input, the second due to d_{12} . As it is required (Eq. 1.2) that $|y_{12}(j\omega)| \leq b_{12}(\omega)$ for all ω , it

is clearly best to let F_{12} , which we can control, be zero. Similarly let $F_{uv} = 0$ for all $u \neq v$. Since G_1 is the same for all 3 structures in the first row of Fig. 1.2, it must be "good enough" (have large enough gain over large enough frequency range) to handle the "feedback needs" of the worst of the three at each ω value. If it is possible to find F_{ij} , G_i which solve these nine single-loop problems, then it is guaranteed that these same F_{ij} , G_i when used as elements of the F , G matrices in Fig. 1.1, are satisfactory for the original mio problem [1]. Thus, the 3×3 mio problem has been converted into three loop problems (choice of G_i) and nine prefilter problems (choice of F_{ij}).

1.2.1 Derivation of Table 1.1.

Table 1.1 lists the demands on the three loop transmission functions $L_i = P_{ii} G_i$ so as to solve the nine single-loop problems of Fig. 1.2, for the BNIC case. They were obtained as follows. In Fig. 1.2 each diagonal y_{uu} element has two components, one due to the unit input, the second due to $d_{uu}(s)$. Let their respective outputs be

$$y_{uu}(s) = \tau_{uu}(s) + \tau_{duu}(s) \quad (1.4a-d)$$

$$\tau_{uu}(s) = \frac{F_u L_u}{1+L_u}, \quad \tau_{duu} = \frac{d_{uu} Q_{uu}}{1+L_u}, \quad L_u = G_u Q_{uu}.$$

Table 1.1

Constraints on the equivalent single-loop structures (BNIC case, diagonal G)

$$\begin{array}{ccc} \underline{A_{11}} & & \underline{B_{11}} \\ \Delta \left| \frac{L_1}{1+L_1} \right| < \frac{b_{11}}{a_{11}} \cdot \frac{1}{|1+L_1|} < \frac{1}{\Delta} \frac{b_{21} \left| \frac{Q_{11}}{Q_{12}} \right| + b_{31} \left| \frac{Q_{11}}{Q_{13}} \right|}{d_{11}} \cdot \frac{b_{12}}{b_{13}} \frac{b_{23} \left| \frac{Q_{11}}{Q_{12}} \right| + b_{33} \left| \frac{Q_{11}}{Q_{13}} \right|}{b_{13}} \end{array}$$

$$\begin{array}{ccc} \underline{D_{21}} & & \underline{A_{22}} \\ \frac{1}{|1+L_2|} < \frac{b_{21}}{b_{11} \left| \frac{Q_{22}}{Q_{21}} \right| + b_{31} \left| \frac{Q_{22}}{Q_{23}} \right|} \cdot \Delta \left| \frac{L_2}{1+L_2} \right| < \frac{b_{22}}{a_{22}} \cdot \frac{1}{|1+L_2|} < \frac{1}{\Delta} \frac{b_{12} \left| \frac{Q_{22}}{Q_{21}} \right| + b_{32} \left| \frac{Q_{22}}{Q_{23}} \right|}{d_{22}} \cdot \frac{b_{23}}{b_{23} \left| \frac{Q_{22}}{Q_{21}} \right| + b_{33} \left| \frac{Q_{22}}{Q_{23}} \right|} \end{array}$$

$$\begin{array}{ccc} \underline{D_{31}} & & \underline{B_{32}} \\ \frac{1}{|1+L_3|} < \frac{b_{31}}{b_{11} \left| \frac{Q_{33}}{Q_{31}} \right| + b_{21} \left| \frac{Q_{33}}{Q_{32}} \right|} \cdot \frac{b_{32}}{b_{12} \left| \frac{Q_{33}}{Q_{31}} \right| + b_{22} \left| \frac{Q_{33}}{Q_{32}} \right|} \cdot \Delta \left| \frac{L_3}{1+L_3} \right| < \frac{b_{33}}{a_{33}} \cdot \frac{1}{|1+L_3|} < \frac{1}{\Delta} \frac{b_{13} \left| \frac{Q_{33}}{Q_{31}} \right| + b_{23} \left| \frac{Q_{33}}{Q_{32}} \right|}{d_{33}} \end{array}$$

$$\underline{A_{33}} \quad \underline{R_{33}}$$

From (1.3) it is necessary that

$$|y_{uu}(j\omega)| \in [a_{uu}(\omega), b_{uu}(\omega)] \quad (1.5)$$

But $|y_{uu}(j\omega)| = |\tau_{uu}(j\omega) + \tau_{duu}(j\omega)|$, and since their relative phases are not known, the harsher condition is used:

$$|\tau_{uu}(j\omega)| + |\tau_{duu}(j\omega)| \in [a_{uu}, b_{uu}] \quad (1.6)$$

$$\text{Suppose } |\tau_{uu}(j\omega)| \in [a'_{uu}(\omega), b'_{uu}(\omega)] \quad (1.7)$$

which must be chosen such that,

$$\begin{aligned} b'_{uu} + \tau_{duu} &\leq b_{uu}, \quad a'_{uu} - \tau_{duu} \geq a_{uu}, \\ [b'_{uu} - a'_{uu} + 2\tau_{duu}]_{\max} &= b_{uu} - a_{uu} \end{aligned} \quad (1.8a-c)$$

For example, suppose $|y_{uu}(j2)| \in [0.9, 1.1]$ is required. This allowance of $1.1 - 0.9 = 0.2$ variation in $|T_{uu}(j2)|$ can be split up in an infinitude of ways between $\tau_{uu}(j2)$ and $\tau_{duu}(j2)$: e.g. $\tau_{duu} = 0.05$, $b'_{uu} = 1.05$, $a'_{uu} = 0.95$ satisfying (1.8c). But $\tau_{duu} = 0.07$, $b'_{uu} = 1.03$, $a'_{uu} = 0.97$ would also be satisfactory, etc. What is the optimum choice? To satisfy (1.7), a minimum value of $|L(j\omega)|$ is needed, and a minimum value of $|L(j\omega)|$ is needed to achieve $|\tau_{duu}| \leq$ its allowed value. Hence, the optimum division is when these two minimum required $|L|$ values are the same.

In table 1.1, the (1.7) obligation on L_u is denoted as an A_{uu} type, of the form

$$\Delta \left| \frac{L_u}{1+L_u} \right| \leq \frac{b'_{uu}}{a'_{uu}} \quad (1.9)$$

while the τ_{duu} is denoted as a B_{uu} type, of form (see Fig. 1.2)

$$\left| \frac{d_{uu} Q_{uu}}{1+L_u} \right| \leq \tau_{duu} .$$

But $-d_{uu} = \sum_{i \neq u} b_{iu} / |Q_{ui}|$, giving

$$\frac{1}{|1 + L_1|} \leq \frac{\tau_{d11}}{b_{21} \left| \frac{Q_{11}}{Q_{12}} \right| + b_{31} \left| \frac{Q_{11}}{Q_{13}} \right|} \quad \text{etc.} \quad (1.10)$$

In the BNIC design, only this type of inequality exists for all off-diagonal elements and is denoted as a D_{uv} type, with b_{uv} replacing τ_{duu} .

1.2.2 Optimization and trade-off

There are interactions between the entries of Table 1.1, via the b_{uv} . For example, suppose b_{21} is decreased from its original value of say 10^{-3} to $\delta < 10^{-3}$, which certainly doesn't violate the requirement $|T_{21}| \leq 10^{-3}$. This helps B_{11} , because $|1 + L_1|$ now may be less than before. It helps D_{31} for the same reason, but clearly makes it harder on D_{21} . But suppose D_{23} imposes a tougher obligation on L_2 than does D_{21} (this is denoted by $D_{23} \succ D_{21}$; $D_{21} \sim D_{23}$ means that each imposes the same requirement on L_2). Then it doesn't matter if b_{21} is decreased to some extent, thereby increasing the D_{21} obligation on L_2 . Note that this interaction is always between the elements of the same column in Table 1.1. Thus b_{11} , b_{21} , b_{31} appear only in the first column; b_{12} , b_{22} , b_{32} only in the second column etc. Similarly, decrease of b_{31} helps (A_{11}, B_{11}) ,

D_{21} but makes it harder on D_{31} .

In the above, it was possible to help L_1 at no expense to the other L 's. Equilibrium is defined as when this is no longer possible. The following has been proven [2]:

Theorem: A necessary and sufficient condition for equilibrium is when all the L_u are dominated by the members of the same column.

For example, D_{12} dominates L_1 , (A_{22}, B_{22}) dominates L_2 , D_{32} dominates L_3 . This does not preclude one or more of $D_{12} \sim D_{13}$, $(A_{22}, B_{22}) \sim D_{21}$ etc.

Trade-off

After equilibrium has been reached, it is still possible and may be desirable to trade-off, i.e. sacrifice one or more L_u for others. For example, if the sensor of y_2 is noisier than the others, or Q_{22} has higher-order modes in a rather low ω range, it is important to reduce $|L_2(j\omega)|$ rapidly vs. ω . This can be done by reducing b_{23} (or b_{33}) if $D_{23} \succ (A_{22}, B_{22})$, D_{21} at the expense of D_{13} , (A_{33}, B_{33}) , thereby imposing greater demands on L_1 (if D_{13} dominates L_1) and/or on L_3 , if (A_{33}, B_{33}) dominates L_3 . Of course, if so, eventually one or more of (A_{22}, B_{22}) , $D_{21} \sim D_{23}$ say the former. Then b_{22} can be decreased but only until it approaches a_{22} in value, whereas any b_{uv} ($u \neq v$) can be reduced by any amount.

Equilibrium and trade-off give the designer valuable flexibility, which he can exploit, according to the circumstances of his specific system.

1.3 Necessary conditions for use of of MIO synthesis technique

Certain conditions must be satisfied in order that the above synthesis technique may be used. These conditions are not difficult to derive, by simply examining the operations involved in executing the design techniques. Normally the plant matrix P is available, so its inverse P^{-1} must exist, in order to evaluate the Q_{uv} from $P^{-1} = [1/Q_{uv}]$. This means that $\det P$ must not be indentially zero for any $P \in \mathcal{P}$. This is the much-touted "controllability" condition. If $\det P \equiv 0$ it means that the plant outputs y_u are not independently realizable, for that specific P .

The other conditions are due to the need that the single-loop problems of Fig. 1.2 be solvable, for only then can the F_u , G_u be found. The uncertainty in the Q_{uu} must be compatible with the specifications on the $T_{uu}(j\omega)$. If $Q_{uu}(s)$ is minimum-phase, then very general Q_{uu} uncertainty and T_{uu} performance tolerances can be handled (see [1] for details). But if $Q_{uu}(s)$ is nonminimum-phase (has zeros in the right half complex plane), then the T_{uu} tolerances must be compatible with the limitations on the realizable bandwidth of $L_u(j\omega)$ [4], due to the right half-plane zeros of $Q_{uu}(s)$. Right half-plane poles of Q_{uu} can be handled [2].

1.3.1 A high-frequency condition

There is an important high-frequency condition on the Q_{uv} which must be satisfied. It will be derived for the 2×2 case, and only stated for the 3×3 case. At high frequencies, the a_{uu} of Fig. 1.2, Table 1.1 and Eq. (1.3) are so small that they can be taken as zero. All the A_{uu} of Table 1.1 then disappear and the B_{uu} have the

same form as the D_{uv} , with b_{uu} replacing the τ_{duu} . In the 2×2 case the inequalities of Table 1.1 then are:

$$\begin{aligned} |1 + L_1|^{-1} &\leq \frac{b_{11}}{b_{21}} \left| \frac{Q_{12}}{Q_{11}} \right|, & \frac{b_{12}}{b_{22}} \left| \frac{Q_{12}}{Q_{11}} \right| \\ |1 + L_2|^{-1} &\leq \frac{b_{21}}{b_{11}} \left| \frac{Q_{21}}{Q_{22}} \right|, & \frac{b_{22}}{b_{12}} \left| \frac{Q_{21}}{Q_{22}} \right| \end{aligned} \quad (1.11a,b)$$

In (1.11a), one might as well let $b_{11}/b_{21} = b_{12}/b_{22}$ since $|1 + L_1|^{-1}$ must satisfy both inequalities. This can't hurt and may help, because suppose $b_{12}/b_{22} > b_{11}/b_{21}$. Reducing b_{12}/b_{22} doesn't hurt (a) but may help (b), if $b_{22}/b_{12} < b_{21}/b_{11}$. For the same reason set $b_{21}/b_{11} = b_{22}/b_{12}$ in (b). These two results are identical: $b_{11}b_{22} = b_{12}b_{21}$, and give

$$|1 + L_1|^{-1} |1 + L_2|^{-1} \leq \left| \frac{Q_{12}Q_{21}}{Q_{11}Q_{22}} \right|. \quad (1.12)$$

Now we know that sooner or later in ω , any practical $|1 + L_u| < 1$, unless L_u is restricted to $|\arg L| \leq \pi/2$ which is impossible in any practical system. (This impractical condition is blithely assumed in the "optimal quadratic regulator," so popular in Modern Control Theory). If we play safe and want to allow $|1 + L_u| < 1$ for all ω larger than some ω_u , then (1.12) requires that there exist a ω_{um} such that

$$\left| \frac{P_{11}P_{22}}{P_{12}P_{21}} \right| = \left| \frac{Q_{12}Q_{21}}{Q_{11}Q_{22}} \right| > 1 \text{ for all } P \in \mathcal{P} \text{ and all } \omega > \omega_{um}. \quad (1.13)$$

The analogous condition in the 3×3 case is more complicated in its derivation [1], so is only stated here:

$$|P_{11}P_{22}P_{33}| > |P_{11}P_{23}P_{32}| + |P_{12}P_{21}P_{33}| + |P_{12}P_{23}P_{31}| \\ + |P_{13}P_{22}P_{31}| + |P_{13}P_{21}P_{32}| \quad (1.14a,b)$$

$$P_{uv} = 1/Q_{uv}$$

The above are not necessary conditions because in (1.12) we could stagger the ω regions in which $|1 + L_u|$, $|1 + L_v|$ are less than unity, i.e. have L_u in the second or third quadrants when L_v is in the first or fourth and vice versa. But it simplifies matters if the condition is satisfied. By renumbering the terminals at the plant input (but not at the output) the new p_{11} is old p_{12} , $(p_{12})_{\text{new}} = (p_{11})_{\text{old}}$ etc. And if this renumbering is done at the plant output,

$(p_{11})_{\text{new}} = (p_{21})_{\text{old}}$ etc. In both case (1.13) becomes

$$\left(\frac{Q_{12}Q_{21}}{Q_{11}Q_{22}} \right)_{\text{new}} = \left(\frac{Q_{11}Q_{22}}{Q_{12}Q_{21}} \right)_{\text{old}} > 1 \quad (1.15)$$

Of course renumbering of either the input or the output terminals of the plant changes the expressions (1.14,1.15). This may be tried if in a specific numbering, the inequality is not satisfied $\forall P \in P$. It is worth noting that Rosenbrock [5] has a condition for his synthesis technique, which is harder to satisfy than (1.13) or (1.15), even though his synthesis technique does not cope with plant parameter uncertainty. His condition is that the diagonal element $|p_{uu}|$ be large than the sum of all the other elements in the same row (or of the same column), and this must be so for all $\omega \in [0, \infty)$.

Finally, suppose that in the 2×2 case neither (1.13) nor (1.15) is satisfied for all $\omega > \text{some } \omega_h$, precluding the use of this synthesis technique in precisely its present form. This is the situation in some of the modes of our aircraft flight control problem, no matter what the numbering of the plant terminals, i.e. (1.14) is not satisfied. Nevertheless, all is far from lost. In the 2×2 case one uses this synthesis technique for designing one of the L_u, F_u (say $u = 1$). So the design of L_u, F_u is that of single-loop system design. Then one uses the exact system equations to design G_2, F_2 . This second part is not difficult because it too becomes a single-loop type of problem, when G_1, F_1 is known:

$$T_{22} = \frac{L_{20}F_2}{L_{20} + \mu}, \quad T_{21} = \frac{\frac{p_{11}p_{21}F_1}{p_{110}} \frac{L_1}{(1+L_1)}}{L_{20} + \mu} \quad (1.16a-d)$$

$$\mu = \frac{p_{11}}{p_{10}} \frac{\left(\frac{\Delta}{p_{11}p_{22}} + L_1 \right)}{(1 + L_1)}, \quad \Delta = p_{11}p_{22} - p_{12}p_{21}$$

$L_{20} = G_2 Q_{220}$ is a nominal loop transmission at some $P_0 \in P$ chosen as the nominal plant. If L_{20} is large enough then from (1.16a) $T_{22} \approx F_2$. In (1.16b), large enough L_{20} also guarantees $|T_{21}|$ can be made as small as desired over any finite ω range. Since F_1 and L_1 are known, it is simple enough to choose L_{20} to satisfy the tolerances on T_{21}, T_{22} . In this way, the restriction (1.13) can be avoided, and in a similar manner restriction (1.14) for the 3×3 system (see Sec. 2.4). The above situation in the YF16CCV system motivated us to research this problem and develop an improvement of the mio synthesis theory. This is presented in Appendix 1. It is a good example of fundamental research motivated by practical problems.

1.4 A shortcoming: use of nondiagonal G

A good criterion of any feedback design technique is that the amount of feedback should be related to the amount of parameter uncertainty and to narrowness of the tolerances. In particular, if there is no uncertainty there is no need for any feedback at all, and the design technique should emerge with this result. As presented so far, the above design technique fails this test because of the existence of the B_{ii} , D_{ij} elements in Table 1.1. This can be corrected by inserting a precompensator H in front of the plant, whose function is to diagonalize the new modified plant PH , as much as possible. If there is no uncertainty it can be done precisely and then $Q_{ij} = \infty$ for all $i \neq j$, and in Table 1.1 the B_{ii} , D_{ij} all give $|1 + L_u|^{-1} \leq \infty$ with no resulting obligation on the L_u .

When there is parameter uncertainty, the elements of H can be chosen to minimize the B_{ii} , D_{ij} factors in the design problem. Let the new modified Q elements be denoted by w_{ij} , the old (due to P alone) by Q_{ij} . For the 2×2 case

$$[1/w_{ij}] = (PH)^{-1} = H^{-1}[1/Q_{ij}] = \begin{bmatrix} \frac{v_{11}}{Q_{11}} \left(1 + \lambda_1 \frac{Q_{11}}{Q_{21}}\right) & \frac{v_{11}}{Q_{12}} \left(1 + \lambda_1 \frac{Q_{12}}{Q_{22}}\right) \\ \frac{v_{22}}{Q_{21}} \left(1 + \lambda_2 \frac{Q_{21}}{Q_{11}}\right) & \frac{v_{22}}{Q_{22}} \left(1 + \lambda_1 \frac{Q_{22}}{Q_{12}}\right) \end{bmatrix} \quad (1.17a-d)$$

$$[v_{ij}] = H^{-1}, \quad \lambda_1 = v_{12}/v_{11}, \quad \lambda_2 = v_{21}/v_{22}$$

In the low and medium ω range where $|L_u|$ is >1 significantly $|1+L_u| \approx |L_u|$, so D_{12} for example becomes closely $|G_1| \geq \frac{b_{22}}{b_{12}w_{12}}$.

Hence it is desirable to choose λ_1 to minimize $\max_p \left| \frac{1}{Q_{11}} + \frac{\lambda_1}{Q_{22}} \right|$.

This is also the best that can be done for (A_{11}, B_{11}) in this ω range.

In the higher ω range where $|L_1| \sim 1$ or less (1.11a,b) apply so then one seeks to minimize

$$\max_p |w_{11}/w_{12}| = \max \left| \frac{\frac{1}{Q_{11}} + \frac{\lambda_1}{Q_{21}}}{\frac{1}{Q_{12}} + \frac{\lambda_1}{Q_{22}}} \right|, \quad (1.18)$$

if the right side in (1.11a) really is the constraint on L_1 . Often the right side is so large that instead one arbitrarily sets a gain margin type of constraint like $|1 + L_1|^{-1} \leq G_m$ db in the higher ω range.

1.5 Summary

We have presented the highlights of a multiple input-output (mio) synthesis technique for uncertain feedback system. Its main attractive feature is its reduction of the highly complex uncertain mio system into a number of single loop uncertain systems. Under very general conditions, the solutions of the latter are guaranteed to be satisfactory for the original mio problem.

The technique was applied very successfully to four linear time invariant mio problems with highly uncertain plants [1-3]. The most complex was 3×3 with a mixture of BNIC and more complex performance tolerances. Also, it was extended to a class of nonlinear uncertain mio plants, including a 2×2 highly nonlinear, uncertain and interacting example [4]. However, all of these were fabricated academic examples. The balance of this report applies this technique for the first time, to a real life practical design problem.

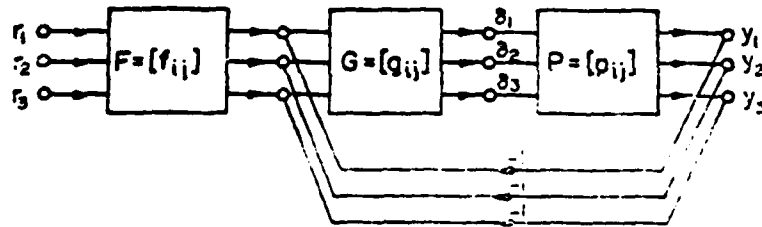


Fig. 1.1 A 3×3 multiple input-output feedback structure
 $\underline{y} = \underline{T} \underline{r}$

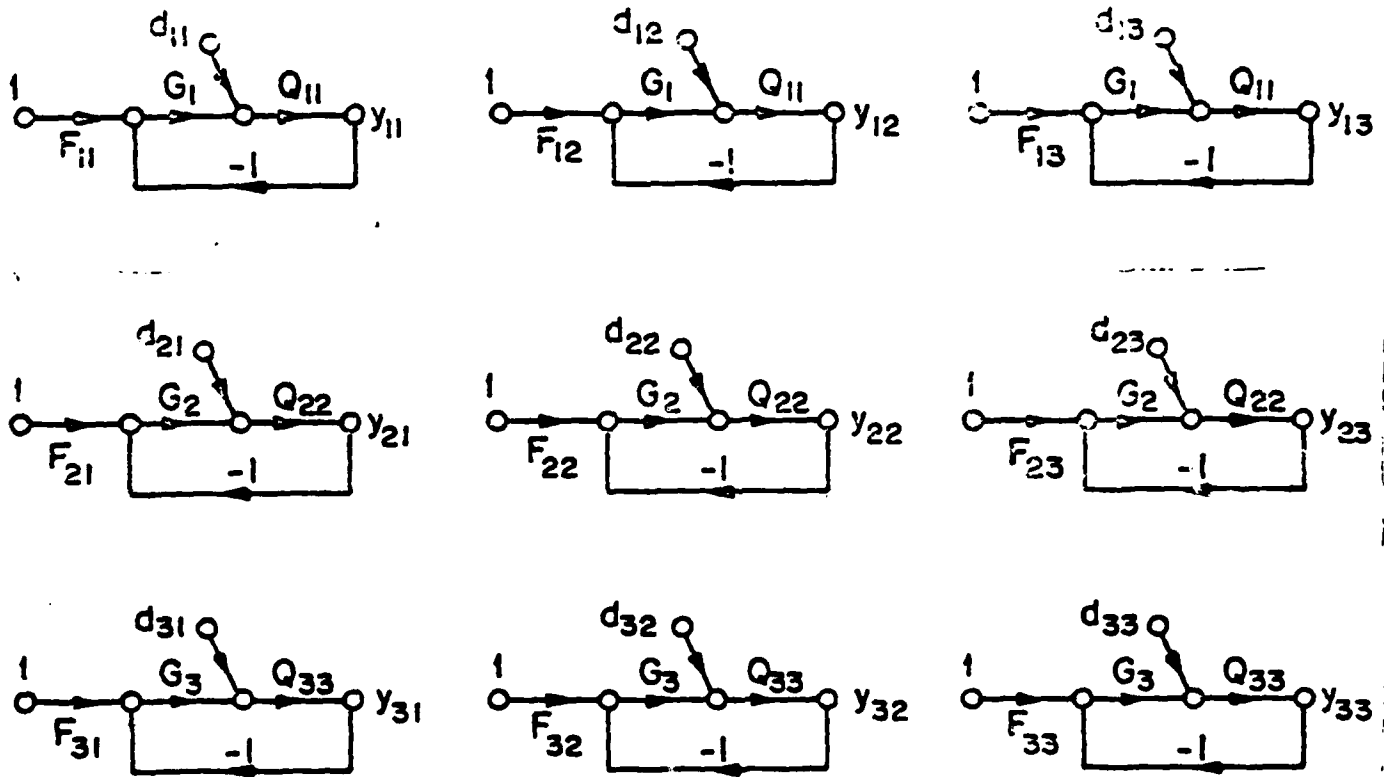


Fig. 1.2 Nine single-loop structures equivalent to Fig. 1.1.

$$P^{-1} = [1/Q_{ij}] \quad ; \quad -d_{uv} = \sum_i \frac{b_{iv}}{Q_{ui}} \quad , \quad i \neq u$$

CHAPTER 2

DESIGN FOR DIRECT SIDE FORCE MODE

The synthesis technique of Chapter 1 is applied to the design of the "Direct Side Force (A_y)" mode of a fighter CCV aircraft. Direct side force (A_y) is commanded and the objective is to achieve specified A_y step response tolerances, while maintaining specified small sideslip (β) and roll (ϕ). The control surfaces are δ_r (rudder), δ_a (ailerons), δ_c (canard). The definition and units of the symbols are all listed in the List of Symbols at the beginning of the report.

2.1 Plant equations

The plant equations are

$$\left. \begin{aligned} s \underline{x} &= A \underline{x} + B \underline{\delta} \quad , \quad \underline{y} = C \underline{x} + D \underline{\delta} \\ \underline{x} &= [p, r, \beta]' \quad , \quad \underline{\delta} = [\delta_r, \delta_a, \delta_c]' \\ \underline{y} &= [\beta, \phi, A_y]' \quad , \quad p = \dot{\phi} \quad , \quad r = \dot{\psi} = \text{yaw rate} \end{aligned} \right\} \quad (2.1a-g)$$

$$A = \frac{qSb}{2V} \begin{bmatrix} C_{lp} & C_{lr} & \frac{2VC_{l\beta}}{b} \\ C_{np} & C_{nr} & \frac{2VC_{n\beta}}{b} \\ C_{yp} + E & C_{yr} - \frac{2mV^2}{qSb} & \frac{2VC_{y\beta}}{b} \end{bmatrix} \quad (2.2)$$

$$B = q S \phi \begin{bmatrix} C_{\ell \delta r} & C_{\ell \delta a} & C_{\ell \delta c} \\ C_{n \delta r} & C_{n \delta a} & C_{n \delta c} \\ C_{y \delta r} & C_{y \delta a} & C_{y \delta c} \end{bmatrix} \quad (2.3)$$

$$\phi = \begin{bmatrix} b/I_x & 0 & 0 \\ 0 & b/I_z & 0 \\ 0 & 0 & 1/mV \end{bmatrix}, \quad E = \left(\alpha + \frac{Y \phi}{s} \right) \frac{2mV^2}{qSb} \quad (2.4a,b)$$

$$C = \begin{bmatrix} 0 & 0 & 1 \\ 1/s & 0 & 0 \\ c_{31} & c_{32} & c_{33} \end{bmatrix}, \quad D = \begin{bmatrix} 0 & 0 & 0 \\ 0 & 0 & 0 \\ C_{y \delta r} & C_{y \delta a} & C_{y \delta c} \end{bmatrix} \frac{q S}{m} \quad (2.5a,b)$$

$$(c_{31}, c_{32}, c_{33}) = \frac{bqS}{2Vm} (C_{yp}, C_{yr}, \frac{2V}{b} C_{y\beta}) \quad (2.6a)$$

Note that the third row of D is precisely the product of V and the third row of B .

$$\text{From (2.1a)} \quad \underline{x} = (sI - A)^{-1} B \underline{\delta},$$

$$\underline{y} = [C(sI - A)^{-1} B + D] \underline{\delta} \stackrel{\Delta}{=} P \underline{\delta} \quad (2.6b)$$

Our technique requires evaluation of $P^{-1} = [1/Q_{ij}]$. Let

$$R \stackrel{\Delta}{=} DB^{-1} = \begin{bmatrix} 0 & 0 & 0 \\ 0 & 0 & 0 \\ 0 & 0 & V \end{bmatrix} \quad (2.6c)$$

from (2.3, 2.5b), so

$$\begin{aligned} [1/Q_{ij}] &= P^{-1} = \{[C(sI-A)^{-1} + DB^{-1}]B\}^{-1} = B^{-1}[R + C(sI-A)^{-1}]^{-1} \\ &= B^{-1}\{[R(sI-A)+C](sI-A)^{-1}\}^{-1} = B^{-1}(sI-A)[R(sI-A)+C]^{-1} \end{aligned} \quad (2.7)$$

It is readily found that

$$Cs + R(s^2I - As) = \begin{bmatrix} 0 & 0 & s \\ 1 & 0 & 0 \\ -(\alpha s + Y_\phi)V & Vs & Vs^2 \end{bmatrix} \quad (2.8a)$$

and its inverse is

$$\begin{bmatrix} 0 & 1 & 0 \\ -1 & (\alpha s + Y_\phi)/s & 1/sV \\ 1/s & 0 & 0 \end{bmatrix} \quad (2.8b)$$

$P^{-1} = [1/Q_{ij}]$ is obtained by premultiplying (2.8b) by $B^{-1}(sI-A)$. This was programmed on the digital computer.

2.2 Flight Conditions

Ten flight conditions were considered in pairs of two. Conditions (1,6) are quite similar to each other, so are (2,7), ... (5,10) in having the same mach, velocity etc, differing only in the $C_{i\delta c}$ values, due to the odd cases having v.c. = 15, the even cases v.c. = 25. The parameter values for these conditions are listed in Table 2.2. The Q_{uv}^{-1} transfer functions for the 10 cases are listed in Table 2.3 in the form $Q_{uv}^{-1} = k\pi(s+p_1)$. The value of k is listed first, followed by the p_1 . At the end in brackets is the zero frequency value of Q_{uv}^{-1} . For

example in Case 1, $Q_{11}^{-1} = .0723(s+.907+j\ 8.2)(s+.907-j\ 8.2)$,
whose value at $s = 0$, is 4.92 . $Q_{31}^{-1} = -.0909(s+6.13)(s-6.10)$ whose
value at $s = 0$ is 3.40 , etc.

The ten flight conditions give at each frequency ten different values
of $Q_{uv}(j\omega)$. The sets $\{Q_{uu}(j\omega)\}$, denoted as "templates" $Tp_{uu}(\omega)$,
are needed in the synthesis technique. A number of these are shown in
Figs. 2.1-3, in Nichols chart coordinates. A missing flight condition
number in these figures, means that its $Q_{ii}(j\omega)$ value is very close to
that for another flight condition. The star refers to Case 10.

Table 2.2

Fighter CCV, Trimmed Aero Data, 01/18/79

Area, $S = 280,000 \text{ ft}^2$; Mac, $c = 10.9 \text{ ft}$; Span, $b = 29.0 \text{ ft}$.

$I_{xp} = 12.606$, $I_{xy} = 12.824$, Load factor = 1.0,

CG location 35.300 % Mac, at W.L. 93,200. $I_{xx} = 8100$, $I_{yy} = 47000$,

$I_{zz} = 53300$, $I_{xz} = 354 \text{ slug ft}^2$.

Flight Conditions	1 6	2 7	3 8	4 9	5 10
Mach	.6	.8	.9	.6	.9
Altitude (ft)	0	20000	0	30000	30000
Impact P, Q_c	582.98	510.38	1462.84	173.48	435.30
Dynamic P, q (lb/ft ²)	533.22	435.97	1199.75	158.67	357.01
P_s/P_o	1.00	.460	1.00	.298	.298
Q_c/P_s	.276	.524	.691	.276	.691
Vel (ft/sec)	669.84	828.32	1004.76	596.94	895.41

TRIMMED LATERAL DIRECTION DATA

α (degrees)	1.890	2.145	.901	6.129	2.470
$10^3 C_{n\beta}$ (1/deg)	2.291	2.759	2.169	3.463	2.947
$10^3 C_{l\beta}$ (1/deg)	-1.836	-1.999	-1.721	-2.705	-2.005
$10^2 C_{y\beta}$ (1/deg)	-2.030	-2.201	-2.100	-2.203	-2.220
$10^2 C_{np}$ (1/rad)	-1.949	-2.658	.9888	-2.709	-2.780
$10(C_{ip})$ (1/rad)	-2.908	-3.148	-3.180	-2.790	-3.203
$10C_{yp}$ (1/rad)	1.054	1.329	.5486	1.495	1.227
$10(C_{nr})$ (1/deg)	-3.834	-3.665	-3.562	-3.863	-3.837

Con't Table 2.2

$10C_{\ell r}(1/\text{deg})$	1.752	2.109	1.608	2.324	2.136
$10C_{yr}(1/\text{deg})$	6.910	6.896	6.434	7.218	7.351
$10^3 C_{n\delta r}(1/\text{deg})$	-1.217	-1.166	- .6989	-1.485	-1.136
$10^4 C_{\ell\delta r}(1/\text{deg})$	3.720	3.090	2.057	3.229	3.306
$10^3 C_{y\delta r}(1/\text{deg})$	2.347	2.147	1.240	2.873	2.080
$10^3 C_{n\alpha}(1/\text{deg})$	-1.008	-1.082	-1.067	-.9541	-1.107
$10^3 C_{\ell\delta a}$	-1.012	-1.060	- .9443	-1.089	-1.082
$10^3 C_{y\delta a}$	2.343	2.567	2.508	2.352	2.671
$10^3 C_{n\delta c}$	1.310	1.314	1.306	1.190	1.310
	1.010	1.008	1.027	.8761	.9977
$10^4 C_{\ell\delta c}$	2.091	2.253	3.058	1.290	2.816
	2.104	2.199	3.075	1.293	2.727
$10^3 C_{y\delta c}$	2.066	2.027	2.207	1.396	1.965
	1.800	1.770	1.912	1.248	1.720

Table 2.1

Transfer functions of q_{uv}^{-1} for 10 flight conditions

Case 1		(See Sec. 2.2)	
.0723;	.9071, 18.2(4.92)	.0195;	3.06, -.105(-6.26E-03)
.00778; -1.141, 19.5(.712)		-.024;	3.50, -.01(8.48E-04)
-.0909;	6.13, -6.10(3.40)	.00506;	1.20, .0193(.12E-03)
Case 6			
.0793;	.8281, 17.7(4.76)	.0192;	3.10, -.106(-6.31E-03)
.00602;	-1.471, 11.2(.768)	-.0239;	3.51, -.010(8.56E-04)
-.111;	6.13, -6.10(4.15)	.0062;	1.20, 1.93(.206E-03)
Case 2			
.0973;	.6321, 17.8(5.96)	.0265;	2.15, -.0835(-4.76E-03)
.00509; -2.361, 11(.644)		-.0283;	2.52, -.0131(9.34E-04)
-.109;	5.81, -5.85(3.7)	.00773;	-.0207(1.6E-04)
		-.117E-03;	-114(.0133)
		-.615E-05;	-1280(7.87E-03)
		.132E-03;	140(.018)

Cont Table 2.3

Case 7		
.107; .576; 17.3(5.74)	.0259; 2.18,-.0843(-4.76E-03)	-.129E-03; -91.8(.0118)
.00327; -3.67; 14.2(.703)	-.0282; 2.52,-.0131(9.31E-04)	-.395E-05; -2080(8.22E-03)
-.134; 5.81,-5.85(4.55)	.00946; 1.00,-.0207(-1.96E-04)	.162E-03; 140(.023)
Case 3		
.0637; 1.16; 11.3(8.22)	.0181; 5.38,-.0485(-4.72E-03)	-.634E-04; -103(.00653)
.00168; -3.0; 15.8(1.13)	-.0108; 5.65,-.00531(3.24E-04)	-.167-05; -2130(3.0E-03)
-.0377; 9.80,-9.85(3.64)	.00205; 3.60,-.00869(-.641E-04)	.375E-04; 173(.0065)
Case 8		
.0694; 1.06; 10.4(7.58)	.0178; 5.41,-.049(-4.72E-03)	-.691E-04; -80.4(.00556)
.000328; -15.3; 160.2(1.26)	-.0107; 5.66,-.0053(3.21E-04)	-.326E-06; -11600(3.78E-03)
-.0454; 9.8,-9.85(4.38)	.00247; 3.60,-.00869(.64E-04)	.452E-04; 173(.0078)

(cont'd) Table 2.3

Case 4		
.178; .404; 1.7(5.81)	.0422; .877, -.209(-7.73E-03)	-.298E-03; -126(.0375)
.00783; -9.51, 3.45(-.257)	-.0822; 1.10, -.0283(2.56E-03)	-.131E-04; -1420(.0186)
-.379; 3.32, -1.33(4.19)	.0517; .427, -.00874(-1.93E-04)	.635E-03; 97.5(.0619)
Case 9 (nominal)		
.203; .353 15.2(5.51)	.0387; .910, -.220(-7.75E-03)	-.341E-03; -97.6(.0333)
.00384; -15.8, 1.49(-.212)	-.0816; 1.10, -.0283(2.54E-03)	-.644E-05; -2990(.0193)
-.475; 3.32, -1.33(5.25)	.0648; .427, -.00874(-.242E-03)	.796E-03; 97.5(.078)
Case 5		
.172; .479±j7.0(8.47)	.044; 1.68, -.0797(-5.89E-03)	-.19.E-03; -113(.0217)
.0352; .183±j8.4(2.48)	-.0243; 2.05, .0093(-.46E-03)	-.393E-04; -376(.0148)
-.0661; 9.79, -10.9(7.05)	.0283; 1.39, -.0648(-2.55E-03)	.738E-04; 425(.0314)
Case 10		
.180; .432±j6.4(7.41)	.0405; 1.71, -.0808(-5.6E-03)	-.201E-03; -87.9(.0177)
.0355; .176±j8.3(2.44)	-.0244; 2.05, .00902(-.451E-03)	-.397E-04; -369(.0146)
-.077; 9.79, -10.9(8.22)	.0330; 1.39, -.0648(-2.97E-03)	.860E-04; 425(.0366)

2.3 Design procedure

It was found that condition (1.14) was not satisfied for all $P \in P$, no matter what plant terminal numbering was tried. The modification described in Sec. 1.3, was therefore used: The technique is used in its original form to derive L_1 and L_2 . Then the exact equation is used to derive L_3 . First, the bounds on $|T_{33}(j\omega)|$ are needed. Examination of the simulation data supplied by the contractor (A_y mode response - Fig. 2.4), suggests modelling $T_{33}(s)$ as a second-order function with a pair of poles at approximately -5 . This gives a first cut at $|T_{33}(j\omega)|$. Then, curves of larger and smaller values are tried in order to widen the acceptable set. In this way the bounds shown in Fig. 2.5 were obtained. It is required (recall 1.3)), that

$$a_{33}(\omega) \leq |T_{33}(j\omega)| \leq b_{33}(\omega) \quad . \quad (2.9)$$

This approach may be criticized as rather crude for translating time-domain into ω -domain tolerances, but we found it highly reliable in many design examples for example [8,9], and it is easy to execute. Reasons for working in the frequency domain rather than in state-space, have been given in [10,11].

In this mode $r_2 = r_3 = 0$, so the only command input is r_3 of Fig. 1.1, and in Table 1.1 only D_{13} , D_{23} , (A_{33}, B_{33}) are applicable. Consider D_{13} written as

$$|1 + L_1| \geq \frac{b_{23} \left| \frac{Q_{11}}{Q_{12}} \right| + b_{33} \left| \frac{Q_{11}}{Q_{13}} \right|}{b_{13}} \quad . \quad (2.10)$$

Recall that $b_{13}(\omega)$ is the maximum allowable value of $|T_{13}(j\omega)|$, $b_{23}(\omega)$ that of $|T_{23}(j\omega)|$. If a command of lg for A_y is to result in a

maximum of one degree steady-state value of β , then

$b_{13}(0) = 1/(57.3)(32.2) = (.5)10^{-3}$. We can prescribe this value for all ω . Comparing this value to b_{33} in Fig. 2.5, clearly $b_{33} \gg b_{23}$, at least from $\omega = 0$ to $\omega \sim 20$. But if it will help in the design, b_{33} can be decreased right down to a_{33} . This will make it harder on the design of L_3 , because the tolerances on $|T_{33}(j\omega)|$ are then narrower, but it is later found that the demands on L_1 , L_2 are much harder than those on L_3 .

Returning to (2.10) since $b_{33} \gg b_{23}$ in the low frequency range, $b_{33} \left| \frac{Q_{11}}{Q_{13}} \right|$ will dominate in the numerator unless $|Q_{11}/Q_{12}| \gg |Q_{11}/Q_{13}|$. We therefore sketch in Fig. 2.6a,b these two ratios from the data available in Table 2.3. Cases 1-5 suffice, because Cases 6-10 are pairwise very similar to Cases 1-5. Clearly, $b_{33}|Q_{11}/Q_{13}|$ dominates at least up to $\omega = 10$, so in this ω range, we need

$$|1 + L_1| = |1 + G_1 Q_{11}| \geq \frac{b_{33}}{b_{13}} \left| \frac{Q_{11}}{Q_{13}} \right| \quad (2.11)$$

which is $\sim 66\text{db} + (-50\text{db}) = 16\text{db}$ for $\omega \in [0,6]$. It helps to approximate $|1 + G_1 Q_{11}|$ by $|G_1 Q_{11}|$, because (2.11) then becomes

$$|G_1(j\omega)| \geq b_{33}/b_{13} |Q_{13}| \quad (2.12)$$

and the bounds on G_1 are easily determined in this range. The value $(1500)^{-1}$ was chosen for b_{13} , corresponding to 1.5° max β for A_y of $1g$. The maximum value of $|Q_{13}|^{-1} = .0375$ for Case 4, giving 55 for $|G_1|_{\min}$. Case 9 was chosen as the nominal plant case Q_{10} , with the nominal loop transmission $L_{10} = G_1 Q_{110}$. It is convenient to have the bounds on L_{10} rather than on G_1 , because in the higher ω

range one can no longer take $|1 + L_1| \doteq L_1$. In any case, the procedure for finding the bounds on L_{10} in the low ω range is fairly clear from the above.

As ω increases, b_{33} decreases (see Fig. 2.5) and so does $|Q_{11}/Q_{13}|$ (see Fig. 2.6b). The first term $\frac{b_{23}}{b_{13}} \left| \frac{Q_{11}}{Q_{12}} \right|$ in (2.10) is never large, so the demand on $|1 + L_1|$ in (2.10) steadily decreases. Eventually $|1 + L_1|$ may be quite small which would permit $L_1 \rightarrow -1$. But it is sensible to impose reasonable stability margins on the L_1 loop by itself. Physically, this would correspond to the case $y_2 = \phi = 0$, $y_3 = A_y = 0$ and the only feedback is from β because then in $\underline{\delta} = P^{-1} \underline{y}$ (see Eq. (2.5)), $\delta_1 = y_1/Q_{11}$. So in the higher ω range bounds were found on L_{10} such that $|1 + L_1|^{-1} \leq 2\text{db}$. The resulting bounds on L_{10} are shown in the Nichols chart in Fig. 2.7. The next step is to find a $L_{10}(s)$, such that $L_{10}(j\omega)$ satisfies the bounds of Fig. 2.7. This was done simply by cut and try. The Bode plots of $L_{10}(j\omega)$ are shown in Fig. 2.8, and $L_{10}(j\omega)$ is also shown in Fig. 2.7.

The resulting $|G_1(j\omega)| = |L_{10}/Q_{110}|$ is sketched in Fig. 2.13, and it is seen it must be greater than one, over an extremely large ω range. The reason for this is evident from Fig. 2.7. The intrinsic demands on $|L_{10}|$ due to the specifications, become negligible at $\omega = 25$. However, $|L_{10}(j\omega)|$ cannot decrease very rapidly vs ω , because its phase lag is not allowed to be more than $\sim 130^\circ$. And this constraint holds until $|L_{10}(j\omega)|$ has decreased to about -24 db . This is due to the large spread in the high frequency values of Q_{11} (see Fig. 2.1). The present design is clearly overly conservative. At $\omega = 8$, $|L_{10}|$ is about 3 db larger than necessary. From 15 to -24 db levels there is a change of 39 db, at an average slope of $-\frac{130}{180} \times 12 = -8.7\text{ db/octave}$, requiring $39/8.7 = 4.5$ octaves, giving $(8) 2^{4.5} \approx 180$ for the frequency at which $|L_{10}| \sim -24\text{ db}$.

The decrease of $|L_{10}|$ can be more rapid thereafter, but again we have been rather conservative.

There is a trade-off between the complexity of the compensation function (the number of its poles and zeros), and the bandwidth of G_1 . It is clearly possible to decrease G_1 more rapidly in the mid-frequency range. Also more far-off poles can be inserted in the higher ω range. All this requires more careful shaping of $L_{10}(j\omega)$, with more poles and zeros. This will be done in later designs.

It is also noted that a significant reason for the large bandwidth of G_1 , is the large gain margin (about 25 db) needed for L_{10} , because of the large spread in the high-frequency value of Q_{11} (see Fig. 2.1). This spread can be reduced by high-frequency scheduling, which is done in Sec. 2.8. The analytic expressions for the $L_{0i}(s)$, $G_i(s)$ etc are given in Appendix 1 of this chapter.

We next turn to the design of $L_{20}(s)$. From Table 1.1, the only requirement here (since only A_y is being commanded) is D_{23} of Table 1.1,

$$|1 + L_2| \geq \frac{b_{13} \left| \frac{Q_{22}}{Q_{21}} \right| + b_{33} \left| \frac{Q_{22}}{Q_{23}} \right|}{b_{23}} \quad (2.13)$$

The bounds on $L_{20}(j\omega)$ are obtained in the same manner as those on L_{10} , with the result shown in Fig. 2.9. This figure has precisely the same features as Fig. 2.7 and for precisely the same reasons - especially the even larger gain margin needed, due to the larger spread in the high-frequency gain factor of Q_{22} (see Fig. 2.2). The $L_{20}(j\omega)$ chosen is shown in Fig. 2.10, and is also rather conservative. It should be noted that as Q_{220} has a right half-plane pole at .0283 (see Table 1.2, Case 9), it is imperative that L_{20} has this same pole; otherwise there

is attempted right half-plane pole cancellation, which would give a dipole in the right half-plane, and the system would then be unstable.

2.4 Design of third (A_y) Loop

It is recalled that condition (1.14) could not be satisfied in this problem, so the design of the third loop is performed by using the exact equation. In Fig. 1.1,

$$T = (I + L)^{-1} L F, \quad L = P G. \quad (2.14)$$

We are interested in the actual expression for

$$T_{33} = \frac{L_3 F_3 [(1+L_1)(1+L_2) - \gamma_{12}]}{(1+L_1)(1+L_2)(1+L_3) - [\gamma_{12}(1+L_3) + \gamma_{13}(1+L_2) + \gamma_{23}(1+L_1)] + \Gamma} \quad (2.15)$$

$$\left. \begin{aligned} \gamma_{12} &= \frac{Q_{11} Q_{22}}{Q_{12} Q_{21}}, \quad \gamma_{13} = \frac{Q_{11} Q_{33}}{Q_{13} Q_{31}}, \quad \gamma_{23} = \frac{Q_{22} Q_{33}}{Q_{23} Q_{32}} \\ \Gamma &= Q_{11} Q_{22} Q_{33} \left(\frac{1}{Q_{12} Q_{23} Q_{31}} + \frac{1}{Q_{21} Q_{32} Q_{13}} \right) \end{aligned} \right\} \quad (2.16a-d)$$

The above was obtained by expanding the matrices in (2.14). For purpose of design of L_3 , it is desirable to rewrite (2.15) in the following form:

$$T_{33} = \frac{F_{33} L_{30} / \psi}{\frac{L_{30}}{\psi} + 1}, \quad L_{30} = G_3 Q_{330} \quad (2.17a,b)$$

$$\psi(j\omega) = \frac{Q_{330}}{Q_{33}} \left\{ 1 - \frac{[\gamma_{13}(1+L_2) + \gamma_{23}(1+L_1) - \Gamma]}{(1+L_1)(1+L_2) - \gamma_{12}} \right\} \quad (2.18)$$

Of course, ψ is a function of ω and of the plant parameters. There is a different ψ value for each of the ten flight conditions.

The procedure is to find the templates $T_{p_j}(\omega)$, of $\psi(j\omega)$ i.e. $T_{p_j}(\omega) = \{\psi(j\omega)\}$. Some templates are shown in Fig. 2.11. It is required

that

$$a_{33}(\omega) \leq |T_{33}(j\omega)| \leq b_{33}(\omega) \quad (2.19)$$

of Fig. 2.5. The function of L_{30} is to guarantee that over the range

$$\Delta \log \left| \frac{L_{30}/\psi}{1 + \frac{L_{30}}{\psi}} \right| \leq \log \frac{b_{33}}{a_{33}} \quad (2.20)$$

The Nichols chart is the perfect design tool for this purpose because it contains loci of constant $|L/(1+L)|$. Here L_{30}/ψ takes the place of L . As there is no uncertainty in L_{30} , the template (set $\{L_{30}/\psi\}$) of L_{30}/ψ is simply the template of $1/\psi$ shifted by the value of $L_{30}(j\omega)$. One positions the template of $1/\psi$ on the Nichols chart until (2.20) is barely satisfied, giving a bound on L_{30} . The design procedure is in fact precisely the same as in single-loop design, described in detail in [3].

The bounds on L_{30} thus obtained are shown in Fig. 2.11, together with the $L_{30}(j\omega)$ chosen. A Bode plot of L_{30} is shown in Fig. 2.12. There is here too the same phenomenon as in the design of L_{10} , L_{20} (Figs. 2.7, 2.9). In the higher ω range, an additional constraint of the form $|1 + L_3|^{-1} < \text{some specified value}$ becomes more demanding on L_3 than (2.19). Also, the large spread in the value of the high-frequency gain factor of Q_{33} (see Fig. 2.3), forces $|L_{30}(j\omega)|$ to be decreased slowly until $|L_{30}| \sim -30$ db. However, since $|Q_{330}(j\omega)|$ is considerably larger than $|Q_{110}|$ and $|Q_{22}|$, the demand on $G_3 = |L_{30}/Q_{330}|$ is considerably less than on G_1 , G_2 , as seen in the Bode plots of the (asymptotic) G_1 , G_2 , $G_3(j\omega)$ in Figs. 2.13, and 2.14.

Proper choice of L_{30} only guarantees that the change in $|T_{33}(j\omega)|$ is within the amount allowed by (2.20). The role of $F_3(j\omega)$ in Fig. 1.1, is to position $|T_{33}(j\omega)|$ within the tolerances of (2.19). For example if $a_{33}(10) = -23.5$ db, $b_{33}(10) = -8.5$, and if $(L_{30}/\omega)/(1+(L_{30}/\omega))$ in practice ranges from -10 db to +2 db at $\omega = 10$, then it is necessary that, $-13.5 \leq |F_3(j10)| \leq -10.5$ db. Bounds in $|F_3(j\omega)|$ are obtained in this manner and then, by cut and try, $F_3(s)$ was selected which satisfied these bounds (see Appendix 1 for $F_3(s)$).

Note that $T_{33}(j\omega) \doteq F_3(j\omega)$ over the significant frequency range, because the bandwidth of $L_3(j\omega)$ is so much larger than that of $T_{33}(j\omega)$. This happens in systems in which large parameter uncertainty demands large loop bandwidths.

2.5 Simulation results, Design 1

The system was simulated on the digital computer for lg step command of A_y . The responses are shown in Figs. 2.15a-c in degrees for β , ϕ and g 's for A_y . The A_y responses for the five cases were very similar, so result in almost a single curve in Fig. 2.15c. The other five cases (6, 7, ..., 10) are pairwise very similar to these first five and are not shown. The control surface deflections δ_r , δ_a , δ_c in degrees are shown in Fig. 2.16a-c. The control surface rates are shown in Figs. 2.17a-c. The actual control surface limits are respectively $\pm 30^\circ$, $\pm 20^\circ$, $\pm 25^\circ$ for δ_r , δ_a , δ_c , so Case 3 is well below saturation, while Case 1 barely causes canard saturation (25.7°). The other canard values are 33° , 120° , 54° for Cases 2, 4, 5 respectively, so that to avoid this amplitude limiting, A_y commanded must be reduced to .76, .21, .46 g's respectively. In all cases

the canard is the limiting surface.

The rate limits are 120, 56, 100 deg/sec for $\dot{\delta}_r$, $\dot{\delta}_a$, $\dot{\delta}_c$ whereas Fig. 2.17 shows that in Case 4, the canard rate is a somewhat greater limiting factor than the canard amplitude, limiting A_y to .17 g for this Case 4. This can be improved by slowing up T_{33} . If the step response of A_y is slowed up by λ (the time scale in Figs. 2.15 multiplied by λ , then the $\dot{\delta}$'s will be reduced by this factor very closely, because as noted in Sec. 2.4, $T_{33}(j\omega) \doteq F_3(j\omega)$ over the significant range of $T_{33}(j\omega)$. This slowing up by a factor λ is achieved by multiplying each of the F_{33} poles by λ . The reason is that F_{33} with its much smaller bandwidth than the L_1 , dominates the system response to commands (see Sec. 2.10).

2.6. Responses under amplitude and rate limiting

The control surfaces amplitude and rate limits were incorporated into the system model, in both cases as simple algebraic nonlinearities. If the rate saturates first, the amplitude can continue to increase until it becomes saturated, and vice versa. The commanded A_y input was in each case made so high as to force the system to saturate. The resulting δ_1 responses are shown in Figs. 2.18a-c, and the δ_i responses in Figs. 2.19a-c. In all cases the canard rate was the first to saturate and the canard amplitude eventually also saturated. Figs. 2.20a-c show the β , ϕ , A_y responses under these very hard saturated conditions. In all cases, the responses are very nice, with little overshoot. Note that in all cases except 3, 3.1 g's were commanded and 9.3 g for Case 3, so as to deliberately drive the system into very hard saturation.

2.7 Design two

Several more designs were made, primarily in order to decrease the bandwidths of G_1 , G_2 . In design 2 some sacrifice was made in the final values of β and ϕ when A_v is commanded. This is evident from the smaller values of $G_1(0)$, $G_2(0)$ in this design as compared to Design 1. Also, an additional two far-off poles were assigned to $G_1(s)$, $G_2(s)$ in order that they may reach zero db magnitude at a considerably smaller frequency than in the first design - compare Designs 1, 2 in Figs. 2.13-4. Otherwise, the design procedure is identical to that of Design 1, and is therefore not described. Because of the faster reduction of $|L_{10}|$, $|L_{20}|$ a greater burden was imposed on L_3 , so G_3 in Fig. 2.13 has a larger bandwidth for Design 2, than in Design 1. But this is acceptable, because the demand on G_3 is so much less than on G_1 , G_2 . The Bode plots of L_{10} , L_{20} , L_{30} are shown in Fig. 2.21a-c. The computer simulation results are shown in Fig. 2.22. It is seen that the β , ϕ responses are as expected somewhat poorer than those in Figs. 2.15-2.17 for Design 1.

2.8 A design with scheduling

One of the reasons for the large G_1 , G_2 bandwidths of Design 1, noted in Sec. 2.3, was the large gain margins needed (Figs. 2.7, 2.9) for L_{10} , L_{20} . This was due to the large uncertainty in the high-frequency gain factors of Q_{11} , Q_{22} (Figs. 2.1, 2.2). A significant decrease in the G_1 , G_2 bandwidths should be possible, if there can be a significant decrease in this high-frequency uncertainty. We therefore examine Eqs. 2.1-8 for $\lim_{s \rightarrow \infty} Q_{uv}$. The results are (letting $q_{uv} = Q_{uv}^{-1}$):

$$q_{11} = Q_{11}^{-1} \rightarrow \frac{-s^2 (C_{y\delta a} C_{\ell\delta c} - C_{\ell\delta a} C_{y\delta c})}{q S_b I_z \Delta} \quad (2.22a-c)$$

$$q_{12} \rightarrow \frac{s^2}{q S_b I_z} \left(\frac{C_{n\delta a} C_{y\delta c} - C_{y\delta a} C_{n\delta c}}{I_x} \right) - q_{11}$$

$$q_{13} \rightarrow -\frac{q_{11}}{V_s}$$

$$q_{21} \rightarrow -\frac{s^2}{q S_b \Delta I_z} (C_{\ell\delta r} C_{y\delta c} - C_{y\delta r} C_{\ell\delta c})$$

$$q_{22} \rightarrow \frac{s^2}{q S_b \Delta} \frac{(C_{n\delta c} C_{y\delta r} - C_{n\delta r} C_{y\delta c})}{I_x} - \alpha q_{21}$$

$$q_{23} \rightarrow -\frac{q_{21}}{sV}$$

$$q_{31} \rightarrow \frac{-s^2}{q S_b \Delta I_z} (C_{y\delta r} C_{\ell\delta a} - C_{\ell\delta r} C_{y\delta a})$$

$$q_{32} \rightarrow \frac{s^2}{q S_b \Delta} \frac{C_{n\delta r} C_{y\delta a} - C_{y\delta r} C_{n\delta a}}{I_x} - \alpha q_{31}$$

$$q_{33} \rightarrow -\frac{q_{31}}{sV}$$

$$\Delta = C_{\ell\delta r} (C_{n\delta a} C_{y\delta c} - C_{y\delta a} C_{n\delta c}) - C_{n\delta r} (C_{\ell\delta a} C_{y\delta c} - C_{y\delta a} C_{\ell\delta c}) + C_{y\delta r} (C_{\ell\delta a} (C_{n\delta c} - C_{n\delta a} C_{\ell\delta c})$$

(2.24a-d)

Thus all the Q_{uv} are inversely proportional to q as $s \rightarrow \infty$. Hence, the part of the uncertainty due to the q variations could be eliminated, if q can be accurately measured rapidly enough. We assume that q can be measured with $\pm 20\%$ error, i.e. the measured value may in fact be between .8 and 1.2 times the correct value. The zero ω values

of the Q_{uv} are independent of q , so the measured q are to be used only in the higher ω range. Accordingly, we insert in front of the plant a diagonal scheduled compensator, each of whose elements is

$$J(s) = \frac{1}{1 + s q_m \tau_s}, \quad \tau_s = \frac{1}{1200} \quad (2.25)$$

where q_m is the measured value of q . One should really experiment with the value of τ_s . But our primary purpose here is to demonstrate how well-known techniques, such as scheduling, can be incorporated into our design procedure.

This incorporation of scheduling into our design technique is very simple. Let the new plant be $P_n = PJ(s)$, so the new

$$P_n^{-1} = [1/Q_{uvn}] = \frac{P^{-1}}{J(s)} = \frac{[1/Q_{uv}]}{J(s)} \quad (2.26)$$

with $J(s)$ a function of q and therefore of each flight condition. The procedure is now exactly the same as before, but Q_{uvn} (functions of the flight condition) replace Q_{uv} . But now there are thirty cases because for each flight condition q_m in (2.25) may be $.8 q$, q or $1.2 q$.

Some of the templates of Q_{uun} are shown in Figs. 2.23-2.25, for Q_{11n} , Q_{22n} . Comparing with the templates of Q_{uu} (old) in Figs. 2.1-3, it is seen that there is little difference at low ω values, but with significant changes of the templates at higher ω values. The new template Q_{11n} at large ω (100) is actually larger in size than the unscheduled Q_{11} (100). However, the nominal (Case 9) Q_{11n} is near the top of its template, rather than the bottom as it was for the unscheduled case. So the resulting bound on L_{10} at high ω is not so far down, we don't need as large a gain margin and $|G_1(j100)|$ for

the scheduled design is much smaller than for Design 1 or 2. In finding these templates of Q_{uun} , three different values were assigned to q_m of (2.25) for each flight condition. These were $q_m = .8q$, q and $1.2q$.

The bounds on the Nichols chart analogous to those in the first design (Figs. 2.7, 2.9, 2.11) are shown in Figs. 2.26a-c, which also include $L_{u0}(j\omega)$. Bode plots of the L_{u0} are shown in figs. 2.27a-c. Digital simulation results are shown in Figs. 2.28a-c. For each flight condition three runs are shown, one for the case $q_m = .8q$, the second if q_m happened to be q , and the third for $q_m = 1.2q$.

Figs. 2.13, 2.14 show that a scheduled design can be more economical in G_u bandwidths required. We have probably overestimated the measurement error i.e. the allowance $\epsilon [0.8q, 1.2q]$ is probably much more than the actual error. Also experimentation in the value of τ_s used in (2.25) will lead to better results, as would a more sophisticated $J(s)$ function of (2.25). In any case, our main point was to demonstrate how easily scheduling may be incorporated into this new design technique. Also how the design technique reveals the frequency ranges in which scheduling is worth implementing.

2.9 Nondiagonal G

The three designs presented so far, all have the shortcoming discussed in Sec. 1.4. They are the products of a design technique which requires loop transmissions, even when there is no uncertainty. The remedy was given in Sec. 1.4. One precedes the plant with a nondiagonal matrix, say $H = [h_{ij}]$ which diagonalizes the new effective plant PH as much as possible. The design technique is then applied to the new plant PH .

In our problem only A_y is commanded so there is need only for h_{13} , h_{23} . The others of diagonal elements can be made zero. In general, the elements of H may be functions of frequency. But as our primary purpose is to demonstrate the new technique, we shall concentrate on $\omega = 0$, and indicate the procedure which can be followed for ω in general.

Recall from Sec. 1.3, (Eqs. 2.10, 2.13) that the bounds on L_{10} , L_{20} are determined by the requirements that

$$\left. \begin{aligned} |1 + L_1| &\geq \frac{b_{23} \left| \frac{Q_{11}}{Q_{12}} \right| + b_{33} \left| \frac{Q_{11}}{Q_{13}} \right|}{b_{13}} \\ |1 + L_2| &\geq \frac{b_{13} \left| \frac{Q_{22}}{Q_{21}} \right| + b_{33} \left| \frac{Q_{22}}{Q_{23}} \right|}{b_{23}} \end{aligned} \right\} \quad (2.27a,b)$$

Recall also that it was shown in Sec. 1.3 that the second terms in the above involving Q_{13} , Q_{23} easily dominated the right sides of (2.27a,b) up to about 10 ~ 15 rps. Hence, it is desirable to make the new Q_{13} , Q_{23} very large. Let the new P be $P_n = PH$, so the new $[1/Q_{uvn}] = H^{-1}P^{-1} = H^{-1}[1/Q_{uv}]$. Let $h_{11} = h_{22} = h_{23} = 1$, $h_{13} = \alpha$, $h_{23} = \beta$, the others zero and then

$$\left. \begin{aligned} Q_{13n} &= (P_{13} - \alpha P_{33})^{-1}, \quad Q_{23n} = [P_{23} - \beta P_{33}]^{-1} \\ P_{uv} &= 1/Q_{uv} \end{aligned} \right\} \quad (2.28a-c)$$

If the b_{13} , b_{33} values were the same for all flight conditions, then a reasonable objective, at any ω , is to choose α , β to minimize $\max |P_{13} - \alpha P_{33}|$ over various flight conditions. However, in

practice the maximum A_y commanded is generally different. Hence, if say a constant maximum β angle is tolerable independently of A_y commanded, then b_{13} should be inversely proportional to A_y commanded. This was assumed here, so an estimate was needed of the maximum A_y commanded for each flight condition. The estimate was made approximately on the basis of the A_y needed to achieve amplitude saturation in earlier designs with lg the maximum value:

$$\begin{aligned} \text{Cases 1,6} &- 1g ; \text{Cases 2,7} &- .6g ; \text{3,8} &- 1g ; \\ 4,9 &- .25g ; \text{5,10} &- .5g . \end{aligned} \quad (2.29)$$

Accordingly, we seek to $\min[\max |W_1(P_{13} - \alpha P_{33})|]$, where $W_1 = b_{33}/b_{13}$, whose values are now: 2000, 1200, 2000, 500, 1000 respectively for the cases (1,6), (2,7), ..., (5,10). The result is $\alpha = .571$, giving 5.64 for the min. max. value, which is 15 db needed for G_1 at $\omega = 0$, instead of 55 (= 34.8 db) needed previously. Similarly, the optimum β is found to be .347, with only 12 db needed for G_2 at $\omega = 0$. In principle, this process can be continued as a function of frequency, but was not done here because there is not much change in the above parameters up to $\omega = 10$. So a matrix of constants is used here for H .

Hereafter, the design procedure is precisely the same. New templates Q_{uun} must be found, and the values of the new Q_{uun} calculated for use in (2.27a,b). The new Q_{uun} are:

$$\left. \begin{aligned} Q_{11n} &= (P_{11} - \alpha P_{31})^{-1}, \quad Q_{22n} = (P_{22} - P_{32})^{-1}, \\ Q_{33n} &= Q_{33}, \quad P_{uv} = 1/Q_{uv} \end{aligned} \right\} \quad (2.30a-c)$$

Some of these new Q_{11n} , Q_{22n} templates are shown in Figs. 2.29a,b. They are somewhat larger than those of the diagonal G design, in Figs. 2.1, 2.2. But the much greater reduction of off-diagonal elements in (2.28a,b) leads to the nondiagonal design being significantly more economical than the diagonal. However, this point should not be overlooked. The choice of H should consider the effect on the uncertainty ranges of the new Q_{uun} . A more sophisticated optimization technique is needed for this purpose. The new bounds on L_{10} , L_{20} are shown in Figs. 2.30a, b and Bode plots in Figs. 2.31 a, b. The new G_1 , G_2 values are shown in Figs. 2.13 , 2.14 where it is seen that they are significantly more economical than those in previous designs.

Simulation results are shown in Figs. 2.32a-c: β , ϕ , A_y in Fig. 2.32a ; δ_r , δ_a , δ_c in Fig. 2.32 b and $\dot{\delta}_r$, $\dot{\delta}_a$, $\dot{\delta}_c$ in Fig. 2.32c. In these simulation results, we deliberately commanded sufficient A_y so as to obtain the maximum available 25° canard value, except for Cases 3, 8. The commanded A_y values are given in brackets in the A_y responses in Fig. 2.32a. Exceedingly small β , ϕ values are achieved in this design, part of the reason being the smaller A_y being commanded for 6 of the 10 cases. There is no rate limiting in all of these cases. The A_y commanded are (in g's):

$$\begin{aligned} \text{Case 1, 1g ; 2, .8g ; 3, 1g; 4, .23g ; 5, .5g ; 6, .73g ;} \\ 7, .6g ; 8, 1g ; 9, .17g ; 10, .35g . \end{aligned} \quad (2.31)$$

From Fig. 2.13, 2.14, it is seen that this is the most economical design so far. It could, of course, be made even more economical by incorporating "scheduling" as well.

2.10 Trade-off between speed of response and rate limiting

It was noted in Sec. 2. that one could achieve smaller peak control surface rates, by slowing up the A_y response. This is illustrated here for Design 1 of Sec. 2.3-2.5, simply by changing the prefilter F_3 . In Design 1,

$$F_3 = F_{3a} = \frac{100}{(s+5)(s+20)} \quad (2.32a)$$

This was changed to

$$F_3 = F_{3b} = \frac{36}{(s+3)(s+12)} \quad (2.32b)$$

The G matrix is not changed, so β , ϕ should be only secondary affected and A_y slowed up. The simulation results for Cases 1-5 are shown in Fig. 2.33 and should be compared with those in Fig. 2.15. The control surface deflections δ_i , $\dot{\delta}_i$ are shown in Fig. 2.34, and should be compared to those in Figs. 2.16, 2.17. It is seen that it is primarily the $|\dot{\delta}_i|_{\max}$ which are significantly reduced. Hence, this method may be used to trade-off between the speed of A_y response and $|\dot{\delta}_i|_{\max}$.

APPENDIX 2.1

COMPENSATION FUNCTIONS FOR VARIOUS DESIGNS

Design 1 (Sects. 2.3-5)

$$L_{10} = \frac{(260)10^4(s+7)(s+60)}{(s^2 + .706s + 27.3)(s + 25)[s^2 + 400s + (400)^2]}$$

$$G_1 = \frac{(52)10^4(s+7)(s+60)}{(s + 25)[s^2 + 400s + (400)^2]}$$

$$L_{20} = \frac{(5)10^5(s+10)(s+180)}{(s - .0283)(s + 1.1)(s + 60)[s^2 + 280s + (350)^2]}$$

$$G_2 = \frac{-(4.08)10^4(s + 180)(s+10)}{(s + 60)[s^2 + 280s + (350)^2]}$$

$$L_{30} = \frac{28,100(s^2+12s+100)(s+200)}{(s^2 + 4s + 6.25)(s + 25)(s + 60)(s + 600)}$$

$$G_3 = \frac{(22.5)(s+100)(s^2+12s+100)(s+200)}{(s^2 + 4s + 6.25)(s + 25)(s + 60)(s + 600)}$$

$$F_3 = \frac{100}{(s + 5)(s + 20)}$$

Design 2

$$G_2 = \frac{-5.4(1 + .1s) \left(1 + \frac{s}{80}\right)}{\left(1 + \frac{s}{40}\right) \left[1 + \left(\frac{s}{350}\right) + \left(\frac{s}{350}\right)^2\right]^2}$$

$$G_1 = \frac{34.9 (1+.1s) \left(1 + \frac{s}{85}\right)}{\left(1 + \frac{s}{40}\right) \left[1 + \frac{s}{350} + \left(\frac{s}{350}\right)^2\right]^2}$$

$$G_3 = \frac{8 (1+.01s) \left(1 + \frac{s}{150}\right)}{1 + \frac{s}{6} \left(1 + \frac{s}{30}\right) \left(1 + \frac{s}{600}\right)}$$

$$F_3 = \frac{100}{(s + 5)(s + 20)}$$

Scheduling design

$$L_{10} = \frac{(4.14) 10^5 (s^2 + 12s + 100)(s + 75)}{(s^2 + .706s + 27.3)(s^2 + 45s + 625)[s^2 + 136s + (170)^2]^2}$$

$$G_1 = \frac{0.84 \times 10^5 (s^2 + 12s + 100)(s + 75)(1 + s/s_0)}{(s^2 + 45s + 625)[s^2 + 136s + (170)^2]^2}$$

$$L_{20} = \frac{(1.029) 10^{10} (s + 5)(s + 30)(s + 60)}{(s - .0283)(s^2 + 48s + 1600)[s^2 + 170s + (170)^2]^2 (s + 1.1)}$$

$$G_2 = \frac{-(4.195) 10^9 (1 + .2s)(s + 30)(s + 60)(1 + s/s_0)}{(s^2 + 48s + 1600)[s^2 + 170s + (170)^2]^2}$$

$$L_{30} = \frac{(4.8)10^4 (s+25)}{(s+3)(s+10)(s+400)}$$

$$G_3 = \frac{38.4(s+25)(s+100)}{(s+3)(s+10)(s+400)}$$

$$F_3 = \frac{100}{(s+5)(s+20)^2}$$

$$L_i = G_i Q_{ii}(\text{old}) \frac{1}{(1 + s/7.56)}$$

Nondiagonal design

$$L_{10} = \frac{(93.6)10^6 (s+2.3)(s+14)}{(s+6)(s^2+0.296s+5.4)[s^2+83s+(83)^2]^2}$$

$$G_1 = \frac{(44.6)10^6 (s+2.3)(s+14)}{(s+6)[s^2+83s+(83)^2]^2}$$

$$L_{20} = \frac{(50)10^8 (s+4)(s+40)}{(s-.0264)(s+.957)(s+10)[s^2+200s+(200)^2]^2}$$

$$G_2 = \frac{-5.2 \times 10^8 (s+4)(s+40)}{(s+10)[s^2+200s + (200)^2]^2}$$

$$G_3 = \frac{1.2}{1 + 1.67s}$$

$$F_3 = \frac{100}{(s+5)(s+20)}$$

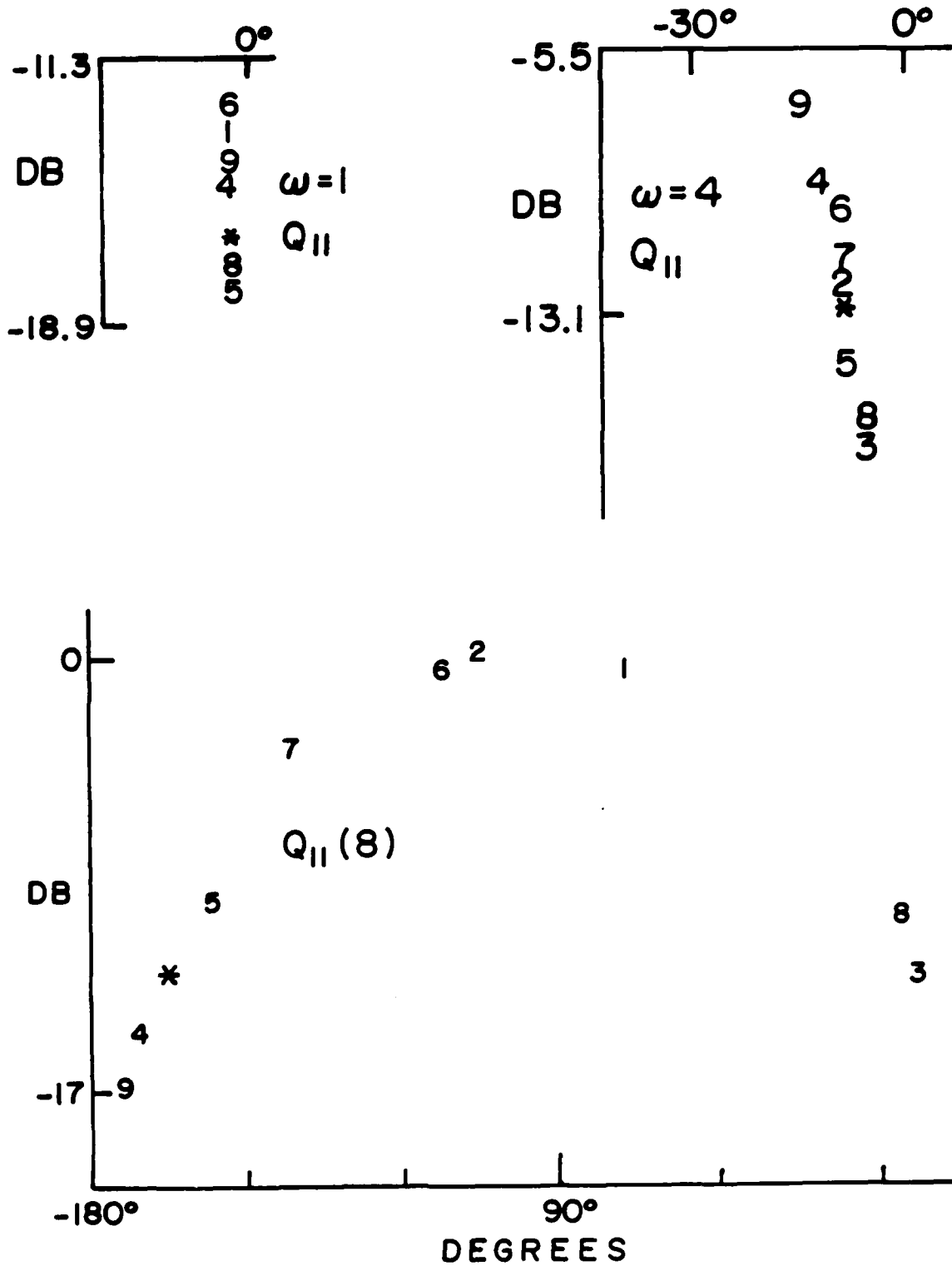
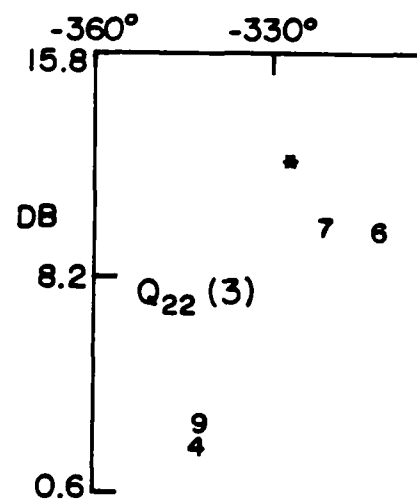
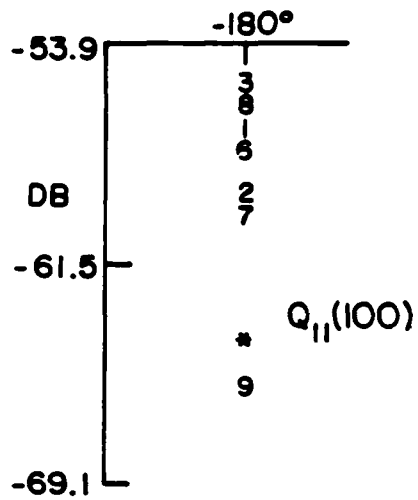
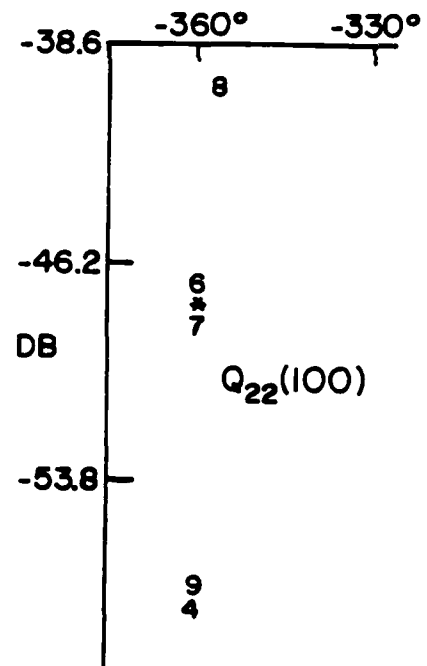
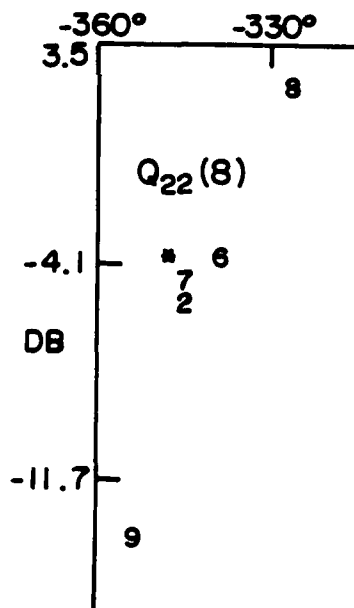


Fig. 2.1 Templates of Q_{11} at $\omega = 1, 4, 8, 100$



2.1 (continued)

Fig. 2.2 Templates of Q_{22} at $\omega = 3, 8, 100$

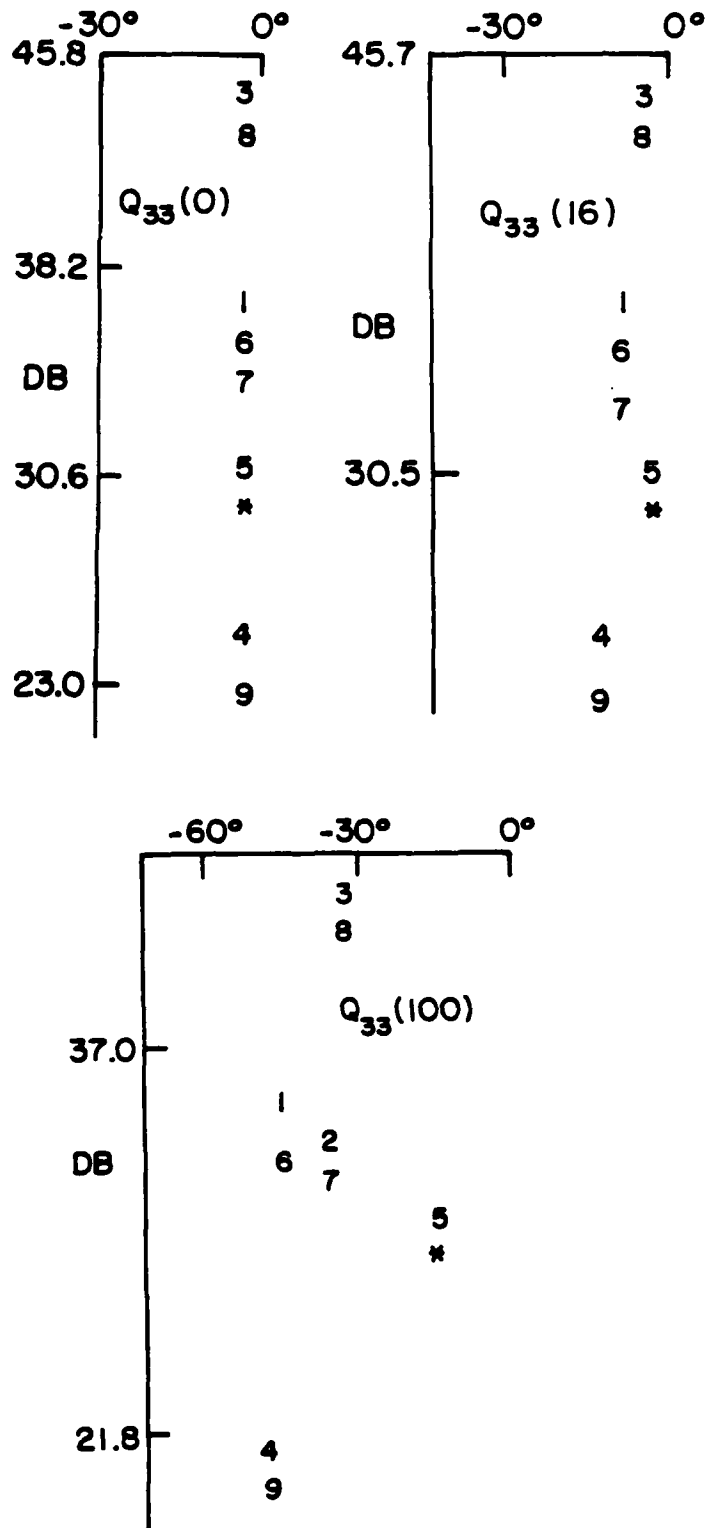


Fig. 2.3 Templates of Q_{33} at $\omega = 0, 16, 100$

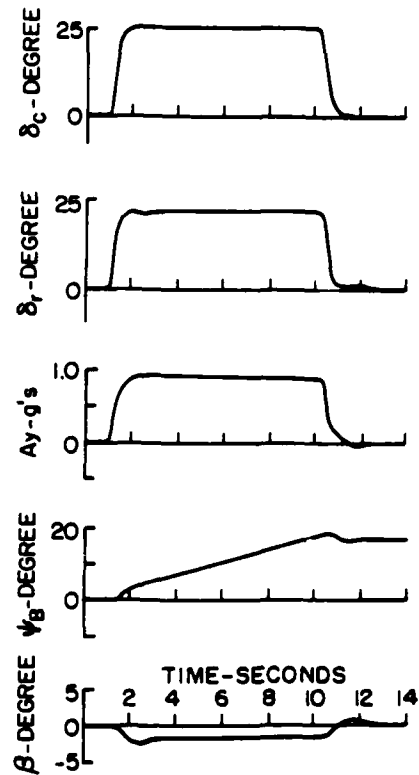


Fig. 2.4 Simulation data, A_y mode response; 9M, 30,000 ft CG, 35% MAC (supplied by contractor)

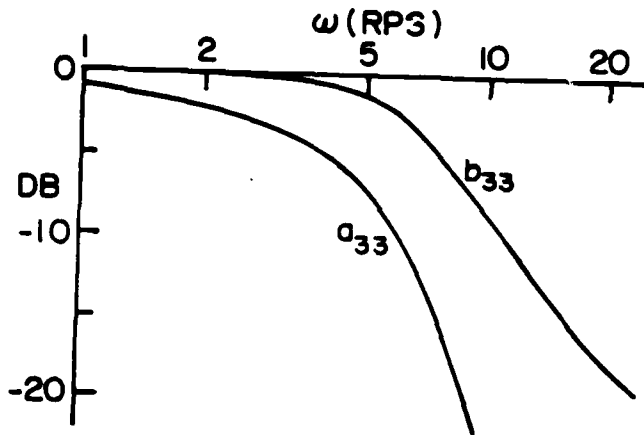


Fig. 2.5 Tolerances on $|T_{33}(j\omega)|$

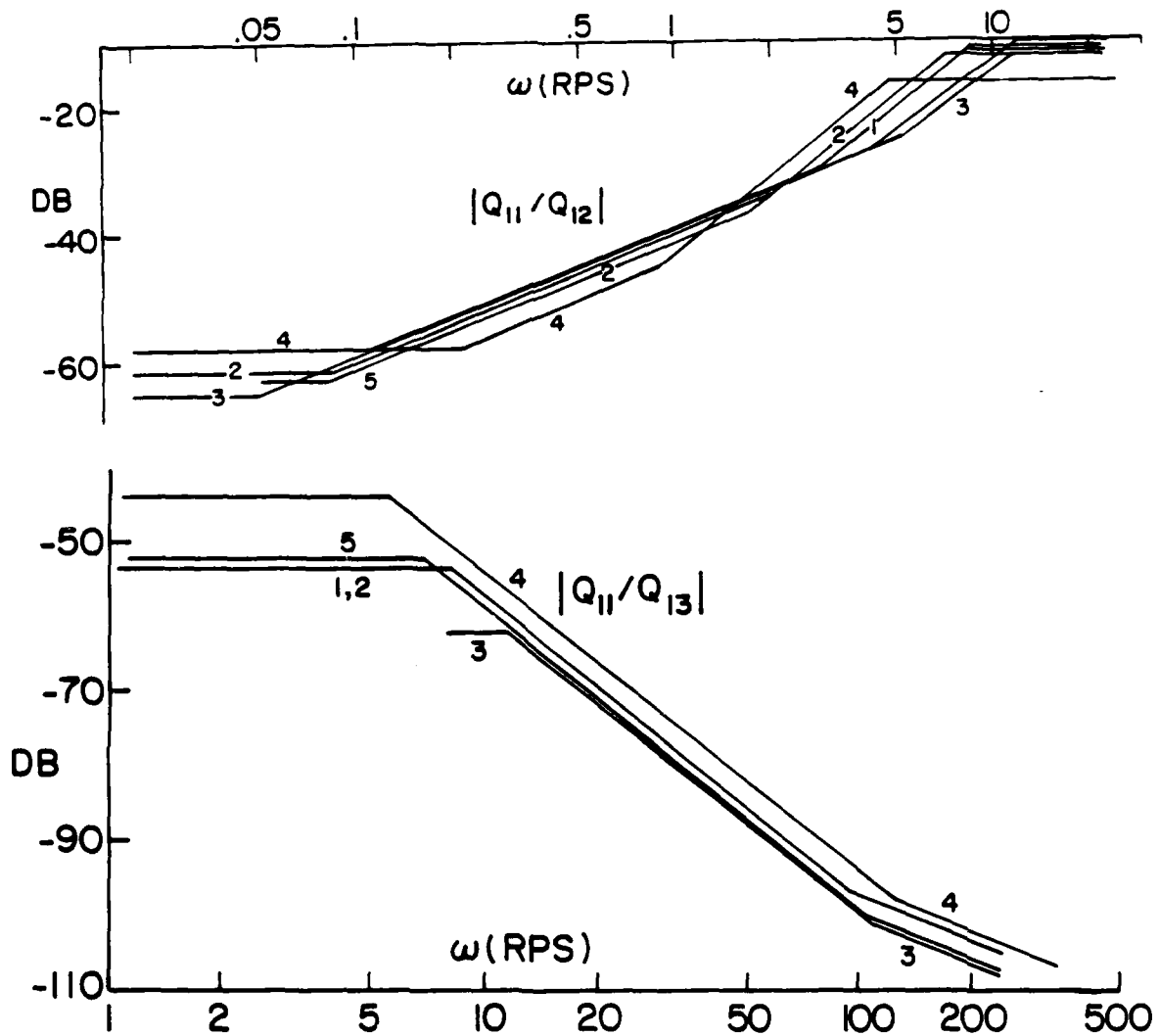


Fig. 2.6a,b Bode plots (asymptotic) of $|Q_{11}/Q_{12}|$, $|Q_{11}/Q_{13}|$.

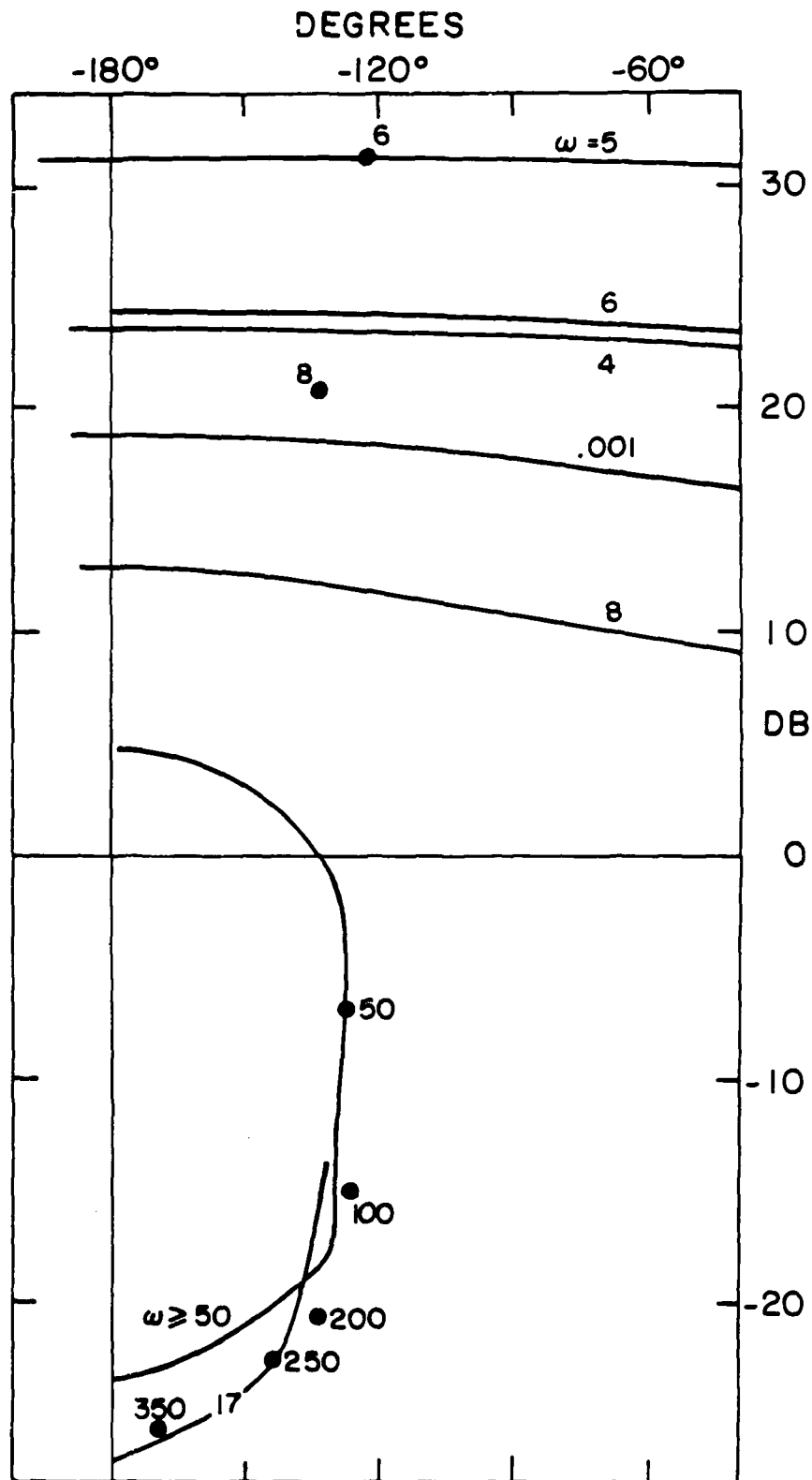


Fig. 2.7 Bounds on L_{10} in Nichols Chart, Design 1. (• indicate $L_{10}(j\omega)$ values).

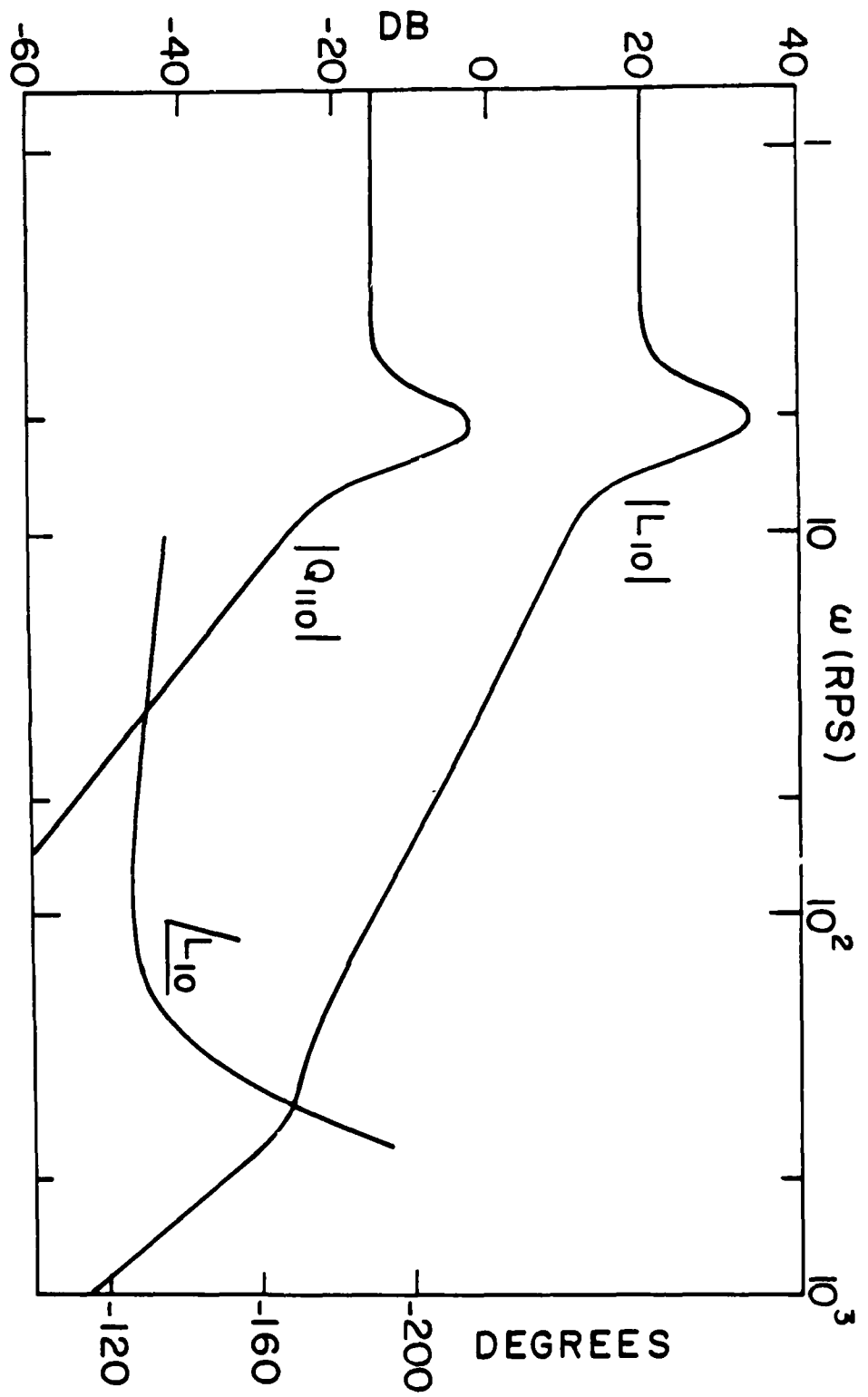


Fig. 2.8 Bode plots of L_{10} , Q_{110} . Design 1.

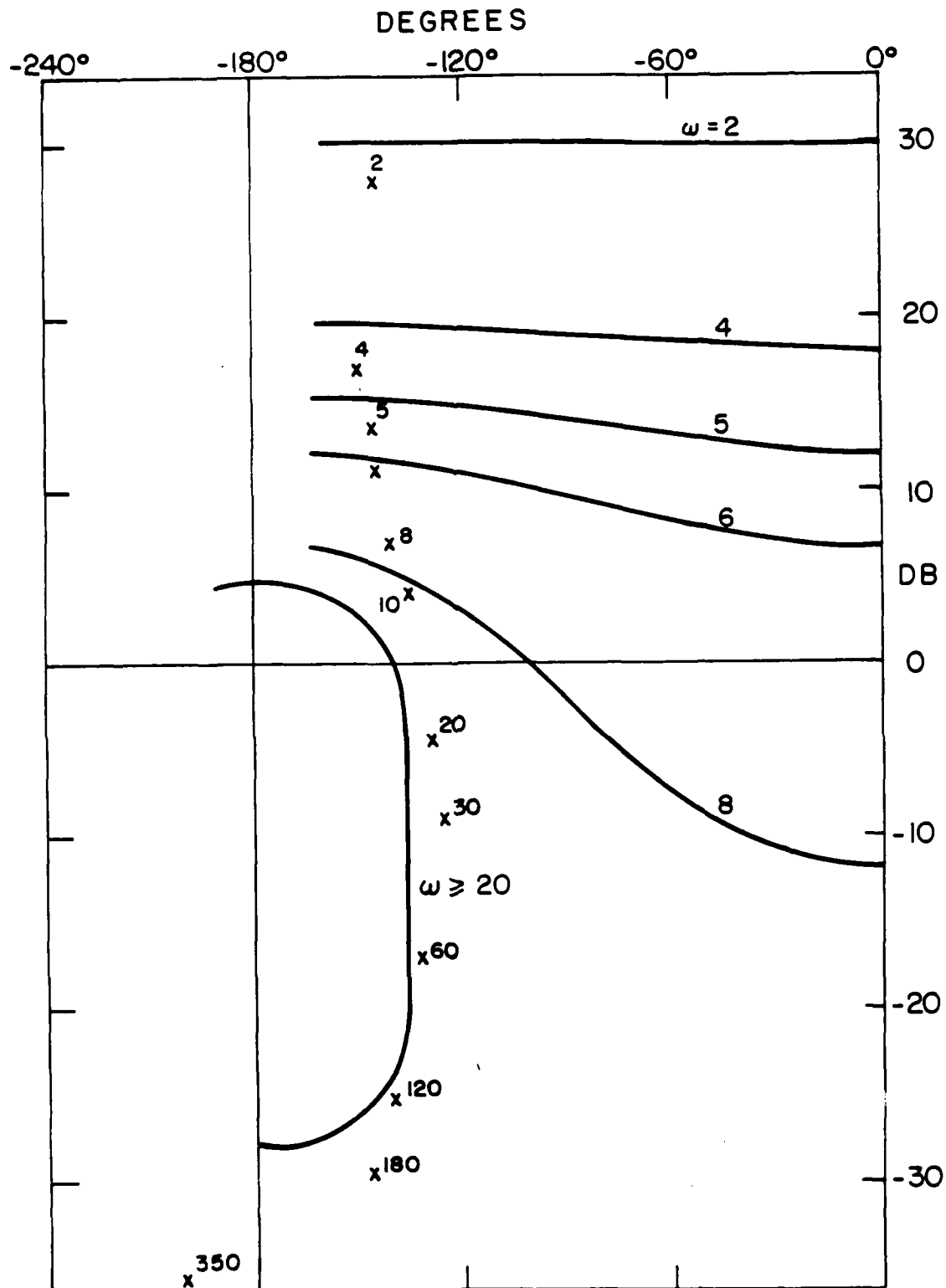


Fig. 2.9 Bounds on L_{20} in Nichols Chart, Design 1 (x are $L_{20}(j\omega)$ values).

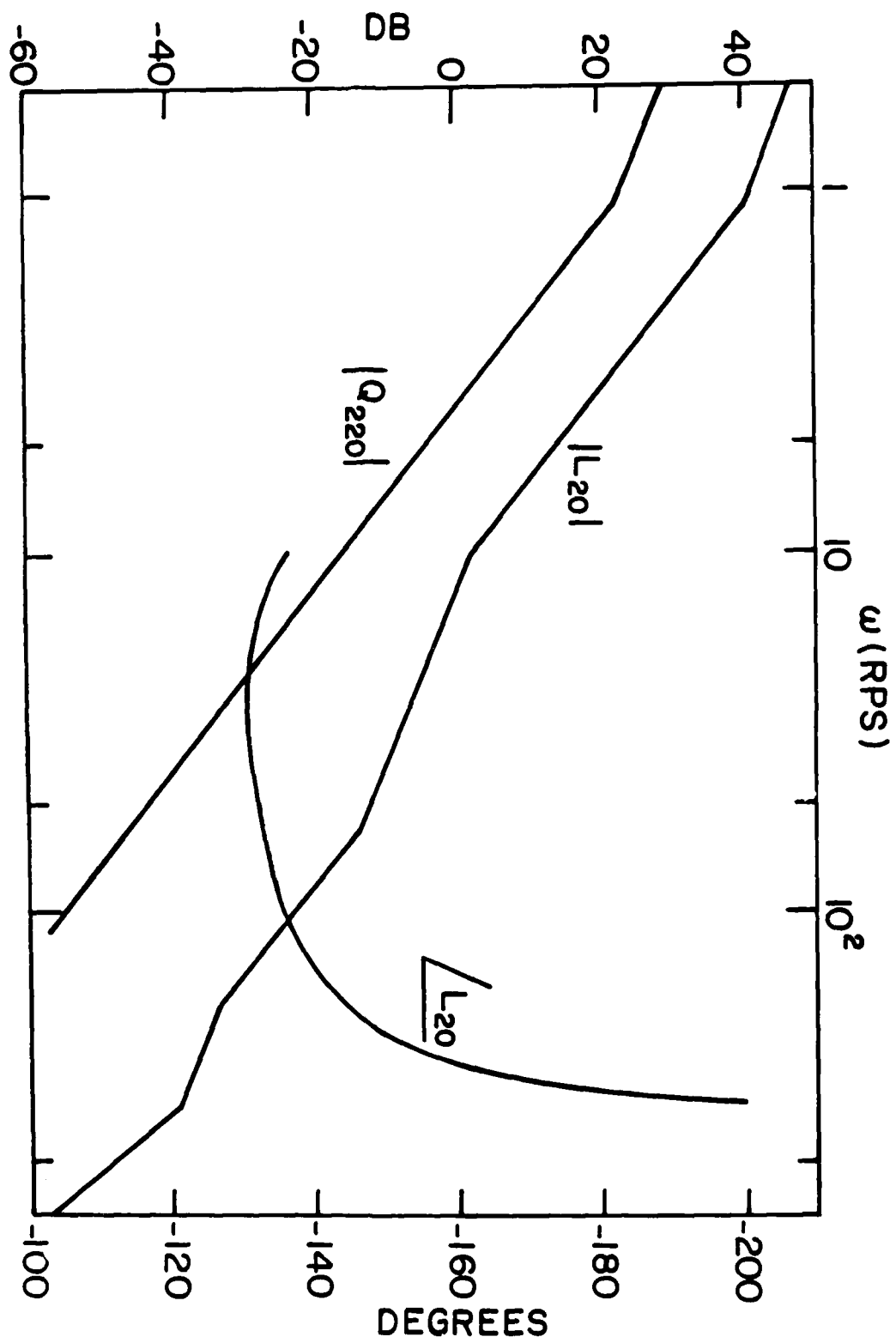


Fig. 2.10 Bode plots of L_{20} , Q_{220} : Design 1 (asymptotes)

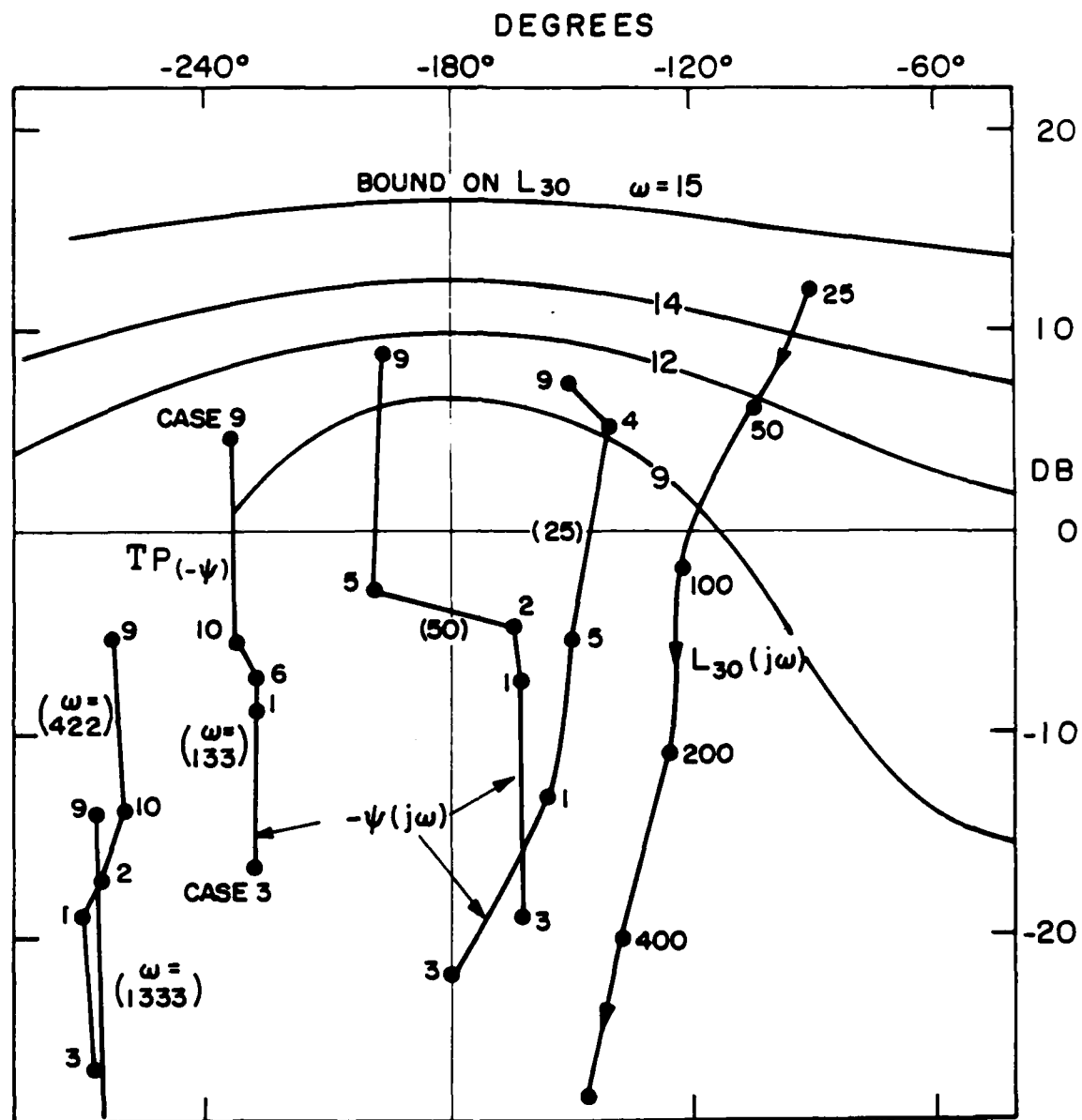


Fig. 2.11 Some templates of $-\psi(j\omega)$ ($T_p(-\omega)$) and bounds

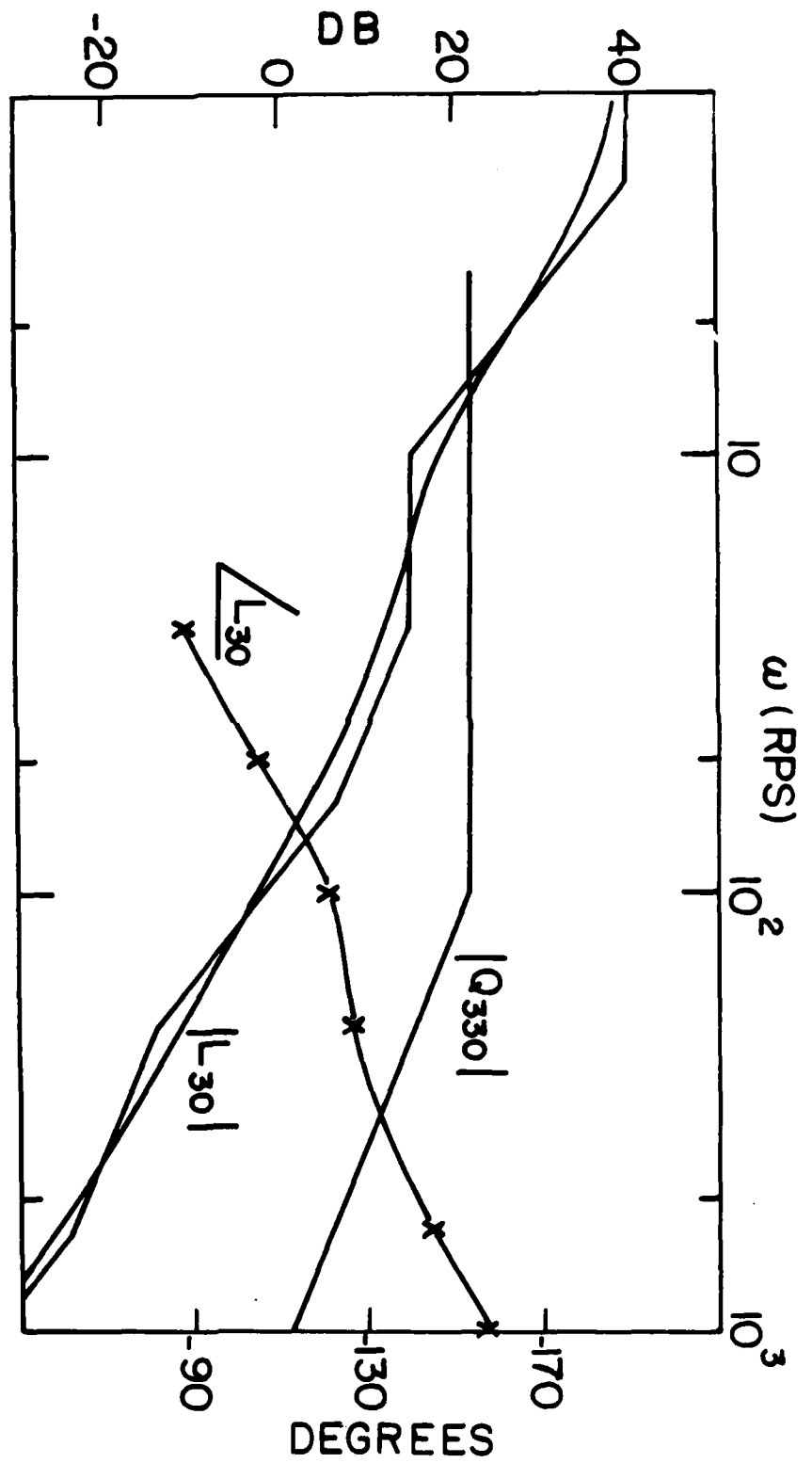


Fig. 2.12 Bode plots of L_{30} , Q_{330} : Design 1.

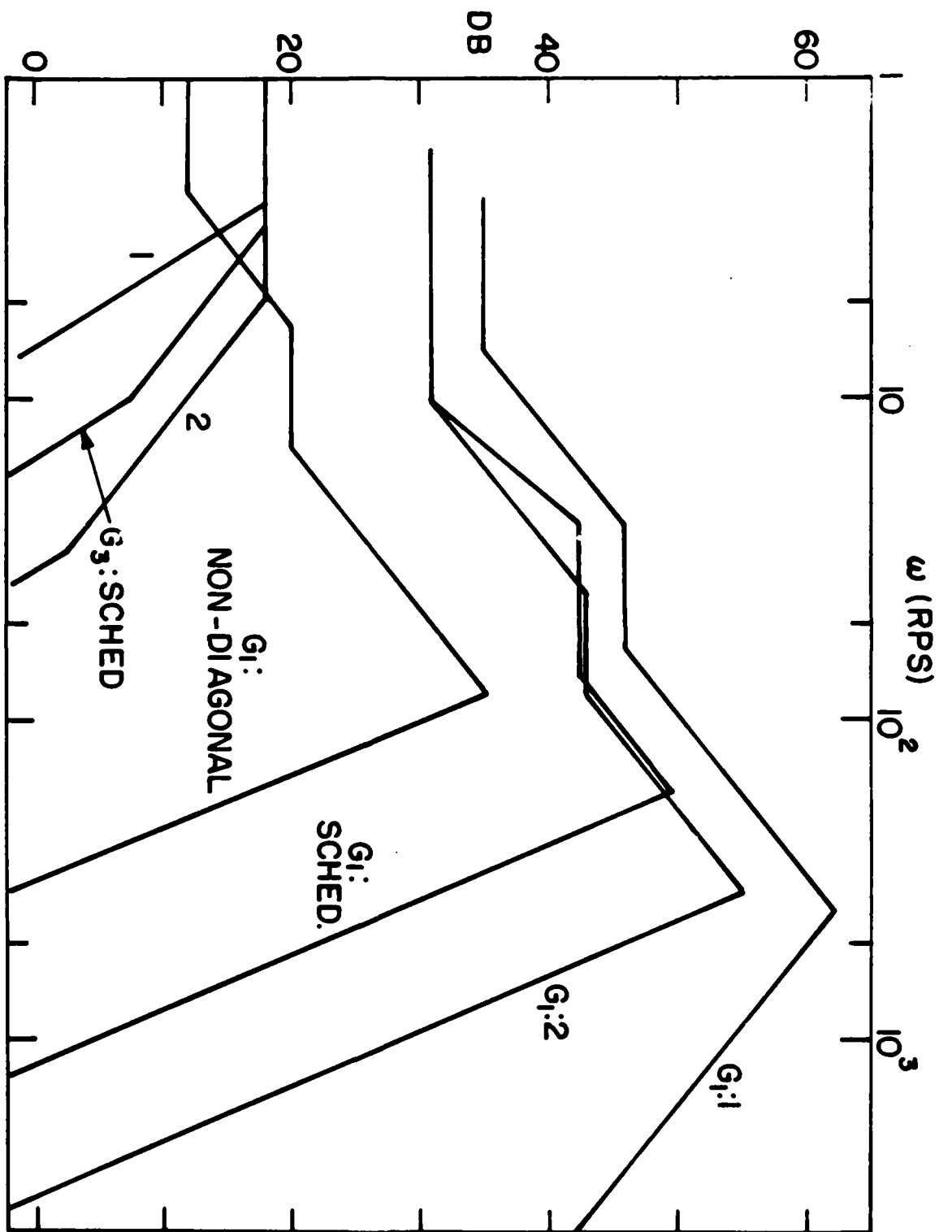


Fig. 2.13 Comparison of G_1 , $G_3(\omega)$ of various designs.

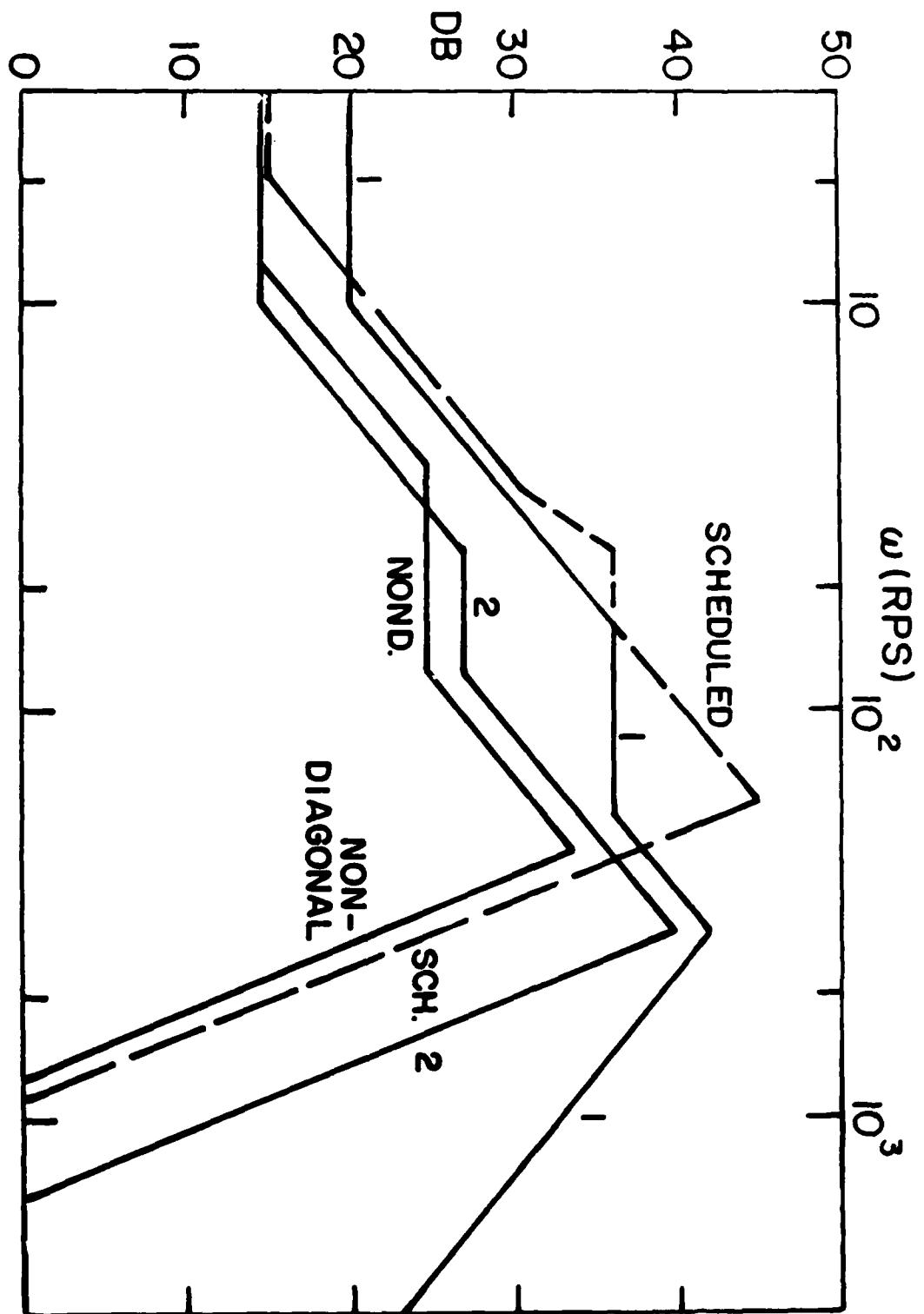


Fig. 2.14 Comparison of $G_2(j\omega)$ of various designs.

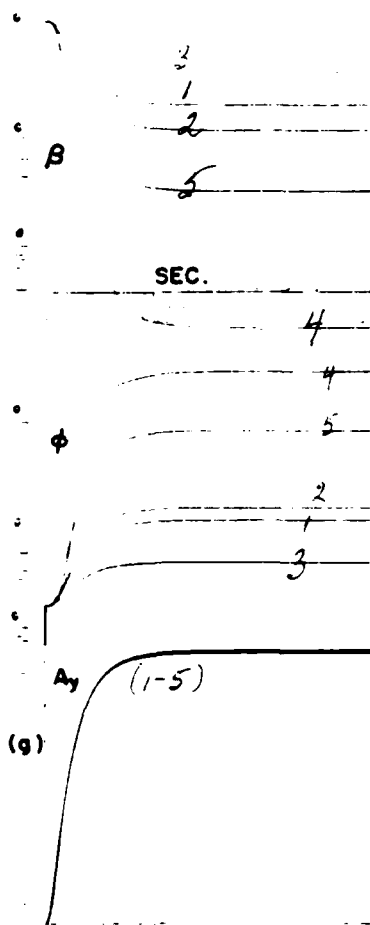


Fig. 2.15

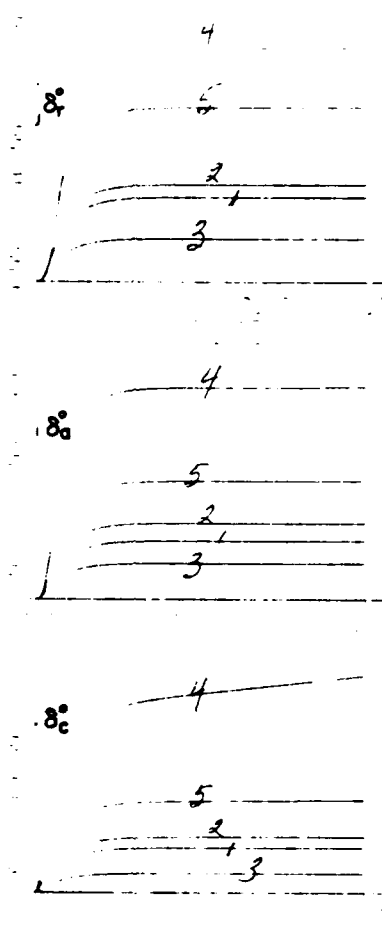


Fig. 2.16

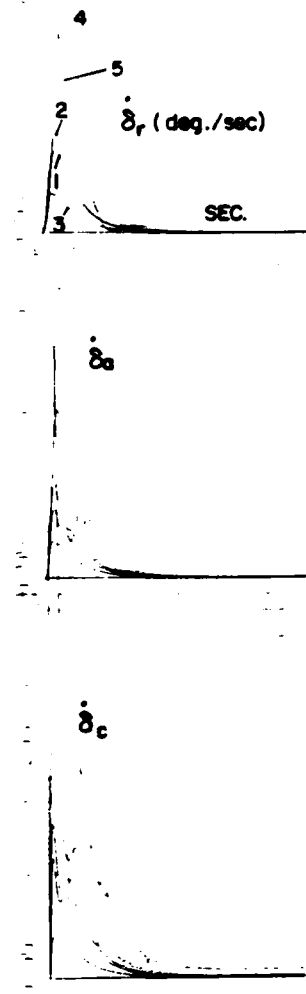


Fig. 2.17

Fig. 2.15-2.17 Computer simulations of design 1, for A_y command of 1g.
 (15) β, ϕ (deg.), (16) δ_1 (degrees), (17) A_y (g's).

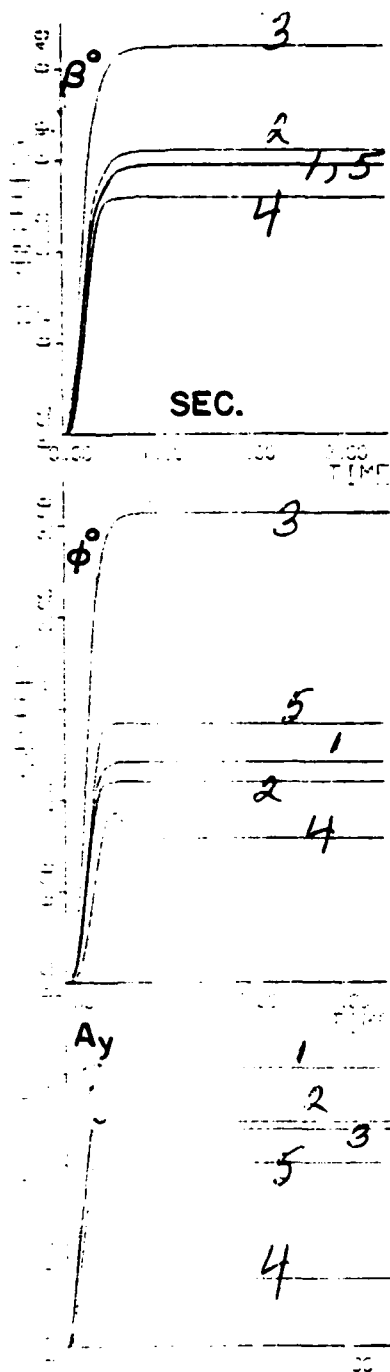


Fig. 2.20

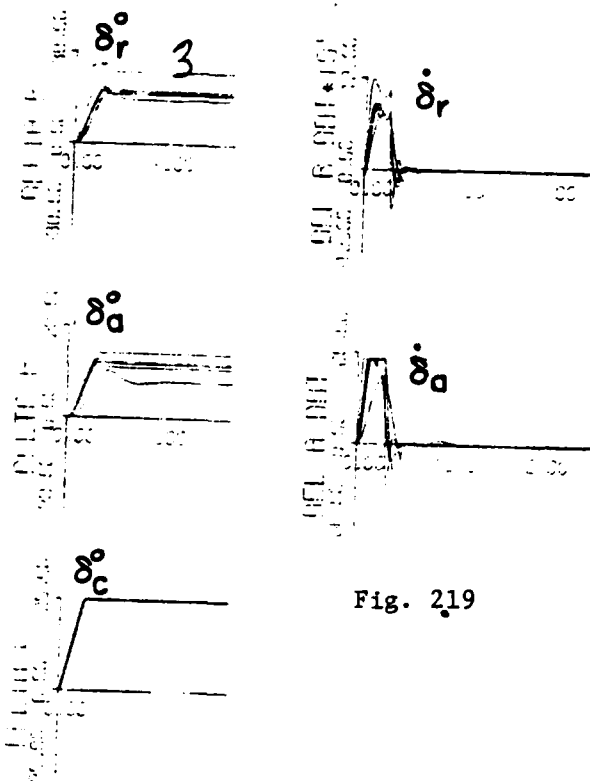


Fig. 2.18

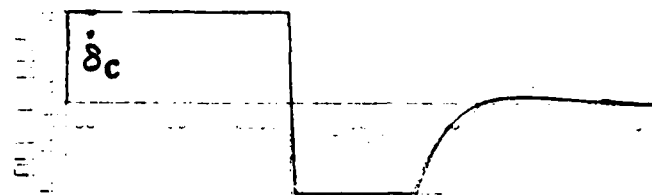


Fig. 2.19

Figs. 2.18-2.20 Responses due to very large A_y commands causing saturation; 9.3g for case 3, 3.1g for others.

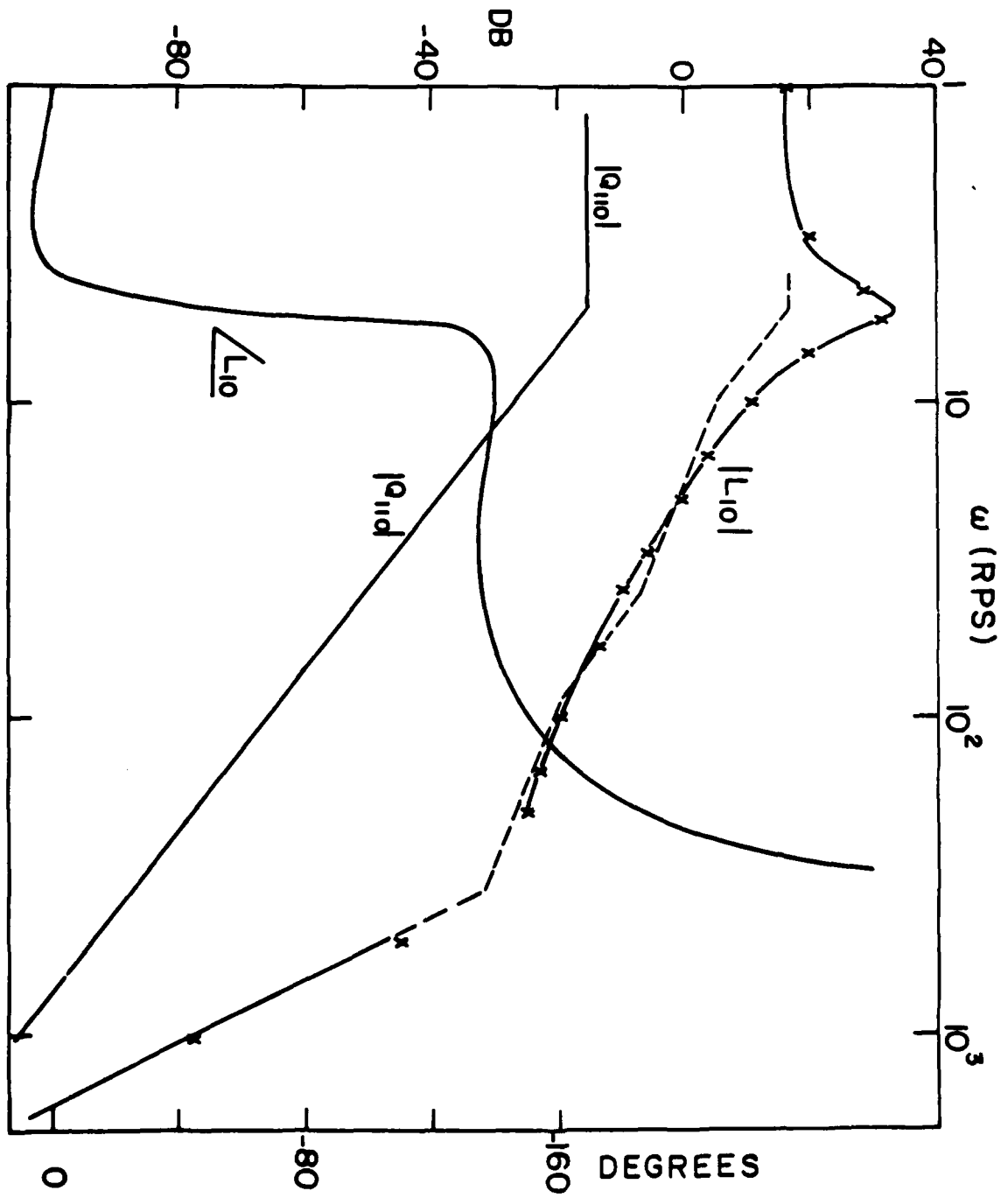


Fig. 2.21a Bode plots of L_{10} , L_{20} , L_{30} : Design 2.

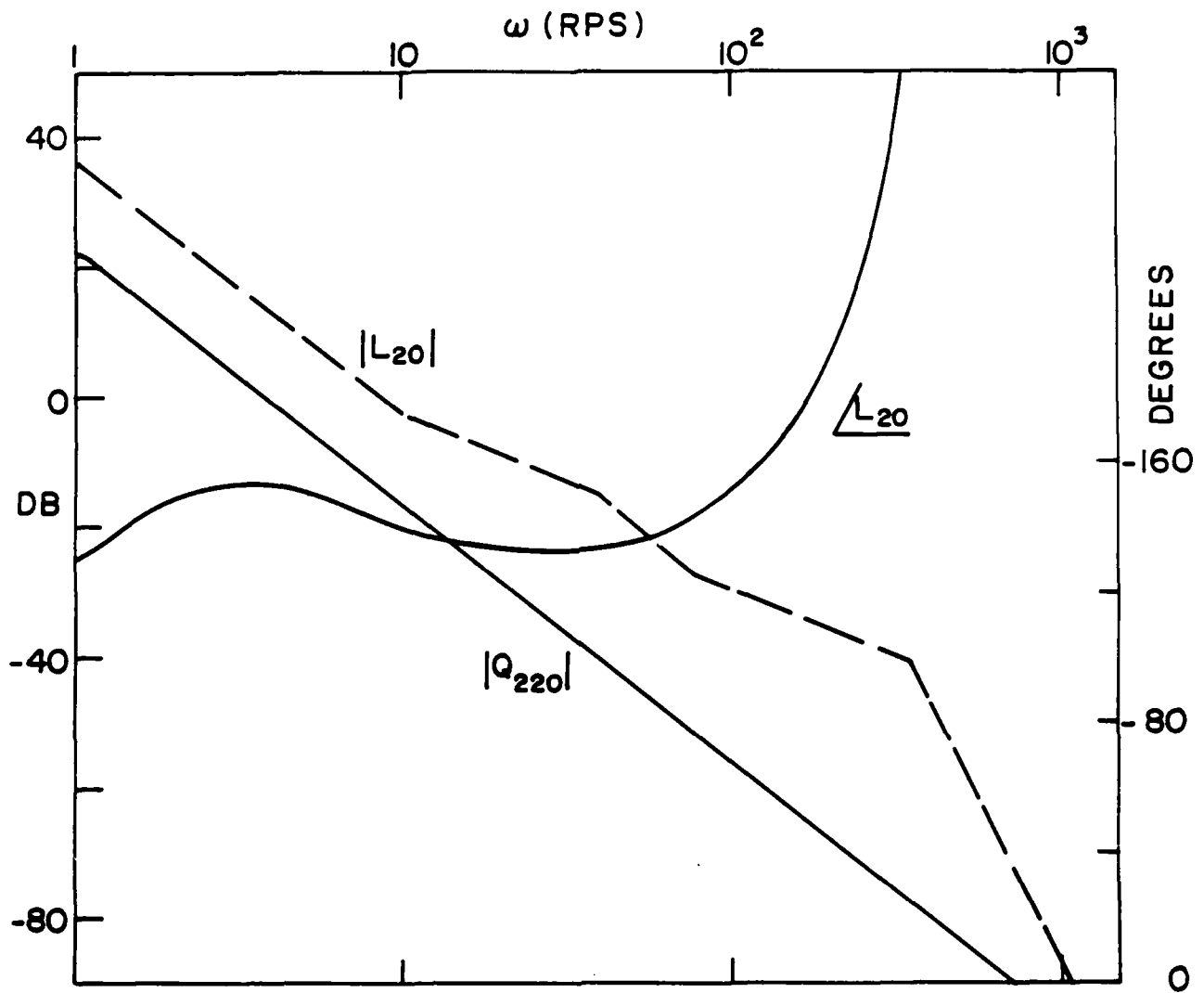


Fig. 2.21b Bode plots of L_{10} , L_{20} , L_{30} : Design 2.

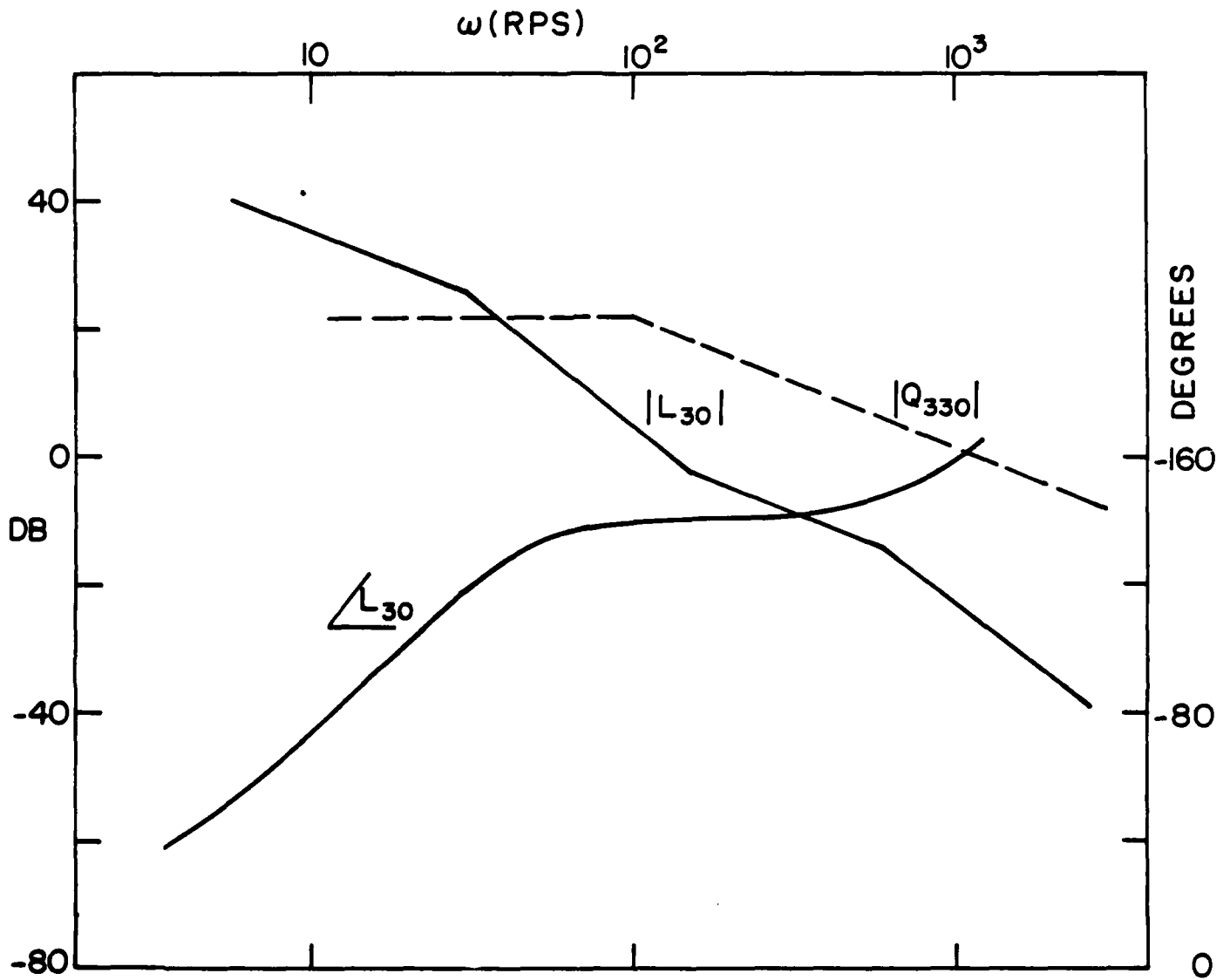


Fig. 2.21c Bode plots of L_{10} , L_{20} , L_{30} : Design 2.

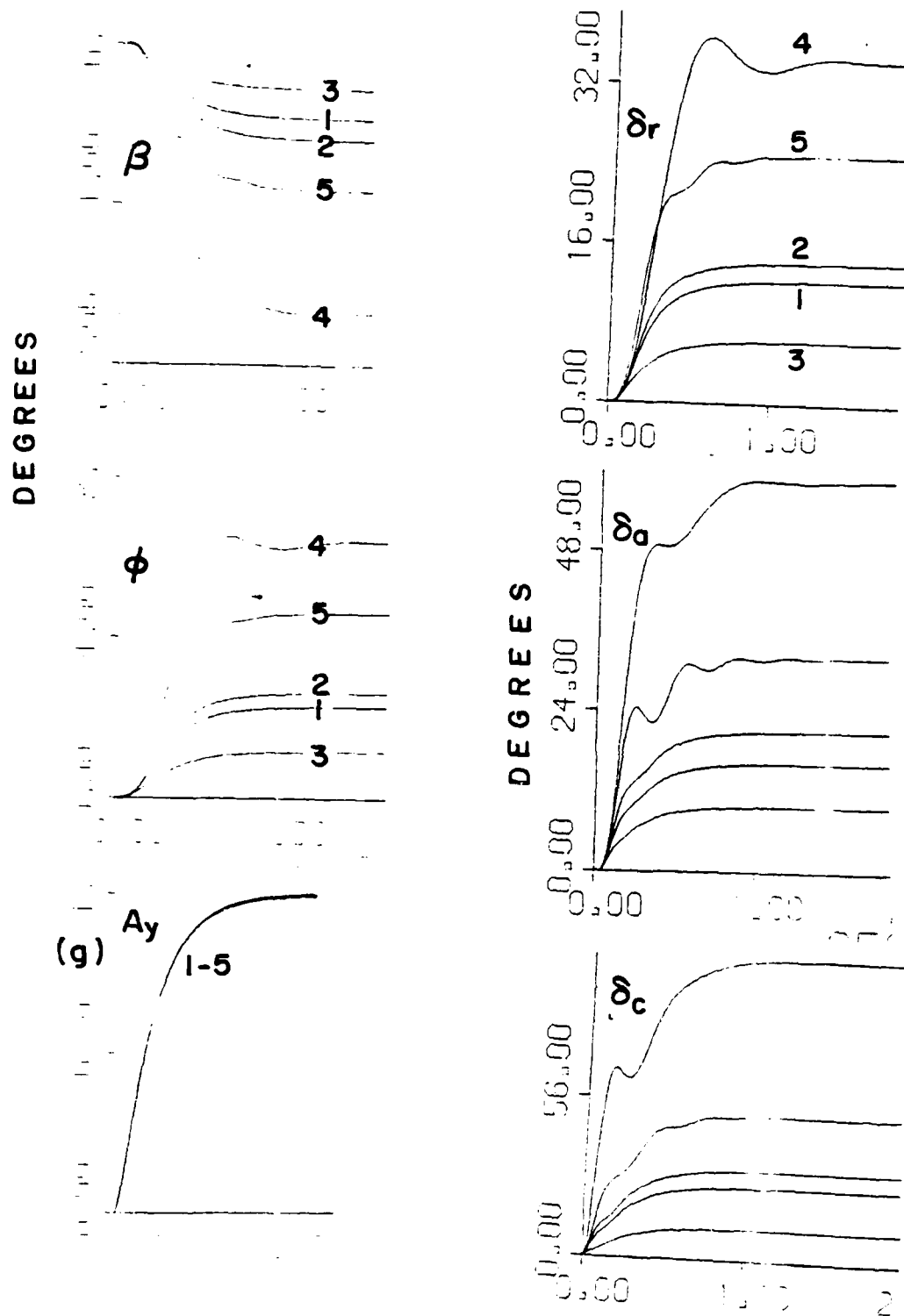


Fig. 2.22 Computer simulations for design 2.

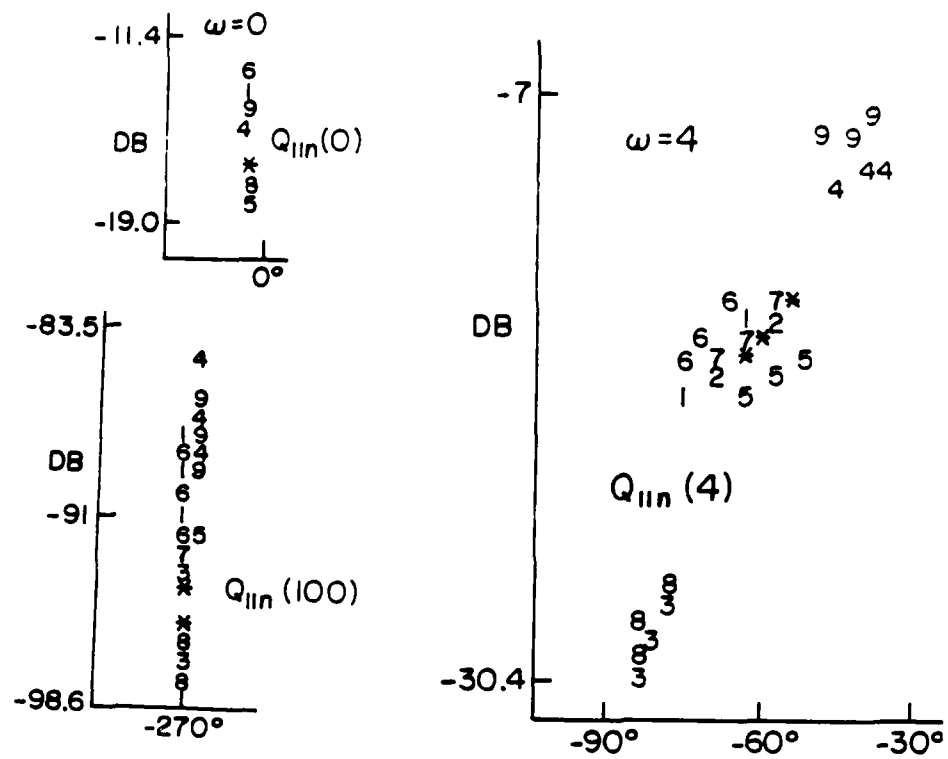


Fig. 2.23 Templates of Q_{lln} , scheduled design

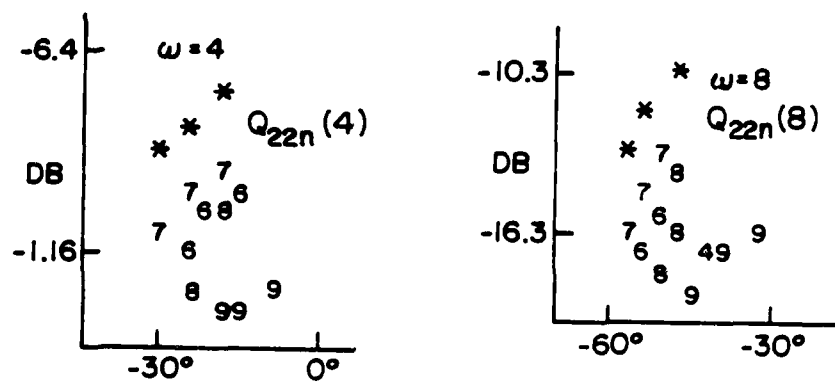


Fig. 2.24 Templates of Q_{22n} , scheduled design

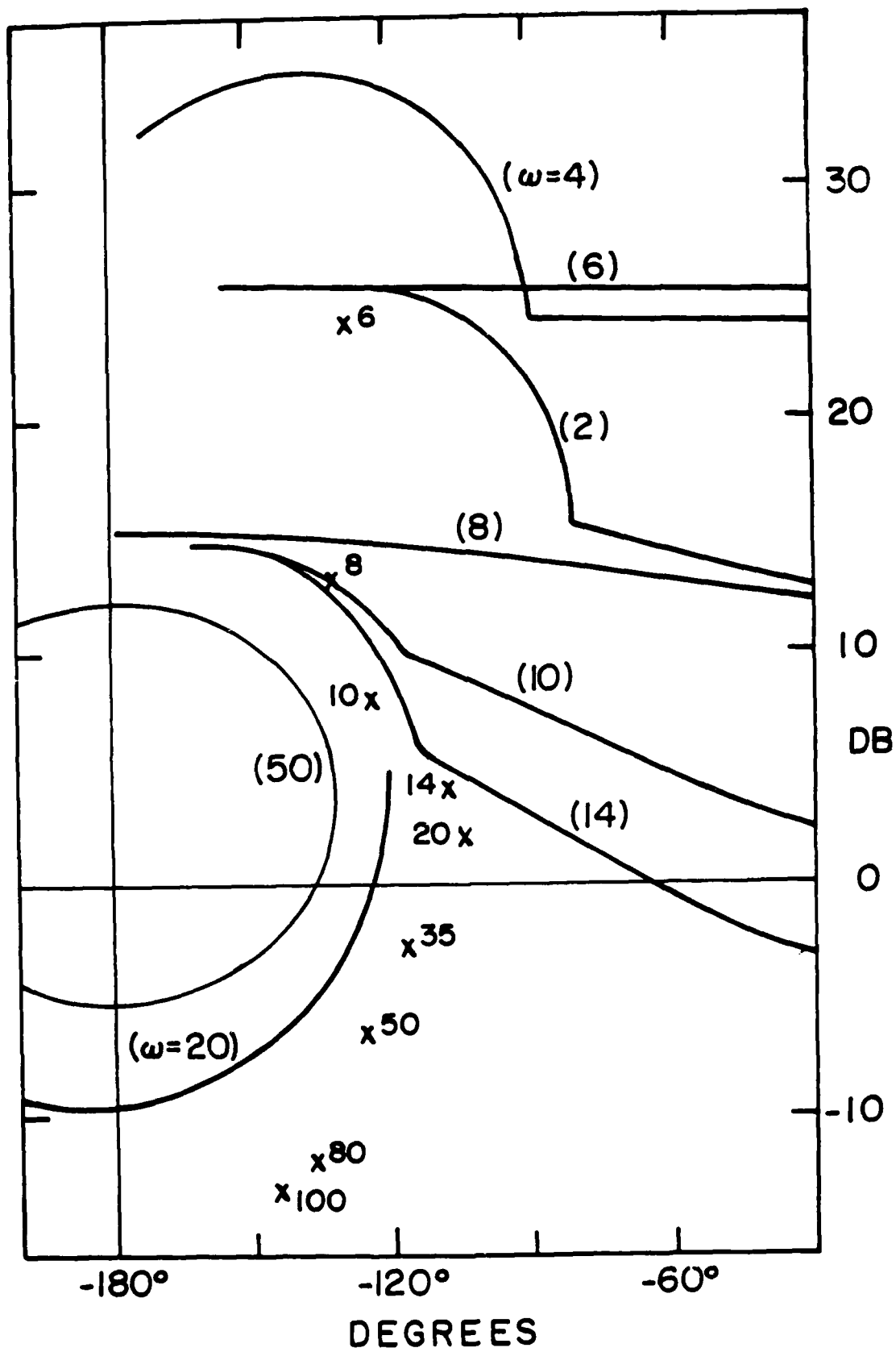


Fig. 2.26a Bounds on L_{10} , scheduled design (x gives $L_{10}(j\omega)$).

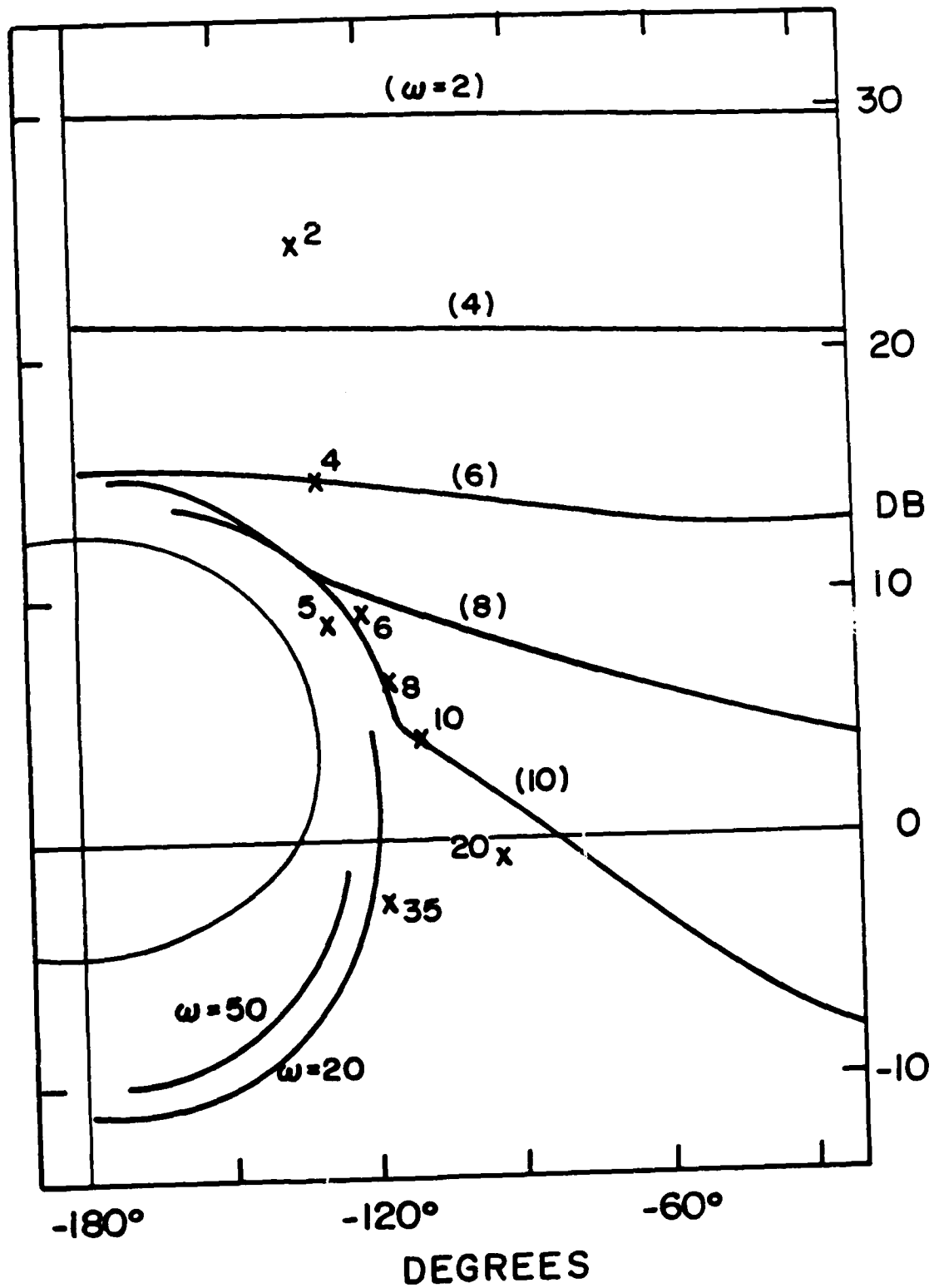


Fig. 2.26b Bounds on L_{20} and $L_{20}(j\omega)$ values, scheduled design.

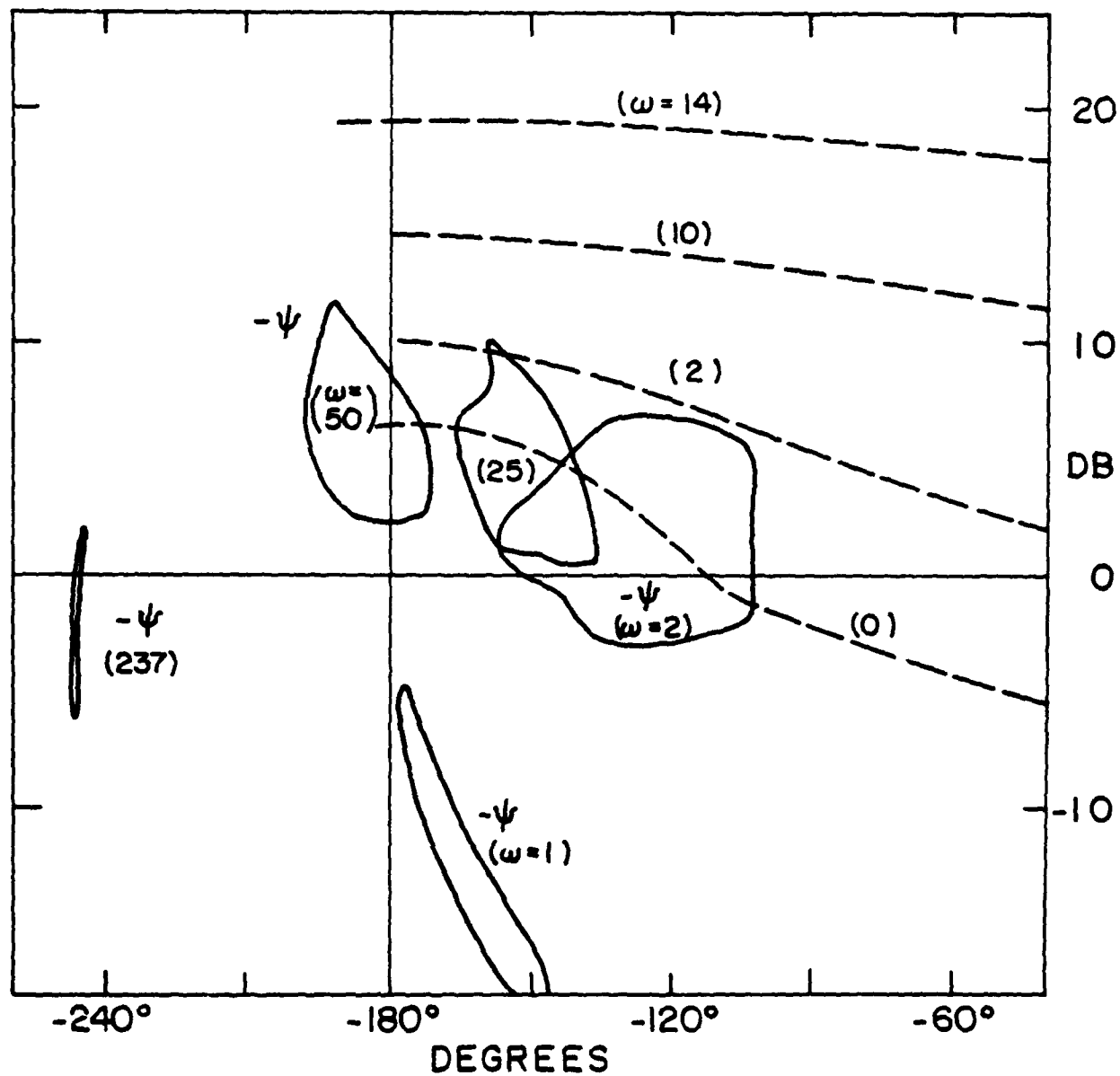


Fig. 2.26c Bounds on L_{30} and templates of $-\psi$, scheduled design

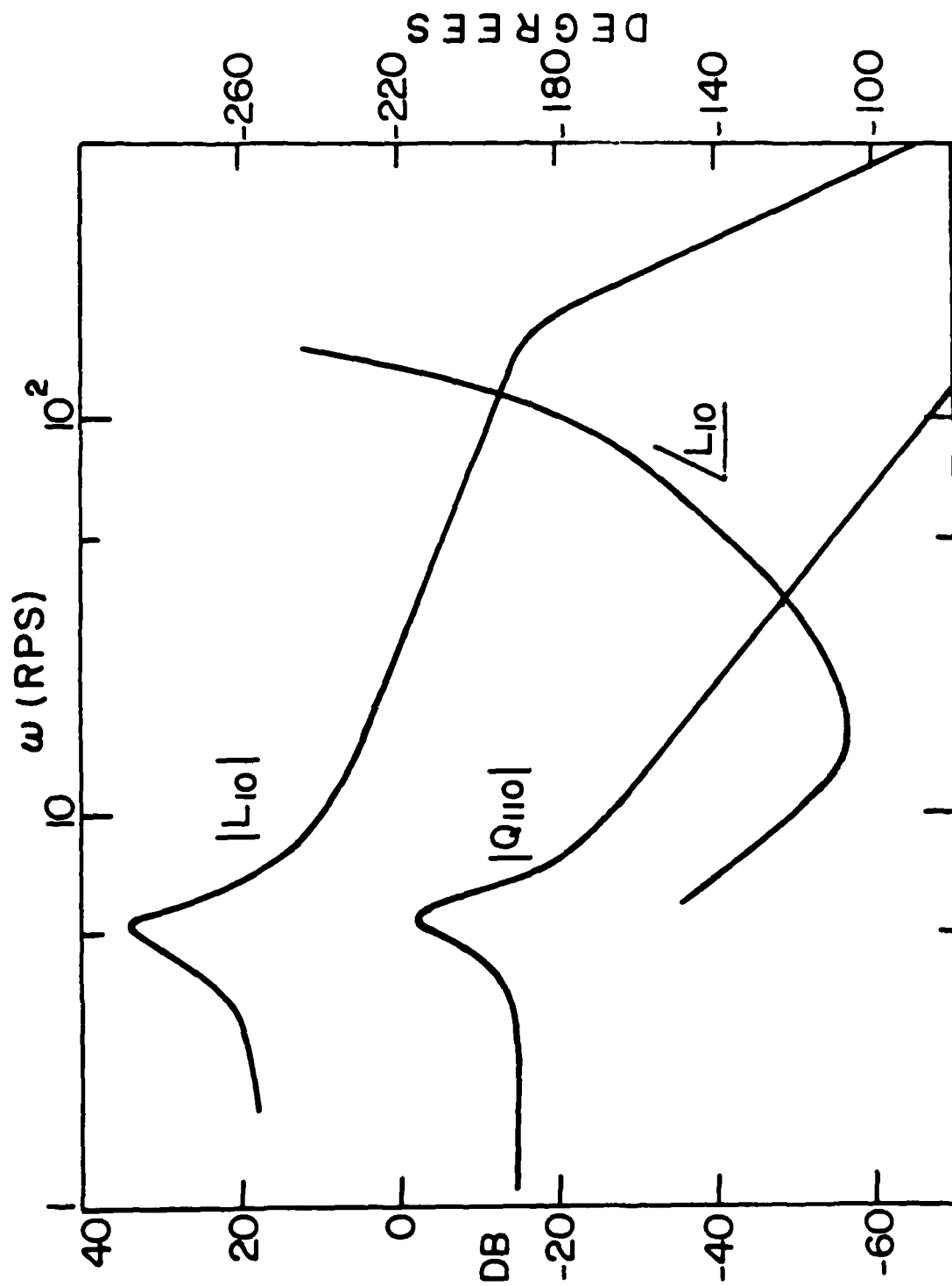


Fig. 2.27a Bode plots L_{10} , scheduled design

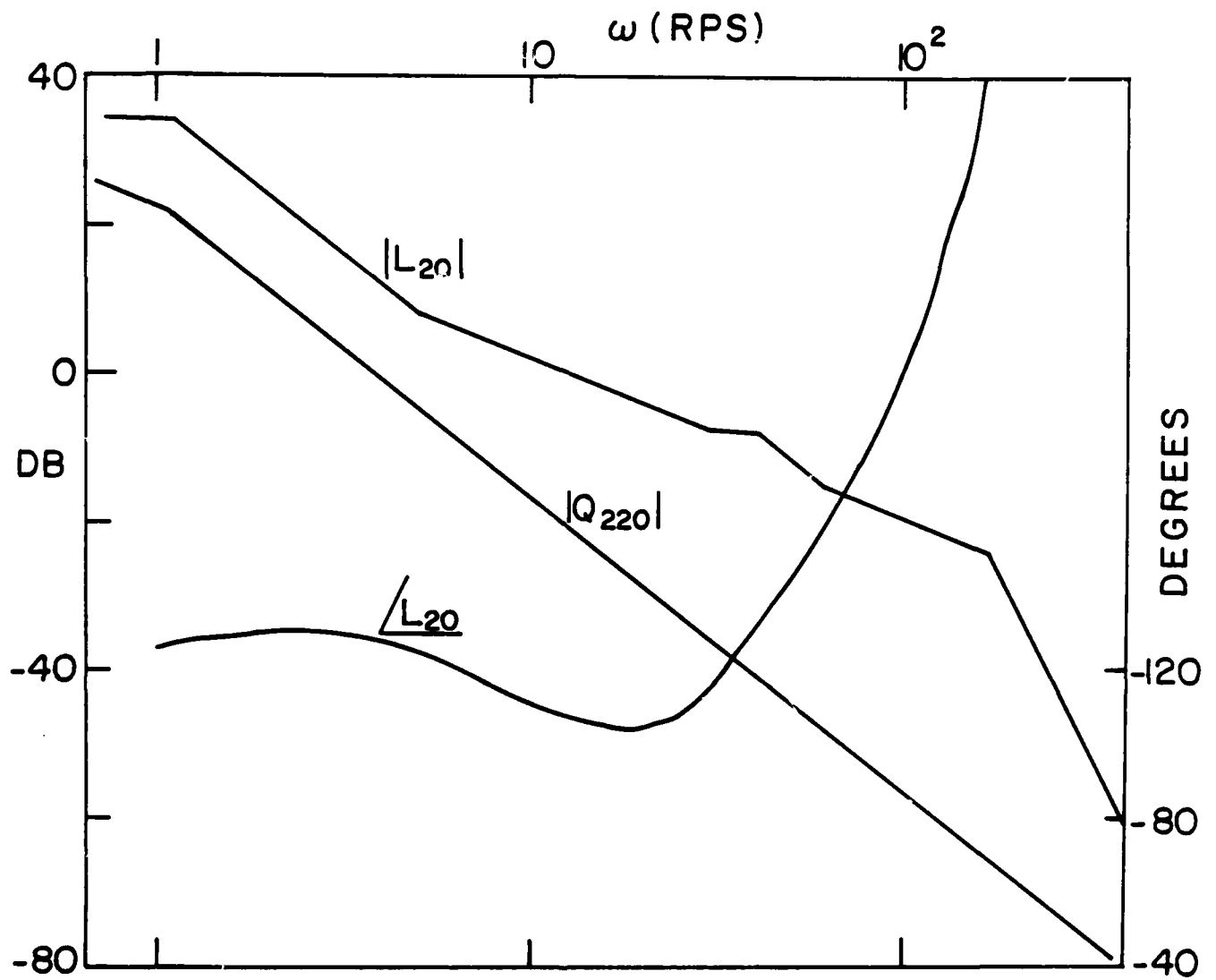


Fig. 2.27b Bode plots L_{20} , scheduled design

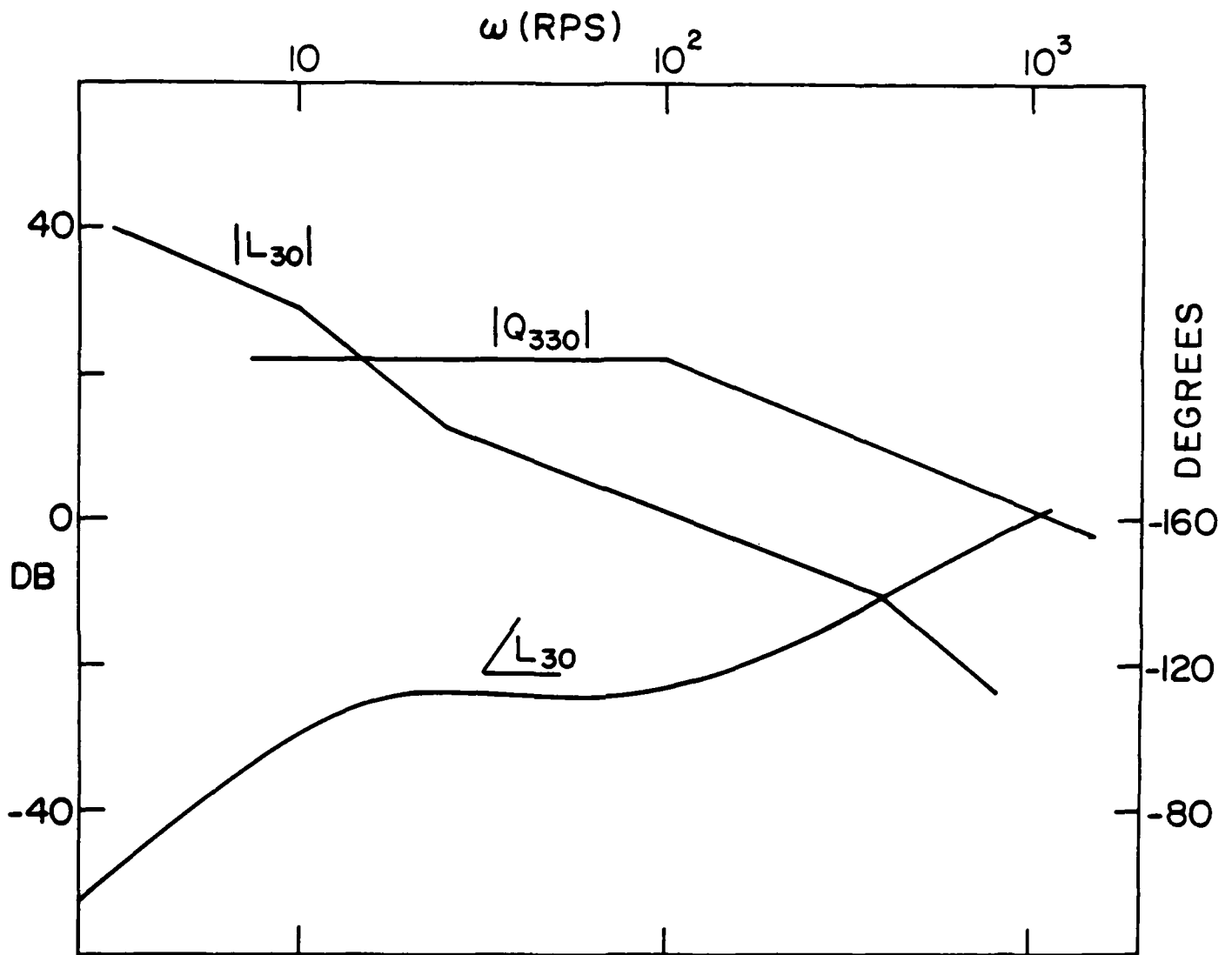


Fig. 2.27c Bode plots L_{30} , scheduled design

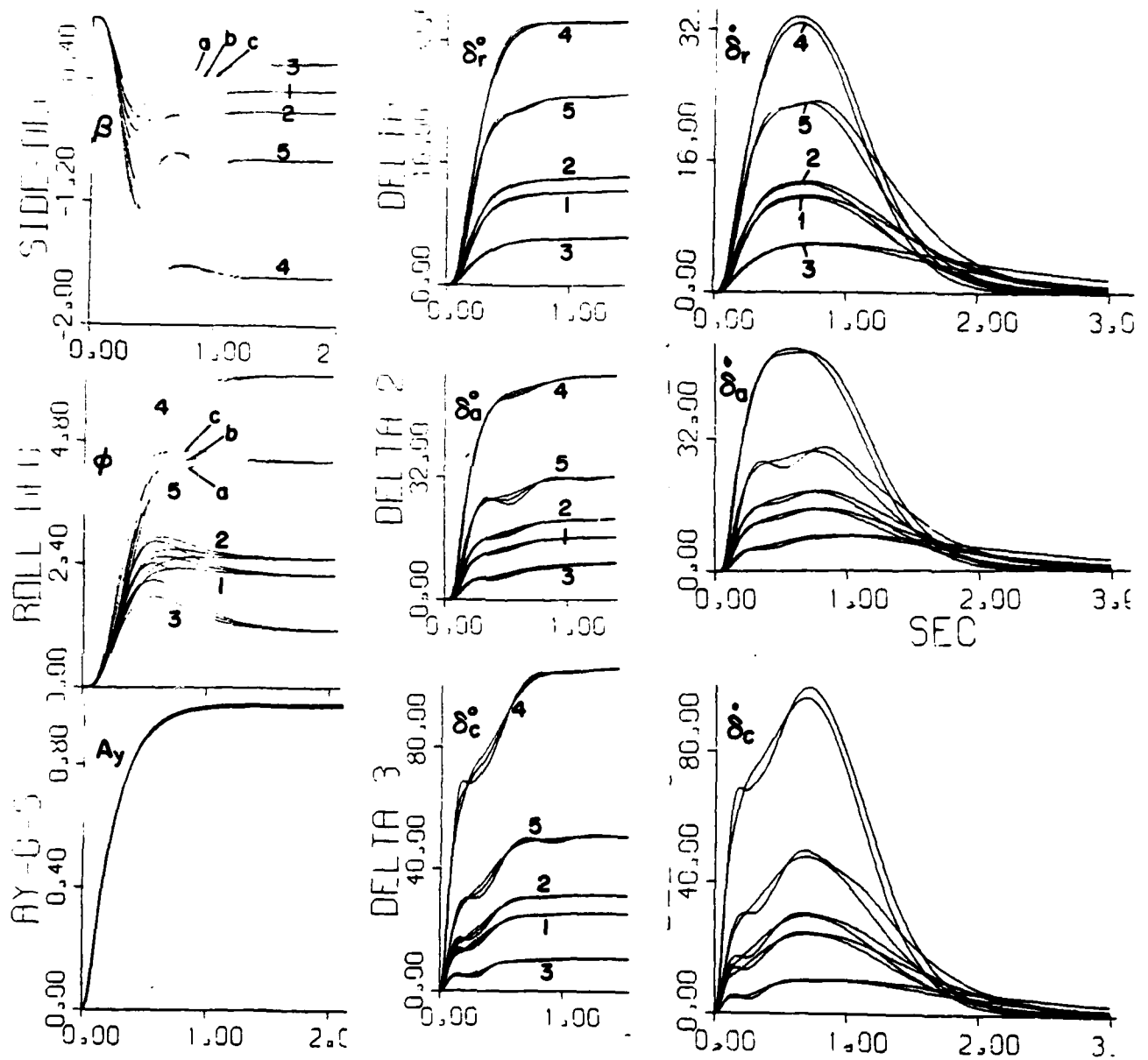


Fig. 2.28a-c. Scheduled design, simulation results for A_y command = 1g.
 (a) β, ϕ (deg.), A_y (g's) (b) δ_1 (degrees) (c) $\dot{\delta}_1$ (deg./sec.)

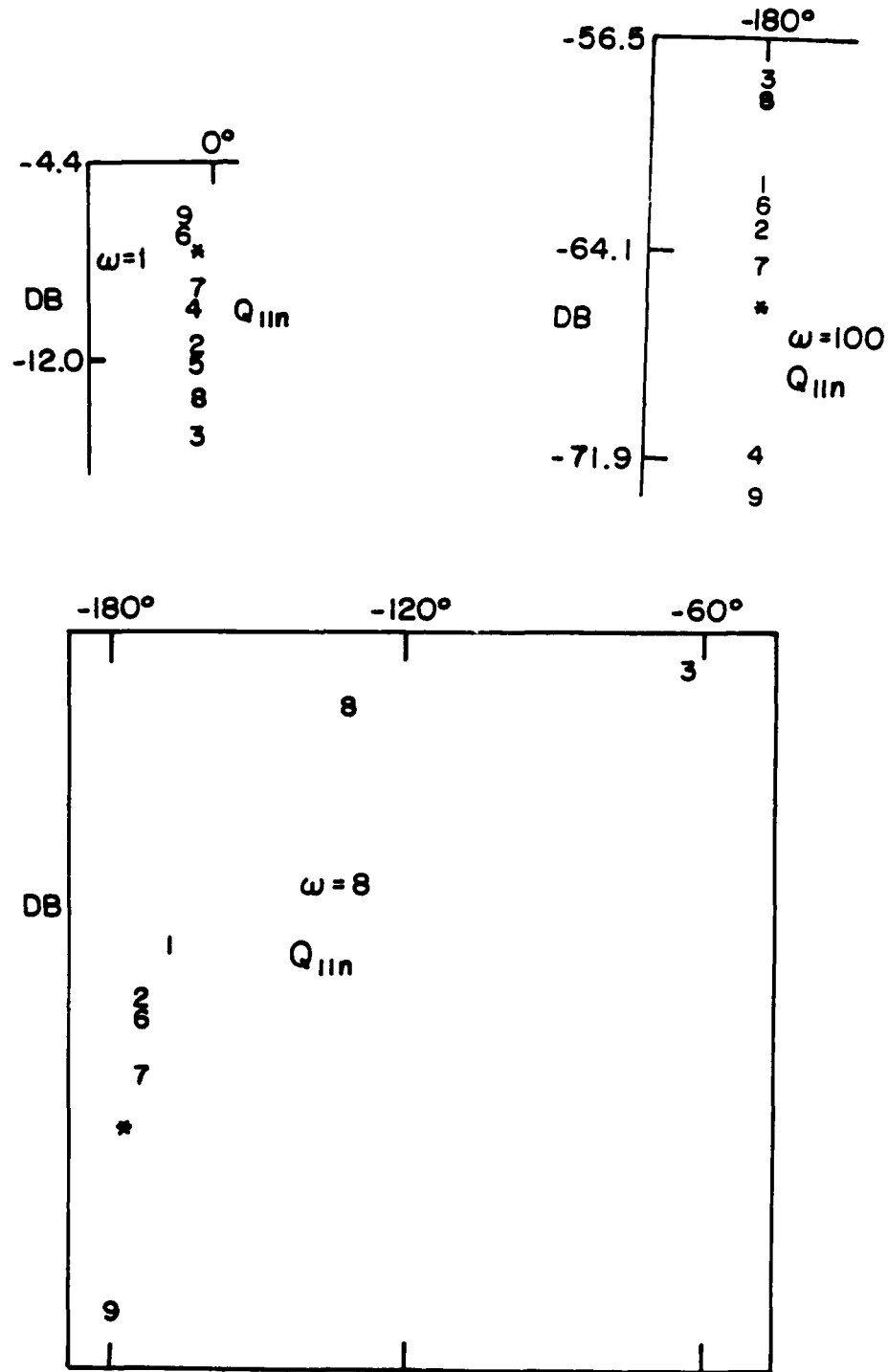


Fig. 2.29a Template of the new Q_{11n}, Q_{22n} , for non-diagonal compensation design.

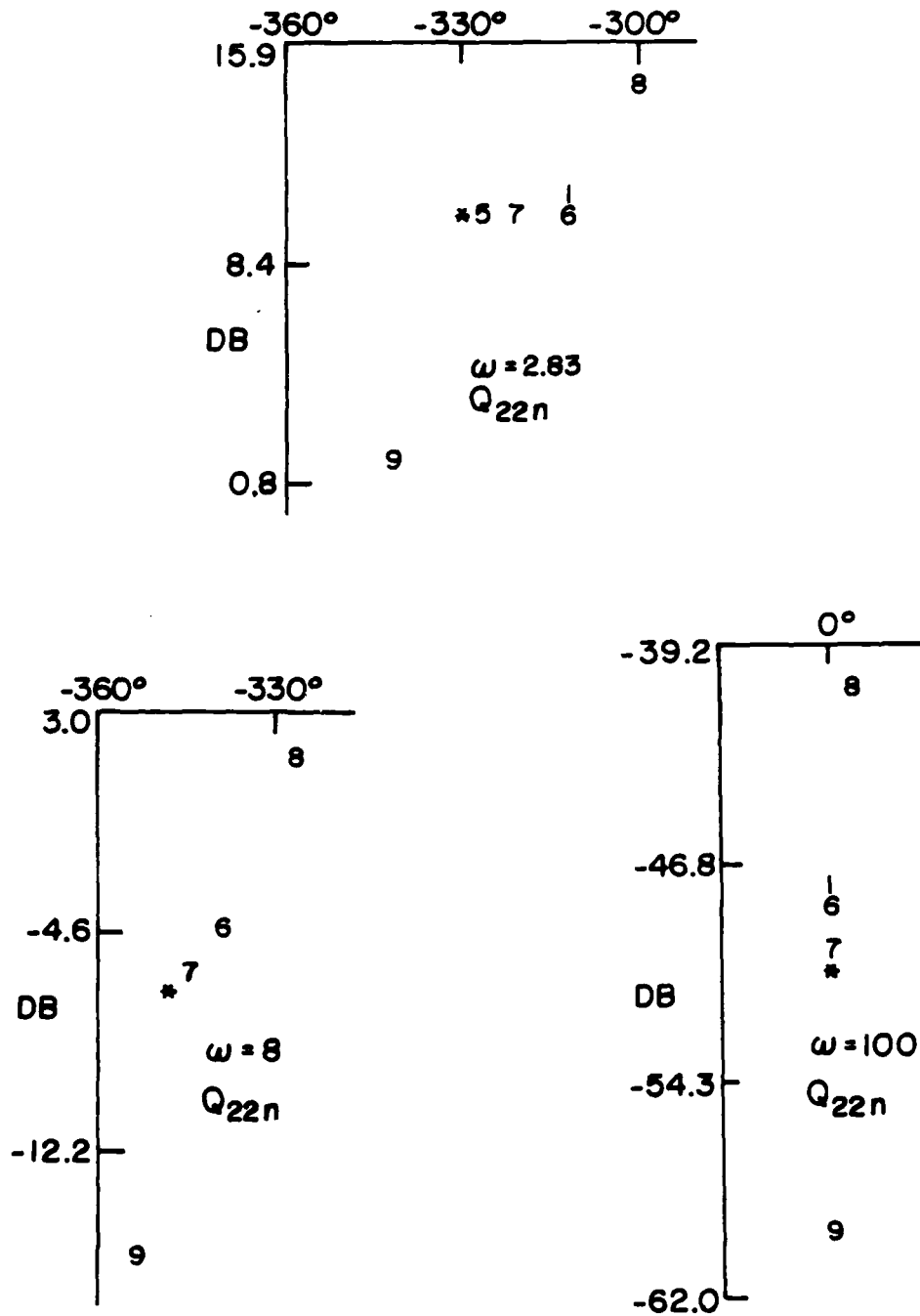


Fig. 2.29b Template of the new Q_{11n} , Q_{22n} , for non-diagonal compensation design.

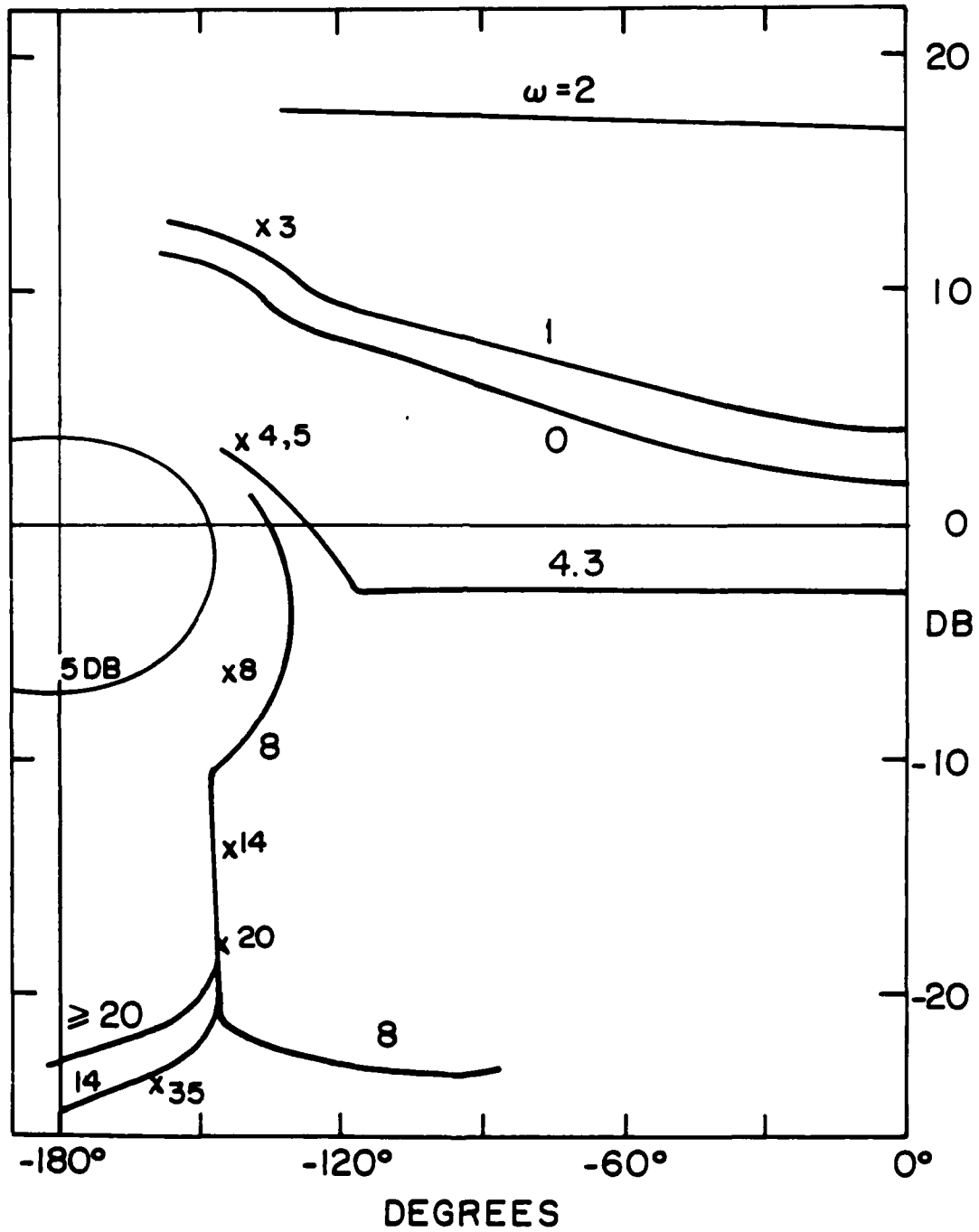


Fig. 2.30a Bounds on L_{10} in nondiagonal compensation design.

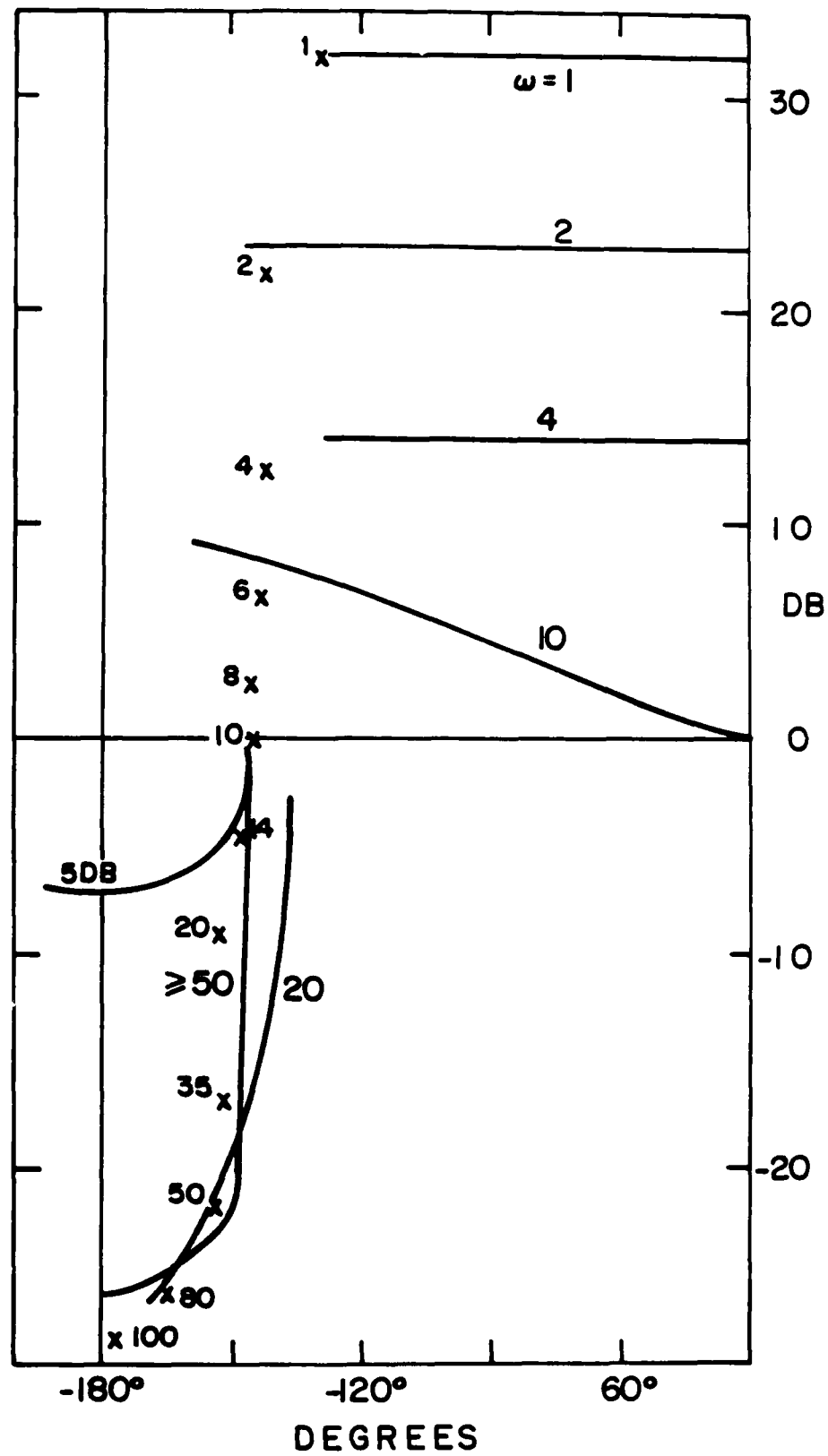


Fig. 2.30b Bounds on L_{20} in nondiagonal compensation design.

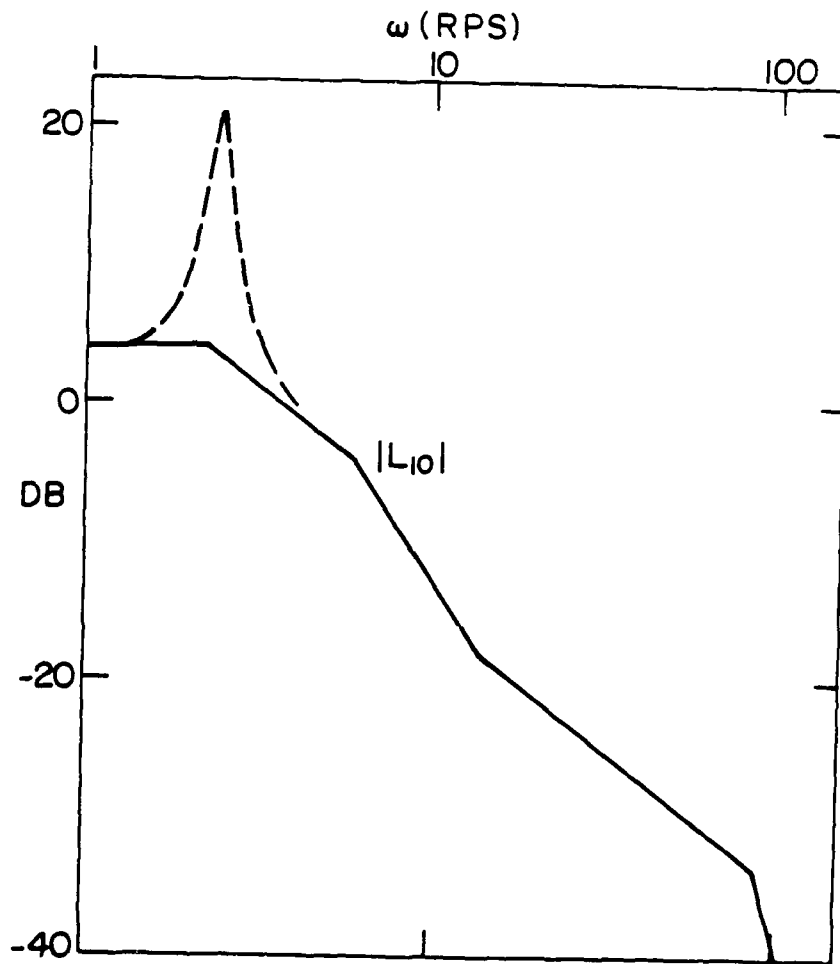


Fig. 2.31a Bode plot of L_{10} in nondiagonal compensation design.

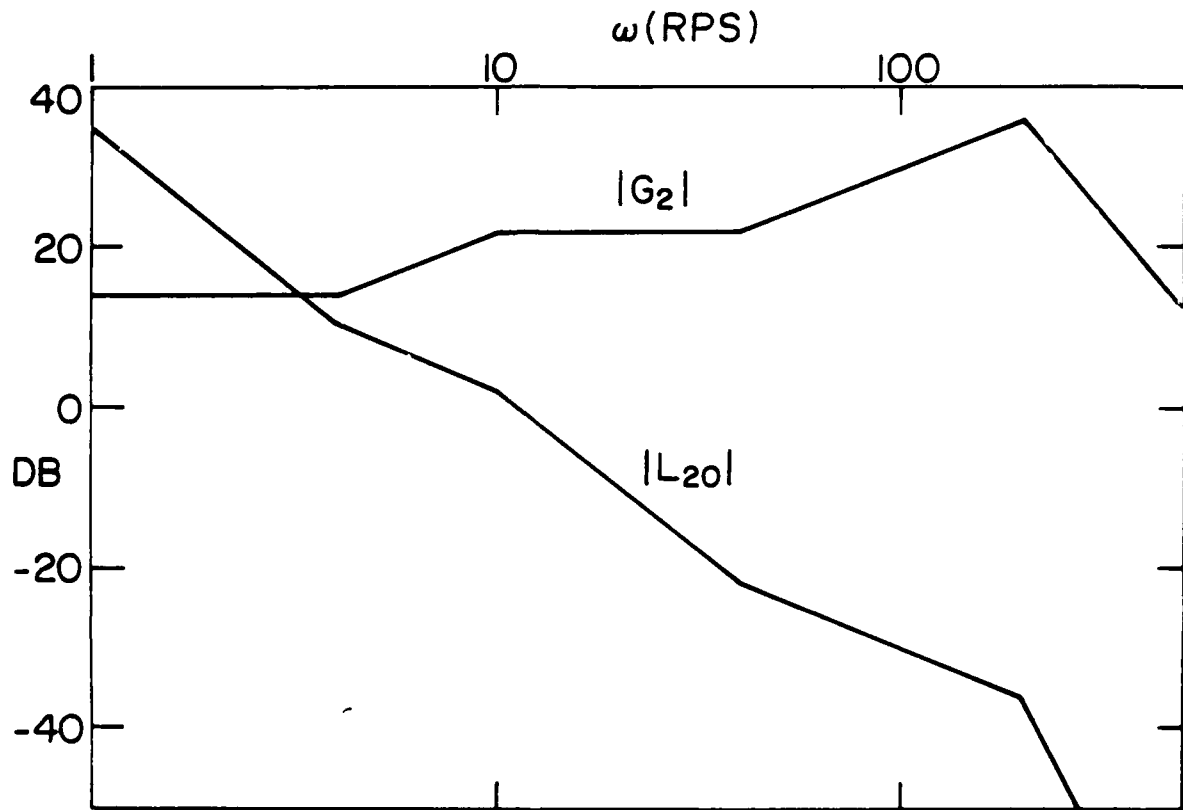


Fig. 2.31b Bode plot of L_{20} in nondiagonal compensation design.

AD-A135 738

MULTIVARIABLE FLIGHTCONTROL DESIGN WITH UNCERTAIN
PARAMETERS(U) WEIZMANN INST OF SCIENCE REHOVOTH
(ISRAEL) DEPT OF APPLIED MA. I HOROWITZ ET AL. SEP 82

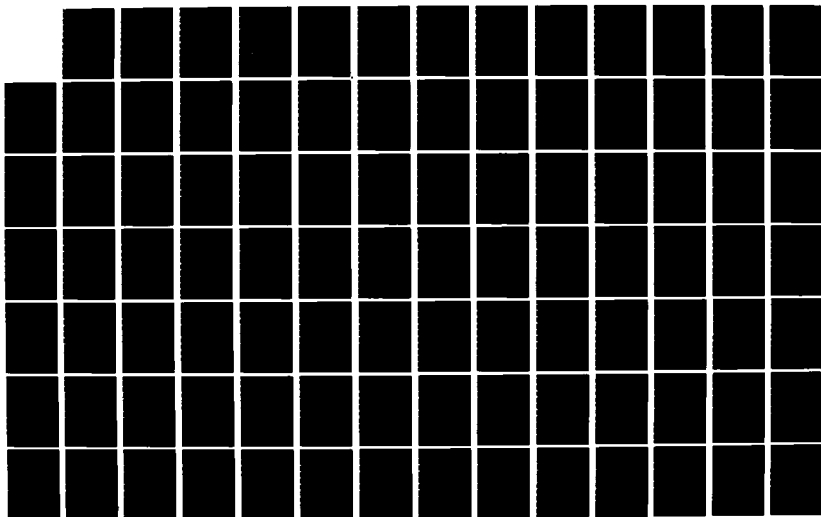
2/4

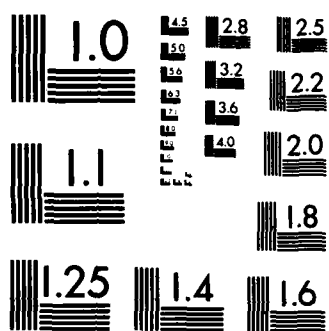
UNCLASSIFIED

AFWAL-TR-83-3036 AFOSR-80-0213

F/G 1/3

NL





MICROCOPY RESOLUTION TEST CHART
NATIONAL BUREAU OF STANDARDS-1963-A

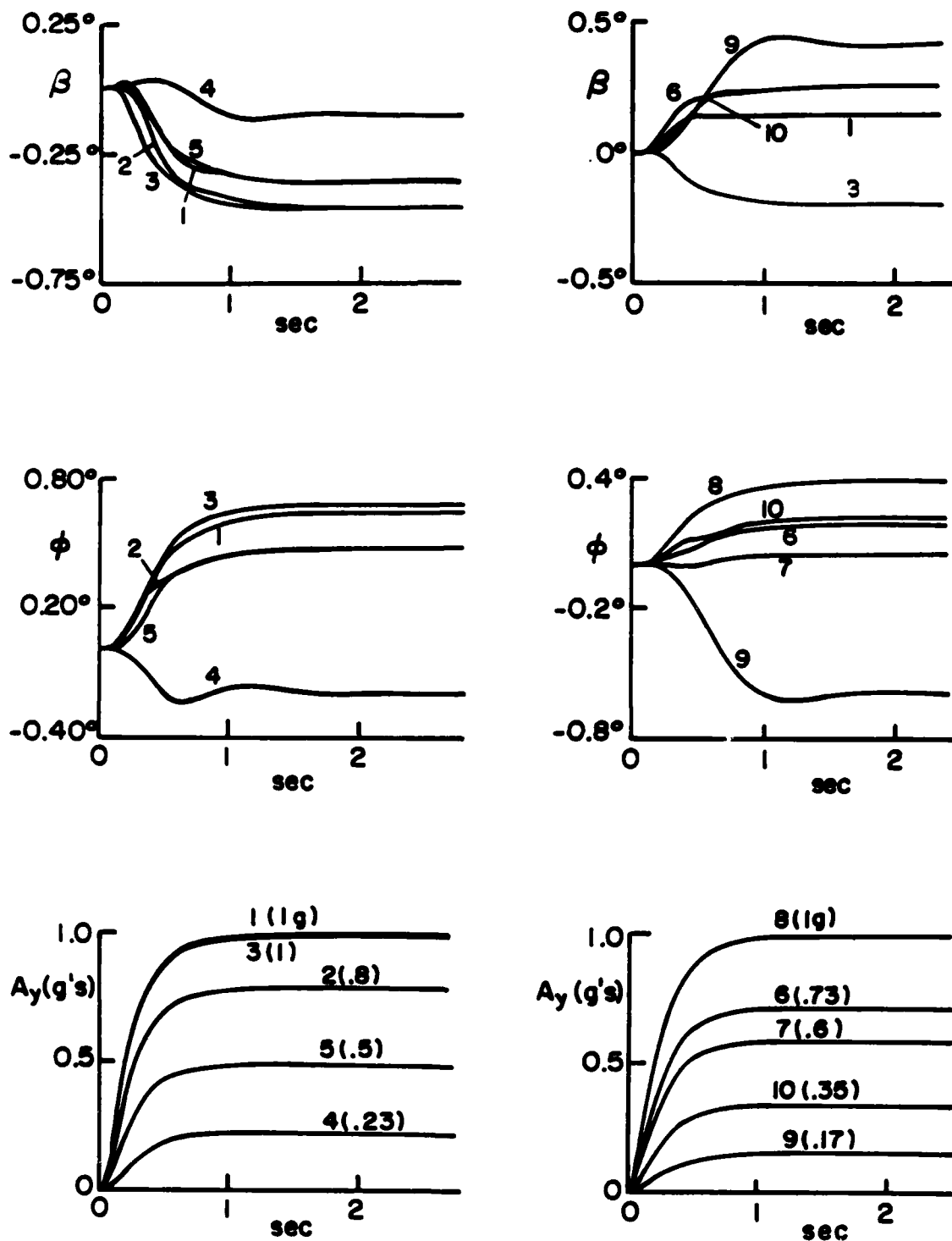


Fig. 2.32a Simulation results for nondiagonal G design:

β , ϕ , A_y

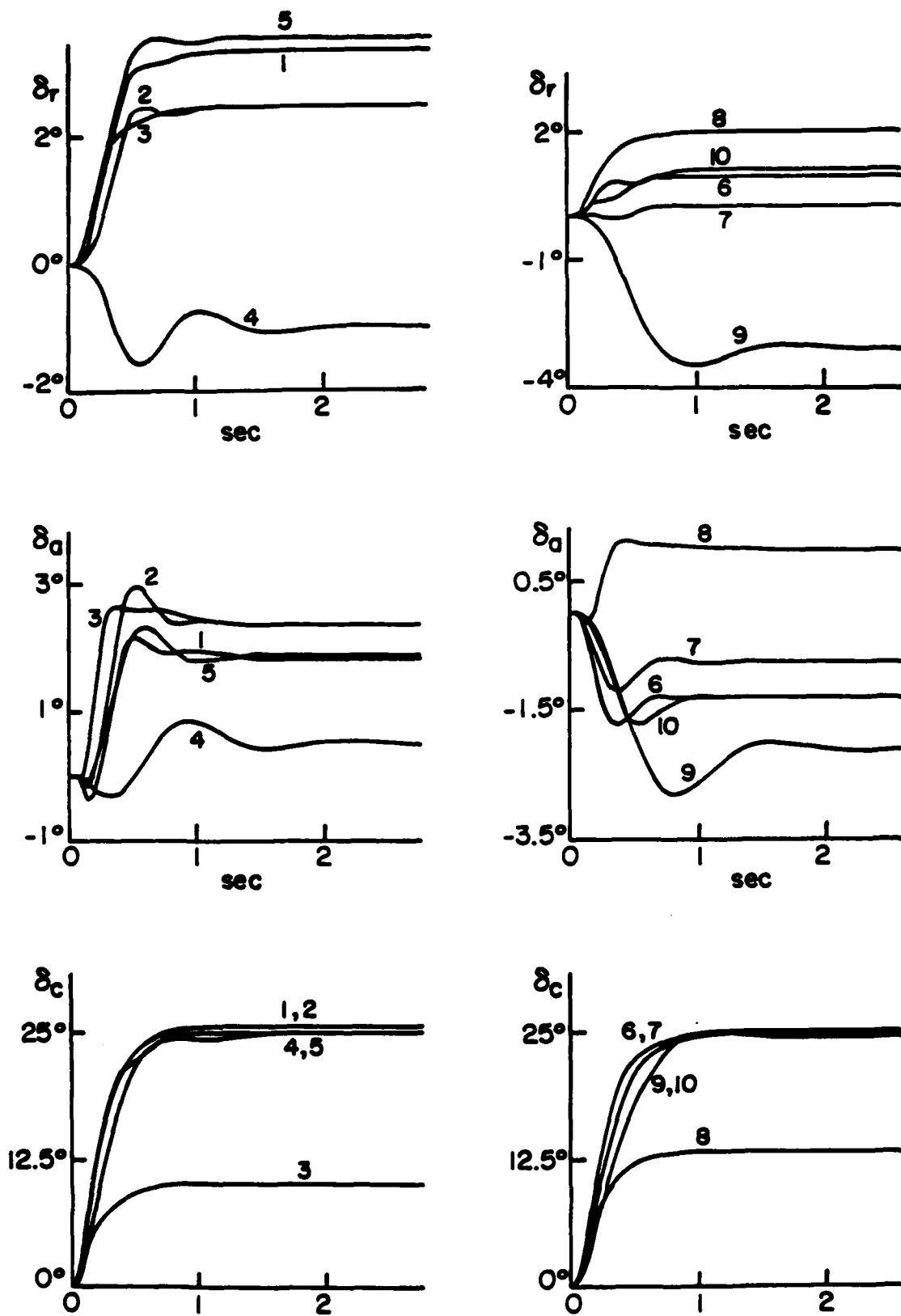


Fig. 2.32b Simulation results for nondiagonal G design:

δ_r , δ_a , δ_c

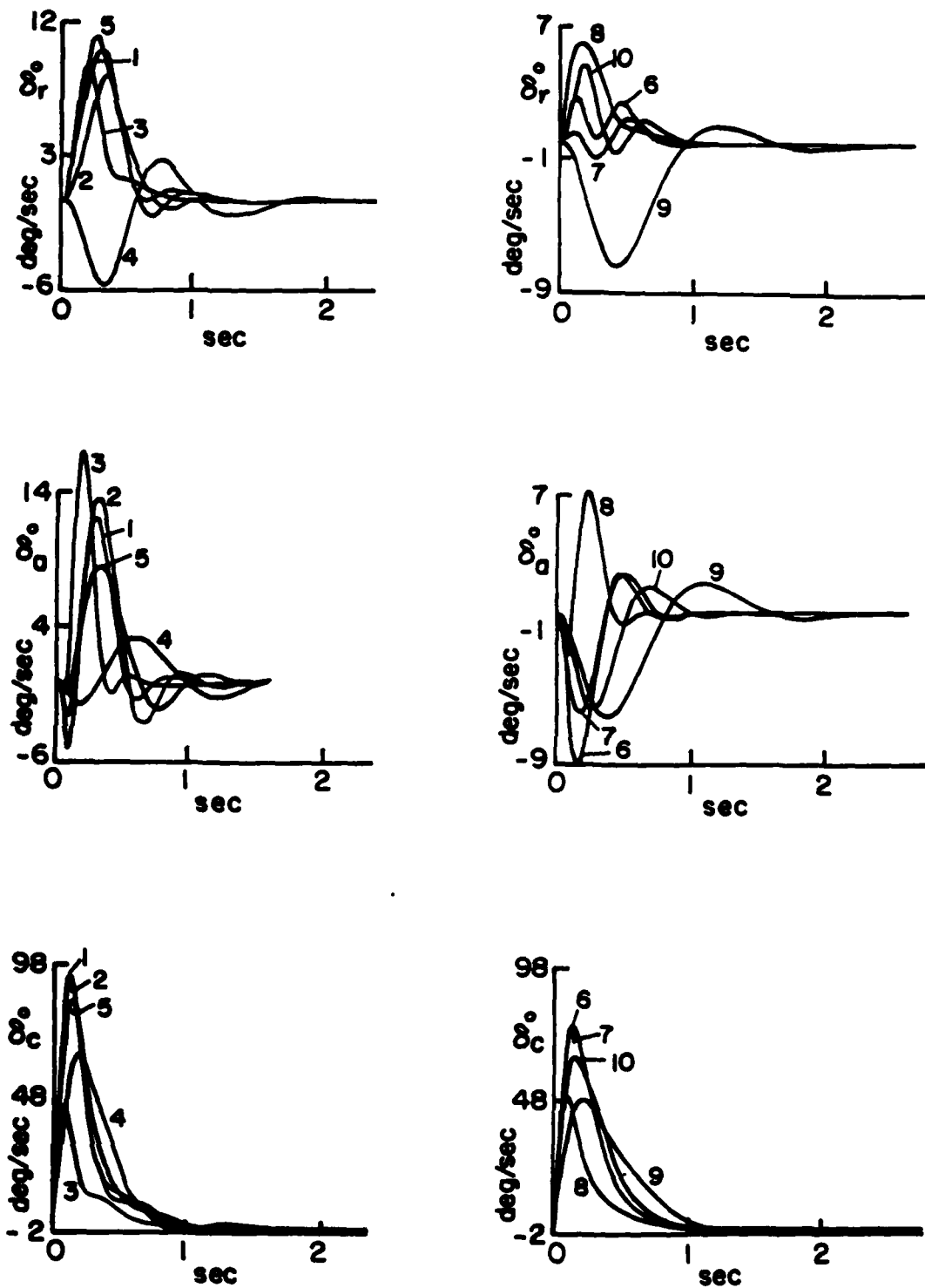


Fig. 2.32c Simulation results for nondiagonal G design:

$\dot{\delta}_r$, $\dot{\delta}_a$, $\dot{\delta}_c$ (commanded A_y values are given in brackets in Fig. 2.32a)

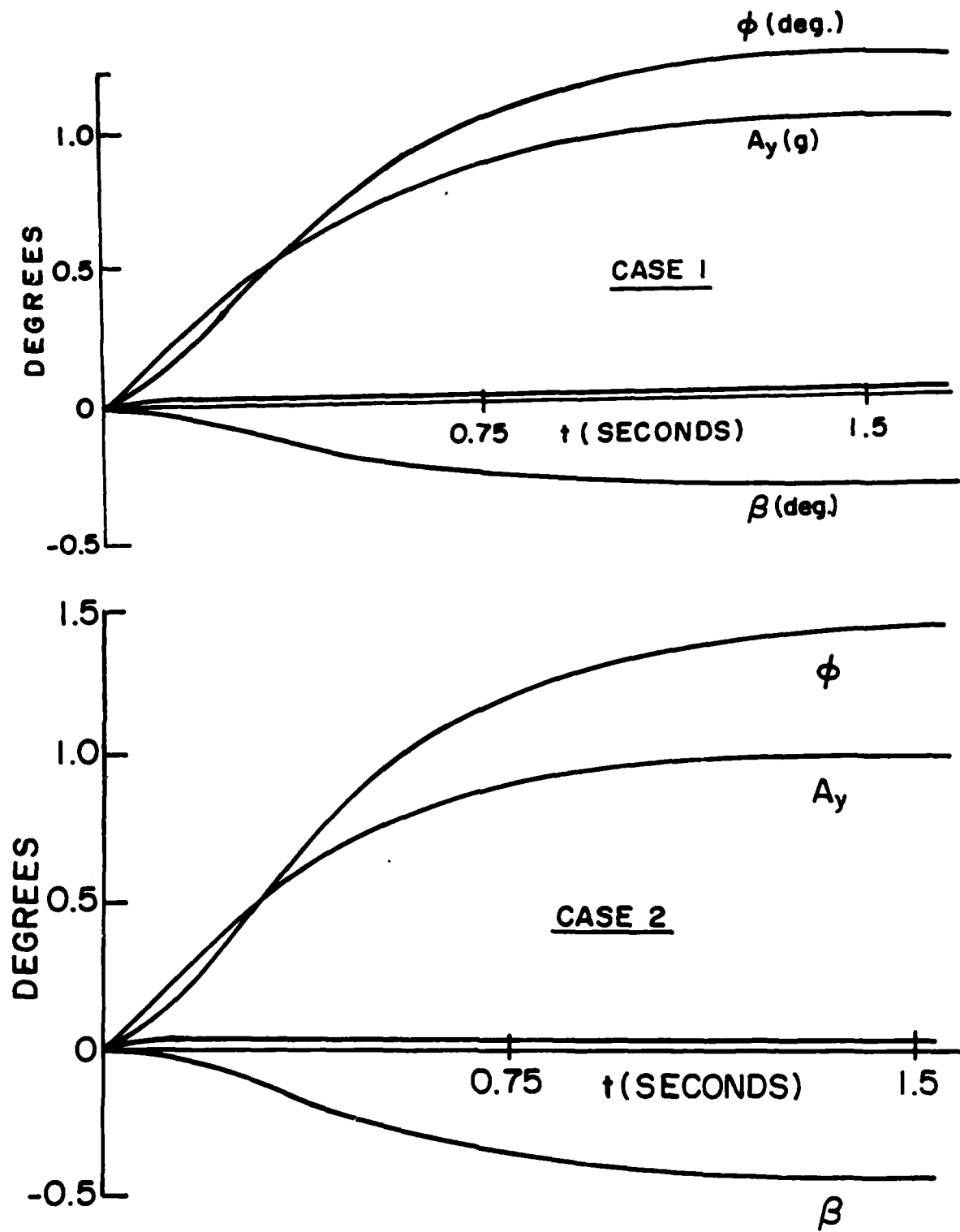


Fig. 2.33 Simulation results for design 1 (β, ϕ, A_y) with $F_3 = F_{3b} = 36/(s+3)(s+12)$

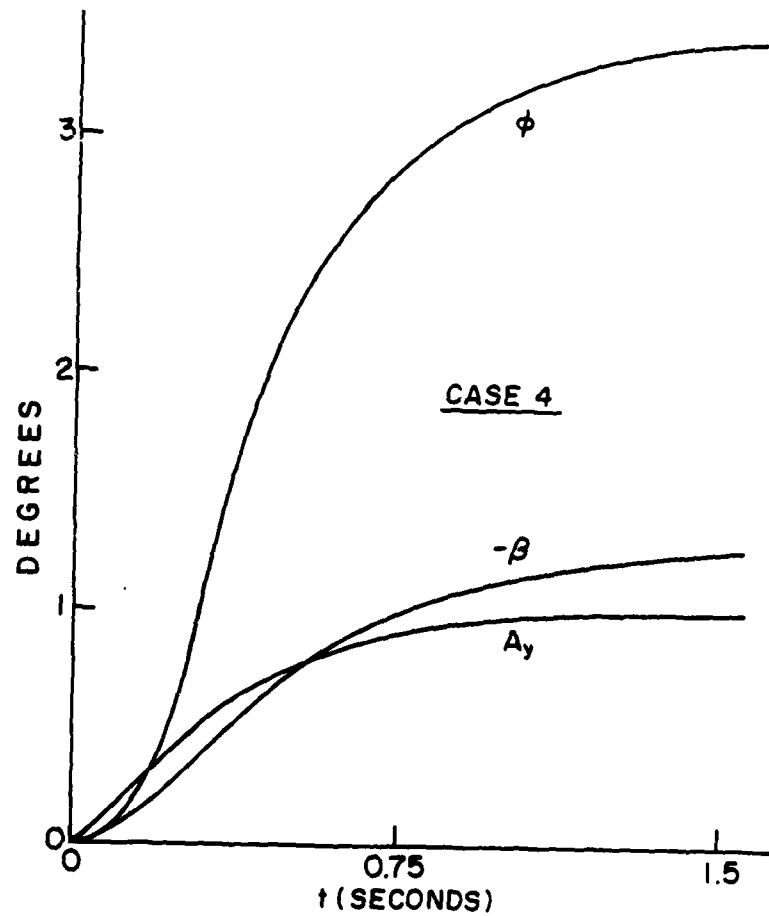
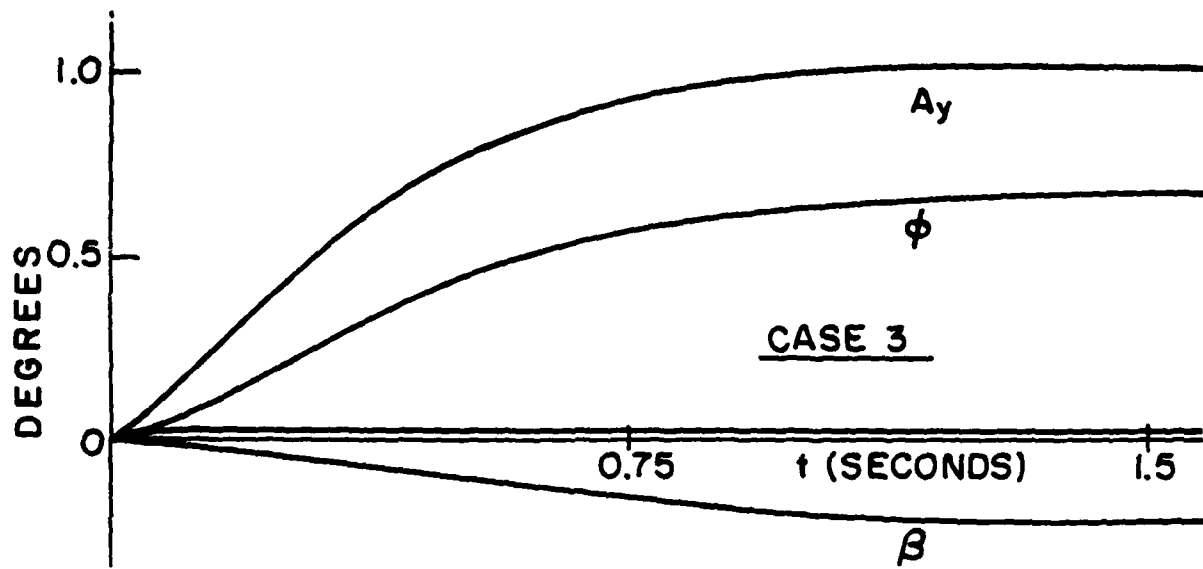


Fig. 2.33 (cont.) Simulation results for design 1 (β, ϕ, A_y) with $F_3 = F_{3b} = 36/(s+3)(s+12)$

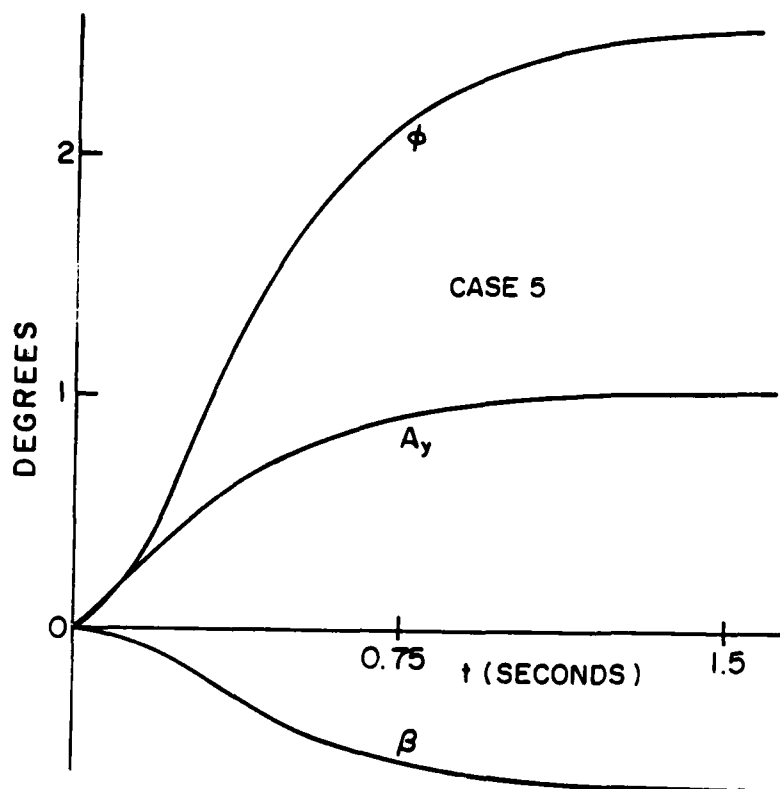


Fig. 2.33 (cont.)
Simulation results for design
1 ($\delta, \dot{\delta}, A_y$) with $F_3 = F_{3b}$
 $= 36/(s+3)(s+12)$

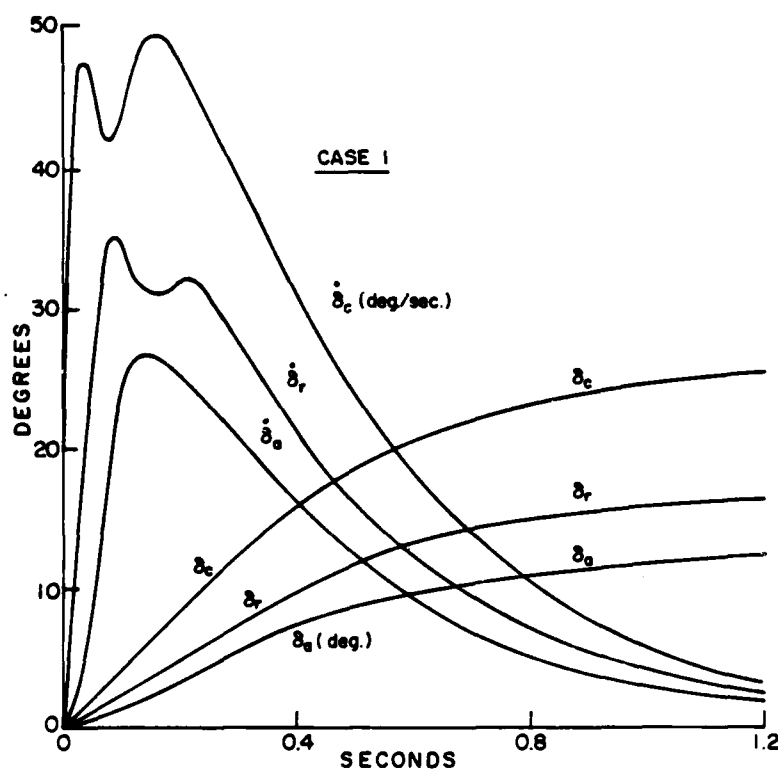


Fig. 2.34 Simulation results for design 1 ($\delta_1, \dot{\delta}_1$) with $F_3 = F_{3b} = 36/(s+3)(s+12)$

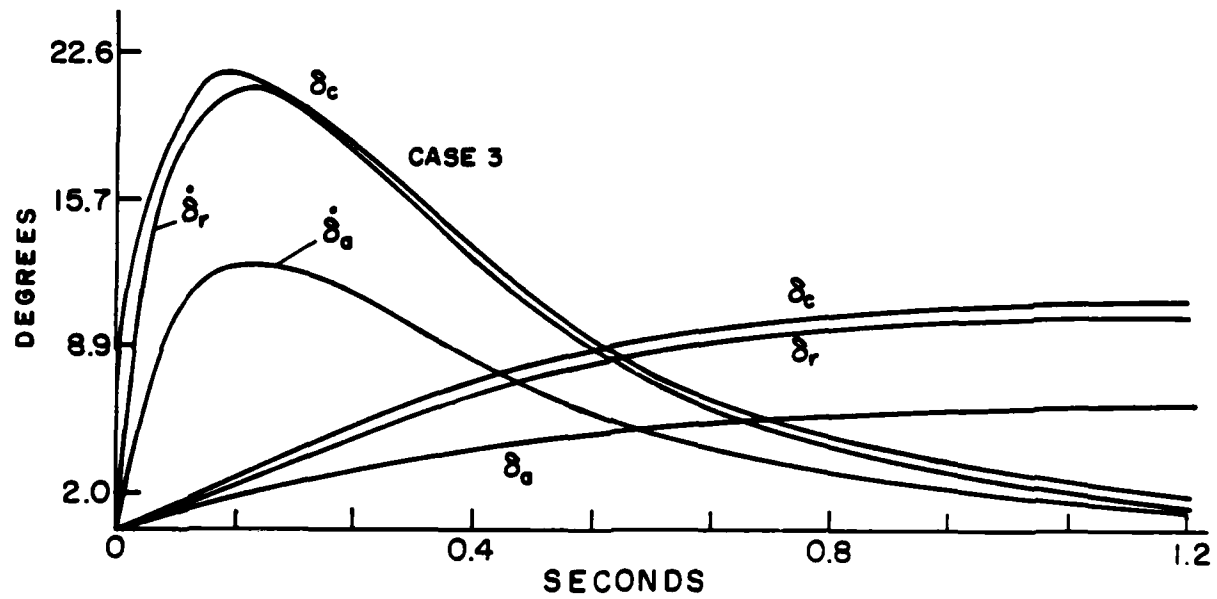
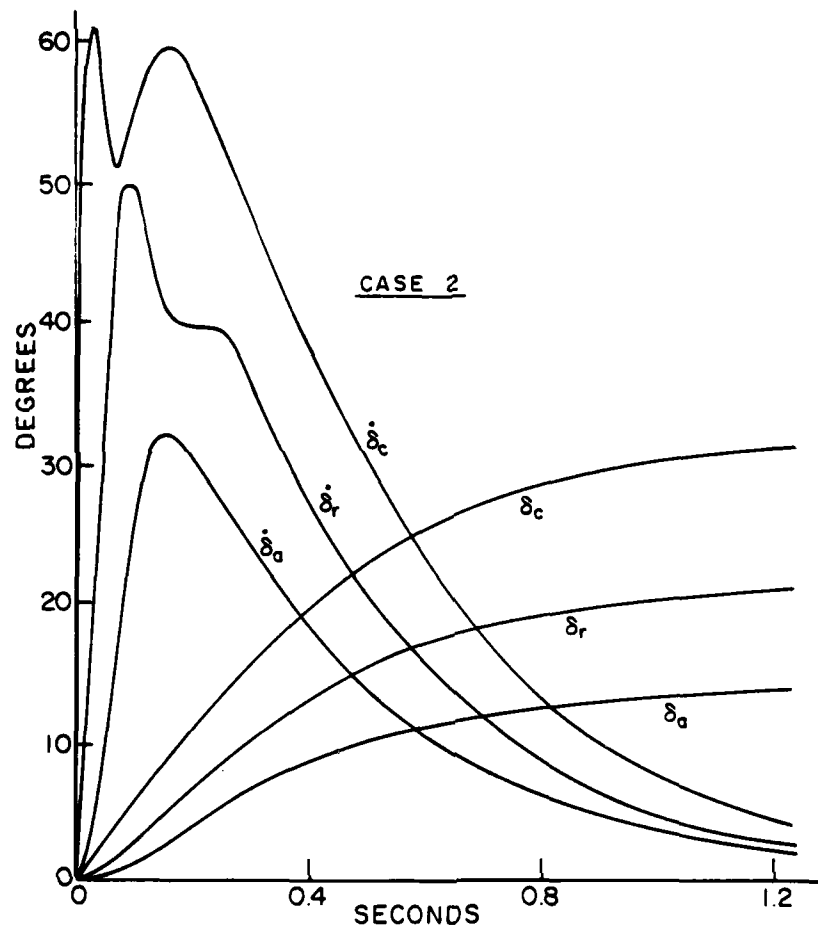


Fig. 2.34 (cont.) Simulation results for design 1 ($\delta_i, \dot{\delta}_i$) with $F_3 = F_{3b} = 36/(s+3)(s+12)$

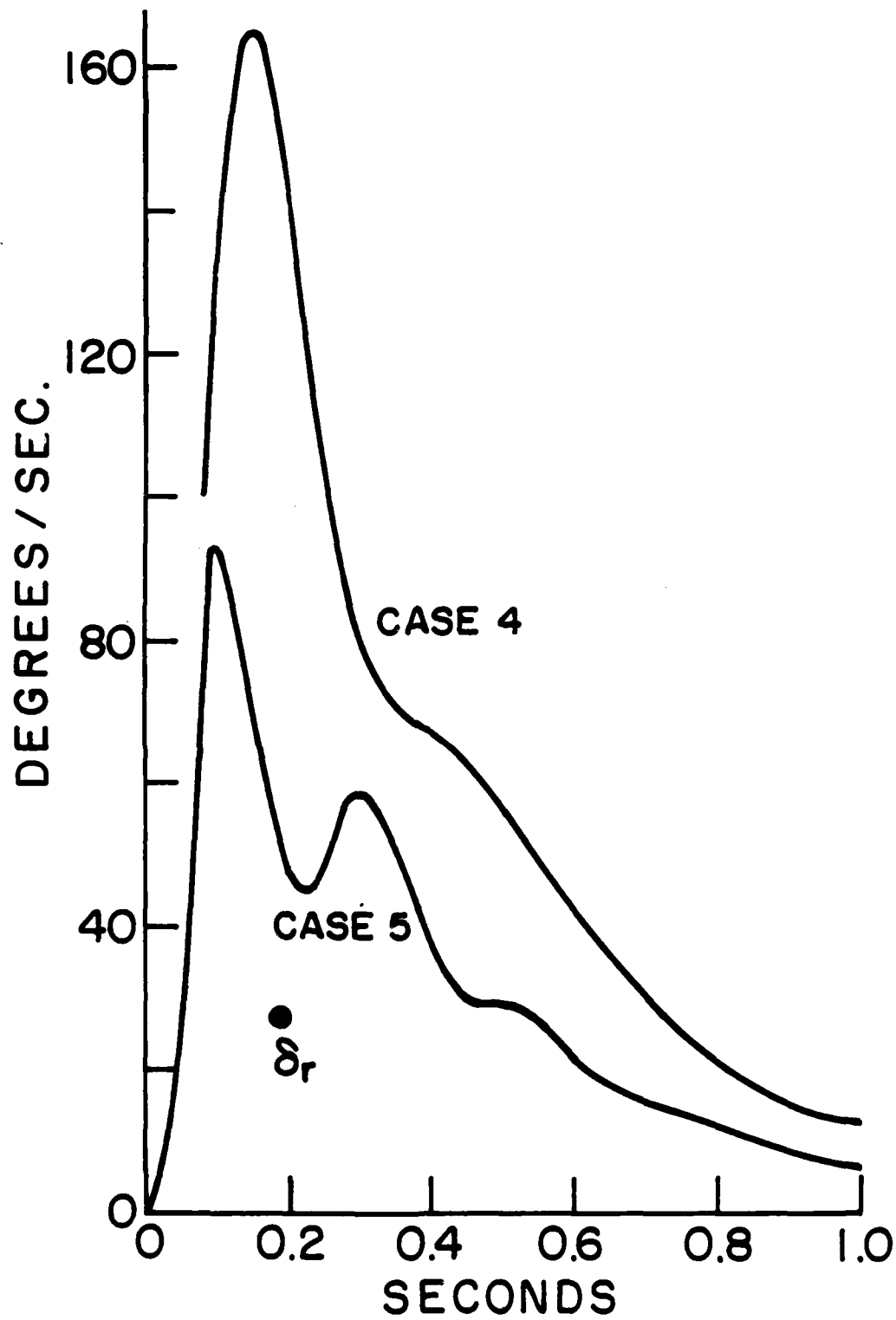


Fig. 2.34 (cont.) Simulation results for design 1 ($\dot{\delta}_1, \dot{\delta}_1$) with $F_3 = F_{3b} = 36/(s+3)(s+12)$

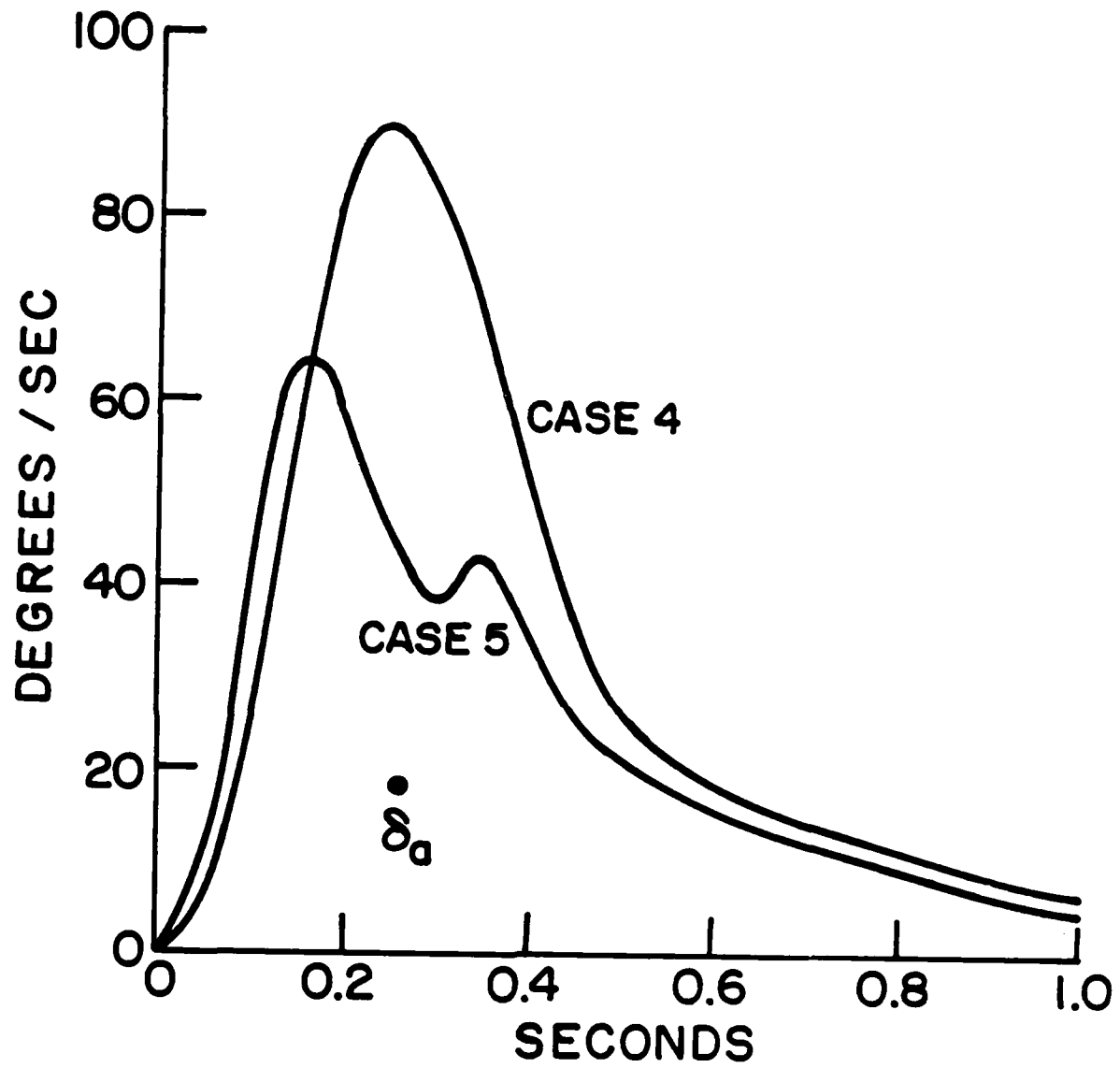


Fig. 2.34 (cont.) Simulation results for design 1 ($\delta_i, \dot{\delta}_i$) with $F_3 = F_{3b} = 36/(s+3)(s+12)$

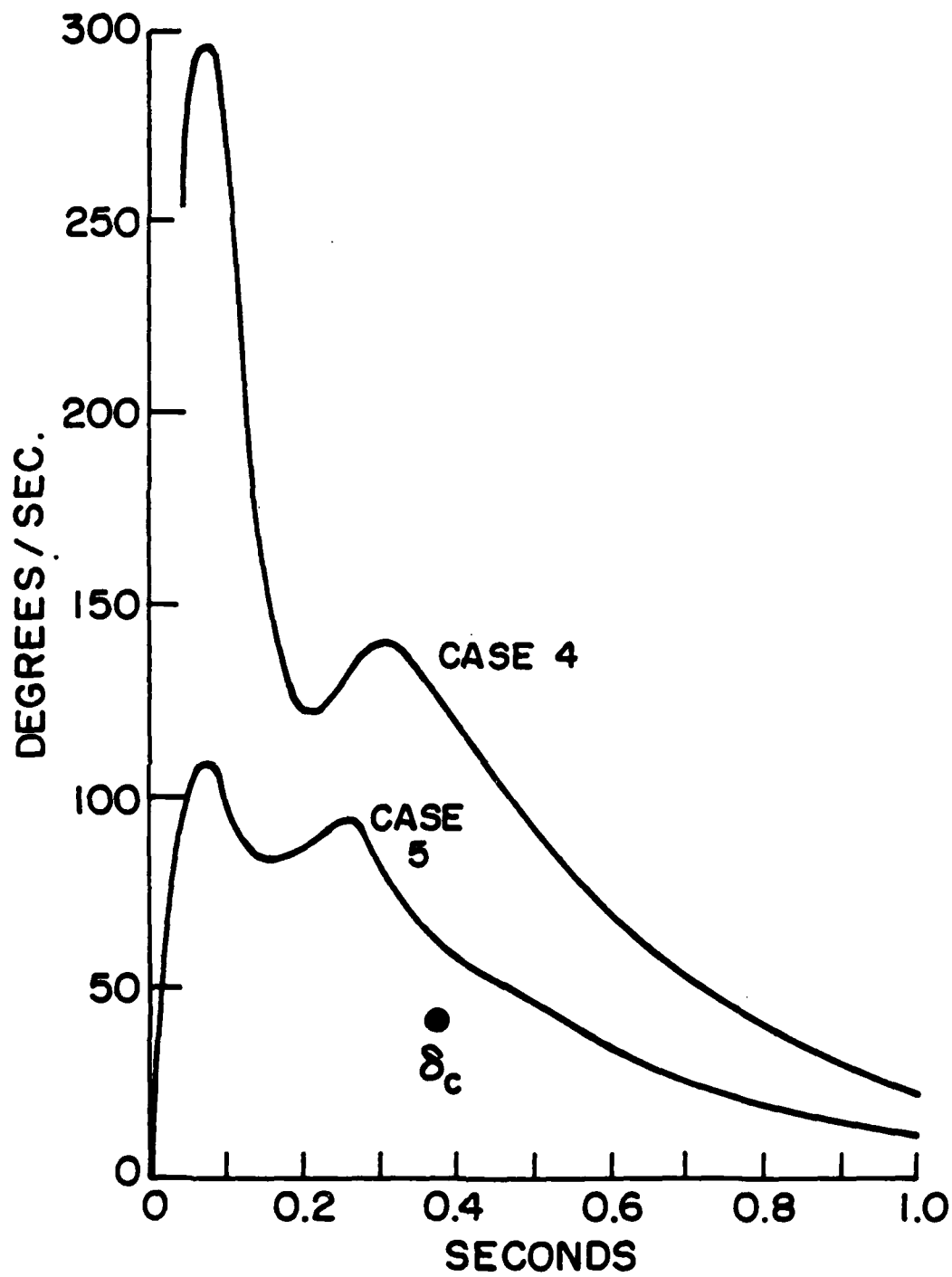


Fig. 2.34 (cont.) Simulation results for design 1 ($\delta_1, \dot{\delta}_1$) with $F_3 = F_{3b} = 36/(s+3)(s+12)$

CHAPTER 3

VERTICAL TRANSLATION MODE (α_2)

Chapter 3 is devoted to a longitudinal mode in which vertical velocity (V_z) and pitch angle (θ) are the output variables of interest. The plant inputs (δ_i control surfaces) are the elevator and flaps (Fig. 3.1).

3.1 Plant equations

The plant equations are gotten from [12, pp. 292-8], modified for inclusion of flaps. The parameters are defined in

$$y = [u, w, \theta]' \quad , \quad \delta = [\delta_e, \delta_f]' \quad (3.1a,b)$$

$$Ay = B\delta \quad , \quad z = [a, \theta] = My \quad (3.2a,b)$$

$$A = \begin{bmatrix} s-X_u & X_w & g \cos \alpha \\ -Z_u & s-Z_w & -Vs \\ 0 & -M_w & s(s-M_q) \end{bmatrix} \quad (2.3)$$

$$B = \begin{bmatrix} X_{\delta} & X_f \\ X_{\delta} & Z_f \\ M_{\delta} & M_f \end{bmatrix} = \frac{\rho S V^2}{2} \begin{bmatrix} \frac{-C_{D\delta}}{m} & \frac{-C_{Df}}{m} \\ \frac{-C_{L\delta}}{m} & \frac{-C_{Lf}}{m} \\ \frac{cC_{M\delta}}{I_y} & \frac{cC_{Mf}}{I_y} \end{bmatrix} \quad (3.4)$$

$$M = \begin{bmatrix} 0 & s & 12.6s^2 - sV \\ 0 & 0 & 1 \end{bmatrix} \quad (3.5)$$

Since P is defined by $z = P\dot{\phi}$, we have $z = M\dot{y} = MA^{-1}B\dot{\phi}$, so

$$P = MA^{-1}B = [P_{ij}] \quad (3.6)$$

$$\left. \begin{aligned} X_u &= -\rho S V C_D / m, & X_w &= \rho S V (C_L - C_{D\alpha}) / 2m \\ X &= -\rho S V^2 C_{D\delta} / 2m, & X_f &= -S V^2 C_{Df} / 2m, \\ M_w &= \rho S c^2 C_{M\dot{\alpha}} / 4I_y, & M_w &= \rho S V c C_{M\alpha} / 2I_y, \\ Z_u &= -\rho S V C_L / m, & Z_w &= -\rho S V (C_{L\alpha} + C_D) / 2m, \\ Z_\delta &= -\rho S V^2 C_{L\delta} / 2m, & Z_f &= -\rho S V^2 C_{Lf} / 2m, \\ M_q &= \rho S V c^2 C_{Mq} / 4I_y, & M_\delta &= \rho S V^2 c C_{M\delta} / 2I_y, \\ Z_{\dot{w}} &= -\rho S c C_{L\dot{\alpha}} / 4m, & M_f &= S V^2 c C_{Mf} / 2I_y \\ & & Z_q &= -S V c C_{Lq} / 4m \end{aligned} \right\} \quad (3.7)$$

$$P_{11} = \frac{\rho S V^2}{2 \det A} [p_{11}(1)s^4 + p_{11}(2)s^3 + p_{11}(3)s^2 + p_{11}(4)s] \quad (3.8a)$$

$$P_{12} = \frac{\rho S V^2}{2 \det A} [p_{12}(1)s^4 + p_{12}(2)s^3 + p_{12}(3)s^2 + p_{12}(4)s] \quad (3.8b)$$

$$P_{21} = \frac{\rho S V^2}{2 \det A} [p_{21}(1)s^2 + p_{21}(2)s + p_{21}(3)] \quad (3.8c)$$

$$P_{22} = \frac{\rho S V^2}{2 \det A} [p_{22}(1)s^2 + p_{22}(2)s + p_{22}(3)] \quad (3.8d)$$

$$\begin{aligned}
 p_{11}(1) &= b_{21} + 12.6b_{31} \\
 p_{11}(2) &= -b_{11}a_{21} - b_{21}(X_u + M_q) - 12.6b_{21}a_{32} - 12.6b_{31}(X_u + Z_w) \\
 p_{11}(3) &= b_{11}(a_{21}M_q + 12.6a_{21}a_{32}) + b_{21}(X_uM_q + 12.6a_{32}X_u + a_{32}V) + \\
 &\quad + b_{31}(12.6X_uZ_w + VZ_w - 12.6a_{12}a_{21}) \\
 p_{11}(4) &= -b_{11}a_{21}a_{32}V - b_{21}a_{32}X_uV + b_{31}(a_{21}a_{13} - VX_uZ_w + a_{12}a_{21}V)
 \end{aligned}
 \quad (3.9a-d)$$

$$\begin{aligned}
 p_{12}(1) &= b_{22} + 12.6b_{32} \\
 p_{12}(2) &= -b_{12}a_{21} - b_{22}(X_u + M_q) - 12.6b_{22}a_{32} - 12.6b_{32}(X_u + Z_w) \\
 p_{12}(3) &= b_{12}(a_{21}M_q + 12.6a_{21}a_{32}) + b_{22}(X_uM_q + 12.6a_{32}X_u + a_{32}V) + \\
 &\quad + b_{32}(12.6X_uZ_w + VZ_w - 12.6a_{12}a_{21}) \\
 p_{12}(4) &= -b_{12}a_{21}a_{32}V - b_{22}a_{32}X_uV + b_{32}(a_{21}a_{13} - VX_uZ_w + a_{12}a_{21}V)
 \end{aligned}
 \quad (3.10a-d)$$

$$\begin{aligned}
 p_{21}(1) &= b_{31} \\
 p_{21}(2) &= -b_{21}a_{32} - b_{31}(X_u + Z_w) \\
 p_{21}(3) &= b_{11}a_{21}a_{32} + b_{21}a_{32}X_u + b_{31}(X_uZ_w - a_{12}a_{21})
 \end{aligned}
 \quad (3.11a-c)$$

$$\left. \begin{aligned} p_{22}(1) &= b_{32} \\ p_{22}(2) &= -b_{22}a_{32}-b_{32}(X_u+Z_w) \\ p_{22}(3) &= b_{12}a_{21}a_{32}+b_{22}a_{32}X_u+b_{32}(X_uZ_w-a_{12}a_{21}) \end{aligned} \right\} \quad (3.12a-c)$$

$$\left. \begin{aligned} \det A &= s^4 - s^3(Z_w M_q + X_u) + s^2 [Z_w M_q + a_{32} V + X_u (Z_w M_q) - a_{21} a_{12}] \\ &\quad - s [X_u (Z_w M_q + V a_{32}) - a_{21} a_{12} M_q] + a_{21} a_{32} a_{13} \end{aligned} \right\} \quad (3.13)$$

$$\left. \begin{aligned} Q_{11} &= \frac{\rho S V^2}{2 \det A} \frac{Q Q}{[p_{22}(1)s^2 + p_{22}(2)s + p_{22}(3)]} \\ Q_{12} &= \frac{-\rho S V^2}{2 \det A} \frac{Q Q}{[p_{12}(1)s^4 + p_{12}(2)s^3 + p_{12}(3)s^2 + p_{12}(4)s]} \\ Q_{21} &= \frac{-\rho S V^2}{2 \det A} \frac{Q Q}{[p_{21}(1)s^2 + p_{21}(2)s + p_{21}(3)]} \\ Q_{22} &= \frac{\rho S V^2}{2 \det A} \frac{Q Q}{[p_{11}(1)s^4 + p_{11}(2)s^3 + p_{11}(3)s^2 + p_{11}(4)s]} \end{aligned} \right\} \quad (3.14a-d)$$

$$\begin{aligned}
 Q(1) &= p_{11}(1)p_{22}(1) - p_{12}(1)p_{21}(1) \\
 Q(2) &= p_{11}(2)p_{22}(1) + p_{11}(1)p_{22}(2) - p_{12}(2)p_{21}(1) - p_{12}(1)p_{21}(2) \\
 Q(3) &= p_{11}(3)p_{22}(1) + p_{11}(2)p_{22}(2) + p_{11}(1)p_{22}(3) - p_{12}(3)p_{21}(1) \\
 &\quad - p_{12}(2)p_{21}(2) - p_{12}(1)p_{21}(3) \\
 Q(4) &= p_{11}(4)p_{22}(1) + p_{11}(3)p_{22}(2) + p_{11}(2)p_{22}(3) - p_{12}(4)p_{21}(1) \\
 &\quad - p_{12}(3)p_{21}(2) - p_{12}(2)p_{21}(3) \\
 Q(5) &= p_{11}(4)p_{22}(2) + p_{11}(3)p_{22}(3) - p_{12}(4)p_{21}(2) - p_{12}(3)p_{21}(3) \\
 Q(6) &= p_{11}(4)p_{22}(3) - p_{12}(4)p_{21}(3) \\
 QQ &= Q(1)s^6 + Q(2)s^5 + Q(3)s^4 + Q(4)s^3 + Q(5)s^2 + Q(6)s
 \end{aligned}
 \tag{3.15a-g}$$

3.2 Flight conditions

As in Chapter 2, there are five different combinations of mach and altitude. The aerodynamic coefficients C_{Li} , C_{Mi} , C_{Di} of the Tables below are functions of the elevator and flap angles, and were supplied for five different values of elevator angle and for two of flap angle. Since these surfaces work generally in opposite directions, only such combinations were used, giving a total of five cases for each of the five flight conditions - a total of 25 different sets of plant parameter values. Some of the data common to both the lateral and longitudinal modes, has already been listed in Table 2.2, so is not repeated in Table 3.1.

Table 3.1

FIGHTER CCV TRIMMED AERO DATA

(see Table 2.2)

Flight conditions	1a-e	2a-e	3a-e	4a-e	5a-e
Mach	.6	.8	.9	.6	.9
Altitude(ft)	0	20000	0	30000	30000
Impact P, Q_c	582.98	510.38	1462.84	173.48	435.30
P/P_0	1.000	.460	1.000	.298	.298
Q_c/P_s	.276	.524	.691	.276	.691
Vel(V) ft/sec.	669.84	828.32	1004.76	596.94	895.41
C_L	.13061	.15974	.05805	.43891	.19507
C_D	.03887	.04118	.03893	.07175	.04336
α (deg.)	1.89033	2.14492	.90073	6.12879	2.46976
DH	-1.06832	-1.10976	-1.98904	.14267	-1.75449
L.E. Flap	.60491	0	0	6.60607	0
$C_{L\alpha}$ (1/deg.)	.07093	.07477	.08044	.07437	.08292
$C_{M\alpha}$ (1/deg.)	.00373	.00384	.00320	.00484	.00380
$C_{D\alpha}$ (1/deg.)	.00289	.00329	.00276	.01256	.00283
$C_{L\dot{\alpha}}$ (1/rad.)	1.30081	1.05000	1.30000	1.20421	1.37000
$C_{M\dot{\alpha}}$ (1/rad.)	-1.41235	-1.55333	-2.2600	-1.26443	-2.37000

Con't Table 3.1

	<u>1a-e</u>	<u>2a-e</u>	<u>3a-e</u>	<u>4a-e</u>	<u>5a-e</u>
C_{Lq} (1/rad.)	3.48856	3.78339	4.61065	3.47297	4.72313
C_{Mq} (1/rad.)	-3.93490	-4.15044	4.96202	-3.94221	-5.10697
elev=-20					
$C_{L\delta}$ (1/deg.)	.00631	.00613	.00544	.00761	.00610
$C_{M\delta}$ (1/deg.)	-.00753	-.00717	-.00700	-.00824	-.00754
$C_{D\delta}$ (1/deg.)	-.00188	-.00183	-.00193	-.00118	-.00180
elev = -10:					
$C_{L\delta}$ (1/deg.)	.00872	.00941	.00815	.00951	.00860
$C_{M\delta}$ (1/deg.)	-.01043	-.01083	-.00995	-.01095	-.01139
$C_{D\delta}$	-.00086	-.00086	-.00106	-.00007	-.00080
elev = +10:					
$C_{L\delta}$ (1/deg.)	.01035	.01016	.00926	.01032	.00990
$C_{M\delta}$	-.01184	-.01247	-.01216	-.01250	-.01319
$C_{D\delta}$.00158	.00186	.00136	.00239	.00199

Con't Table 3.1

	<u>1a-e</u>	<u>2a-e</u>	<u>3a-e</u>	<u>4a-e</u>	<u>5a-e</u>
elev = +20					
$C_{L\delta}$ (1/deg.)	.00771	.00740	.00694	.00757	.00701
$C_{M\delta}$	-.00921	-.00938	-.00902	-.00933	-.00981
$C_{D\delta}$.00242	.00253	.00228	.00313	.00259
elev = +30:					
$C_{L\delta}$ (1/deg.)	.00625	.00623	.00615	.00597	.00630
$C_{M\delta}$	-.00720	-.00717	-.00731	-.00729	-.00755
$C_{D\delta}$.00264	.00256	.00241	.00328	.0026
flap = +10:					
C_{L_f} (1/deg.)	.01132	.01184	.00796	.01168	.01130
C_{M_f} (1/deg.)	-.00096	-.00185	-.00205	-.00051	-.00254
C_{D_f} (1deg.)	.00058	.00074	.00072	.00116	.00109
flap = -10					
C_{L_f} (1/deg.)	.01300	.01444	.00796	.01510	.01600
C_{M_f}	-.00093	-.00154	-.00205	-.00041	-.00265
C_{D_f}	.00002	.00007	.00072	.00074	.00005

Con't Table 3.1

A total of 25 flight conditions were taken $1a, b, \dots e$; $2a, \dots e$; \dots ; $5a, \dots e$, where cases $a-e$ are due to the following 5 combinations of Elev. and Flap:

Case	Elev.	Flap
a	-20	+10
b	-10	10
c	10	-10
d	20	-10
e	30	-10

3.3 Transfer functions for 25 flight conditions

The transfer functions for the 25 flight conditions of Sec. 3.2, are in Appendix 3.1. Those of the elements p_{ij} of $P = [p_{ij}]$, as well as those of the inverse $P^{-1} = [1/p_{ij}]$ are presented. "gain" refers to the high-frequency gain factor. Thus $p_{ij} \rightarrow k_{ij}/s^{e_{ij}}$ as $s \rightarrow \infty$, and "gain" refers to k_{ij} for p_{ij} or Q_{ij} , as the case may be.

3.4 Problem statement and response specifications

The original problem statement was "Vertical velocity $v_z = \int_0^t A_n dt$ is commanded. This is to be achieved with very small effect on the pitch (θ) angle -would like 0.1° max., but $.5^\circ$ may have to be accepted. The elevator and flap are needed for this purpose. For test results and responses see " α_2 mode response" (Fig. 3.2b here) -- try for steady state achieved in < 4 seconds, hopefully in 2 seconds. Re maximum values, see how much can be done. About 25ft/sec. rate of climb was about the maximum achieved in test results, but more would be desirable".

Suppose we allow $.165^\circ$ for θ due to 25 ft/sec. Then b_{21} of Chapter 1 (the equivalent of Table 1.1 for $n = 2$, and of Eq. 1.2) is

$$b_{21} = \frac{.165}{57.3 \times 25} = (1.15)10^{-4} \quad (-78.7\text{db}) \quad (3.16a)$$

To find (a_{11}, b_{11}) , suppose we use a critically damped second-order model, and ask for 90% response in 2.8 seconds. From the response curves at $\zeta = 1$ e.g. [13, p. 200], this corresponds to $\omega_n 2.8 = 4$, so $\omega_n = 1.4$. We shall use $\omega_n = 1.4$, i.e. the $T_{11}(s)$ model is

$$T_{11}(s) = \frac{(1.4)^2}{s^2 + 2(1.4)s + (1.4)^2} \quad (3.16b)$$

and shall use $|T_{11}(j\omega)| = b_{11}(\omega)$, because preliminary examination indicates that as in Chapter 2, $|L_{11}(j\omega)|$ (here, cf. $L_{33}(j\omega)$; there) will be very large, so $\Delta T_{11}(j\omega)$ due to varying flight conditions will be small over the important ω range. Accordingly, $b_{11}(\omega) = |T_{11}(j\omega)|$ is sketched in Fig. 3.2a.

3.5 Bounds and design of $L_{20}(j\omega)$

The equivalent (for $n = 2$) of D_{21} of Table 1.1 is used, written as

$$|1 + L_2| \geq \frac{b_{11}}{b_{21}} \left| \frac{Q_{22}}{Q_{21}} \right|, \quad L_2 = G_2 Q_{22} \quad (3.17a)$$

In the low ω range, $|L_2| \gg 1$ so write $|1 + L_2| \doteq |L_2| = |G_2 Q_{22}|$, so (3.17a) can be written

$$|G_2(j\omega)| \geq \left| \frac{b_{11}}{b_{21} Q_{21}(j\omega)} \right| = \frac{(.86)10^4 b_{11}}{|Q_{21}|} \quad (3.17b)$$

Clearly, at any given ω , $\min |Q_{21}|$ is needed, so we prepare asymptotic plots of $|Q_{21}(j\omega)|$. This was done only in cases 1a to 5a, shown in Fig. 3.3. We also want to check when the approximation $|1 + G_2 Q_{22}| \doteq |G_2 Q_{22}|$ is no longer valid, so similarly prepare asymptotic plots of $|Q_{22}|$, shown in Fig. 3.4. Case 4a was chosen as the nominal case. With these sketches, it was relatively easy to prepare Table 3.2 based only on Cases 1a-5a.

Table 3.2
Calculation of bounds on $L_{20}(j\omega)$

ω	b_{11} (db)	$ Q_{21} _{\min}$ (db)	$ G_2 _{\text{Bound}}$ (3.17b) (db)	$ G_2 Q_{22} _{\min}$ (db)	$ Q_{220} $ (db)	$ L_{20} $ (db)
0	0	24	54.7	21.7	-25.3	29.4
.01	0	30	48.7	23.7	-20	28.7
.05	0	35	43.7	25.7	-17	26.7
.1	0	38	40.7	22.7	-17	23.7
.2	0	39	39.7	21.7	-17	22.7
1	-3.5	33	42.2	24.2	-17	25.7
2	-10	27	41	23	-17	24
5	-25	20	33.7	15.7	-20	13.7

For $\omega \geq 10$, we use the constraint $|1 + L_{20}|^{-1} < 5 \text{ db}$, and use the templates of Q_{22} to obtain the bounds on $L_{20}(j\omega)$, which are shown in the Nichols Chart in Fig. 3.5. Some templates of Q_{22} needed for this purpose, are shown in Fig. 3.6. Note that L_{20} has a half-plane pole, which must be present in L_{20} , so $\text{Arg } L_{20} = -180^\circ$ at $\omega = 0$. By cut and try a $L_{20}(j\omega)$ which satisfies the bounds of Fig. 3.5, was found. Its Bode plot is shown in Fig. 3.7, and it is also shown in Fig. 3.5. The resulting $|G_2(j\omega)|$ is sketched in Fig. 3.8. The dashed lines show the greater reduction of $|G_2(j\omega)|$ vs ω that may be achieved (should this be important) by adding a zero at -400 and a pair of complex poles with $\zeta = .3$ and $\omega_n = 800$.

3.6 Design of G_1 , F_1

The exact equation for $T_{11}(s)$ is used to determine $L_{10}(s)$. It is

$$T_{11}(s) = \frac{F_1 L_1 (1+L_2)}{(1+L_1)(1+L_2) - \gamma}, \quad \gamma = \frac{Q_{11} Q_{22}}{Q_{12} Q_{21}}, \quad L_i = G_i Q_{ii}. \quad (3.18a-c)$$

This can be manipulated into

$$T_{11}(s) = \frac{F_1 L_1^*}{1+L_1^*}, \quad L_1^* = \frac{L_1}{1 - \frac{\gamma}{1+L_2}}. \quad (3.19a,b)$$

Since (3.19a) is exactly the expression for a single loop system with plant

$$Q_{11}^* = \frac{Q_{11}}{1 - \frac{\gamma}{1+L_2}}, \quad (3.20)$$

single-loop synthesis theory [3] may be used to find the bounds on

$$L_{10}^* = G_1 Q_{110}^*,$$

$$\left. \begin{aligned} Q_{110}^* &= \frac{Q_{110}}{1 - \frac{\gamma_0}{1+L_{20}}} , \\ \gamma_0 &= \frac{Q_{110} Q_{220}}{Q_{120} Q_{210}} \end{aligned} \right\} \quad (3.11.5)$$

To do such a design, the templates of Q_{11}^* are needed, and are available because L_{20} is known. Some of these templates of Q_{11}^* are shown in Fig. 3.9. The small circle marks the nominal Q_{110}^* . In order to get an idea of how large G_1 in $L_1^* = G_1 Q_{11}$ must be, in order to handle the $T_{11}(j\omega)$ problem, we sketch $Q_{110}^*(j\omega)$ in Fig. 3.10, and see that it is very large over the bandwidth of $T_{11}(j\omega)$. A Nyquist sketch of Q_{110}^* makes it obvious that it has a net right half-plane pole; excess of right half-plane poles over right half-plane zeros = 1, so $Q_{110}^*(s)$ was factored on the computer and found to have a pole at 3.94 (due to Q_{220})

There is no need to find bounds on L_{10}^* , because it is so easy to have $|L_1^*/(1+L_1^*)|$ almost invariant over the significant ω range of $T_{11}(j\omega)$. Rather $G_1(j\omega)$ is simply chosen to achieve reasonable stability margins for T_{11} over the various flight conditions. The correspondingly $L_{10}^*(j\omega)$ chosen is sketched in Fig. 3.11. The locus of the templates of $L_1^* = G_1 Q_{11}^*(j\omega)$, is shown in Fig. 3.12, with the triangles marking L_{10}^* .

Finally $F_1(s)$ is chosen to achieve $T_{11}(j\omega)$ of Fig. 3.3.

The compensation functions for the above design, are:

$$\left. \begin{aligned} G_1(s) &= \frac{-(1 + \frac{s}{35})(1 + \frac{s}{1500})}{(1 + \frac{s}{70})(1 + \frac{s}{300})(1 + \frac{s}{3000})} \\ G_2(s) &= \frac{230(1 + \frac{s}{4.5})(1 + \frac{s}{4})(1 + \frac{s}{80})}{(1 + \frac{s}{.6})(1 + \frac{s}{40}) \left[1 + \frac{s}{350} + \left(\frac{s}{350} \right)^2 \right]} \\ F_1(s) &= \frac{1}{1 + \frac{2s}{1.4} + \left(\frac{s}{1.4} \right)^2} \end{aligned} \right\} \quad (3.22a-c)$$

3.7 Simulation results

Computer simulations of the design are shown in Fig. 3.13 for commanded V_z of 25 ft/sec. and it is seen that the specifications of Sec. 3.4 are remarkably well satisfied. Also, for this V_z command of 25 ft/sec., the saturation value of $\delta_f(20^\circ)$ is exceeded moderately only for Case 3 (mach .9; alt. 0 ft). The rate saturation value $\dot{\delta}_f(56^\circ/\text{sec})$ is exceeded only for Case 4 (mach .6; alt. 30,000 ft.)

Fig. 3.14 shows the faster responses achieved by using the faster prefilter $F_1 = 1.4/(s + 1.4)$. In both cases, the results are highly satisfactory.

APPENDIX 3.1

Transfer Functions for 25 Flight Conditions

$$\dot{X} = AX + BU, \quad Y = CX + DU, \quad X = [x_1, x_2, x_3]^T, \quad U = [u_1, u_2]^T, \quad P^{-1} = [p_{ij}]_{ij}$$

"Gain" refers to high-frequency gain factor.

```

CASE No. 10          (A,B) MEANS A+JB
-----
P11 = -277.
ZEROS OF P11
(-0.404E+01, 0.0)   ( 0.142E+01, 0.0)
(-0.155E-01, 0.0)   ( 0.0, 0.0)
POLES OF P11
(-0.404E+01, 0.0)   ( 0.142E+01, 0.0)
(-0.155E-01, -0.755E-01) (-0.155E-01, 0.755E-01)
GAIN P11 = -184.
ZEROS OF P12
(-0.404E+01, 0.0)   ( 0.352E+01, 0.0)
(-0.257E-01, 0.0)   ( 0.0, 0.0)
POLES OF P12
(-0.404E+01, 0.0)   ( 0.142E+01, 0.0)
(-0.155E-01, -0.755E-01) (-0.155E-01, 0.755E-01)
GAIN P12 = -14.9
ZEROS OF P21
(-0.157E+01, 0.0)   (-0.306E-01, 0.0)
POLES OF P21
(-0.404E+01, 0.0)   ( 0.142E+01, 0.0)
(-0.155E-01, -0.755E-01) (-0.155E-01, 0.755E-01)
GAIN P21 = -1.90
ZEROS OF P22
(-0.244E+01, 0.0)   (-0.272E-01, 0.0)
POLES OF P22
(-0.404E+01, 0.0)   ( 0.142E+01, 0.0)
(-0.155E-01, -0.755E-01) (-0.155E-01, 0.755E-01)

```

GAIN Q11 = 0.116E+04
Q11(0) = C.
ZERGES OF Q11
(-0.211E-01, 0.0) (0.0 , 0.0)
POLES OF Q11
(-0.244E+01, 0.0) (-0.272E-01, 0.0)
GAIN Q12 = -12.1
Q12(0) = -20.5
ZERGES OF Q12
(-0.211E-01, 0.0)
POLES OF Q12
(-0.480E+01, 0.0) (0.352E+01, 0.0)
(-0.253E-01, 0.0)
GAIN Q21 = -148.
Q21(0) = C.
ZERGES OF Q21
(-0.211E-01, 0.0) (0.0 , 0.0)
POLES OF Q21
(-0.157E+01, 0.0) (-0.306E-01, 0.0)
GAIN Q22 = 8.
Q22(0) = 3.70
ZERGES OF Q22
(-0.211E-01, 0.0)
POLES OF Q22
(-0.829E+01, 0.0) (0.685E+01, 0.0)
(-0.277E-01, 0.0)

CASE NO. 18

(A,B) MEANS A+JB

GAIN P11 = -384.

ZERGES OF P11

(-0.329E+01, 0.0) (0.686E+01, 0.0)
(-0.263E-01, 0.0) (0.0 , 0.0)

POLES OF P11

(-0.404E+01, 0.0) (0.142E+01, 0.0)
(-0.155E-01, -0.755E-01) (-0.155E-01, 0.755E-01)

GAIN P12 = -184.

ZERGES OF P12

(-0.480E+01, 0.0) (0.352E+01, 0.0)
(-0.253E-01, 0.0) (0.0 , 0.0)

POLES OF P12

(-0.404E+01, 0.0) (0.142E+01, 0.0)
(-0.155E-01, -0.755E-01) (-0.155E-01, 0.755E-01)

GAIN P21 = -20.7

ZERGES OF P21

(-0.157E+01, 0.0) (-0.298E-01, 0.0)

POLES OF P21

(-0.404E+01, 0.0) (0.142E+01, 0.0)
(-0.155E-01, -0.755E-01) (-0.155E-01, 0.755E-01)

GAIN P22 = -1.90

ZERGES OF P22

(-0.244E+01, 0.0) (-0.272E-01, 0.0)

POLES OF P22

(-0.404E+01, 0.0) (0.142E+01, 0.0)
(-0.155E-01, -0.755E-01) (-0.155E-01, 0.755E-01)

GAIN Q11 = 0.161E+04
 Q11(0) = C.
 ZERGES OF Q11
 (-0.226E-01, C.0) (0.0 , 0.0)
 POLES OF Q11
 (-0.244E+01, 0.0) (-0.272E-01, 0.0)
 GAIN Q12 = -16.7
 Q12(0) = -27.6
 ZERGES OF Q12
 (-0.226E-01, C.0)
 POLES OF Q12
 (-0.480E+01, 0.0) (0.352E+01, 0.0)
 (-0.253E-01, C.0)
 GAIN Q21 = -148.
 Q21(0) = C.
 ZERGES OF Q21
 (-0.226E-01, C.0) (0.0 , 0.0)
 POLES OF Q21
 (-0.157E+01, 0.0) (-0.258E-01, C.0)
 GAIN Q22 = 8.00
 Q22(0) = 3.70
 ZERGES OF Q22
 (-0.226E-01, C.0)
 POLES OF Q22
 (-0.829E+01, C.0) (0.686E+01, 0.0)
 (-0.268E-01, C.0)

CASE NO. 1C

(A,B) MEANS A+JB

GAIN P11 = -442.

ZERGES OF P11

(-0.82E+01, 0.0) (0.682E+01, 0.0)
 (-0.258E-01, 0.0) (0.0 , 0.0)

POLES OF P11

(-0.404E+01, 0.0) (0.142E+01, 0.0)
 (-0.155E-01, -0.755E-01) (-0.155E-01, 0.755E-01)

GAIN P12 = -207.

ZERGES OF P12

(-0.464E+01, 0.0) (0.336E+01, 0.0)
 (-0.272E-01, 0.0) (0.0 , 0.0)

POLES OF P12

(-0.404E+01, 0.0) (0.142E+01, 0.0)
 (-0.155E-01, -0.755E-01) (-0.155E-01, 0.755E-01)

GAIN P21 = -23.5

ZERGES OF P21

(-0.158E+01, 0.0) (-0.287E-01, 0.0)

POLES OF P21

(-0.404E+01, 0.0) (0.142E+01, 0.0)
 (-0.155E-01, -0.755E-01) (-0.155E-01, 0.755E-01)

GAIN P22 = -1.85

ZERGES OF P22

(-0.261E+01, 0.0) (-0.290E-01, 0.0)

POLES OF P22

(-0.404E+01, 0.0) (0.142E+01, 0.0)
 (-0.155E-01, -0.755E-01) (-0.155E-01, 0.755E-01)

GAIN Q11 = 0.219E+04

Q11(0) = C.

ZERGES OF Q11
(-0.294E-01, C.0) (0.0 , 0.0)

POLES OF Q11
(-0.261E+01, C.0) (-0.290E-01, 0.0)

GAIN Q12 = -19.5

Q12(0) = -29.9

ZERGES OF Q12
(-0.294E-01, C.0)

POLES OF Q12
(-0.464E+01, C.0) (0.336E+01, 0.0)
(-0.272E-01, C.0)

GAIN Q21 = -172.

Q21(0) = C.

ZERGES OF Q21
(-0.294E-01, C.0) (0.0 , 0.0)

POLES OF Q21
(-0.158E+01, 0.0) (-0.287E-01, 0.0)

GAIN Q22 = 9.14

Q22(0) = 4.09

ZERGES OF Q22
(-0.294E-01, C.0)

POLES OF Q22
(-0.824E+01, C.0) (0.682E+01, 0.0)
(-0.258E-01, C.0)

CASE NO. 10

(A,B) MEANS A+JB

GAIN P11 = -339.

ZEROES OF P11

(-0.323E+01, 0.0) (0.586E+01, 0.0)
(-0.252E-01, 0.0) (0.0, 0.0)

POLES OF P11

(-0.404E+01, 0.0) (0.142E+01, 0.0)
(-0.155E-01, -0.755E-01) (-0.155E-01, 0.755E-01)

GAIN P12 = -207.

ZEROES OF P12

(-0.464E+01, 0.0) (0.336E+01, 0.0)
(-0.272E-01, 0.0) (0.0, 0.0)

POLES OF P12

(-0.404E+01, 0.0) (0.142E+01, 0.0)
(-0.155E-01, -0.755E-01) (-0.155E-01, 0.755E-01)

GAIN P21 = -18.3

ZEROES OF P21

(-0.158E+01, 0.0) (-0.281E-01, 0.0)

POLES OF P21

(-0.404E+01, 0.0) (0.142E+01, 0.0)
(-0.155E-01, -0.755E-01) (-0.155E-01, 0.755E-01)

GAIN P22 = -1.85

ZEROES OF P22

(-0.261E+01, 0.0) (-0.290E-01, 0.0)

POLES OF P22

(-0.404E+01, 0.0) (0.142E+01, 0.0)
(-0.155E-01, -0.755E-01) (-0.155E-01, 0.755E-01)

GAIN Q11 = 0.171E+04

Q11(0) = C.

ZEROES OF Q11

(-0.304E-01, 0.0) (0.0 , 0.0)

POLES OF Q11

(-0.261E+01, 0.0) (-0.290E-01, 0.0)

GAIN Q12 = -15.2

Q12(0) = -22.6

ZEROES OF Q12

(-0.304E-01, 0.0)

POLES OF Q12

(-0.464E+01, 0.0) (0.336E+01, 0.0)
(-0.272E-01, 0.0)

GAIN Q21 = -173.

Q21(0) = C.

ZEROES OF Q21

(-0.304E-01, 0.0) (0.0 , 0.0)

POLES OF Q21

(-0.158E+01, 0.0) (-0.281E-01, 0.0)

GAIN Q22 = 9.3

Q22(0) = 4.09

ZEROES OF Q22

(-0.304E-01, 0.0)

POLES OF Q22

(-0.828E+01, 0.0) (0.696E+01, 0.0)
(-0.252E-01, 0.0)

CASE NO. 1E	(A,B)	MEANS	A+JB

GAIN P11 = -268.			
ZEROCES OF P11			
(-0.824E+01, 0.0)	(0.633E+01, 0.0)
(-0.247E-01, 0.0)	(0.0	, 0.0
POLES OF P11			
(-0.404E+01, 0.0)	(0.142E+01, 0.0)
(-0.155E-01, -0.755E-01))	(-0.155E-01, 0.755E-01))
GAIN P12 = -207.			
ZEROCES OF P12			
(-0.464E+01, 0.0)	(0.336E+01, 0.0)
(-0.272E-01, 0.0)	(0.0	, 0.0
POLES OF P12			
(-0.404E+01, 0.0)	(0.142E+01, 0.0)
(-0.155E-01, -0.755E-01))	(-0.155E-01, 0.755E-01))
GAIN P21 = -14.3			
ZEROCES OF P21			
(-0.158E+01, 0.0)	(-0.276E-01, 0.0)
POLES OF P21			
(-0.404E+01, 0.0)	(0.142E+01, 0.0)
(-0.155E-01, -0.755E-01))	(-0.155E-01, 0.755E-01))
GAIN P22 = -1.85			
ZEROCES OF P22			
(-0.261E+01, 0.0)	(-0.290E-01, 0.0)
POLES OF P22			
(-0.404E+01, 0.0)	(0.142E+01, 0.0)
(-0.155E-01, -0.755E-01))	(-0.155E-01, 0.755E-01))

GAIN Q11 = 0.133E+04
Q11(0) = C.
ZERGES OF Q11
(-0.311E-C1, C.0) (0.0 , 0.0)
PCLES OF Q11
(-0.261E+C1, C.0) (-0.290E-C1, 0.0)
GAIN Q12 = -11.9
Q12(0) = -17.4
ZERGES OF Q12
(-0.311E-C1, C.0)
PCLES OF Q12
(-0.464E+C1, C.0) (0.336E+C1, 0.0)
(-0.272E-01, 0.0)
GAIN Q21 = -172.
Q21(0) = C.
ZERGES OF Q21
(-0.311E-C1, C.0) (0.0 , 0.0)
PCLES OF Q21
(-0.158E+C1, 0.0) (-0.276E-C1, 0.0)
GAIN Q22 = 9.17
Q22(0) = 4.09
ZERGES OF Q22
(-0.311E-C1, C.0)
PCLES OF Q22
(-0.824E+01, C.0) (0.683E+C1, 0.0)
(-0.247E-C1, C.0)

CASE NO. 2A

(A,B) MEANS A+JB

GAIN P11 = -217.

ZERGES OF P11

(-0.749E+01, 0.0) (0.649E+01, 0.0)
(-0.167E-01, 0.0) (0.0 , 0.0)

PCLES OF P11

(-0.341E+01, 0.0) (0.155E+01, 0.0)
(-0.105E-01, -0.579E-01) (-0.105E-01, 0.579E-01)

GAIN P12 = -174.

ZERGES OF P12

(-0.493E+01, 0.0) (0.403E+01, 0.0)
(-0.171E-01, 0.0) (0.0 , 0.0)

PCLES OF P12

(-0.341E+01, 0.0) (0.155E+01, 0.0)
(-0.105E-01, -0.579E-01) (-0.105E-01, 0.579E-01)

GAIN P21 = -11.6

ZERGES OF P21

(-0.110E+01, 0.0) (-0.215E-01, 0.0)

PCLES OF P21

(-0.341E+01, 0.0) (0.155E+01, 0.0)
(-0.105E-01, -0.579E-01) (-0.105E-01, 0.579E-01)

GAIN P22 = -3.00

ZERGES OF P22

(-0.140E+01, 0.0) (-0.192E-01, 0.0)

POLES OF P22

(-0.341E+01, 0.0) (0.155E+01, 0.0)
(-0.105E-01, -0.579E-01) (-0.105E-01, 0.579E-01)

GAIN Q11 = 459.

Q11(0) = C.

ZEROES OF Q11

(-0.108E-01, C.C) (0.0 , 0.0)

POLES OF Q11

(-0.140E+01, 0.0) (-0.192E-01, 0.0)

GAIN Q12 = -7.89

Q12(0) = -14.4

ZEROES OF Q12

(-0.108E-01, C.C)

POLES OF Q12

(-0.493E+01, C.C) (0.403E+01, 0.0)
 (-0.171E-01, 0.0)

GAIN Q21 = -118.

Q21(0) = C.

ZEROES OF Q21

(-0.108E-01, C.C) (0.0 , 0.0)

POLES OF Q21

(-0.110E+01, C.C) (-0.215E-01, 0.0)

GAIN Q22 = 6.34

Q22(0) = 4.28

ZEROES OF Q22

(-0.108E-01, C.C)

POLES OF Q22

(-0.749E+01, C.C) (0.649E+01, 0.0)
 (-0.187E-01, 0.0)

CASE NO. 28

(A,B) MEANS A+JB

GAIN P11 = -330.

ZEROES OF P11

(-0.748E+01, 0.0) (0.648E+01, 0.0)
(-0.181E-01, 0.0) (0.0 , 0.0)

POLES OF P11

(-0.341E+01, 0.0) (0.159E+01, 0.0)
(-0.105E-01, -0.579E-01) (-0.105E-01, 0.579E-01)

GAIN P12 = -174.

ZEROES OF P12

(-0.493E+01, 0.0) (0.403E+01, 0.0)
(-0.171E-01, 0.0) (0.0 , 0.0)

POLES OF P12

(-0.341E+01, 0.0) (0.159E+01, 0.0)
(-0.105E-01, -0.579E-01) (-0.105E-01, 0.579E-01)

GAIN P21 = -17.6

ZEROES OF P21

(-0.110E+01, 0.0) (-0.208E-01, 0.0)

POLES OF P21

(-0.341E+01, 0.0) (0.159E+01, 0.0)
(-0.105E-01, -0.579E-01) (-0.105E-01, 0.579E-01)

GAIN P22 = -3.00

ZEROES OF P22

(-0.140E+01, 0.0) (-0.192E-01, 0.0)

POLES OF P22

(-0.341E+01, 0.0) (0.159E+01, 0.0)
(-0.105E-01, -0.579E-01) (-0.105E-01, 0.579E-01)

GAIN Q11 = 691.

Q11(0) = C.

ZERGES OF Q11
(-0.133E-01, C.0) (0.0 , 0.0)

PCLES OF Q11
(-0.140E+01, C.0) (-0.192E-01, C.0)

GAIN Q12 = -11.9

Q12(0) = -20.9

ZERGES OF Q12
(-0.133E-01, C.0)

PCLES OF Q12
(-0.493E+01, C.0) (0.403E+01, 0.0)
(-0.171E-01, C.0)

GAIN Q21 = -118.

Q21(0) = C.

ZERGES OF Q21
(-0.133E-01, C.0) (0.0 , 0.0)

PCLES OF Q21
(-0.110E+01, C.0) (-0.208E-01, 0.0)

GAIN Q22 = 6.29

Q22(0) = 4.28

ZERGES OF Q22
(-0.133E-01, C.0)

PCLES OF Q22
(-0.744E+01, C.0) (0.648E+01, 0.0)
(-0.181E-01, C.0)

CASE NC. 2C

(A,B) MEANS A+JB

GAIN P11 = -372.

ZERGES OF P11

(-0.754E+01, 0.0) (0.654E+01, 0.0)
 (-0.172E-01, 0.0) (0.0 , 0.0)

POLES OF P11

(-0.341E+01, 0.0) (0.159E+01, 0.0)
 (-0.105E-01, -0.579E-01) (-0.105E-01, 0.579E-01)

GAIN P12 = -198.

ZERGES OF P12

(-0.450E+01, 0.0) (0.360E+01, 0.0)
 (-0.193E-01, 0.0) (0.0 , 0.0)

POLES OF P12

(-0.341E+01, 0.0) (0.159E+01, 0.0)
 (-0.105E-01, -0.579E-01) (-0.105E-01, 0.579E-01)

GAIN P21 = -20.2

ZERGES OF P21

(-0.110E+01, 0.0) (-0.200E-01, 0.0)

POLES OF P21

(-0.341E+01, 0.0) (0.159E+01, 0.0)
 (-0.105E-01, -0.579E-01) (-0.105E-01, 0.579E-01)

GAIN P22 = -2.5

ZERGES OF P22

(-0.155E+01, 0.0) (-0.203E-01, 0.0)

POLES OF P22

(-0.341E+01, 0.0) (0.159E+01, 0.0)
 (-0.105E-01, -0.579E-01) (-0.105E-01, 0.579E-01)

GAIN Q11 = 0.123E+04

Q11(0) = C.

ZEROES OF Q11

(-0.210E-01, C.C) (0.0 , 0.0)

POLES OF Q11

(-0.155E+01, 0.0) (-0.203E-01, 0.0)

GAIN Q12 = -15.5

Q12(0) = -22.5

ZEROES OF Q12

(-0.210E-01, C.C)

POLES OF Q12

(-0.450E+01, C.C) (0.360E+01, 0.0)
 (-0.183E-01, C.C)

GAIN Q21 = -152.

Q21(0) = C.

ZEROES OF Q21

(-0.210E-01, 0.0) (0.0 , 0.0)

POLES OF Q21

(-0.110E+01, C.C) (-0.200E-01, 0.0)

GAIN Q22 = 8.27

Q22(0) = 4.19

ZEROES OF Q22

(-0.210E-01, C.C)

POLES OF Q22

(-0.754E+01, C.C) (0.654E+01, 0.0)
 (-0.172E-01, 0.0)

CASE NC. 2D

(A,B) MEANS A+JB

GAIN P11 = -277.

ZERGES OF P11
(-0.757E+C1, 0.0) (0.658E+C1, 0.0)
(-0.167E-C1, 0.0) (0.0 , 0.0)

POLES OF P11
(-0.341E+C1, 0.0) (0.159E+C1, 0.0)
(-0.105E-01, -0.579E-01) (-0.105E-01, 0.579E-C1)

GAIN P12 = -198.

ZERGES OF P12
(-0.450E+01, 0.0) (0.360E+C1, 0.0)
(-0.183E-C1, 0.0) (0.0 , 0.0)

POLES OF P12
(-0.341E+C1, 0.0) (0.159E+01, 0.0)
(-0.105E-01, -0.579E-01) (-0.105E-01, 0.579E-C1)

GAIN P21 = -15.2

ZERGES OF P21
(-0.109E+01, 0.0) (-0.195E-C1, 0.0)

POLES OF P21
(-0.341E+C1, 0.0) (0.159E+C1, 0.0)
(-0.105E-01, -0.579E-01) (-0.105E-C1, 0.579E-C1)

GAIN P22 = -2.5

ZERGES OF P22
(-0.155E+01, 0.0) (-0.203E-C1, 0.0)

POLES OF P22
(-0.341E+01, 0.0) (0.159E+C1, 0.0)
(-0.105E-C1, -0.579E-01) (-0.105E-01, 0.579E-01)

GAIN Q11 = 930.

Q11(0) = 0.

ZEROES OF Q11
 $(-0.221E-01, 0.0)$) (0.0 , 0.0)

POLES OF Q11
 $(-0.155E+01, 0.0)$) $(-0.203E-01, 0.0)$)

GAIN Q12 = -11.7

Q12(0) = -16.4

ZEROES OF Q12
 $(-0.221E-01, 0.0)$)

POLES OF Q12
 $(-0.450E+01, 0.0)$) (0.360E+01, 0.0)
 $(-0.183E-01, 0.0)$)

GAIN Q21 = -153.

Q21(0) = 0.

ZEROES OF Q21
 $(-0.221E-01, 0.0)$) (0.0 , 0.0)

POLES OF Q21
 $(-0.109E+01, 0.0)$) $(-0.195E-01, 0.0)$)

GAIN Q22 = 8.38

Q22(0) = 4.19

ZEROES OF Q22
 $(-0.221E-01, 0.0)$)

POLES OF Q22
 $(-0.757E+01, 0.0)$) (0.658E+01, 0.0)
 $(-0.167E-01, 0.0)$)

CASE NC. 2E

(A,B) MEANS A+JB

GAIN P11 = -218.

ZEROES OF P11

(-0.747E+01, 0.0) (0.649E+01, 0.0)
 (-0.164E-01, 0.0) (0.0 , 0.0)

POLES OF P11

(-0.341E+01, 0.0) (0.159E+01, 0.0)
 (-0.105E-01, -0.579E-01) (-0.105E-01, 0.579E-01)

GAIN P12 = -198.

ZEROES OF P12

(-0.450E+01, 0.0) (0.360E+01, 0.0)
 (-0.183E-01, 0.0) (0.0 , 0.0)

POLES OF P12

(-0.341E+01, 0.0) (0.159E+01, 0.0)
 (-0.105E-01, -0.579E-01) (-0.105E-01, 0.579E-01)

GAIN P21 = -11.6

ZEROES OF P21

(-0.110E+01, 0.0) (-0.192E-01, 0.0)

POLES OF P21

(-0.341E+01, 0.0) (0.159E+01, 0.0)
 (-0.105E-01, -0.579E-01) (-0.105E-01, 0.579E-01)

GAIN P22 = -2.5

ZEROES OF P22

(-0.155E+01, 0.0) (-0.203E-01, 0.0)

POLES OF P22

(-0.341E+01, 0.0) (0.159E+01, 0.0)
 (-0.105E-01, -0.579E-01) (-0.105E-01, 0.579E-01)

GAIN Q11 = 704.

Q11(0) = C.

ZEROES OF Q11
(-0.229E-01, 0.0) (0.0 , 0.0)

POLES OF Q11
(-0.155E+01, 0.0) (-0.203E-01, 0.0)

GAIN Q12 = -8.88

Q12(0) = -12.4

ZEROES OF Q12
(-0.229E-01, 0.0)

POLES OF Q12
(-0.450E+01, 0.0) (0.36CE+01, 0.0)
(-0.193E-01, 0.0)

GAIN Q21 = -151.

Q21(0) = C.

ZEROES OF Q21
(-0.229E-01, 0.0) (0.0 , 0.0)

POLES OF Q21
(-0.110E+01, 0.0) (-0.192E-01, 0.0)

GAIN Q22 = 8.05

Q22(0) = 4.19

ZEROES OF Q22
(-0.229E-01, 0.0)

POLES OF Q22
(-0.747E+01, 0.0) (0.649E+01, 0.0)
(-0.164E-01, 0.0)

CASE NC. 3A

(A,B) MEANS A+JB

GAIN P11 = -567.

ZEROES OF P11

(-0.134E+02, 0.0) (0.109E+02, 0.0)
(-0.442E-01, 0.0) (0.0 , 0.0)

POLES OF P11

(-0.612E+01, 0.0) (0.146E+01, 0.0)
(-0.219E-01, -0.530E-01) (-0.219E-01, 0.530E-01)

GAIN P12 = -368.

ZEROES OF P12

(-0.986E+01, 0.0) (0.749E+01, 0.0)
(-0.427E-01, 0.0) (0.0 , 0.0)

POLES OF P12

(-0.612E+01, 0.0) (0.146E+01, 0.0)
(-0.219E-01, -0.530E-01) (-0.219E-01, 0.530E-01)

GAIN P21 = -31.2

ZEROES OF P21

(-0.264E+01, 0.0) (-0.450E-01, 0.0)

POLES OF P21

(-0.612E+01, 0.0) (0.146E+01, 0.0)
(-0.219E-01, -0.530E-01) (-0.219E-01, 0.530E-01)

GAIN P22 = -9.15

ZEROES OF P22

(-0.296E+01, 0.0) (-0.434E-01, 0.0)

POLES OF P22

(-0.612E+01, 0.0) (0.146E+01, 0.0)
(-0.219E-01, -0.530E-01) (-0.219E-01, 0.530E-01)

GAIN Q11 = 691.

Q11(0) = 0.

ZEROES OF Q11

(-0.300E-01, 0.0) (0.0 , 0.0)

POLES OF Q11

(-0.296E+01, 0.0) (-0.434E-01, 0.0)

GAIN Q12 = -17.2

Q12(0) = -127.

ZEROES OF Q12

(-0.300E-01, 0.0)

POLES OF Q12

(-0.986E+01, 0.0) (0.749E+01, 0.0)

(-0.427E-01, 0.0)

GAIN Q21 = -202.

Q21(0) = 0.

ZEROES OF Q21

(-0.300E-01, 0.0) (0.0 , 0.0)

POLES OF Q21

(-0.264E+01, 0.0) (-0.450E-01, 0.0)

GAIN Q22 = 11.2

Q22(0) = 40.1

ZEROES OF Q22

(-0.300E-01, 0.0)

POLES OF Q22

(-0.134E+02, 0.0) (0.109E+02, 0.0)

(-0.442E-01, 0.0)

CASE NO. 3b

(A,B) MEANS A+JB

GAIN P11 = -819.

ZERGES OF P11

(-0.133E+02, 0.0) (0.108E+02, 0.0)
 (-0.433E-01, 0.0) (0.0 , 0.0)

PCLES OF P11

(-0.612E+01, 0.0) (0.146E+01, 0.0)
 (-0.219E-01, -0.530E-01) (-0.219E-01, 0.530E-01)

GAIN P12 = -368.

ZERGES OF P12

(-0.986E+01, 0.0) (0.749E+01, 0.0)
 (-0.427E-01, 0.0) (0.0 , 0.0)

PCLES OF P12

(-0.612E+01, 0.0) (0.146E+01, 0.0)
 (-0.219E-01, -0.530E-01) (-0.219E-01, 0.530E-01)

GAIN P21 = -44.4

ZERGES OF P21

(-0.265E+01, 0.0) (-0.446E-01, 0.0)

PCLES OF P21

(-0.612E+01, 0.0) (0.146E+01, 0.0)
 (-0.219E-01, -0.530E-01) (-0.219E-01, 0.530E-01)

GAIN P22 = -9.15

ZERGES OF P22

(-0.296E+01, 0.0) (-0.434E-01, 0.0)

PCLES OF P22

(-0.612E+01, 0.0) (0.146E+01, 0.0)
 (-0.219E-01, -0.530E-01) (-0.219E-01, 0.530E-01)

GAIN Q11 = 968.

G11(0) = 0.

ZERGES OF Q11
 (-0.334E-01, 0.0) (0.0 , 0.0)

POLES OF Q11
 (-0.296E+01, 0.0) (-0.434E-01, 0.0)

GAIN Q12 = -24.1

Q12(0) = -179.

ZERGES OF Q12
 (-0.334E-01, 0.0)

POLES OF Q12
 (-0.986E+01, 0.0) (0.749E+01, 0.0)
 (-0.427E-01, 0.0)

GAIN Q21 = -200.

Q21(0) = 0.

ZERGES OF Q21
 (-0.334E-01, 0.0) (0.0 , 0.0)

POLES OF Q21
 (-0.265E+01, 0.0) (-0.446E-01, 0.0)

GAIN Q22 = 10.8

Q22(0) = 40.1

ZERGES OF Q22
 (-0.334E-01, 0.0)

POLES OF Q22
 (-0.133E+02, 0.0) (0.108E+02, 0.0)
 (-0.432E-01, 0.0)

CASE NC. 3C

(A,B) MEANS A+JB

GAIN P11 = -578.

ZERGES OF P11

(-0.134E+02, 0.0) (0.110E+02, 0.0)
 (-0.432E-01, 0.0) (0.0 , 0.0)

POLES OF P11

(-0.612E+01, 0.0) (0.146E+01, 0.0)
 (-0.219E-01, -0.530E-01) (-0.219E-01, 0.530E-01)

GAIN P12 = -485.

ZERGES OF P12

(-0.916E+01, 0.0) (0.691E+01, 0.0)
 (-0.436E-01, 0.0) (0.0 , 0.0)

POLES OF P12

(-0.612E+01, 0.0) (0.146E+01, 0.0)
 (-0.219E-01, -0.530E-01) (-0.219E-01, 0.530E-01)

GAIN P21 = -54.3

ZERGES OF P21

(-0.284E+01, 0.0) (-0.440E-01, 0.0)

POLES OF P21

(-0.612E+01, 0.0) (0.146E+01, 0.0)
 (-0.219E-01, -0.530E-01) (-0.219E-01, 0.530E-01)

GAIN P22 = -9.73

ZERGES OF P22

(-0.309E+01, 0.0) (-0.443E-01, 0.0)

POLES OF P22

(-0.612E+01, 0.0) (0.146E+01, 0.0)
 (-0.219E-01, -0.530E-01) (-0.219E-01, 0.530E-01)

```

GAIN Q11 =      0.173E+04
Q11(0) =      0.
ZERCES OF Q11
(-0.459E-01, 0.0      ) ( 0.0      , 0.0      )
PCLES OF Q11
(-0.309E+01, 0.0      ) (-0.443E-01, 0.0      )
GAIN Q12 =      -34.6
Q12(0) =      -215.
ZERCES OF Q12
(-0.459E-01, 0.0      )
PCLES OF Q12
(-0.916E+01, 0.0      ) ( 0.681E+01, 0.0      )
(-0.436E-01, 0.0      )
GAIN Q21 =      -309.
Q21(0) =      0.
ZERCES OF Q21
(-0.459E-01, 0.0      ) ( 0.0      , 0.0      )
PCLES OF Q21
(-0.264E+01, 0.0      ) (-0.440E-01, 0.0      )
GAIN Q22 =      17.2
Q22(0) =      45.5
ZERCES OF Q22
(-0.459E-01, 0.0      )
PCLES OF Q22
(-0.134E+02, 0.0      ) ( 0.110E+02, 0.0      )
(-0.432E-01, 0.0      )

```


CASE NO. 30

(A,B) MEANS A+JB

GAIN P11 = -728.

ZERGES OF P11

(-0.134E+02, 0.0) (0.109E+02, 0.0)
 (-0.429E-01, 0.0) (0.0 , 0.0)

PCLES OF P11

(-0.612E+01, 0.0) (0.146E+01, 0.0)
 (-0.219E-01, -0.530E-01) (-0.219E-01, 0.530E-01)

GAIN P12 = -485.

ZERGES OF P12

(-0.916E+01, 0.0) (0.681E+01, 0.0)
 (-0.436E-01, 0.0) (0.0 , 0.0)

PCLES OF P12

(-0.612E+01, 0.0) (0.146E+01, 0.0)
 (-0.219E-01, -0.530E-01) (-0.219E-01, 0.530E-01)

GAIN P21 = -40.3

ZERGES OF P21

(-0.264E+01, 0.0) (-0.437E-01, 0.0)

PCLES OF P21

(-0.612E+01, 0.0) (0.146E+01, 0.0)
 (-0.219E-01, -0.530E-01) (-0.219E-01, 0.530E-01)

GAIN P22 = -9.73

ZERGES OF P22

(-0.309E+01, 0.0) (-0.443E-01, 0.0)

PCLES OF P22

(-0.612E+01, 0.0) (0.146E+01, 0.0)
 (-0.219E-01, -0.530E-01) (-0.219E-01, 0.530E-01)

GAIN Q11 = 0.128E+04
Q11(0) = C.
ZERGES OF Q11
(-0.479E-C1, C.0) (0.0 , 0.0)
PCLES OF Q11
(-0.309E+C1, 0.0) (-0.443E-C1, 0.0)
GAIN Q12 = -25.7
Q12(0) = -158.
ZERGES OF Q12
(-0.479E-C1, C.0)
PCLES OF Q12
(-0.916E+C1, 0.0) (0.681E+01, 0.0)
(-0.436E-C1, C.0)
GAIN Q21 = -309.
Q21(0) = C.
ZERGES OF Q21
(-0.479E-01, 0.0) (0.0 , 0.0)
PCLES OF Q21
(-0.264E+01, C.0) (-0.437E-C1, 0.0)
GAIN Q22 = 17.1
Q22(0) = 45.5
ZERGES OF Q22
(-0.479E-01, C.0)
PCLES OF Q22
(-0.134E+C2, C.0) (0.109E+C2, 0.0)
(-0.429E-C1, C.0)

CASE NO. 3E

(A,B) MEANS A+JB

GAIN P11 = -607.

ZEROS OF P11

(-0.133E+02, 0.0) (0.108E+02, 0.0)
(-0.427E-01, 0.0) (0.0 , 0.0)

POLES OF P11

(-0.612E+01, 0.0) (0.146E+01, 0.0)
(-0.219E-01, -0.530E-01) (-0.219E-01, 0.530E-01)

GAIN P12 = -485.

ZEROS OF P12

(-0.916E+01, 0.0) (0.681E+01, 0.0)
(-0.436E-01, 0.0) (0.0 , 0.0)

POLES OF P12

(-0.612E+01, 0.0) (0.146E+01, 0.0)
(-0.219E-01, -0.530E-01) (-0.219E-01, 0.530E-01)

GAIN P21 = -32.6

ZEROS OF P21

(-0.265E+01, 0.0) (-0.435E-01, 0.0)

POLES OF P21

(-0.612E+01, 0.0) (0.146E+01, 0.0)
(-0.219E-01, -0.530E-01) (-0.219E-01, 0.530E-01)

GAIN P22 = -9.73

ZEROS OF P22

(-0.309E+01, 0.0) (-0.443E-01, 0.0)

POLES OF P22

(-0.612E+01, 0.0) (0.146E+01, 0.0)
(-0.219E-01, -0.530E-01) (-0.219E-01, 0.530E-01)

```

GAIN Q11 =    0.102E+04
Q11(0) =      0.
ZERCOES OF Q11
(-0.491E-01, 0.0      ) ( 0.0      , 0.0      )
POLES OF Q11
(-0.309E+01, 0.0      ) (-0.443E-01, 0.0      )
GAIN Q12 =    -20.5
Q12(0) =     -128.
ZERCOES OF Q12
(-0.491E-01, 0.0      )
POLES OF Q12
(-0.916E+01, 0.0      ) ( 0.681E+01, 0.0      )
(-0.436E-01, 0.0      )
GAIN Q21 =    -304.
Q21(0) =      0.
ZERCOES OF Q21
(-0.491E-01, 0.0      ) ( 0.0      , 0.0      )
POLES OF Q21
(-0.265E+01, 0.0      ) (-0.435E-01, 0.0      )
GAIN Q22 =     16.3
Q22(0) =     45.5
ZERCOES OF Q22
(-0.491E-01, 0.0      )
POLES OF Q22
(-0.133E+02, 0.0      ) ( 0.108E+02, 0.0      )
(-0.427E-01, 0.0      )

```

CASE NO. 4A

(A,B) MEANS A+JB

GAIN P11 = -93.3

ZERGES OF P11

(-0.445E+01, 0.0) (0.394E+01, 0.0)
(-0.149E-01, 0.0) (0.0 , 0.0)

PCLES OF P11

(-0.214E+01, 0.0) (0.124E+01, 0.0)
(-0.959E-02, -0.781E-01) (-0.959E-02, 0.781E-01)

GAIN P12 = -52.9

ZERGES OF P12

(-0.234E+01, 0.0) (0.191E+01, 0.0)
(-0.969E-02, 0.0) (0.0 , 0.0)

PCLES OF P12

(-0.214E+01, 0.0) (0.124E+01, 0.0)
(-0.959E-02, -0.781E-01) (-0.959E-02, 0.781E-01)

GAIN P21 = -4.86

ZERGES OF P21

(-0.556E+01, 0.0) (-0.255E-01, 0.0)

PCLES OF P21

(-0.214E+01, 0.0) (0.124E+01, 0.0)
(-0.959E-02, -0.781E-01) (-0.959E-02, 0.781E-01)

GAIN P22 = -0.301

ZERGES OF P22

(-0.132E+01, 0.0) (-0.141E-01, 0.0)

PCLES OF P22

(-0.214E+01, 0.0) (0.124E+01, 0.0)
(-0.959E-02, -0.781E-01) (-0.959E-02, 0.781E-01)

GAIN Q11 = 761.

Q11(0) = 0.

ZEROES OF Q11
 (-0.576E-02, 0.0) (0.0 , 0.0)

POLES OF Q11
 (-0.132E+01, 0.0) (-0.141E-01, 0.0)

GAIN Q12 = -4.33

Q12(0) = -3.6

ZEROES OF Q12
 (-0.576E-02, 0.0)

POLES OF Q12
 (-0.234E+01, 0.0) (0.191E+01, 0.0)
 (-0.969E-02, 0.0)

GAIN Q21 = -47.1

Q21(0) = 0.

ZEROES OF Q21
 (-0.576E-02, 0.0) (0.0 , 0.0)

POLES OF Q21
 (-0.556E+00, 0.0) (-0.255E-01, 0.0)

GAIN Q22 = 2.46

Q22(0) = 0.337

ZEROES OF Q22
 (-0.576E-02, 0.0)

POLES OF Q22
 (-0.445E+01, 0.0) (0.394E+01, 0.0)
 (-0.149E-01, 0.0)

CASE NO. 48

(A,B) MEANS A+JB

GAIN P11 = -121.

ZEROES OF P11

(-0.443E+01, 0.0) (0.398E+C1, 0.0)
 (-0.140E-01, 0.0) (0.0 , 0.0)

POLES OF P11

(-0.214E+01, 0.0) (0.124E+C1, 0.0)
 (-0.959E-C2, -0.781E-01) (-0.959E-C2, 0.781E-01)

GAIN P12 = -52.9

ZEROES OF P12

(-0.234E+01, 0.0) (0.191E+C1, 0.0)
 (-0.969E-C2, 0.0) (0.0 , 0.0)

POLES OF P12

(-0.214E+01, 0.0) (0.124E+01, 0.0)
 (-0.959E-C2, -0.781E-01) (-0.959E-C2, 0.781E-01)

GAIN P21 = -6.46

ZEROES OF P21

(-0.555E+C0, 0.0) (-0.246E-C1, 0.0)

POLES OF P21

(-0.214E+01, 0.0) (0.124E+C1, 0.0)
 (-0.959E-C2, -0.781E-01) (-0.959E-C2, 0.781E-01)

GAIN P22 = -0.301

ZEROES OF P22

(-0.132E+01, 0.0) (-0.141E-01, 0.0)

POLES OF P22

(-0.214E+01, 0.0) (0.124E+C1, 0.0)
 (-0.959E-C2, -0.781E-01) (-0.959E-C2, 0.781E-01)

GAIN Q11 = 0.101E+04
Q11(0) = C.
ZEROS OF Q11
(-0.646E-02, 0.0) (0.0 , 0.0)
POLES OF Q11
(-0.132E+01, 0.0) (-0.141E-01, 0.0)
GAIN Q12 = -5.77
Q12(0) = -4.48
ZEROS OF Q12
(-0.646E-02, 0.0)
POLES OF Q12
(-0.234E+01, 0.0) (0.191E+01, 0.0)
(-0.969E-02, 0.0)
GAIN Q21 = -47.2
Q21(0) = C.
ZEROS OF Q21
(-0.646E-02, 0.0) (0.0 , 0.0)
POLES OF Q21
(-0.555E+00, 0.0) (-0.246E-01, 0.0)
GAIN Q22 = 2.51
Q22(0) = 0.337
ZEROS OF Q22
(-0.646E-02, 0.0)
POLES OF Q22
(-0.448E+01, 0.0) (0.398E+01, 0.0)
(-0.140E-01, 0.0)

CASE NO. 4C

(A,B) MEANS A+JB

GAIN P11 = -136.

ZERGES OF P11
 $(-0.451E+01, 0.0)$ $(0.401E+01, 0.0)$
 $(-0.127E-01, 0.0)$ $(0.0, 0.0)$

POLES OF P11
 $(-0.214E+01, 0.0)$ $(0.124E+01, 0.0)$
 $(-0.959E-02, -0.781E-01)$ $(-0.959E-02, 0.781E-01)$

GAIN P12 = -66.5

ZERGES OF P12
 $(-0.220E+01, 0.0)$ $(0.176E+01, 0.0)$
 $(-0.128E-01, 0.0)$ $(0.0, 0.0)$

POLES OF P12
 $(-0.214E+01, 0.0)$ $(0.124E+01, 0.0)$
 $(-0.959E-02, -0.781E-01)$ $(-0.959E-02, 0.781E-01)$

GAIN P21 = -7.38

ZERGES OF P21
 $(-0.555E+00, 0.0)$ $(-0.232E-01, 0.0)$

POLES OF P21
 $(-0.214E+01, 0.0)$ $(0.124E+01, 0.0)$
 $(-0.959E-02, -0.781E-01)$ $(-0.959E-02, 0.781E-01)$

GAIN P22 = -0.242

ZERGES OF P22
 $(-0.179E+01, 0.0)$ $(-0.160E-01, 0.0)$

POLES OF P22
 $(-0.214E+01, 0.0)$ $(0.124E+01, 0.0)$
 $(-0.959E-02, -0.781E-01)$ $(-0.959E-02, 0.781E-01)$

GAIN Q11 = 0.189E+04
 Q11(0) = 0.
 ZERGES OF Q11
 (-0.128E-01, 0.0) (0.0 , 0.0)
 PCLES OF Q11
 (-0.179E+01, 0.0) (-0.160E-01, 0.0)
 GAIN Q12 = -6.88
 Q12(0) = -3.99
 ZERGES OF Q12
 (-0.128E-01, 0.0)
 PCLES OF Q12
 (-0.220E+01, 0.0) (0.176E+01, 0.0)
 (-0.128E-01, 0.0)
 GAIN Q21 = -62.0
 Q21(0) = 0.
 ZERGES OF Q21
 (-0.128E-01, 0.0) (0.0 , 0.0)
 PCLES OF Q21
 (-0.555E+00, 0.0) (-0.232E-01, 0.0)
 GAIN Q22 = 3.36
 Q22(0) = 0.419
 ZERGES OF Q22
 (-0.128E-01, 0.0)
 PCLES OF Q22
 (-0.451E+01, 0.0) (0.401E+01, 0.0)
 (-0.127E-01, 0.0)

CASE NO. 4D

(A,B) MEANS A+JB

GAIN P11 = -101.

ZERGES OF P11

(-0.452E+01, 0.0) (0.403E+01, 0.0)
 (-0.117E-01, 0.0) (0.0 , 0.0)

POLES OF P11

(-0.214E+01, 0.0) (0.124E+01, 0.0)
 (-0.959E-02, -0.781E-01) (-0.959E-02, 0.781E-01)

GAIN P12 = -66.5

ZERGES OF P12

(-0.220E+01, 0.0) (0.176E+01, 0.0)
 (-0.128E-01, 0.0) (0.0 , 0.0)

POLES OF P12

(-0.214E+01, 0.0) (0.124E+01, 0.0)
 (-0.959E-02, -0.781E-01) (-0.959E-02, 0.781E-01)

GAIN P21 = -5.51

ZERGES OF P21

(-0.555E+00, 0.0) (-0.222E-01, 0.0)

POLES OF P21

(-0.214E+01, 0.0) (0.124E+01, 0.0)
 (-0.959E-02, -0.781E-01) (-0.959E-02, 0.781E-01)

GAIN P22 = -0.242

ZERGES OF P22

(-0.179E+01, 0.0) (-0.160E-01, 0.0)

POLES OF P22

(-0.214E+01, 0.0) (0.124E+01, 0.0)
 (-0.959E-02, -0.781E-01) (-0.959E-02, 0.781E-01)

```

GAIN Q11 = 0.141E+04
Q11(0) = 0.
ZERGES OF Q11
(-0.132E-01, 0.0 ) ( 0.0 , 0.0 )
POLES OF Q11
(-0.179E+01, 0.0 ) (-0.160E-01, 0.0 )
GAIN Q12 = -5.14
Q12(0) = -2.75
ZERGES OF Q12
(-0.132E-01, 0.0 )
POLES OF Q12
(-0.220E+01, 0.0 ) ( 0.176E+01, 0.0 )
(-0.128E-01, 0.0 )
GAIN Q21 = -62.0
Q21(0) = 0.
ZERGES OF Q21
(-0.132E-01, 0.0 ) ( 0.0 , 0.0 )
POLES OF Q21
(-0.555E+00, 0.0 ) (-0.222E-01, 0.0 )
GAIN Q22 = 3.38
Q22(0) = 0.419
ZERGES OF Q22
(-0.132E-01, 0.0 )
POLES OF Q22
(-0.452E+01, 0.0 ) ( 0.403E+01, 0.0 )
(-0.117E-01, 0.0 )

```

CASE NO. 4E

(A,B) MEANS A+JB

GAIN P11 = -79.3

ZEROES OF P11

(-0.451E+01, 0.0) (0.402E+01, 0.0)
(-0.110E-01, 0.0) (0.0 , 0.0)

POLES OF P11

(-0.214E+01, 0.0) (0.124E+01, 0.0)
(-0.959E-02, -0.781E-01) (-0.959E-02, 0.781E-01)

GAIN P12 = -66.5

ZEROES OF P12

(-0.220E+01, 0.0) (0.176E+01, 0.0)
(-0.128E-01, 0.0) (0.0 , 0.0)

POLES OF P12

(-0.214E+01, 0.0) (0.124E+01, 0.0)
(-0.959E-02, -0.781E-01) (-0.959E-02, 0.781E-01)

GAIN P21 = -4.30

ZEROES OF P21

(-0.556E+00, 0.0) (-0.215E-01, 0.0)

POLES OF P21

(-0.214E+01, 0.0) (0.124E+01, 0.0)
(-0.959E-02, -0.781E-01) (-0.959E-02, 0.781E-01)

GAIN P22 = -0.242

ZEROES OF P22

(-0.179E+01, 0.0) (-0.160E-01, 0.0)

POLES OF P22

(-0.214E+01, 0.0) (0.124E+01, 0.0)
(-0.959E-02, -0.781E-01) (-0.959E-02, 0.781E-01)

GAIN Q11 = 0.110E+04

Q11(0) = C.

ZEROES OF Q11
(-0.136E-01, C.0) (0.0 , 0.0)

POLES OF Q11
(-0.179E+01, 0.0) (-0.160E-01, 0.0)

GAIN Q12 = -4.02

Q12(0) = -2.01

ZEROES OF Q12
(-0.136E-01, C.0)

POLES OF Q12
(-0.220E+01, C.0) (0.176E+01, 0.0)
(-0.128E-01, C.0)

GAIN Q21 = -62.0

Q21(0) = C.

ZEROES OF Q21
(-0.136E-01, C.0) (0.0 , 0.0)

POLES OF Q21
(-0.556E+00, 0.0) (-0.215E-01, 0.0)

GAIN Q22 = 3.37

Q22(0) = 0.419

ZEROES OF Q22
(-0.136E-01, C.0)

POLES OF Q22
(-0.451E+01, 0.0) (0.402E+01, 0.0)
(-0.110E-01, 0.0)

CASE NC. 5A

(A,B) MEANS A+JB

GAIN P11 = -134.

ZERGES OF P11

(-0.713E+01, 0.0) (0.627E+01, 0.0)
(-0.134E-01, 0.0) (0.0 , 0.0)

PCLES OF P11

(-0.305E+01, 0.0) (0.145E+01, 0.0)
(-0.855E-02, -0.536E-01) (-0.855E-02, 0.536E-01)

GAIN P12 = -149.

ZERGES OF P12

(-0.506E+01, 0.0) (0.424E+01, 0.0)
(-0.120E-01, 0.0) (0.0 , 0.0)

PCLES OF P12

(-0.305E+01, 0.0) (0.145E+01, 0.0)
(-0.855E-02, -0.536E-01) (-0.855E-02, 0.536E-01)

GAIN P21 = -10.0

ZERGES OF P21

(-0.915E+00, 0.0) (-0.163E-01, 0.0)

PCLES OF P21

(-0.305E+01, 0.0) (0.145E+01, 0.0)
(-0.855E-02, -0.536E-01) (-0.855E-02, 0.536E-01)

GAIN P22 = -3.37

ZERGES OF P22

(-0.106E+01, 0.0) (-0.144E-01, 0.0)

PCLES OF P22

(-0.305E+01, 0.0) (0.145E+01, 0.0)
(-0.855E-02, -0.536E-01) (-0.855E-02, 0.536E-01)

GAIN Q11 = 259.

Q11(C) = C.

ZEROES OF Q11
(-0.279E-C2, C.0) (0.0 , 0.0)

POLES OF Q11
(-0.106E+01, C.0) (-0.144E-01, 0.0)

GAIN Q12 = -5.86

Q12(0) = -11.4

ZEROES OF Q12
(-0.279E-C2, C.0)

POLES OF Q12
(-0.506E+C1, 0.0) (0.424E+C1, 0.0)
(-0.120E-C1, C.0)

GAIN Q21 = -87.4

Q21(C) = C.

ZEROES OF Q21
(-0.279E-C2, C.0) (0.0 , 0.0)

POLES OF Q21
(-0.915E+00, C.0) (-0.163E-01, 0.0)

GAIN Q22 = 4.76

Q22(0) = 3.96

ZEROES OF Q22
(-0.279E-C2, C.0)

POLES OF Q22
(-0.713E+01, 0.0) (0.627E+C1, C.0)
(-0.134E-C1, C.0)

CASE NO. 58

(A,B) MEANS A+JB

GAIN P11 = -272.

ZERGES OF P11

(-0.713E+01, 0.0) (0.633E+01, 0.0)
 (-0.129E-01, 0.0) (0.0 , 0.0)

PCLES OF P11

(-0.305E+01, 0.0) (0.145E+01, 0.0)
 (-0.855E-02, -0.536E-01) (-0.855E-02, 0.536E-01)

GAIN P12 = -149.

ZERGES OF P12

(-0.506E+01, 0.0) (0.424E+01, 0.0)
 (-0.120E-01, 0.0) (0.0 , 0.0)

PCLES OF P12

(-0.305E+01, 0.0) (0.145E+01, 0.0)
 (-0.855E-02, -0.536E-01) (-0.855E-02, 0.536E-01)

GAIN P21 = -15.1

ZERGES OF P21

(-0.914E+00, 0.0) (-0.157E-01, 0.0)

PCLES OF P21

(-0.305E+01, 0.0) (0.145E+01, 0.0)
 (-0.855E-02, -0.536E-01) (-0.855E-02, 0.536E-01)

GAIN P22 = -3.37

ZERGES OF P22

(-0.106E+01, 0.0) (-0.144E-01, 0.0)

PCLES OF P22

(-0.305E+01, 0.0) (0.145E+01, 0.0)
 (-0.855E-02, -0.536E-01) (-0.855E-02, 0.536E-01)

GAIN Q11 = 398.

Q11(0) = C.

ZERGES OF Q11

(-0.626E-02, C.0) (0.0 , C.C)

PCLES OF Q11

(-0.106E+C1, C.0) (-0.144E-C1, C.C)

GAIN Q12 = -8.99

Q12(0) = -16.5

ZERGES OF Q12

(-0.626E-02, C.0)

PCLES OF Q12

(-0.506E+C1, 0.0) (0.424E+C1, C.0)

(-C.120E-C1, C.0)

GAIN Q21 = -88.7

Q21(0) = C.

ZERGES OF Q21

(-0.626E-02, C.0) (0.0 , C.C)

PCLES OF Q21

(-0.914E+C0, C.0) (-0.157E-C1, C.0)

GAIN Q22 = 4.93

Q22(0) = 3.56

ZERGES OF Q22

(-0.626E-02, C.0)

PCLES OF Q22

(-0.719E+01, 0.0) (0.633E+C1, C.0)

(-0.129E-C1, C.0)

CASE NO. 5C

(A,B) MEANS A+JB

GAIN P11 = -314.

ZERGES OF P11

(-0.719E+C1, 0.0) (0.634E+C1, 0.0)
 (-0.122E-C1, 0.0) (0.0 , 0.0)

POLES OF P11

(-0.305E+01, 0.0) (0.145E+C1, 0.0)
 (-0.855E-C2, -0.536E-01) (-0.855E-C2, 0.536E-01)

GAIN P12 = -196.

ZERGES OF P12

(-0.469E+C1, 0.0) (0.387E+01, 0.0)
 (-0.132E-C1, 0.0) (0.0 , 0.0)

POLES OF P12

(-0.305E+C1, 0.0) (0.145E+C1, 0.0)
 (-0.855E-C2, -0.536E-01) (-0.855E-C2, 0.536E-C1)

GAIN P21 = -17.5

ZERGES OF P21

(-0.914E+00, 0.0) (-0.150E-C1, 0.0)

POLES OF P21

(-0.305E+C1, 0.0) (0.145E+C1, 0.0)
 (-0.855E-C2, -0.536E-01) (-0.855E-C2, 0.536E-C1)

GAIN P22 = -3.52

ZERGES OF P22

(-0.113E+C1, 0.0) (-0.155E-C1, 0.0)

POLES OF P22

(-0.305E+C1, 0.0) (0.145E+C1, 0.0)
 (-0.855E-C2, -0.536E-01) (-0.855E-C2, 0.536E-C1)

GAIN Q11 = 559.
Q11(0) = C.
ZERGES OF Q11
(-0.178E-01, C.0) (0.0 , 0.0)
POLES OF Q11
(-0.113E+01, C.0) (-0.155E-01, 0.0)
GAIN Q12 = -11.9
Q12(0) = -17.6
ZERGES OF Q12
(-0.178E-01, C.0)
POLES OF Q12
(-0.469E+01, C.0) (0.387E+01, 0.0)
(-0.132E-01, C.0)
GAIN Q21 = -132.
Q21(0) = C.
ZERGES OF Q21
(-0.178E-01, C.0) (0.0 , 0.0)
POLES OF Q21
(-0.914E+00, C.0) (-0.150E-01, 0.0)
GAIN Q22 = 7.38
Q22(0) = 4.73
ZERGES OF Q22
(-0.178E-01, C.0)
POLES OF Q22
(-0.719E+01, 0.0) (0.634E+01, 0.0)
(-0.122E-01, C.0)

CASE NO. 5D

(A,B) MEANS A+JB

GAIN P11 = -230.

ZERGES OF P11

(-0.724E+C1, 0.0) (0.638E+01, 0.0)
 (-0.113E-C1, 0.0) (0.0 , 0.0)

PCLES OF P11

(-0.305E+01, 0.0) (0.145E+C1, 0.0)
 (-0.855E-C2, -0.536E-01) (-0.855E-02, 0.536E-01)

GAIN P12 = -196.

ZERGES OF P12

(-0.469E+C1, 0.0) (0.387E+01, 0.0)
 (-0.132E-C1, 0.0) (0.0 , 0.0)

PCLES OF P12

(-0.305E+C1, 0.0) (0.145E+C1, 0.0)
 (-0.855E-C2, -0.536E-01) (-0.855E-02, 0.536E-01)

GAIN P21 = -13.0

ZERGES OF P21

(-0.913E+C0, 0.0) (-0.146E-C1, 0.0)

PCLES OF P21

(-0.305E+C1, 0.0) (0.145E+C1, 0.0)
 (-0.855E-02, -0.536E-01) (-0.855E-02, 0.536E-C1)

GAIN P22 = -3.52

ZERGES OF P22

(-0.113E+C1, 0.0) (-0.155E-C1, 0.0)

PCLES OF P22

(-0.305E+C1, 0.0) (0.145E+C1, 0.0)
 (-0.855E-C2, -0.536E-01) (-0.855E-02, 0.536E-01)

GAIN Q11 = 494.

Q11(0) = C.

ZEROES OF Q11
(-0.193E-01, C.C) (0.0 , 0.0)

PCLES OF Q11
(-0.113E+01, C.C) (-0.155E-01, C.C)

GAIN Q12 = -8.88

Q12(0) = -12.7

ZEROES OF Q12
(-0.193E-01, C.C)

PCLES OF Q12
(-0.469E+01, C.C) (0.387E+01, 0.0)
(-0.132E-01, C.C)

GAIN Q21 = -133.

Q21(0) = C.

ZEROES OF Q21
(-0.193E-01, C.C) (0.0 , 0.0)

PCLES OF Q21
(-0.913E+00, C.C) (-0.146E-01, C.C)

GAIN Q22 = 7.54

Q22(0) = 4.73

ZEROES OF Q22
(-0.193E-01, C.C)

PCLES OF Q22
(-0.724E+01, C.C) (0.638E+01, 0.0)
(-0.118E-01, C.C)

CASE NO. 5E

(A,B) MEANS A+JB

GAIN P11 = -196.

ZERGES OF P11

(-0.709E+01, 0.0) (0.624E+01, 0.0)
 (-0.113E-01, 0.0) (0.0 , 0.0)

POLES OF P11

(-0.305E+01, 0.0) (0.145E+01, 0.0)
 (-0.855E-02, -0.536E-01) (-0.855E-02, 0.536E-01)

GAIN P12 = -196.

ZERGES OF P12

(-0.469E+01, 0.0) (0.387E+01, 0.0)
 (-0.132E-01, 0.0) (0.0 , 0.0)

POLES OF P12

(-0.305E+01, 0.0) (0.145E+01, 0.0)
 (-0.855E-02, -0.536E-01) (-0.855E-02, 0.536E-01)

GAIN P21 = -10.0

ZERGES OF P21

(-0.918E+00, 0.0) (-0.144E-01, 0.0)

POLES OF P21

(-0.305E+01, 0.0) (0.145E+01, 0.0)
 (-0.855E-02, -0.536E-01) (-0.855E-02, 0.536E-01)

GAIN P22 = -3.52

ZERGES OF P22

(-0.113E+01, 0.0) (-0.155E-01, 0.0)

POLES OF P22

(-0.305E+01, 0.0) (0.145E+01, 0.0)
 (-0.855E-02, -0.536E-01) (-0.855E-02, 0.536E-01)

GAIN Q11 = 371.

Q11(0) = C.

ZERGES OF Q11
 (-0.205E-01, C.0) (0.0 , 0.0)

POLES OF Q11
 (-0.113E+01, C.0) (-0.155E-01, 0.0)

GAIN Q12 = -6.68

Q12(0) = -9.61

ZERGES OF Q12
 (-0.205E-01, C.0)

POLES OF Q12
 (-0.469E+01, C.0) (0.387E+01, 0.0)
 (-0.132E-01, C.0)

GAIN Q21 = -130.

Q21(0) = C.

ZERGES OF Q21
 (-0.205E-01, 0.0) (0.0 , 0.0)

POLES OF Q21
 (-0.913E+00, C.0) (-0.144E-01, 0.0)

GAIN Q22 = 7.03

Q22(0) = 4.73

ZERGES OF Q22
 (-0.205E-01, C.0)

POLES OF Q22
 (-0.709E+01, C.0) (0.624E+01, 0.0)
 (-0.116E-01, C.0)

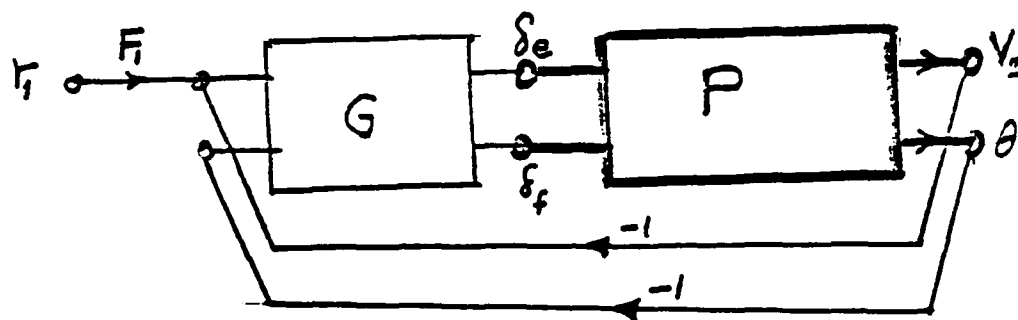


Fig. 3.1 System structure for longitudinal pitch-pointing mode (α_1)

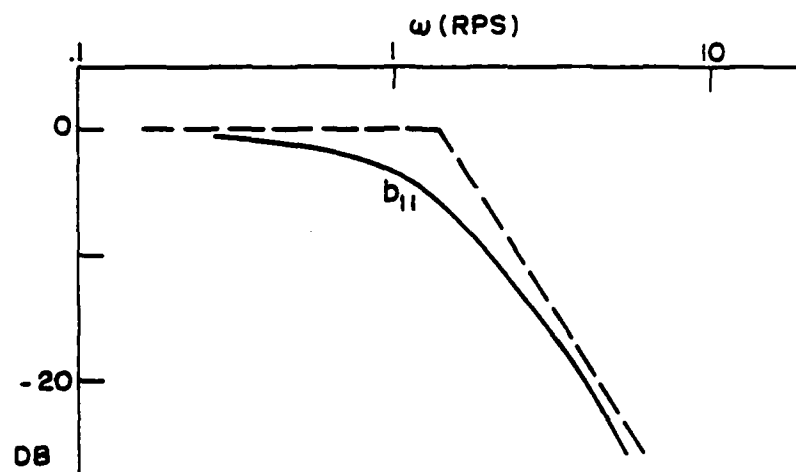
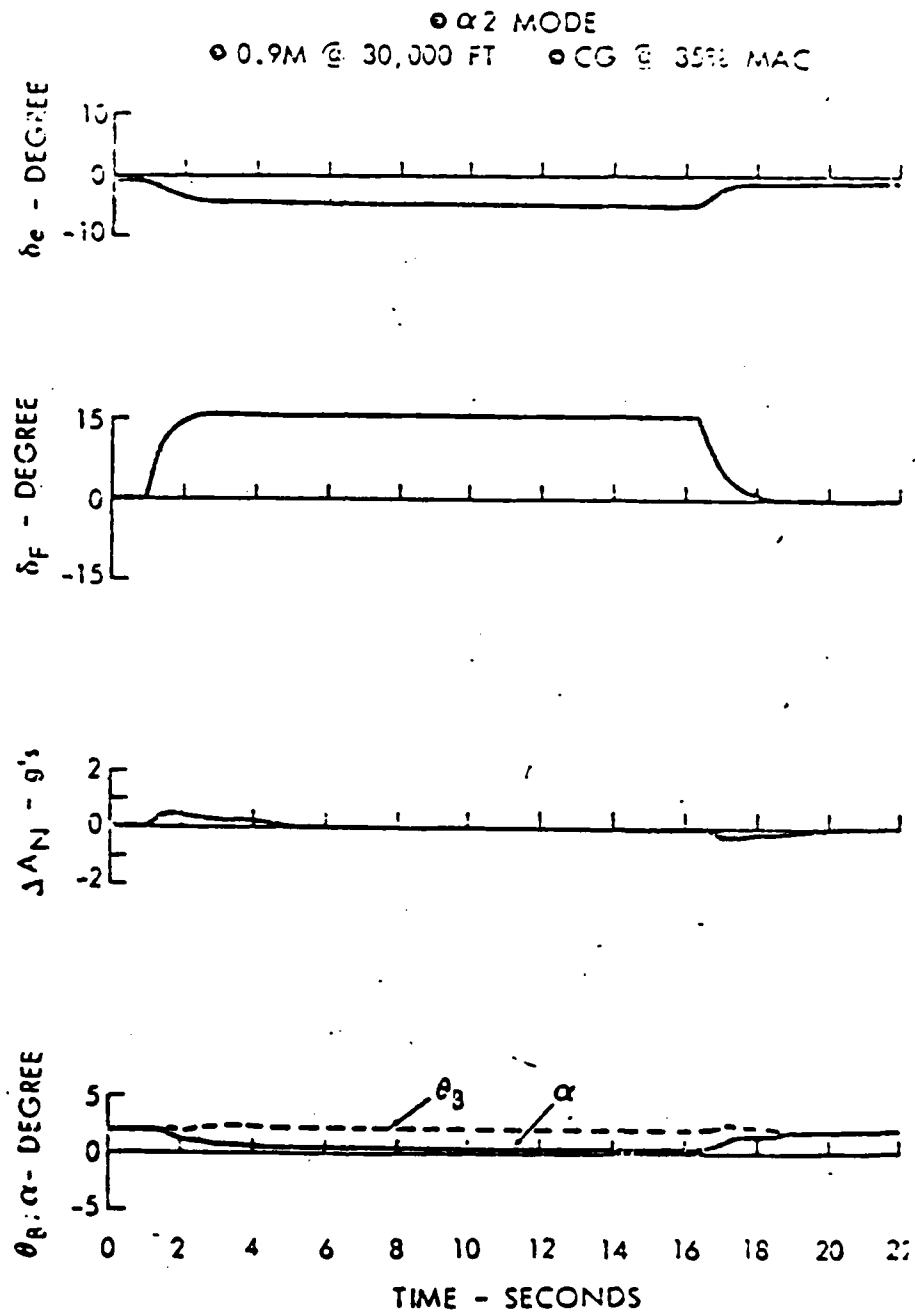


Fig. 3.2a Bode sketch of $b_{11}(\omega)$



α_2 mode response.

Fig. 3.2b α_2 mode response

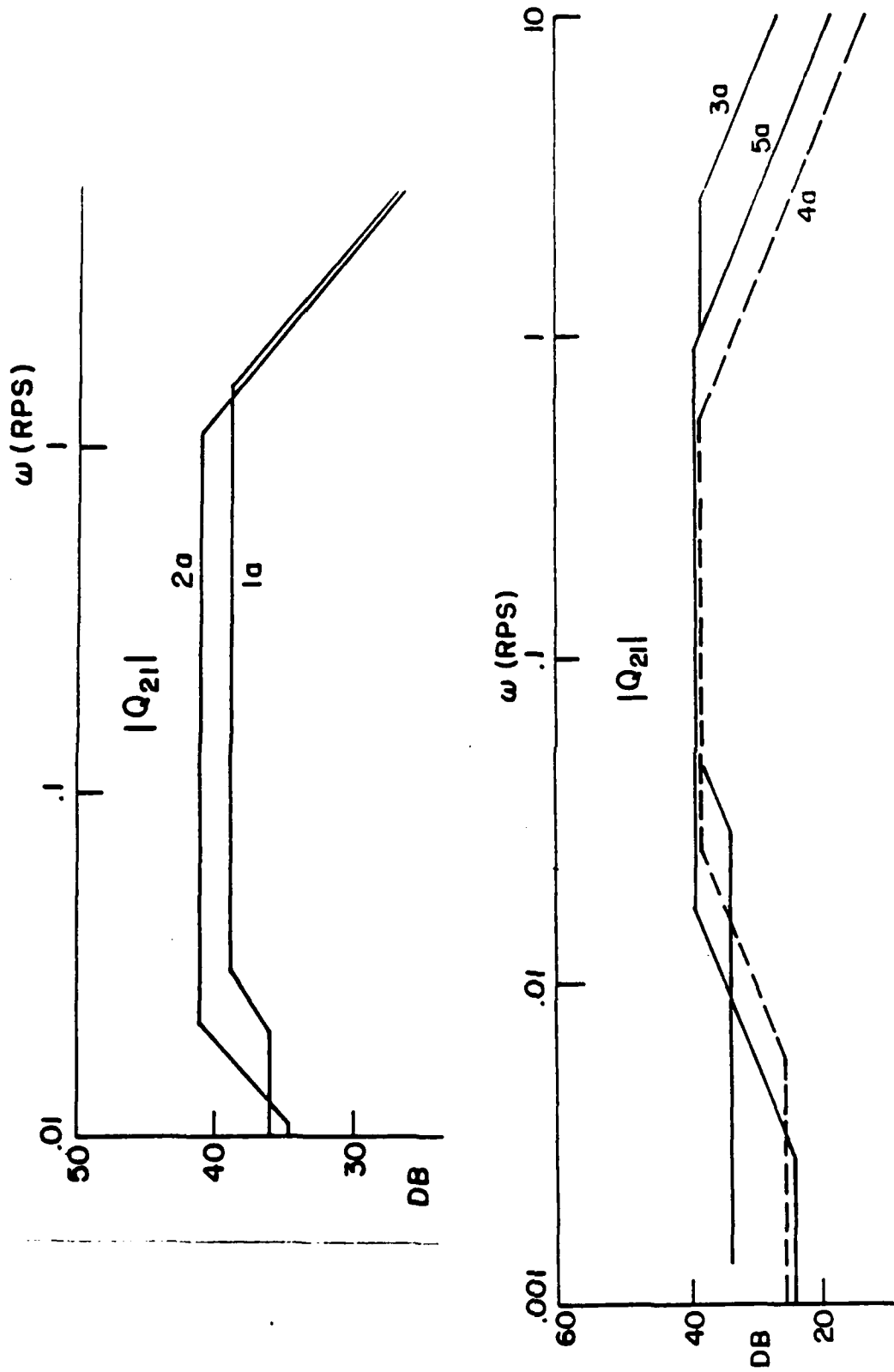


Fig. 3.3 Asymptotic plots of $|Q_{21}(j\omega)|$, Cases 1a-5a.

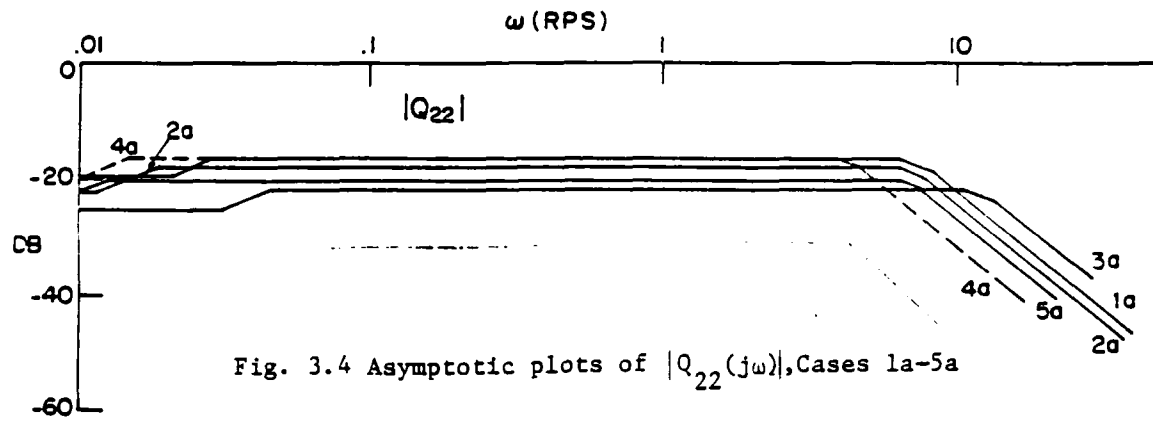


Fig. 3.4 Asymptotic plots of $|Q_{22}(j\omega)|$, Cases 1a-5a

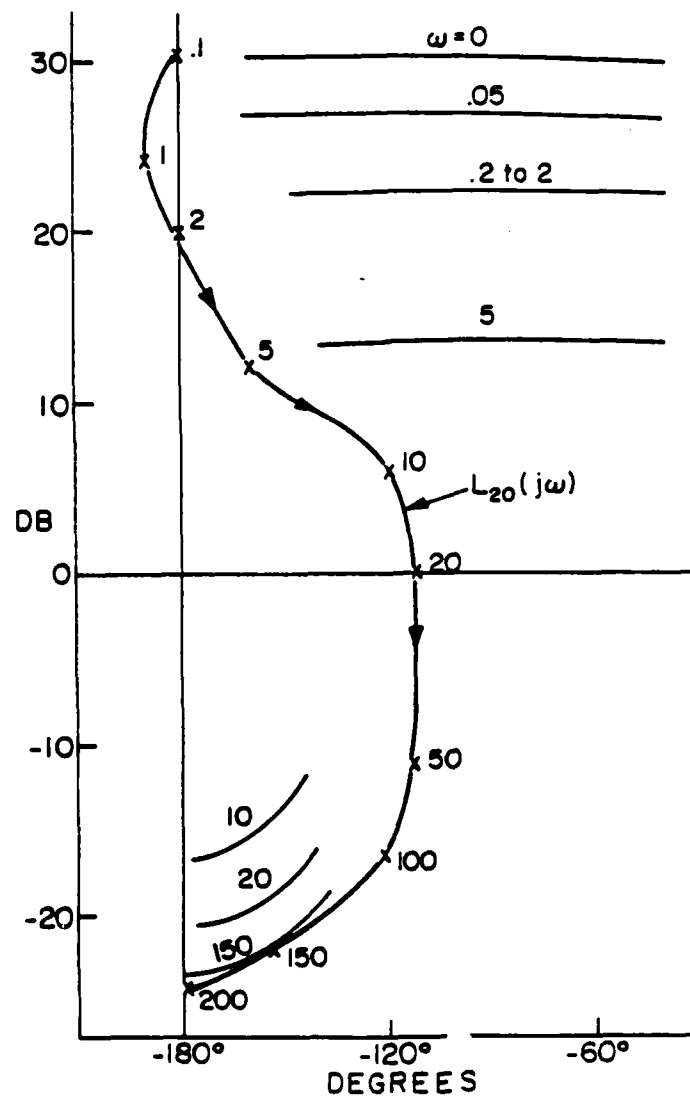


Fig. 3.5 Bounds on $L_{20}(j\omega)$ and final design

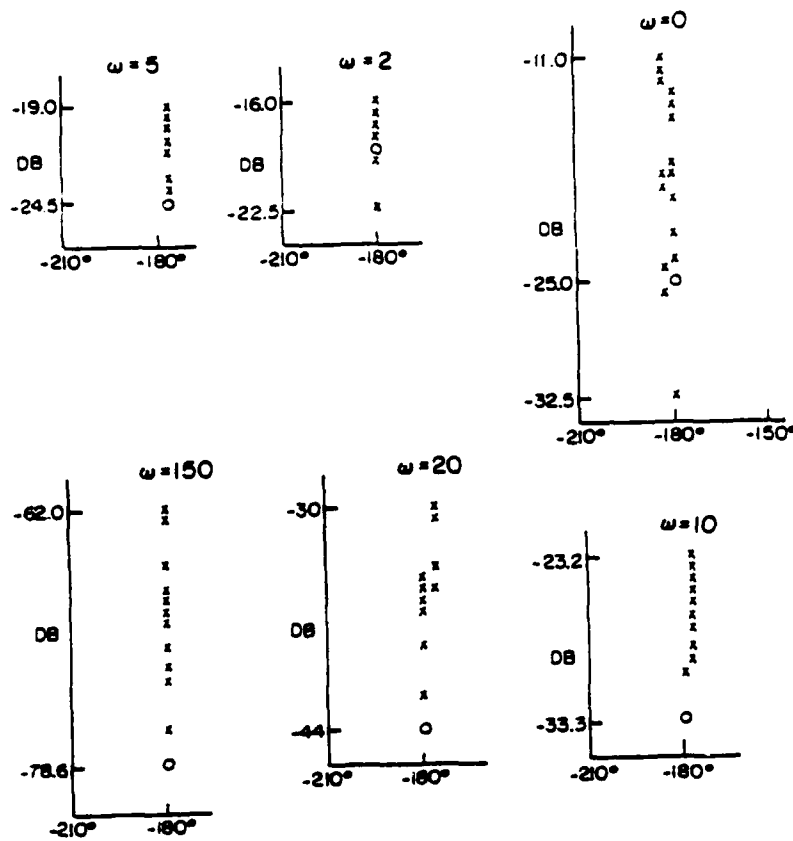


Fig. 3.6 Some templates of $Q_{22}(j\omega)$

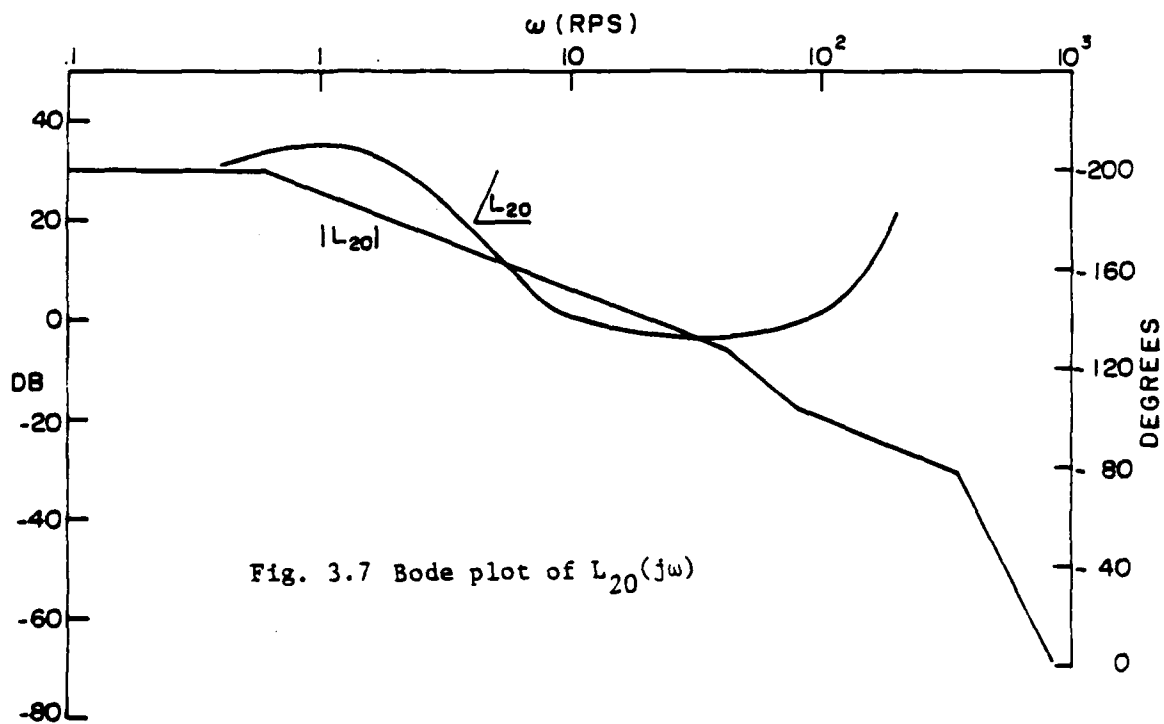


Fig. 3.7 Bode plot of $L_{20}(j\omega)$

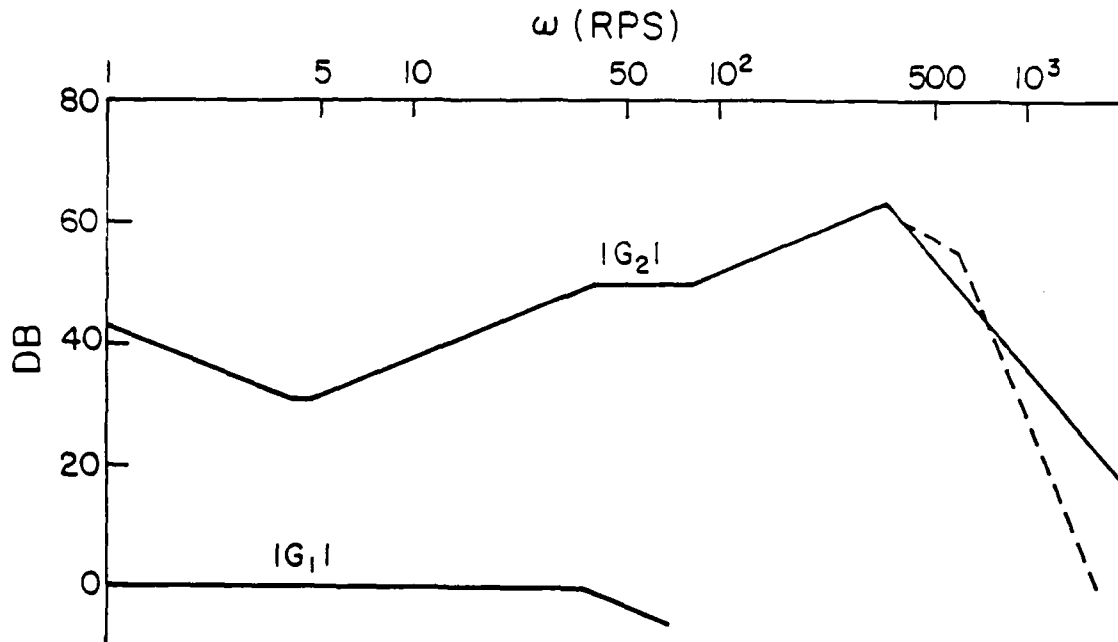


Fig. 3.8 Bode plot of $|G_2(j\omega)|$

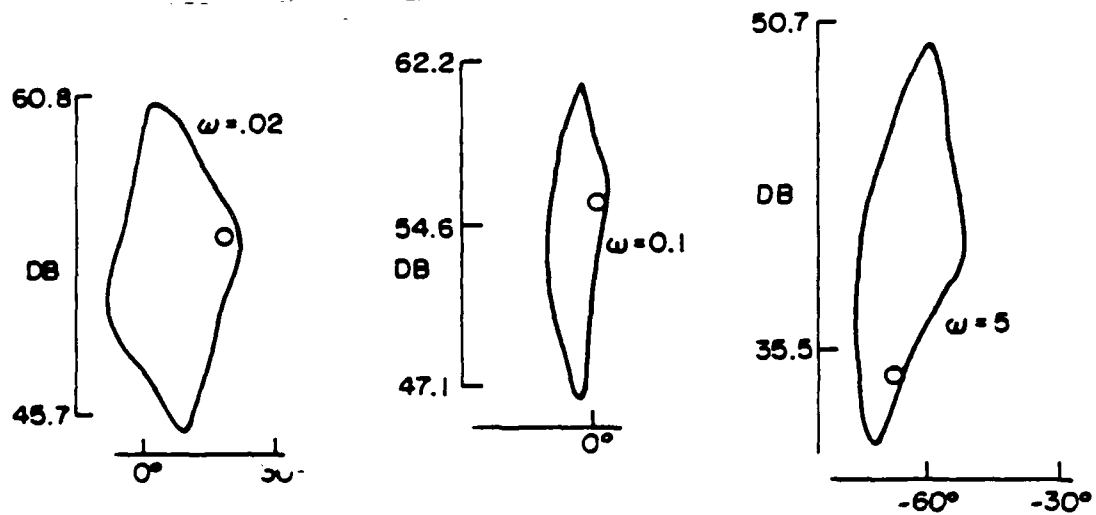


Fig. 3.9 Some templates of $Q_{11}^*(j\omega)$

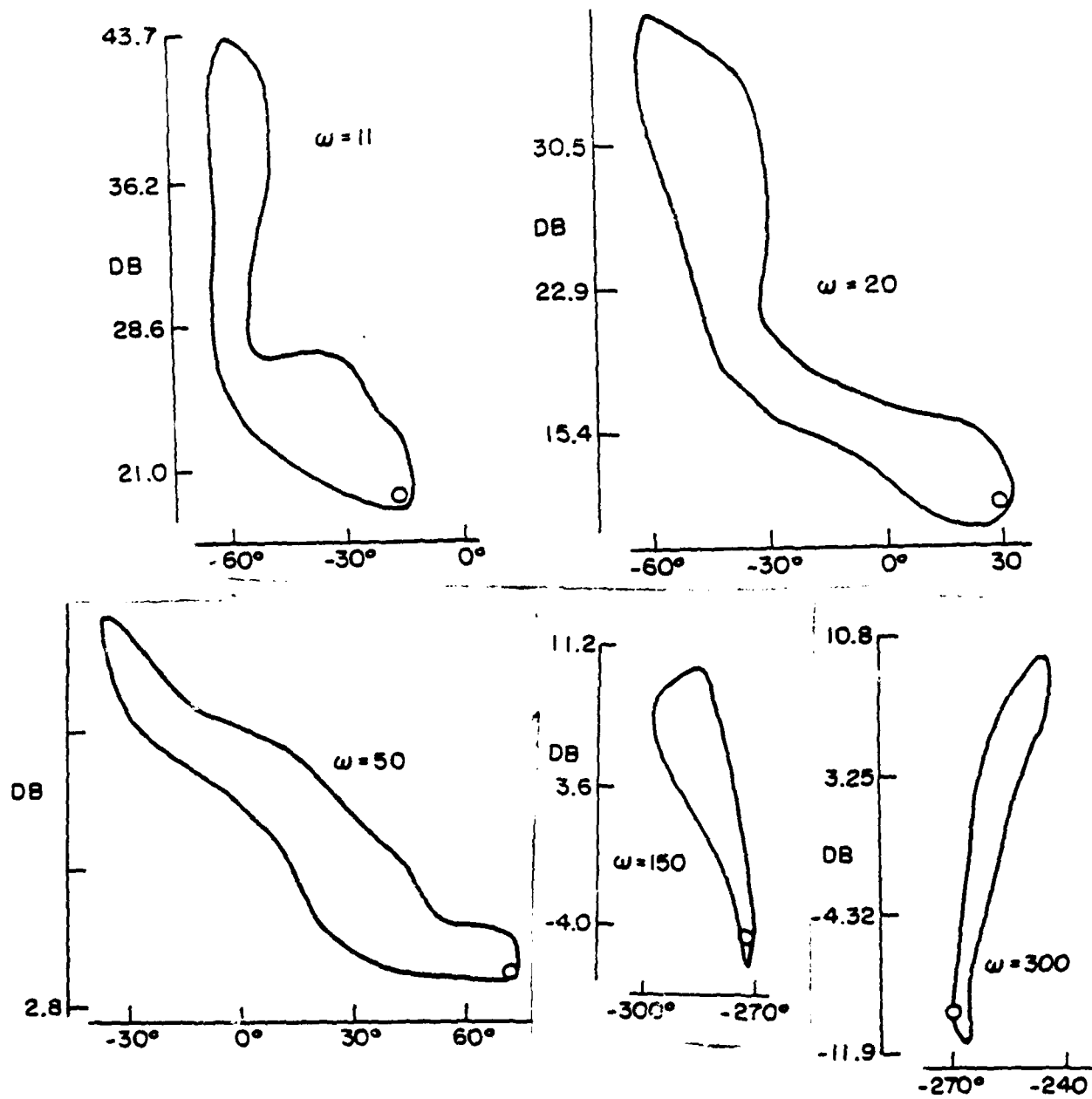


Fig. 3.9 (cont.) Some templates of $Q_{11}^*(j\omega)$

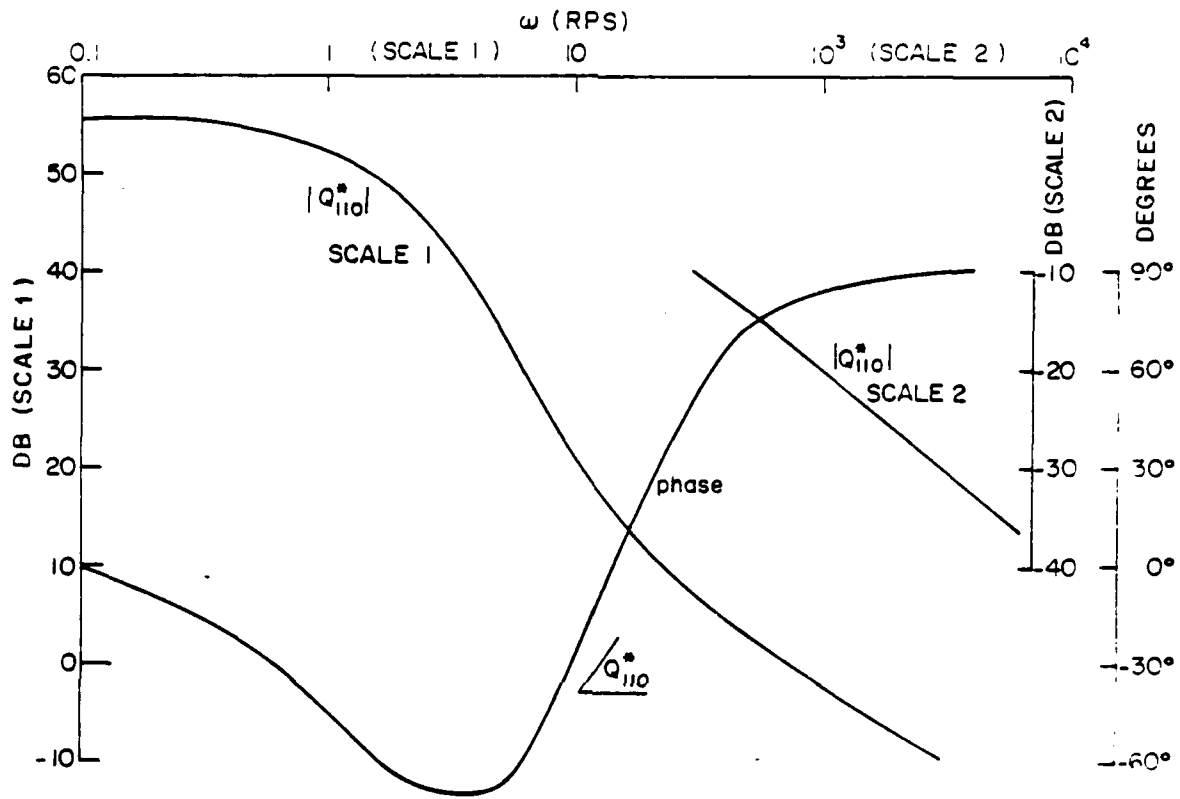


Fig. 3.10 Bode plot of nominal, $Q_{110}^*(j\omega)$

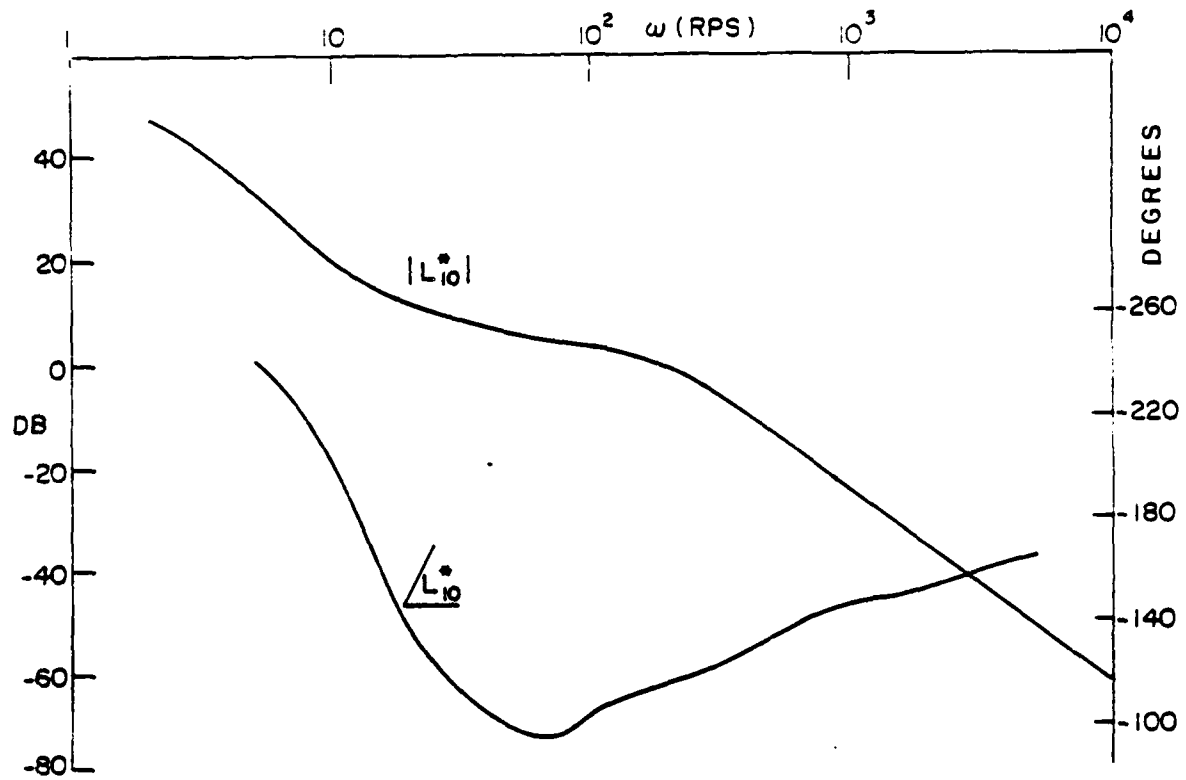


Fig. 3.11 Bode plot of $L_{110}^*(j\omega)$

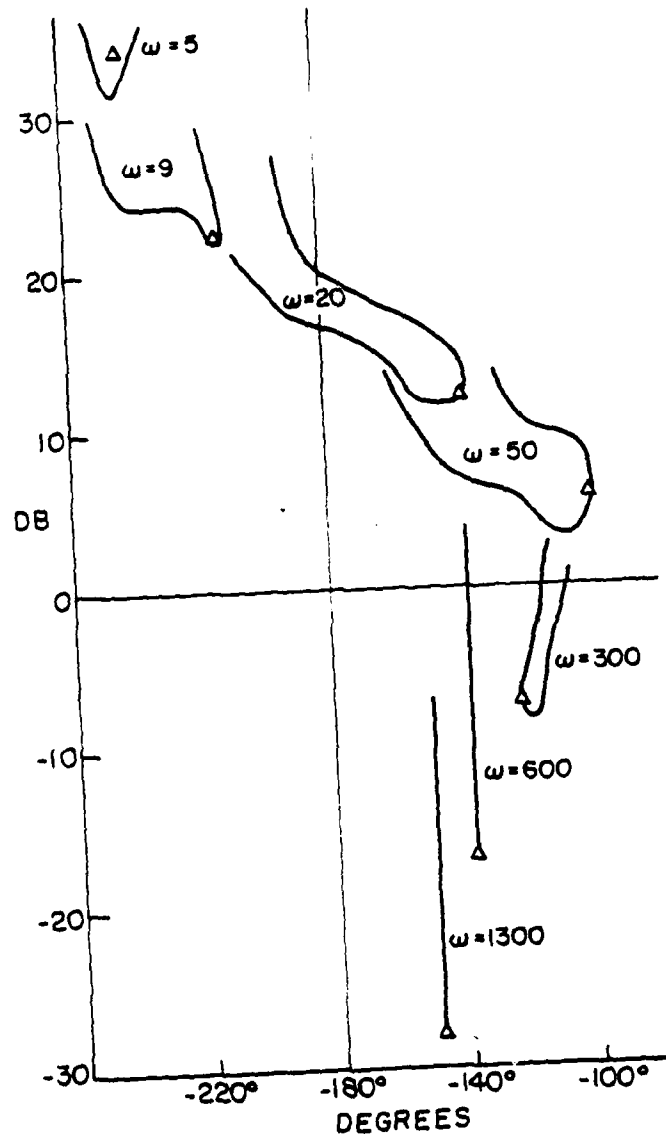


Fig. 3.12 Locus of templates of $L_1^* = G_1 Q_{11}^*(j\omega)$

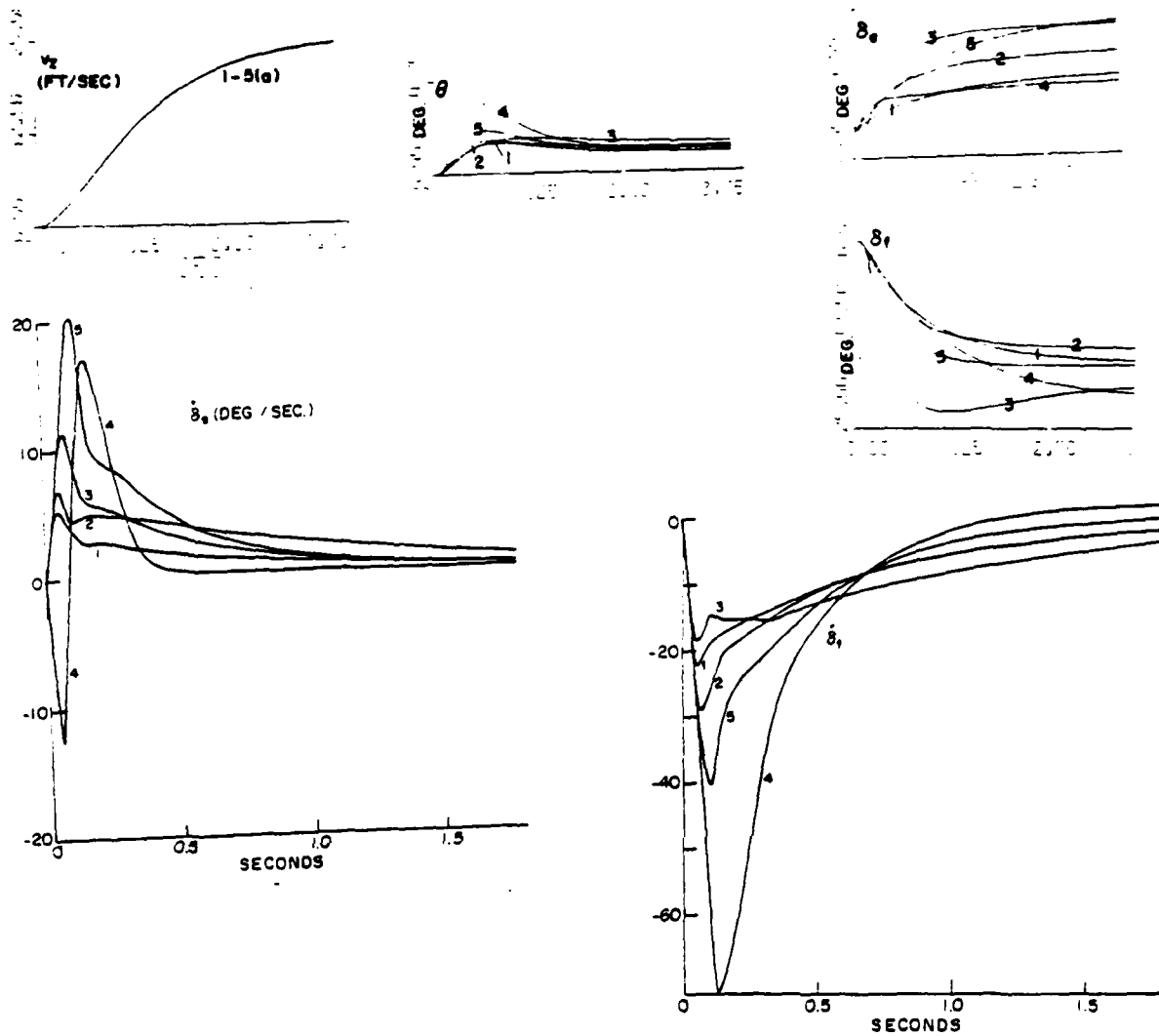


Fig. 3.13 Simulation results

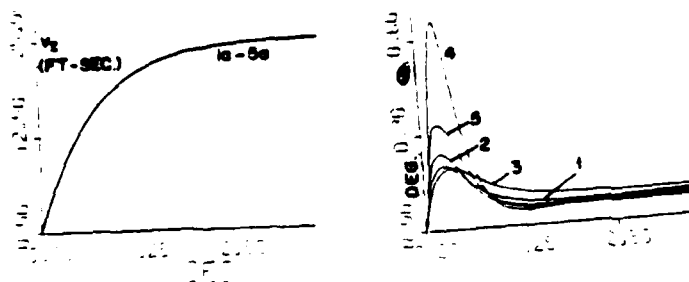


Fig. 3.14 Simulation results for
"faster" filter, $F_1 = \frac{1}{\frac{s}{1.4} + 1}$

Chapter 4

DESIGN OF LATERAL TRANSLATION (ψ) MODE

4.1 Problem statement

In this mode the plant inputs are listed as δ_c , δ_r , δ_a (canard, rudder, aileron), and its outputs are: side velocity $v = \int A_y dt$, yaw $\psi = \int r dt$, roll ϕ (Fig. 4.1). The objective is to achieve a commanded side velocity v_c with small yaw ψ and small roll ϕ angles. For a command of $v_c = 60$ ft/sec, we shall aim for $\leq 1^\circ$ for $|\psi|$, and $\leq 2^\circ$ for $|\phi|$. Hence

$$b_{21} = \frac{1}{(60)57.3} = -70 \text{ db}; \quad b_{31} = 2b_{21} = -64 \text{ db} \quad (4.1a,b)$$

As for b_{11} , we take in the meantime the model

$$T_{11}(s) = \left[\left(1 + \frac{s}{.3} \right) \left(1 + \frac{s}{4} \right)^2 \right]^{-1} \quad (4.2)$$

whose Bode plot is sketched in Fig. 4.2. We do not consider the lower bound $a_{11}(\omega)$ for $|T_{11}(j\omega)|$ at this point, because in the previous designs the corresponding loop transmission was so large that the T_{ii} (T_{33} in Chapter 2, T_{11} in Chapter 3) was almost invariant over its important ω range.

4.2 Plant equations

While the plant system here is essentially the same as in Chapter 2, there the variables of interest were sideslip β , roll ϕ , side force A_y whereas here they are side velocity, yaw and roll, so we get different plant equation. In (2.1), yaw was not present while side slip

was in the output vector \underline{y} . But the procedure for finding the new plant matrix is the same as in Chapter 2, so is not repeated here.

Here,

$$\underline{z} = [v, \dots, z]' = P \underline{x} = [p_c, \dots, p_a]' \quad (4.3)$$

The elements Q_{ij} of $Q = P^{-1} = [1/Q_{ij}]$ for the ten cases listed in Chapter 2 are given in Table 4.1 below, in which the entries are of the form

$$Q_{ij}^{-1} = D_{ij}s^3 + C_{ij}s^2 + A_{ijs} + B_{ij} \quad (4.4a)$$

except for

$$Q_{i3} = s[D_{ij}s^3 + C_{ij}s^2 + A_{uj}s + B_{ij}] \quad (4b)$$

TABLE 4.1 ELEMENTS Q1J (SEE SEC. 4.2)

[illegible]

C A S E 6

I	J	D	C	A	B
1	1	0.0	0.0	0.151E-01	0.552E-02
1	2	0.0	0.134E+00	0.233E-01	0.415E+01
1	3	0.0	0.302E-02	0.137E+00	0.133E+00
2	1	0.0	0.0	0.114E+02	0.670E-02
2	2	0.0	0.765E-01	0.123E+00	0.450E+01
2	3	0.0	0.507E-01	0.123E+00	0.415E+00
3	1	0.0	0.0	0.134E+00	0.415E+01
3	2	0.0	0.134E+00	0.137E+00	0.415E+01
3	3	0.0	0.302E-02	0.137E+00	0.133E+00

C A S E 7

I	J	D	C	A	B
1	1	0.0	0.0	0.226E-01	0.550E-02
1	2	0.0	0.134E+00	0.505E-02	0.456E+01
1	3	0.445E-02	0.460E-02	0.171E+00	0.177E+00
2	1	0.0	0.0	0.120E-01	0.682E-02
2	2	0.0	0.107E+00	0.123E+00	0.565E+01
2	3	0.209E-01	0.653E-01	0.211E+00	0.219E+00
3	1	0.0	0.0	0.818E-02	0.854E-03
3	2	0.0	0.327E-02	0.240E-01	0.707E+00
3	3	0.280E-01	0.736E-01	0.265E-01	0.275E-01

C A S E 8

I	J	D	C	A	B
1	1	0.0	0.0	0.781E-02	0.433E-02
1	2	0.0	0.454E-01	0.243E-02	0.433E+01
1	3	0.176E-02	0.747E-02	0.689E-01	0.140E+00
2	1	0.0	0.0	0.570E-02	0.758E-02
2	2	0.0	0.694E-01	0.147E+00	0.762E+01
2	3	0.189E-01	0.999E-01	0.120E+00	0.244E+00
3	1	0.0	0.0	0.378E-02	0.126E-02
3	2	0.0	0.328E-03	0.100E-01	0.126E+01
3	3	0.107E-01	0.606E-01	0.199E-01	0.405E-01

C A S E 9

I	J	D	C	A	B
1	1	0.0	0.0	0.776E-01	0.379E-02
1	2	0.0	0.475E+00	0.448E-02	0.524E+01
1	3	0.140E-01	0.196E-02	0.561E+00	0.233E+00
2	1	0.0	0.0	0.333E-01	0.932E-02
2	2	0.0	0.203E+00	0.143E+00	0.550E+01
2	3	0.604E-01	0.530E-01	0.595E+00	0.300E+00
3	1	0.0	0.0	0.191E-01	0.356E-03
3	2	0.0	0.384E-02	0.474E-01	0.213E+00
3	3	0.812E-01	0.927E-01	0.227E-01	0.115E-01

C A S E 10

I	J	D	C	A	B
1	1	0.0	0.0	0.366E-01	0.915E-02
1	2	0.0	0.770E-01	0.826E-01	0.819E+01
1	3	0.297E-01	0.445E-01	0.353E+00	0.294E+00
2	1	0.0	0.0	0.178E-01	0.824E-02
2	2	0.0	0.180E+00	0.155E+00	0.737E+01
2	3	0.482E-01	0.790E-01	0.318E+00	0.265E+00
3	1	0.0	0.0	0.147E-01	0.275E-02
3	2	0.0	0.355E-01	0.125E-01	0.246E+01
3	3	0.229E-01	0.483E-01	0.106E+00	0.885E-01

4.3 Design of L_3

The inequality to be satisfied is

$$|1 + L_3| \geq \frac{b_{11} \left| \frac{Q_{33}}{Q_{31}} \right| + b_{21} \left| \frac{Q_{33}}{Q_{32}} \right|}{b_{31}} \triangleq B_3 \quad (4.5)$$

For $\omega \in [0.1, 5]$, $b_{11} \left| \frac{Q_{33}}{Q_{32}} \right| \gg b_{21} \left| \frac{Q_{33}}{Q_{32}} \right|$ and $B_3 > 60$ db, so

we need

$$|1 + L_3| \geq \frac{b_{11}}{b_{31}} \frac{Q_{33}}{Q_{31}} > 60 \text{ db} \quad (4.6)$$

Since $|L_3| = |Q_{33}G_3| \gg 1$, $|1 + L_3| \doteq |L_3|$ (4.6) becomes

$$|G_3| \geq \frac{b_{11}}{b_{31} |Q_{31}|_{\min}} \quad (4.7)$$

The resulting bounds on $|G_3(j\omega)|$ are shown in Fig. 4.3, and on

$L_{30} = Q_{330}G_3$ in Fig. 4.4.

For $\omega > 8$ in (4.5), $B_3 \approx 0$ db, so the only requirement is stability of $(1+L_3)$ and a reasonable margin $|L_3/(1+L_3)| \leq \mu$; $\mu = 5$ db was chosen. The results are shown in Fig. 4.4. Some templates of Q_{33} are shown in Fig. 4.5. At low ω values, a right half-plane pole of Q_{33} near the origin and a zero at $s = 0$ (recall (4b)) dominate, so we use $G_3 \sim -8(s+0.1)/s$ for $\omega < 5$, which handles both $\omega < .1$ and the requirement $|G| > 5$ for $\omega \in [0.1, 5]$. The final $L_{30} = G_3 Q_{330}$ chosen, is shown in Fig. 4.4, with

$$G_3(s) = \frac{-0.8(1+10s)\left(1 + \frac{s}{7.2}\right)}{s \left(1 + \frac{s}{80}\right) \left(1 + \frac{s}{500}\right)} \quad (4.8)$$

4.4 Design of L_2

The inequality to be satisfied (see Chapter 1), is:

$$|1 + L_2| \geq \frac{b_{11} \left| \frac{Q_{22}}{Q_{21}} \right| + b_{31} \left| \frac{Q_{22}}{Q_{23}} \right|}{b_{21}} \triangleq B_2 \quad (4.9)$$

For $\omega \in [1, 5]$, $b_{11} \left| \frac{Q_{22}}{Q_{21}} \right| \gg b_{31} \left| \frac{Q_{22}}{Q_{23}} \right|$, and $B_2 > 70$ db, so as in Eqs. [4.6, 7], we need

$$|G_2| \geq \frac{b_{11}}{b_{21} |Q_{21}|} \geq 30 \text{ db} \quad (4.10)$$

$$\text{For } \omega \text{ small, } b_{31} \left| \frac{Q_{22}}{Q_{23}} \right| \gg b_{11} \left| \frac{Q_{22}}{Q_{21}} \right|$$

because of the zero of Q_{23} at the origin, so G_2 is assigned a pole at the origin and its low frequency form is

$$G_2 \sim \frac{K(10s + 1)}{s}, \quad K \geq 30 \text{ db} \quad (4.11)$$

see Fig. 4.6. For $\omega > 15$, $B_2 \sim 0$ so the only demands are of stability and suitable margin for $|L_2/(1 + L_2)|$. The template of Q_{22} determine the resulting bounds on L_{20} , see Figs. 4.7, 4.8.

$L_{20}(j\omega)$ is sketched in Fig. 4.8, and

$$G_1(s) = \frac{-3.1(10s+1)(.1s+1)}{s \left(\frac{s}{200} + 1 \right)^2} \quad (4.12)$$

4.5 Design of G_1

As in Chapter 2, the exact equation is used for the design of the final loop involving G_1 . The exact expression for T_{11} is manipulated into the form

$$\left. \begin{aligned} T_{11}(s) &= \frac{F_1 L_1^*}{1+L_1^*}, \quad L_1^* = Q_{11}^* G_1, \quad Q_{11}^* = \frac{Q_{11}}{1-\eta} \\ \eta &= \frac{\gamma_{12}(1+L_3) + \gamma_{13}(1+L_2) - \Gamma}{(1+L_2)(1+L_3) - \gamma_{23}} \\ \gamma_{ij} &= \frac{Q_{ii} Q_{jj}}{Q_{ij} Q_{ji}}, \\ \Gamma &= Q_{11} Q_{22} Q_{33} \left[\frac{1}{Q_{12} Q_{23} Q_{31}} + \frac{1}{Q_{21} Q_{32} Q_{13}} \right] \end{aligned} \right\} \quad (4.13a-f)$$

The design of F_1 , G_1 is therefore precisely a single-loop design, for which Ref. [3] is highly appropriate. Templates of Q_{11}^* are obtained (Fig. 4.9). These are used, as described in [3], to obtain bounds on L_{10}^* , such that $\Delta |L_1^* / (1+L_1^*)|$ does not exceed the allowed range. The bounds shown in Fig. 10 were used here. The upper bound does not correspond to that used in Fig. 4.2. This may affect the T_{21} , T_{31} results. If it

does do so too much adversely, we can redesign F_1 . In any case, the resulting bounds on L_{10}^* are shown in Fig. 11, as well as L_{10}^* with

$$G_1(s) = \frac{0.01(5s+1)}{s(.1s+1)} \quad (4.14)$$

which involves very little bandwidth for $G_1(j\omega)$. (It might be a good idea to make G_1 larger.) Two choices of F_1 were tried

$$F_{1a} = \frac{0.3}{(s+.3)} ; \quad F_{1b} = \frac{0.5}{(s+.5)} \quad (4.15a,b)$$

4.6 Simulation of Design

The two designs (F_{1a} , F_{1b}) were simulated on the digital computer. The results are shown in Figs. 4.12, 4.13 respectively and are seen to be very good. The commanded v was adjusted so that in most cases, one of the control surfaces (it was δ_c the canard) saturated. The yaw and roll values obtained are very small.

Obviously, the v responses with F_{1b} are faster than those for F_{1a} . However, the canard then saturates for some cases (those with some overshoot) at smaller commanded v values. One could perhaps eliminate the overshoot for these cases, by careful examination of these cases, and this would be worth doing in a design meant for actual implementation. If the overshoot in some of these δ responses could be eliminated, the limiting factor in speeding up the response of v would be the saturation values of the δ_i rather than those of some of the δ_i . In any case, the results achieved nicely satisfy the specifications of Sec. 4.1.

4.7 Use of Digital Compensation

Digital compensation is becoming increasingly attractive, due to the tremendous progress in microprocessing. The sampling causes the compensation function to be nonminimum phase [], but the extra phase lag decreases as the sampling frequency is increased. In a sophisticated digital design, one could have several parallel digital compensations with different sampling rates. The networks with smaller bandwidth in their transfer functions could be assigned larger sampling periods. The optimum arrangement of such parallel compensation is worthy of study. In the present case, we simply replaced the compensation functions in Design 1, by equivalent digital networks. Tustin's method [] was used in which s is replaced in the transfer function by

$$s = \frac{2}{T} \frac{z - 1}{z + 1} \quad (4.16)$$

Different sampling periods T were tried and it was found that $T = .02$ seconds gave the satisfactory results shown in Fig. 4.14.

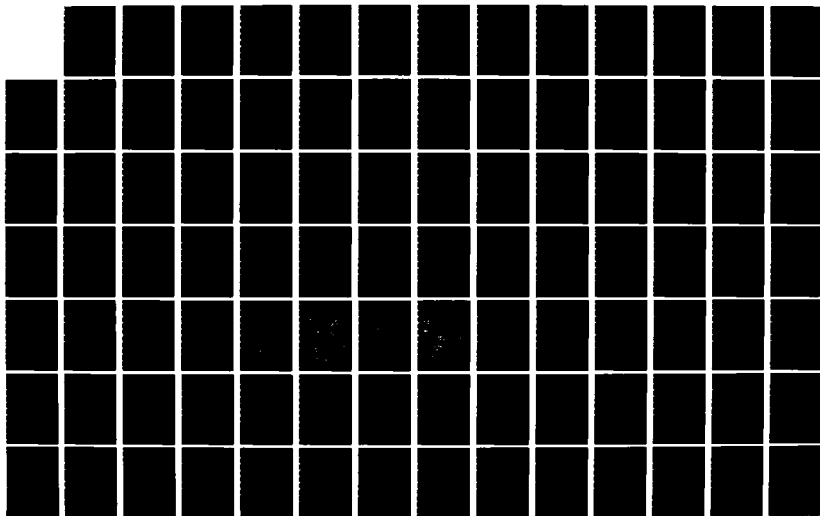
AD-A135 738

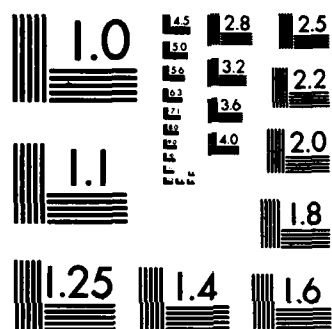
MULTIVARIABLE FLIGHT CONTROL DESIGN WITH UNCERTAIN
PARAMETERS(U) WEIZMANN INST OF SCIENCE REHOVOTH
(ISRAEL) DEPT OF APPLIED MA. I HOROWITZ ET AL. SEP 82
AFWAL-TR-83-3036 AFOSR-80-0213 F/G 1/3

3/4

UNCLASSIFIED

NL





MICROCOPY RESOLUTION TEST CHART
NATIONAL BUREAU OF STANDARDS-1963-A

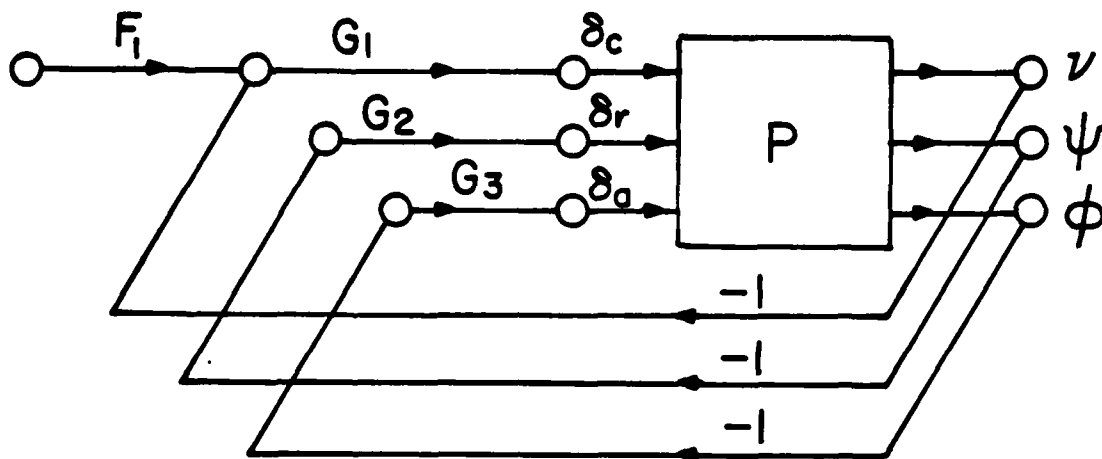


Fig. 4.1 System structure for lateral translation (β_2) mode

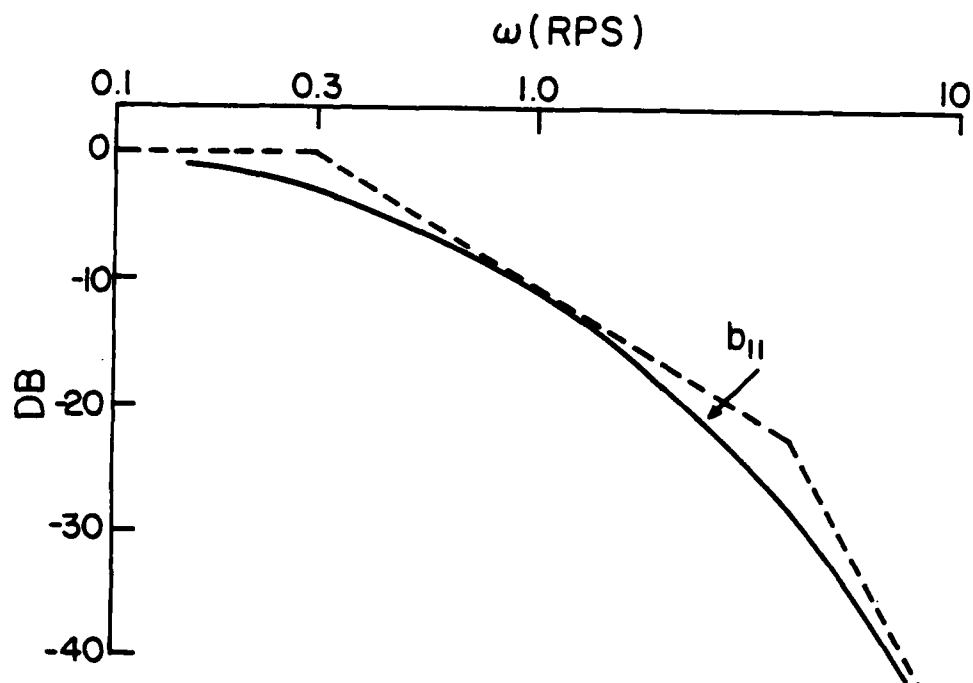


Fig. 4.2 Bode plot of $b_{11}(\omega)$

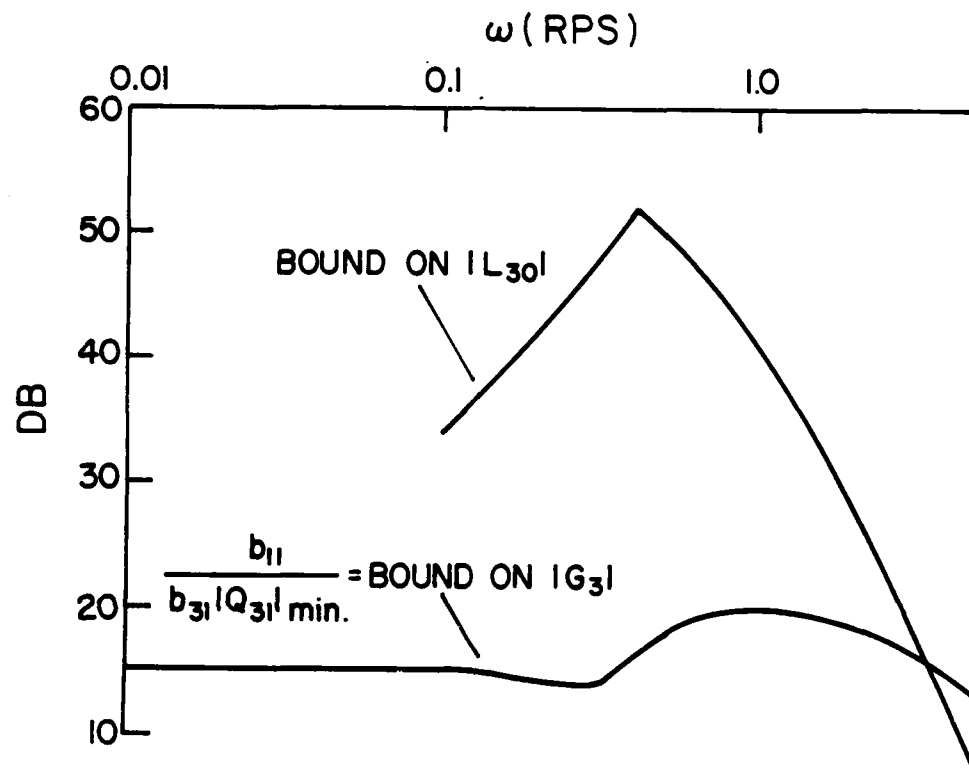


Fig. 4.3 Bounds on $|G_3(j\omega)|$ for part of frequency range

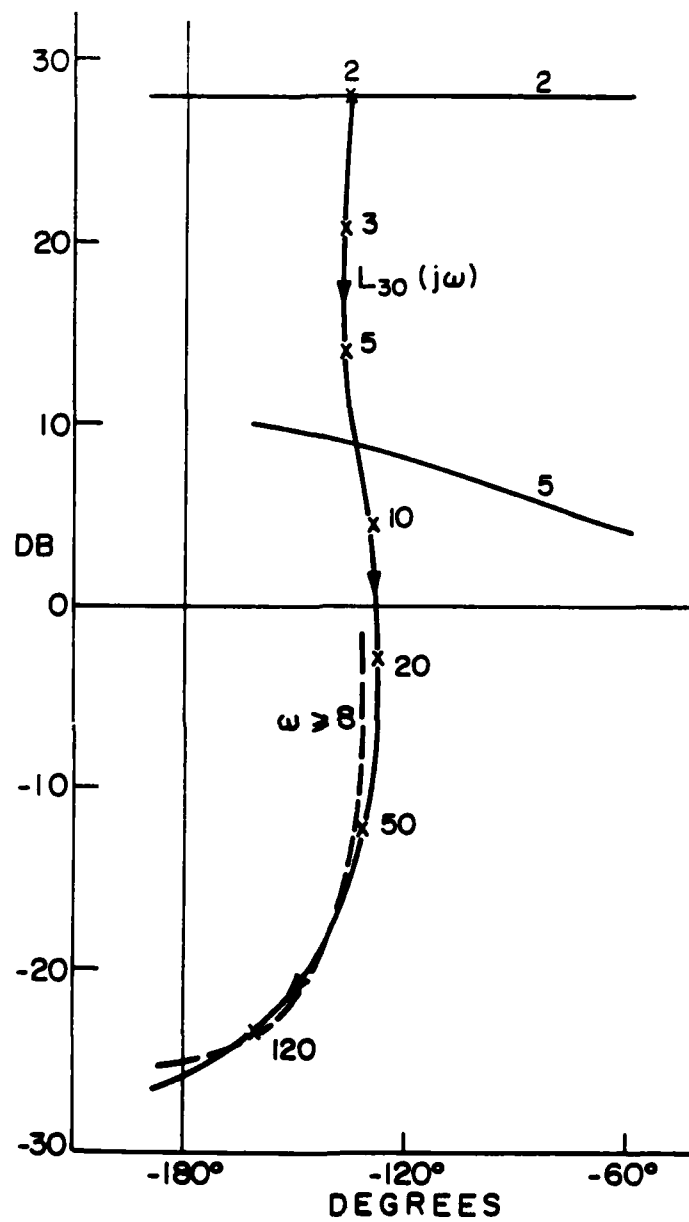


Fig. 4.4 Bounds on L_{30} in Nichols Chart and $L_{30}(j\omega)$

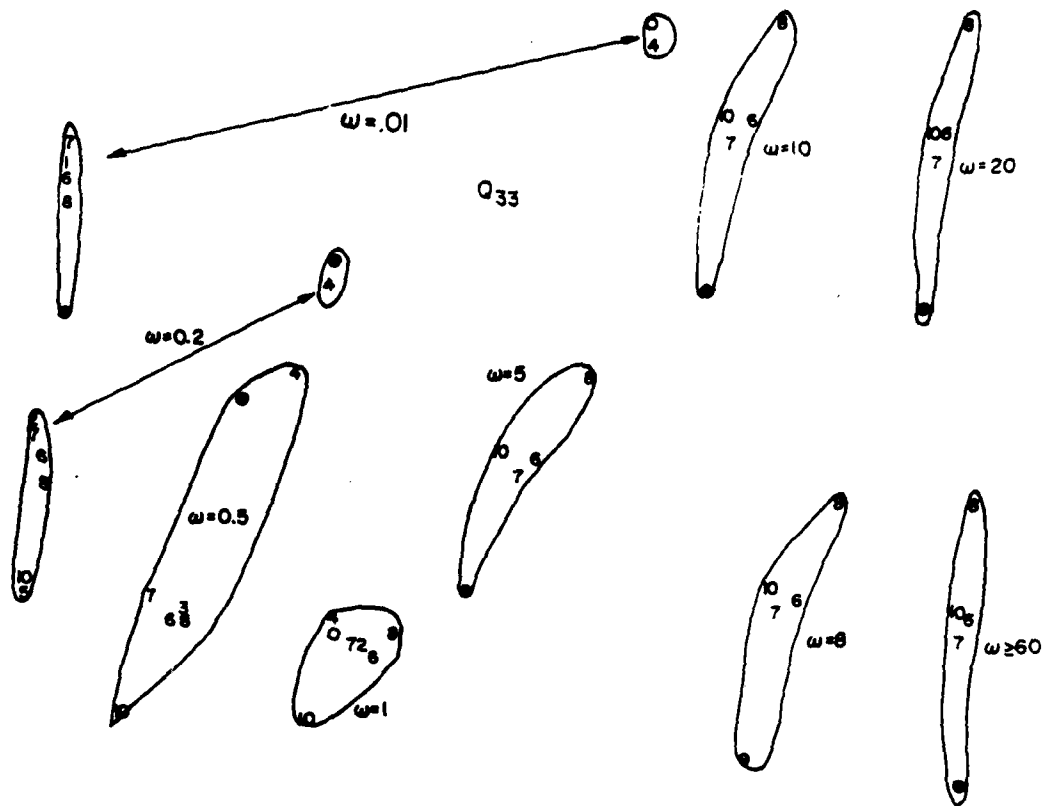


Fig. 4.5 Some templates of $Q_{33}(j\omega)$

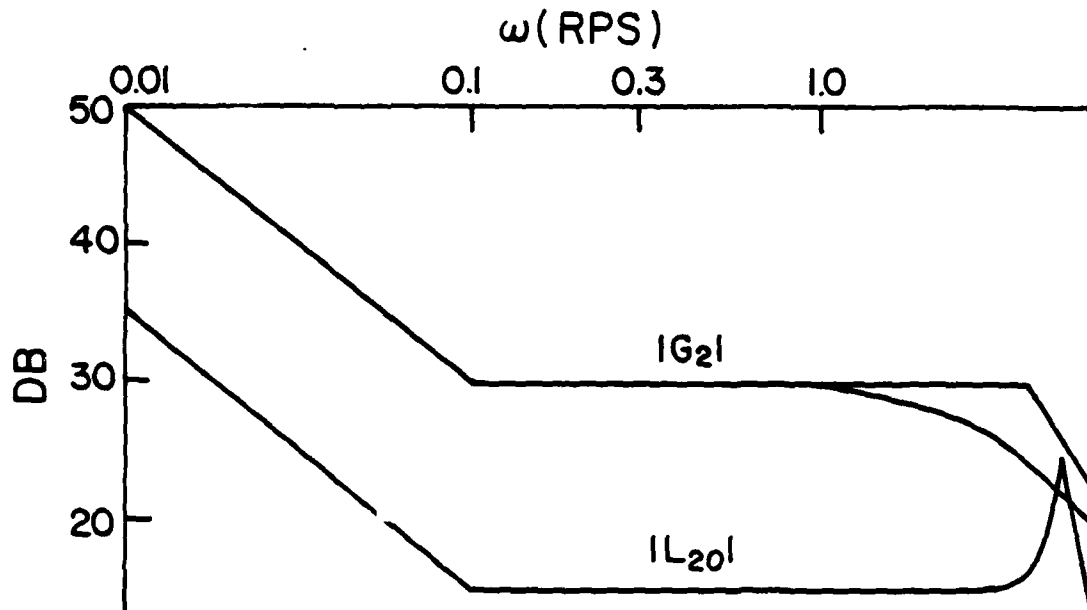


Fig. 4.6 Bounds on $|G_2(j\omega)|$ and on $|L_{20}(j\omega)|$ for part of frequency range.

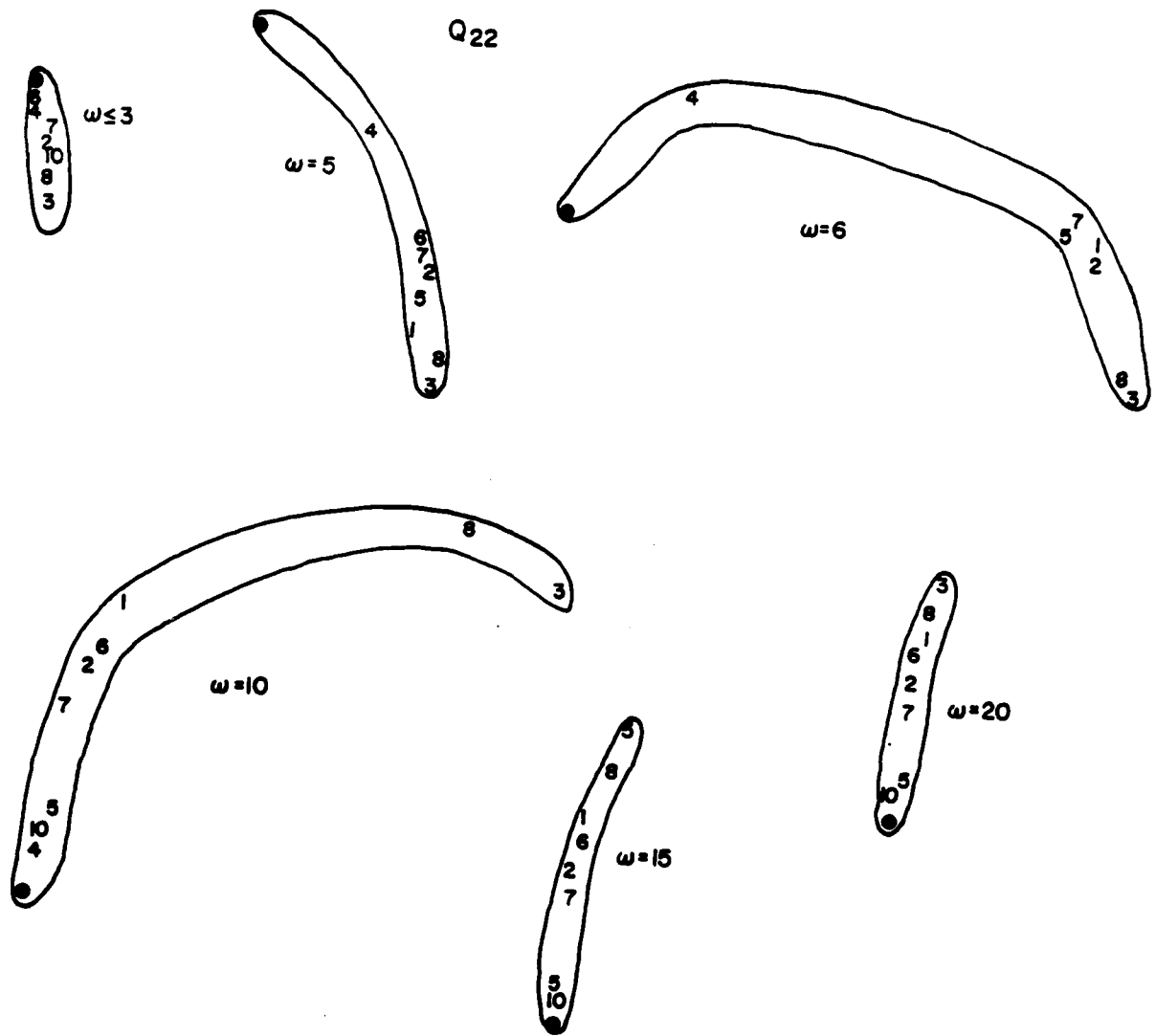


Fig. 4.7 Some templates of $Q_{22}(j\omega)$

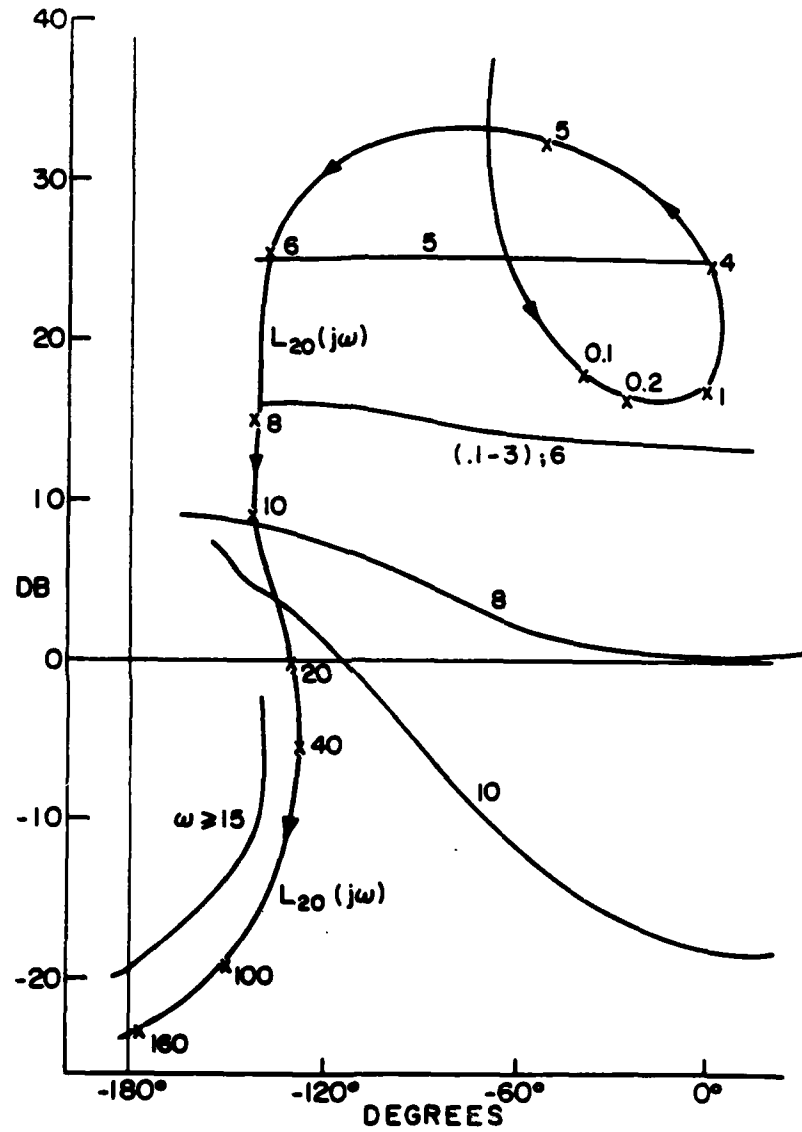


Fig. 4.8 Bounds on $L_{20}(j\omega)$ and $L_{20}(j\omega)$ designed

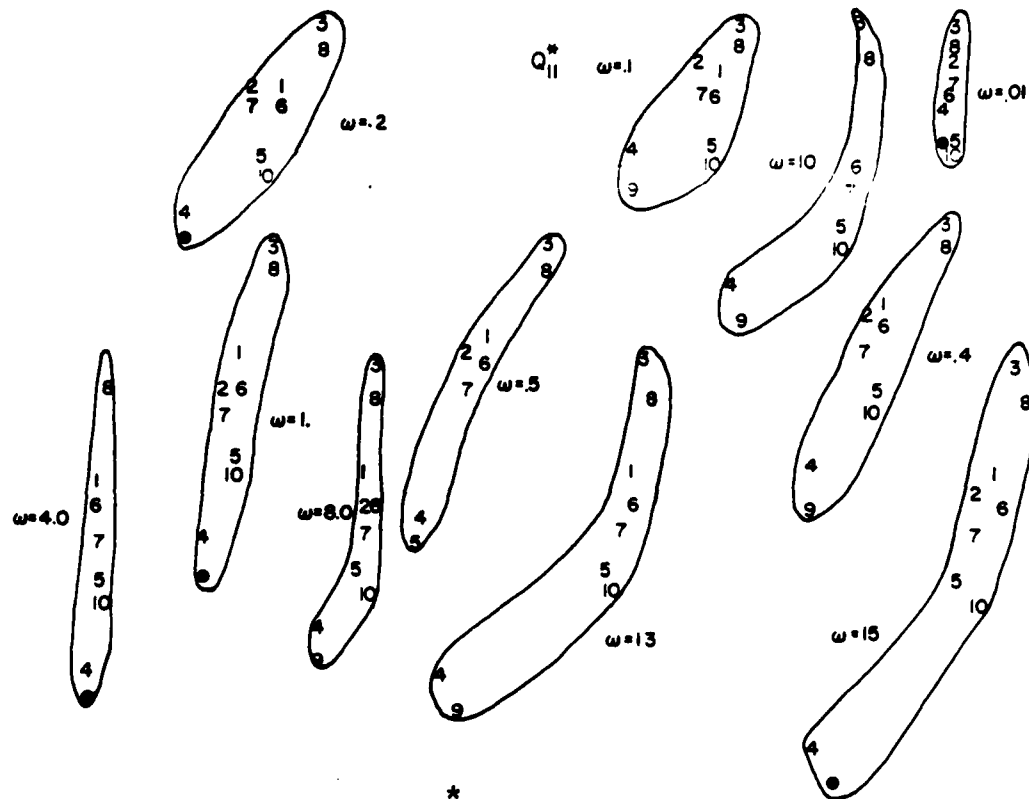


Fig. 4.9 Some templates of $Q_{11}^*(j\omega)$

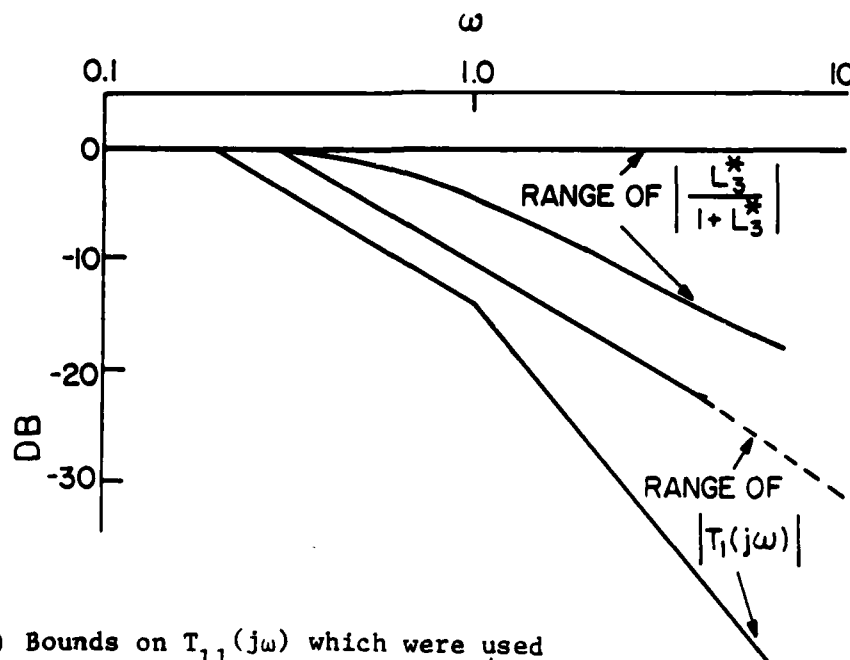


Fig. 4.10 Bounds on $T_{11}(j\omega)$ which were used

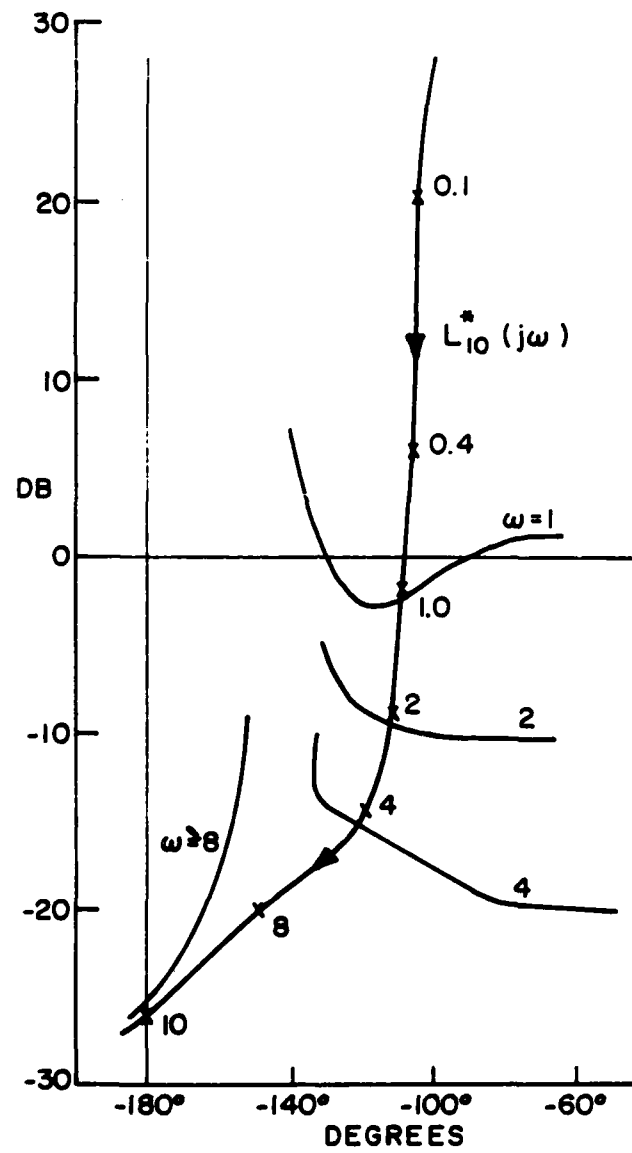


Fig. 4.11 Bounds on $L_{10}^*(j\omega)$ and $L_{10}^*(j\omega)$

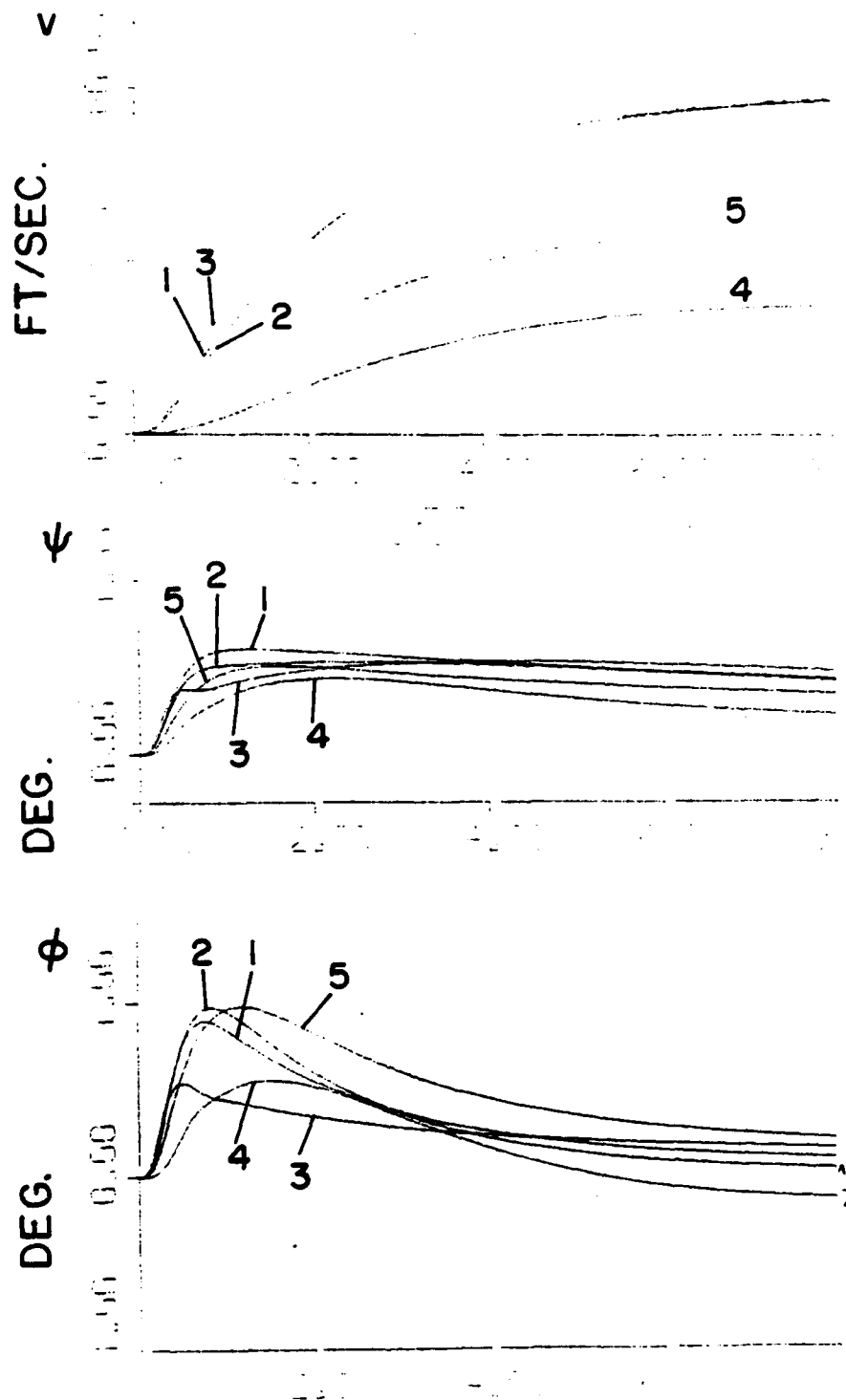


Fig. 4.12 Simulation results, $F_{1a} = 0.3/(s+3)$

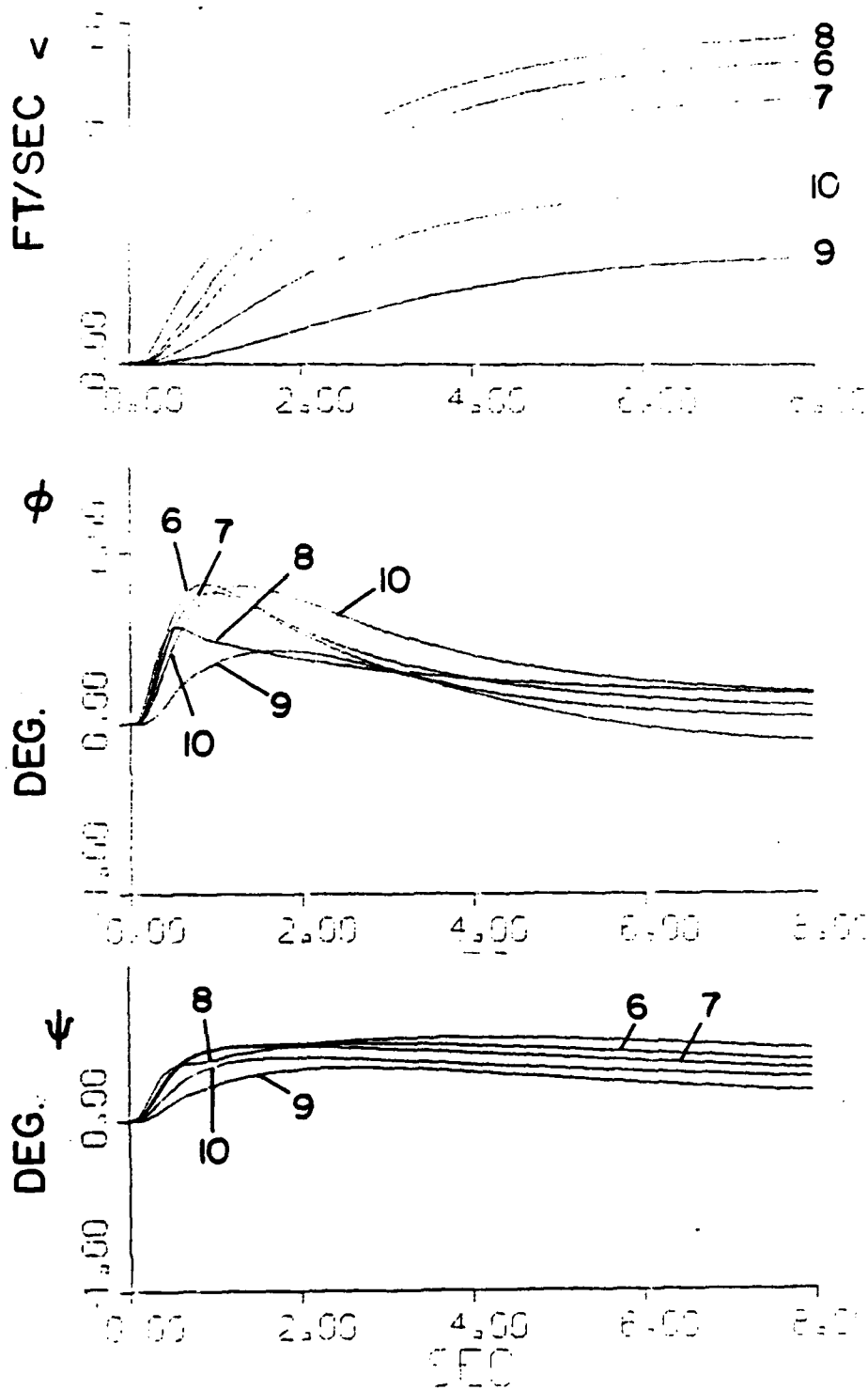


Fig. 4.12 (cont.) Simulation results, $F_{1a} = 0.3/(s+3)$

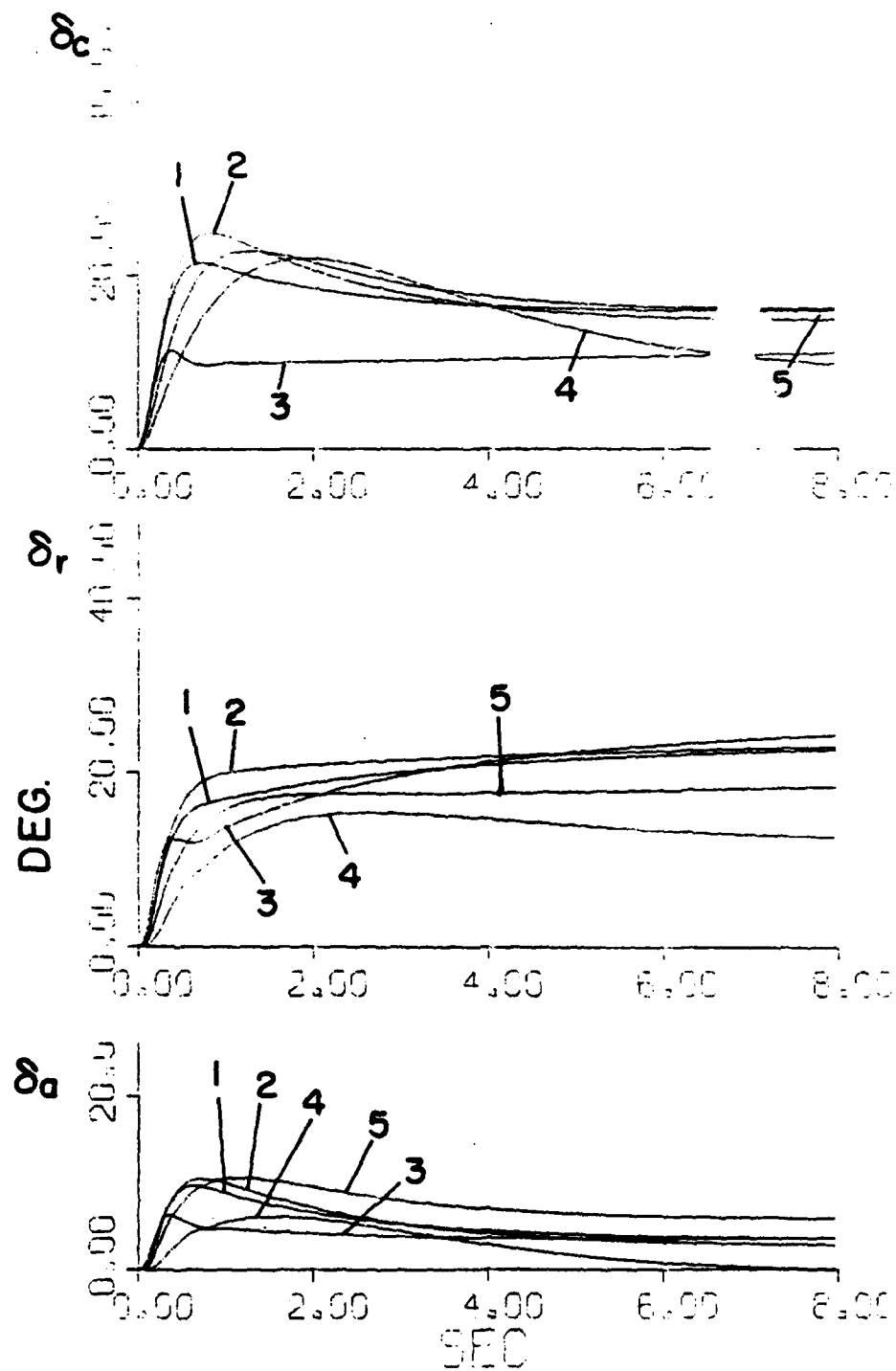


Fig. 4.12 (cont.) Simulation results, $F_{1a} = 0.3/(s+3)$

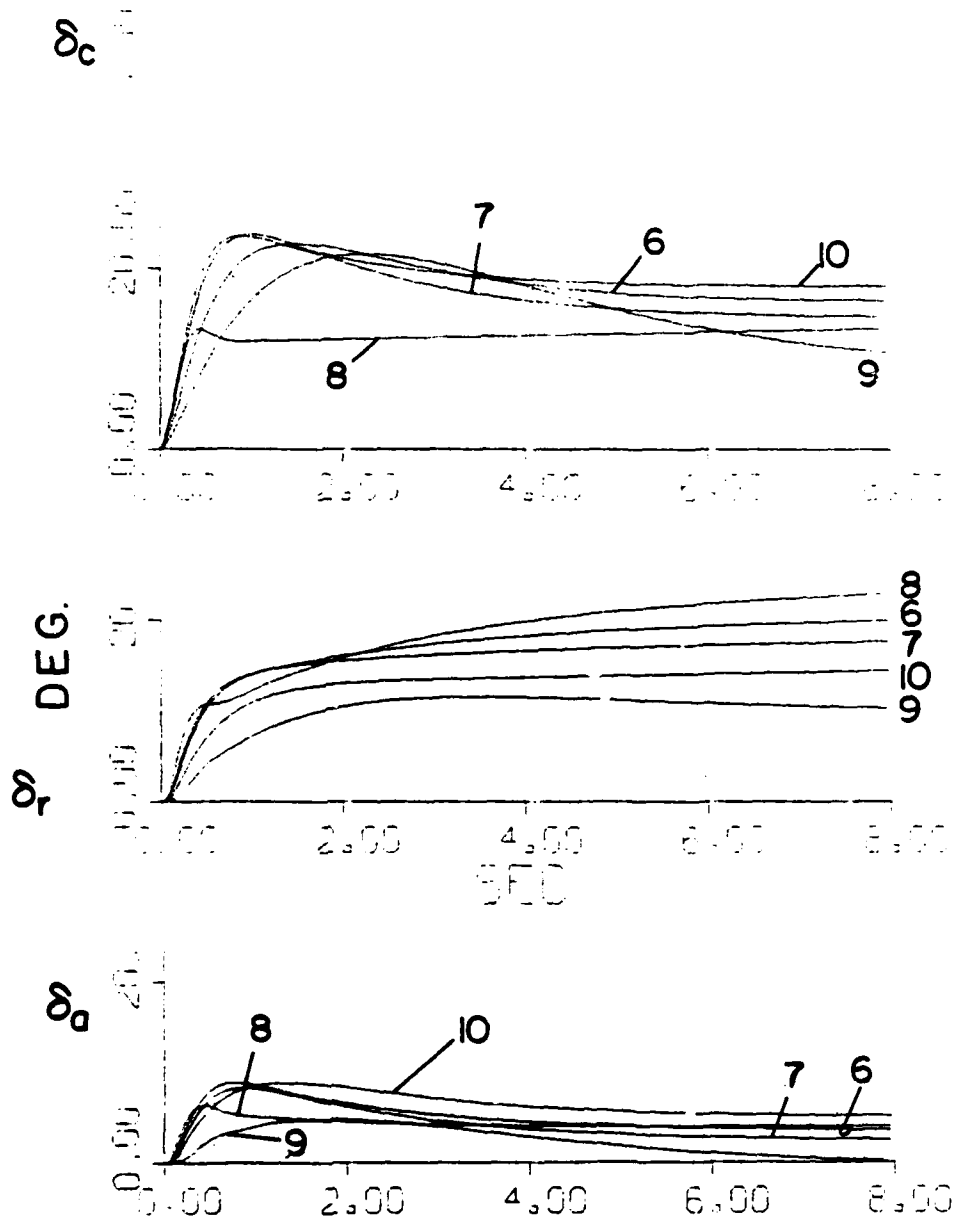


Fig. 4.12 (cont.) Simulation results, $F_{1a} = 0.3/(s+3)$

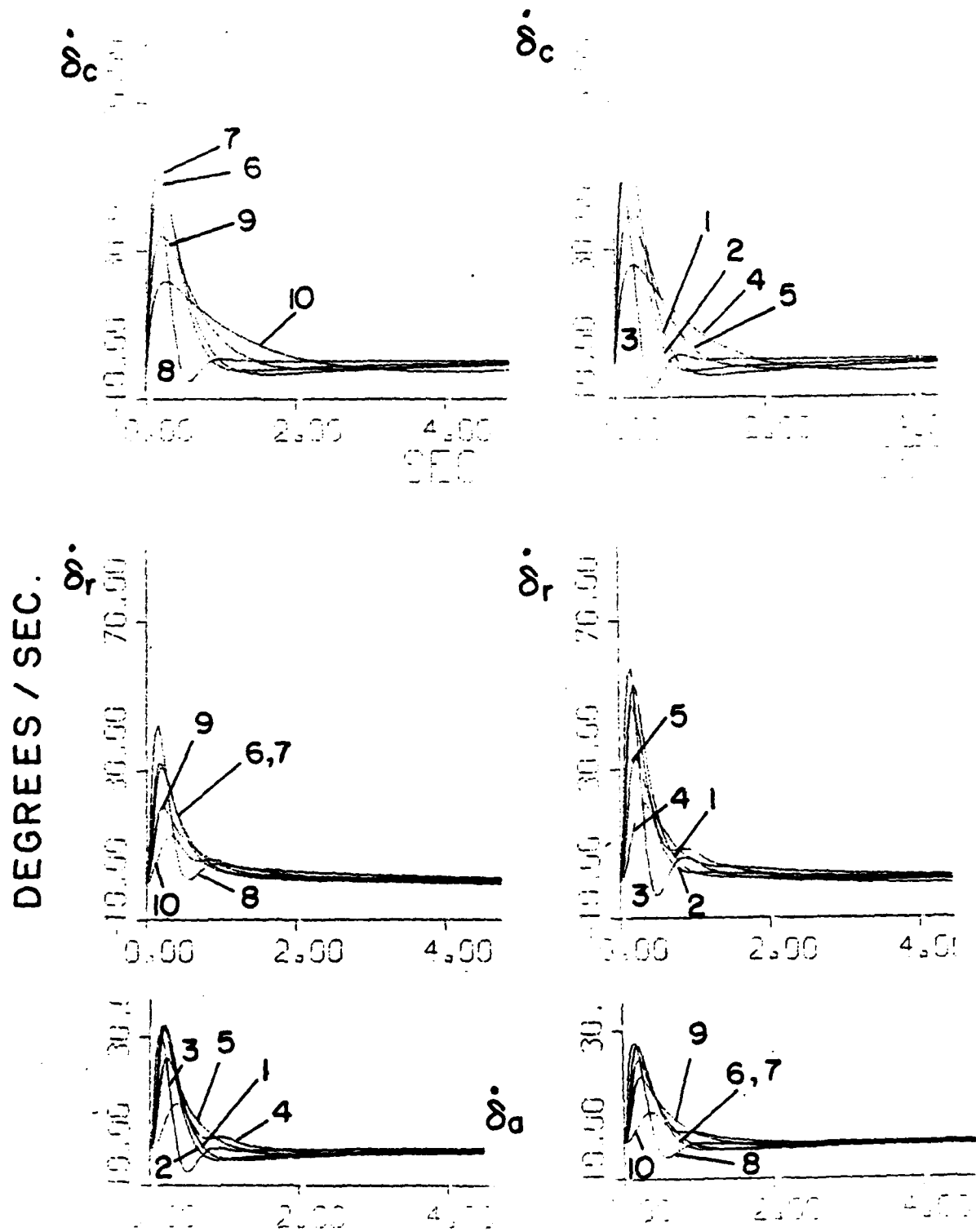


Fig. 4.12 (cont.) Simulation results, $F_{1a} = 0.3/(s+3)$

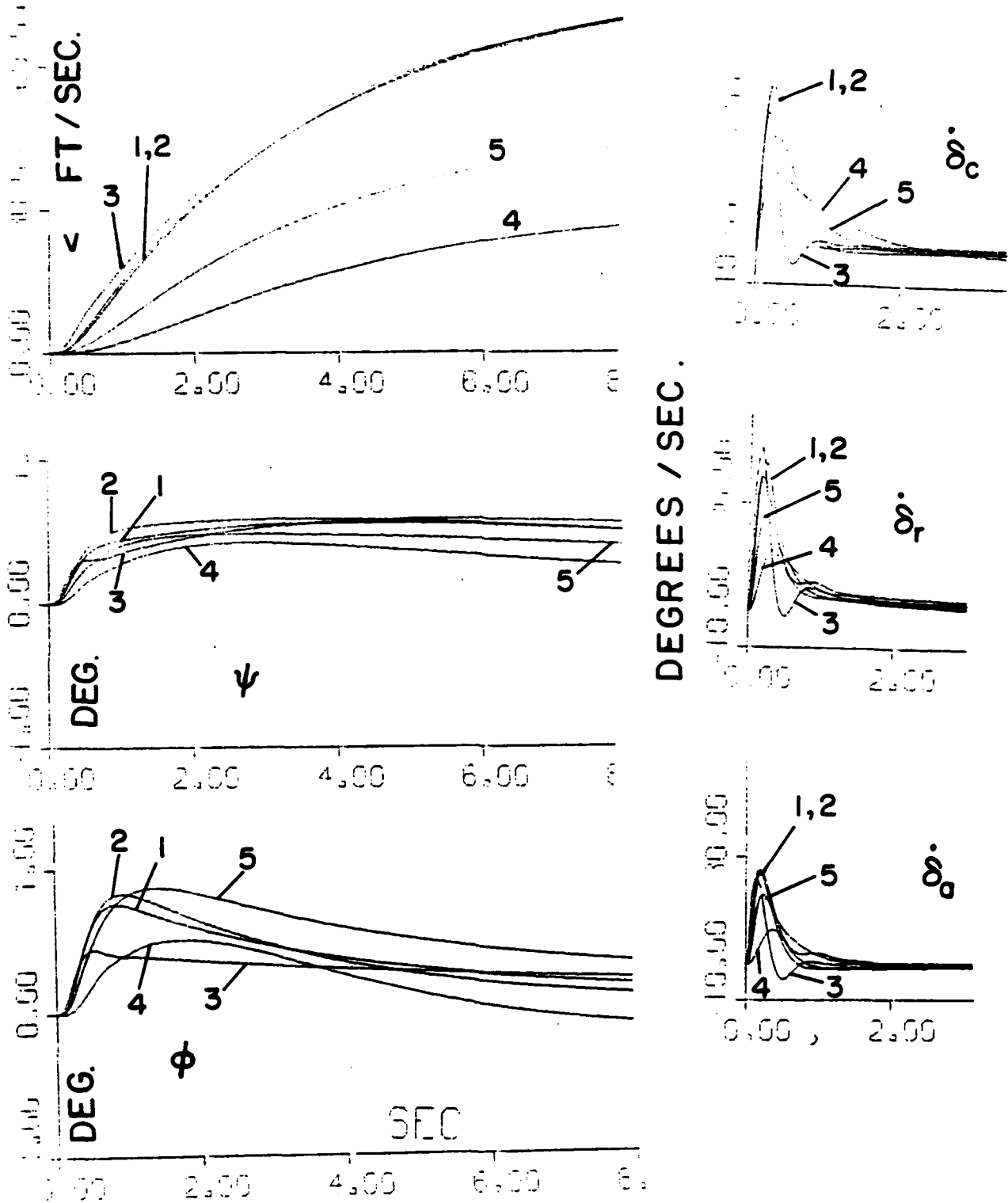


Fig. 4.13 Simulation results, $F_{1b} = 0.5/(s+0.5)$

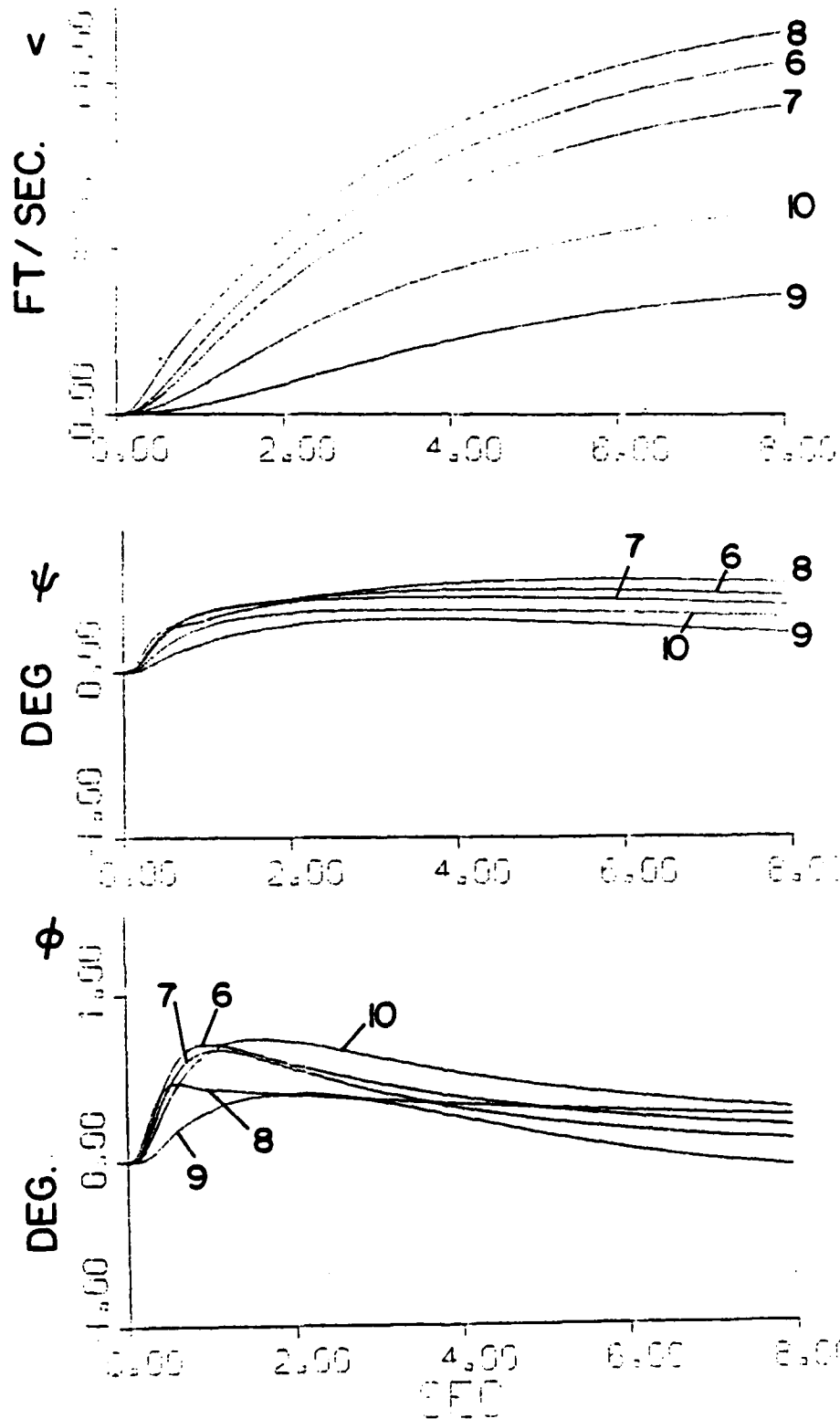


Fig. 4.13 (cont.) Simulation results, $F_{1b} = 0.5/(s+5)$

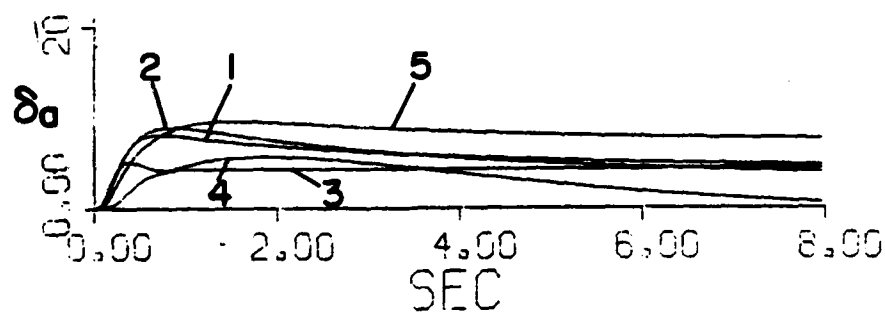
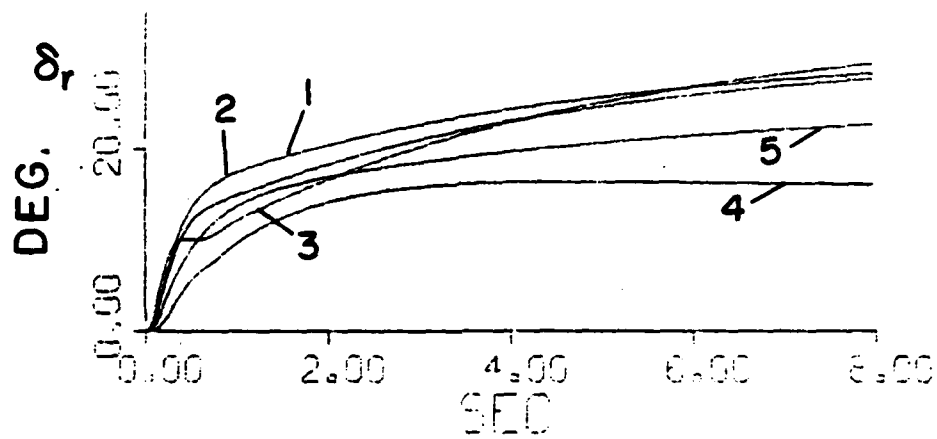
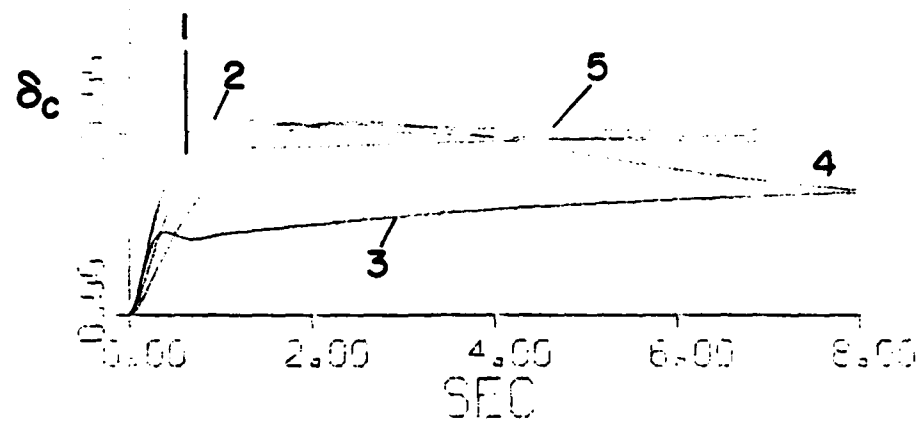


Fig. 4.13 (cont.) Simulation results, $F_{1b} = 0.5/(s+5)$

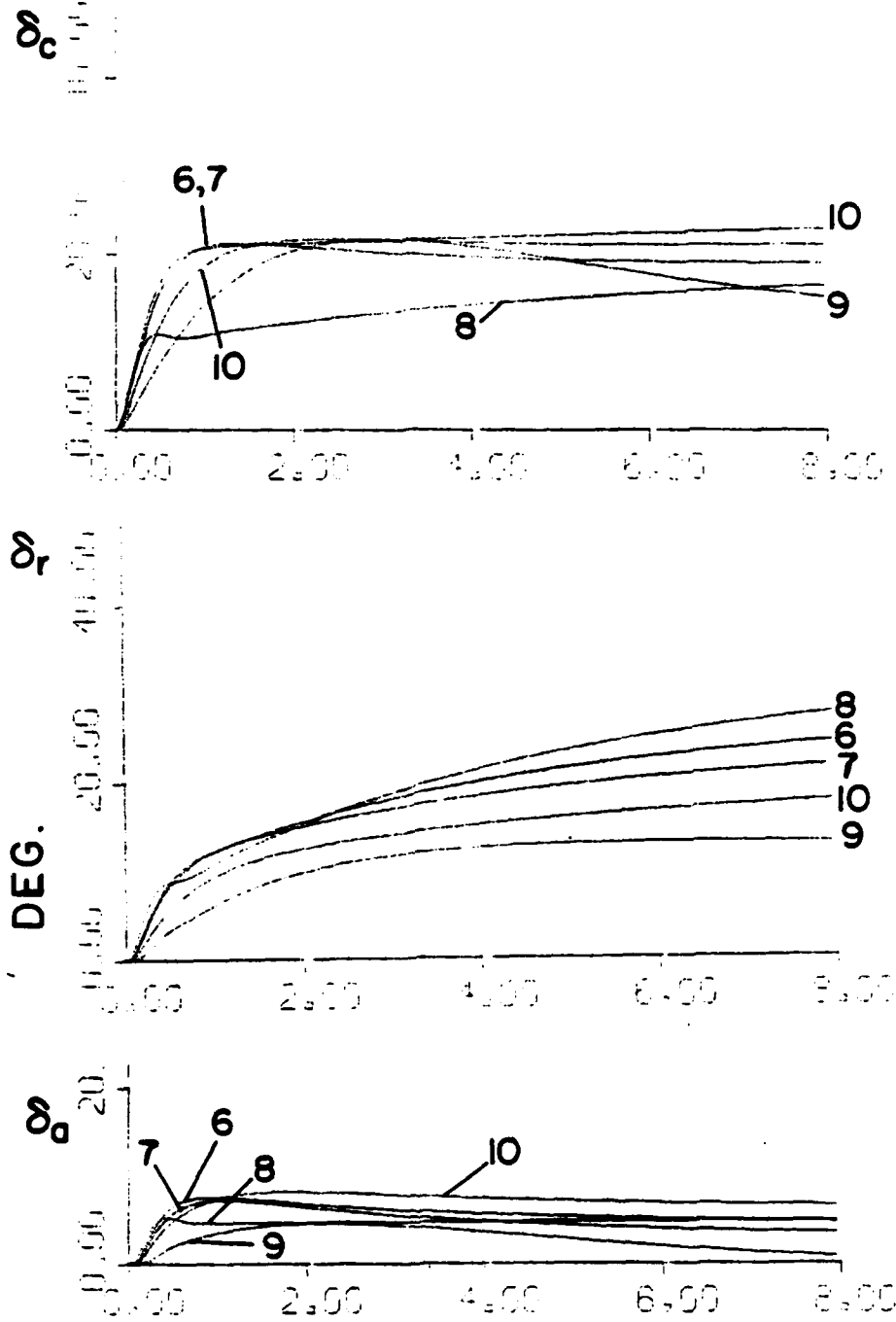


Fig. 4.13 (cont.) Simulation results, $F_{1b} = 0.5/(s+5)$

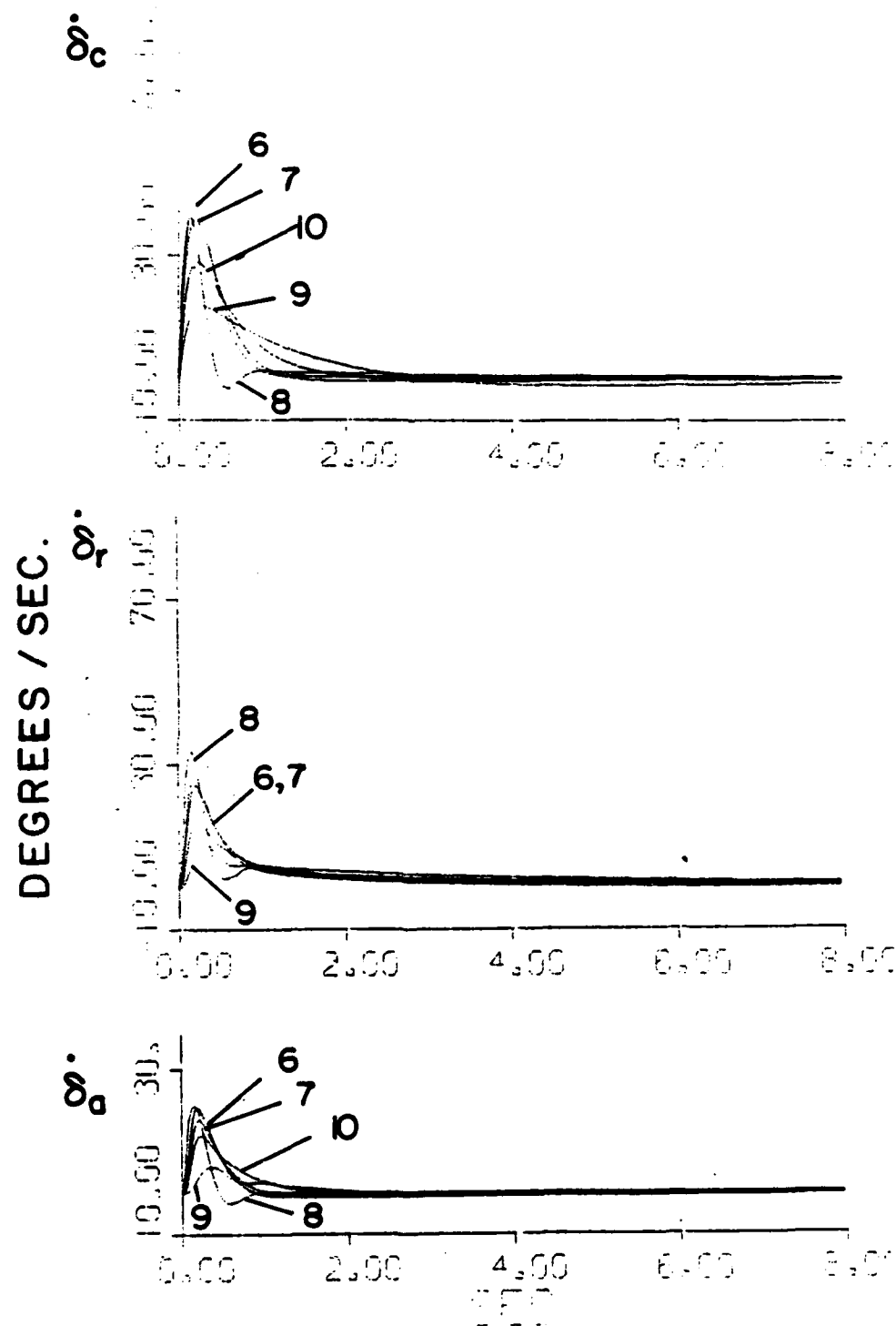


Fig. 4.13 (cont.) Simulation results, $F_{1b} = 0.5/(s+5)$

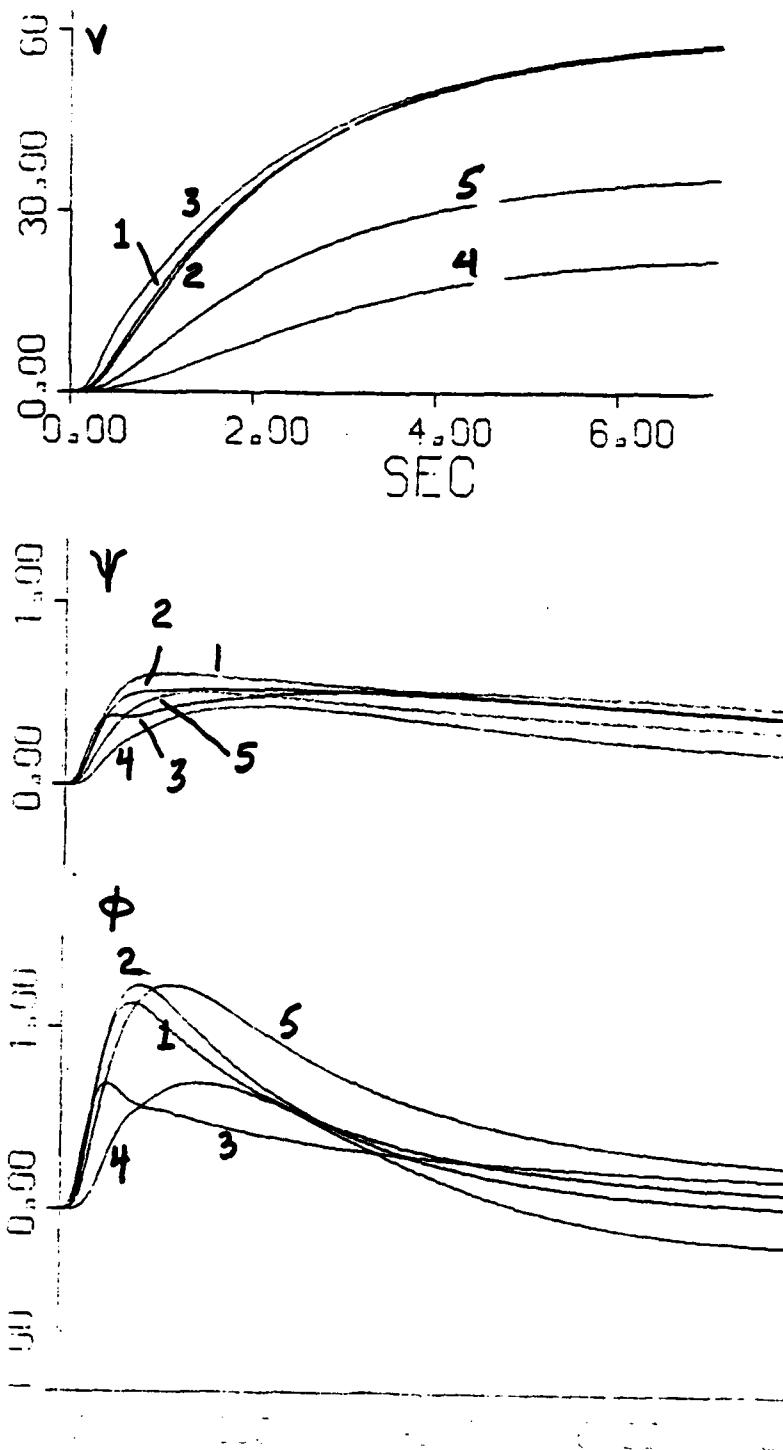


Fig. 4.14 Simulation results with digital compensation, $T = 0.02$ seconds, $F = F_{1a}^*$

Expanded time scale in last two figures

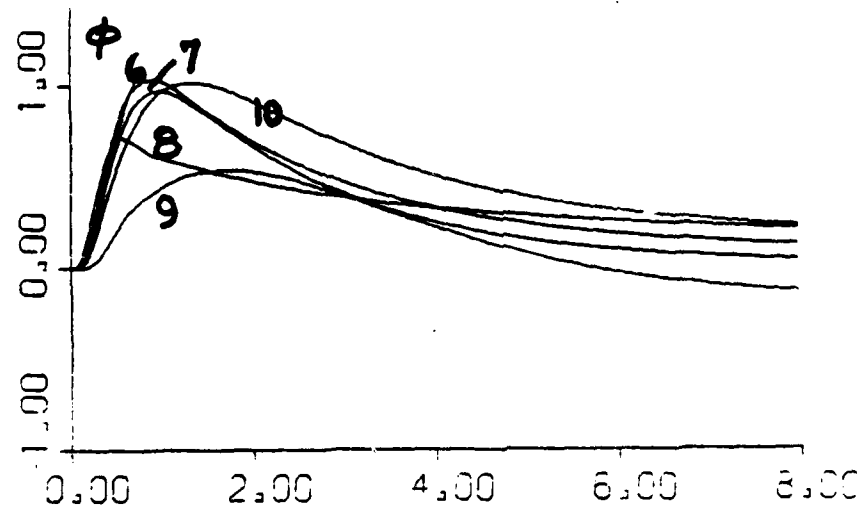
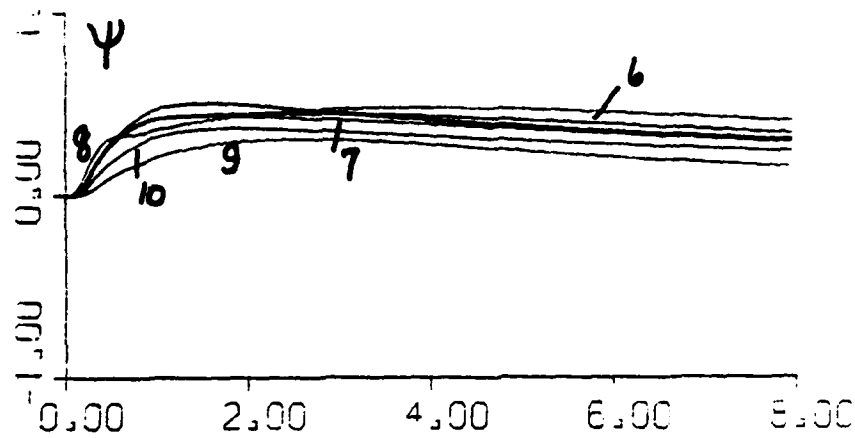
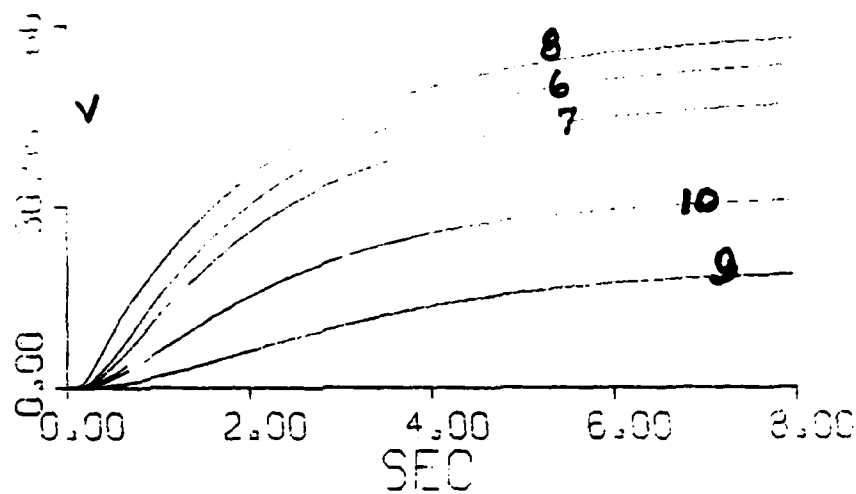


Fig. 4.14 (cont.) Simulation results with digital compensation, $T = 0.02$ seconds, $F = F$

Expanded time scale in last two figures

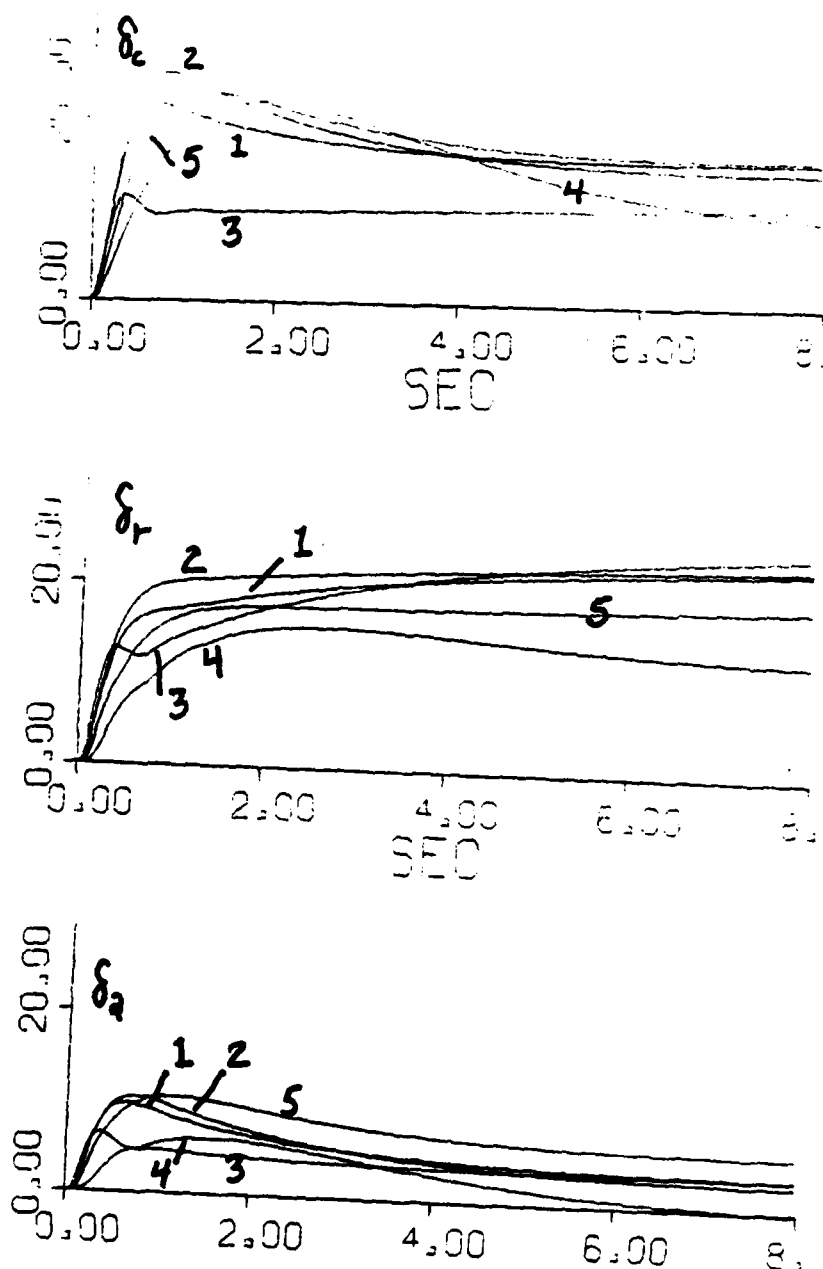


Fig. 4.14 (cont.) Simulation results with digital compensation, $T = 0.02$ seconds, $F = F_{1a}^*$
Expanded time scale in last two figures

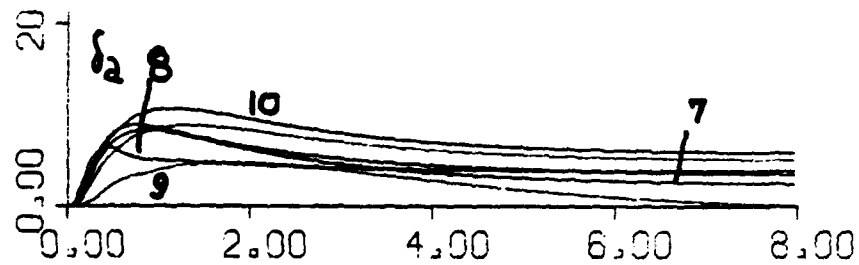
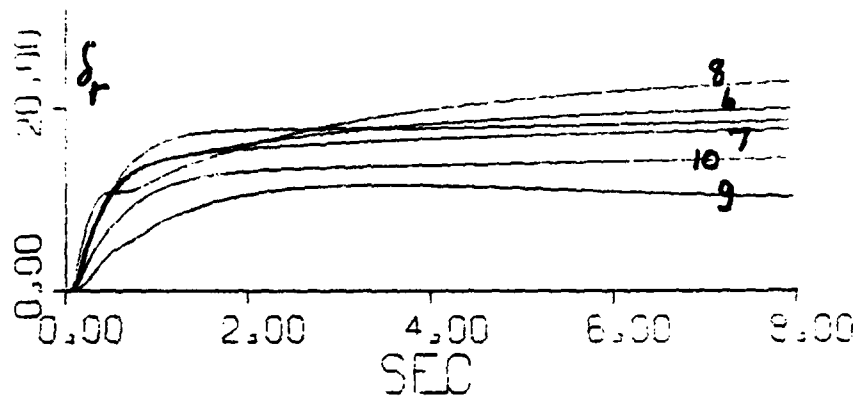
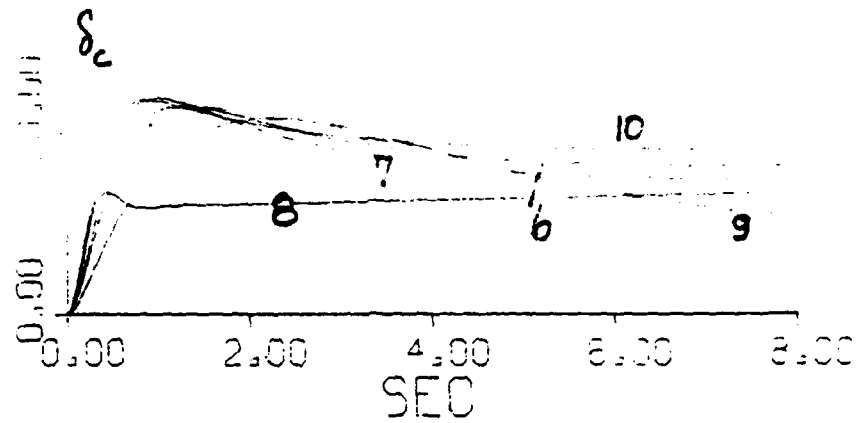


Fig. 4.14 (cont.) Simulation results with digital compensation, $T = 0.02$ seconds, $F = F_{1a}^*$

Expanded time scale in last two figures

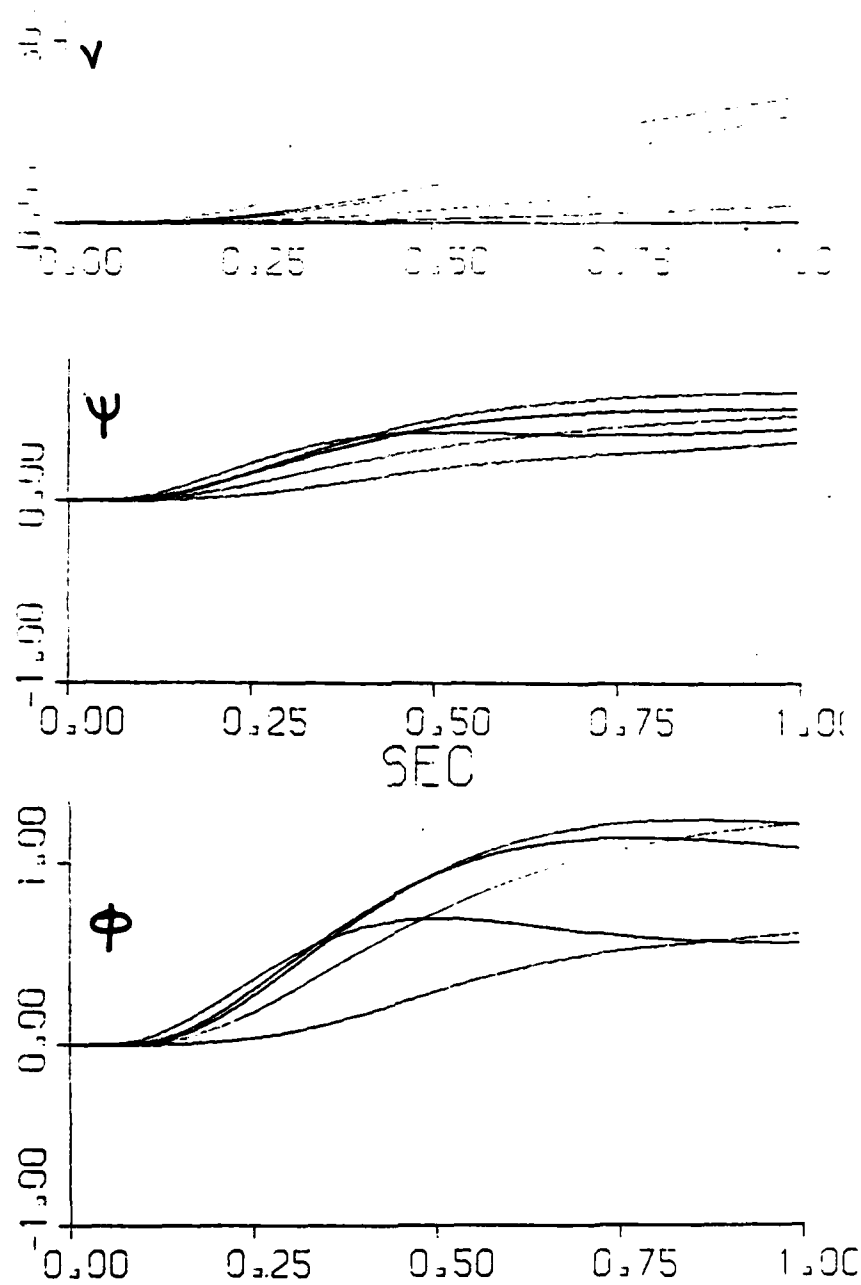


Fig. 4.14 (cont.) Simulation results with digital compensation, $T = 0.02$ seconds, $F = F_{1a}^*$
Expanded time scale in last two figures

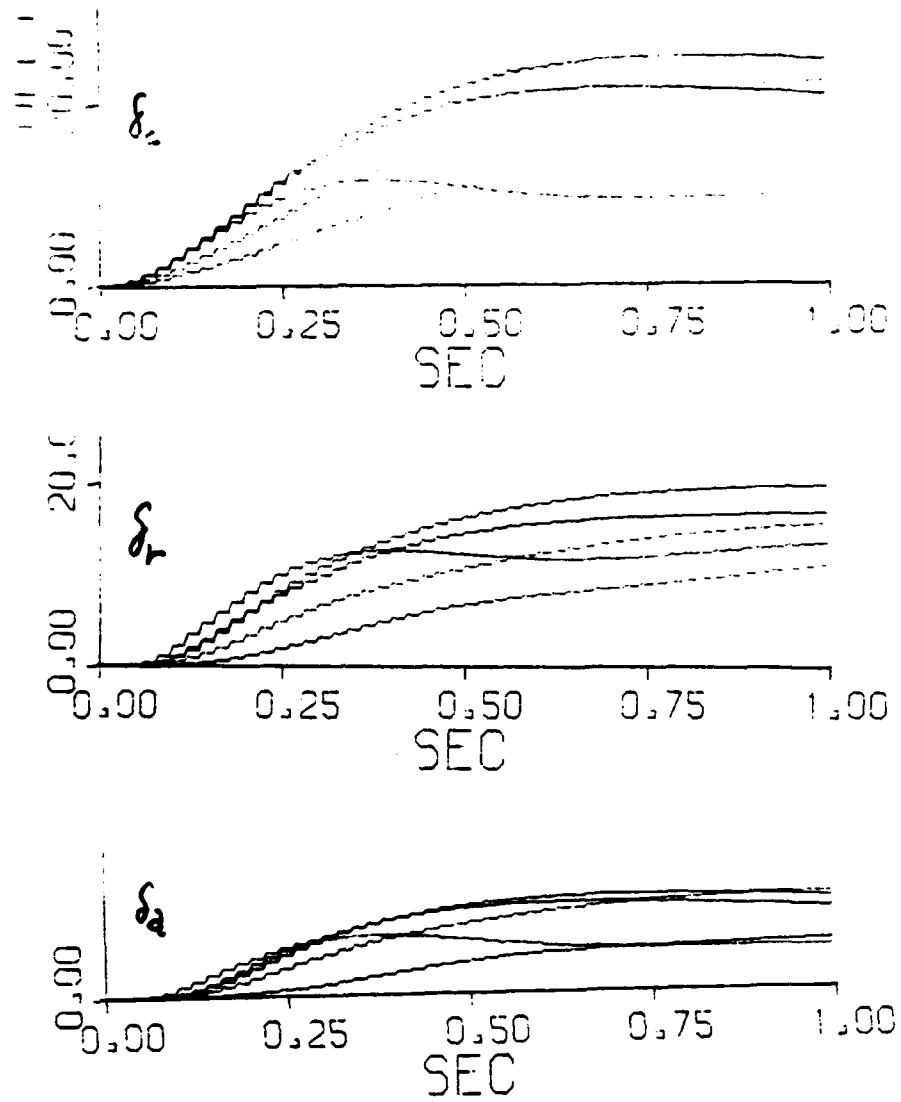


Fig. 4.14 (cont.) Simulation results with digital compensation, $T = 0.02$ seconds, $F = F_{la}^*$
Expanded time scale in last two figures

Chapter 5

DESIGN BASED ON NONLINEAR MULTIPLE
INPUT-OUTPUT PLANT MODEL5.1 Nonlinear MIO Design Technique

In the preceeding chapters a linear MIO (multiple input-output) model was used for the plant. Such a model is only an approximation of the more accurate nonlinear model (Eqs. 5.1-5.5 below). Our design technique is able to cope precisely with a large class of highly uncertain nonlinear MIO plants. It is emphasized that the design technique is exact. The rigorous development of the technique with two detailed numerical examples, is given in [4]. For the sake of completeness, a qualitative description of the technique is here included.

Let $y_i = wx_i$ be the nonlinear relation between a n -vector x_i of plant inputs and a n -vector y_i of plant outputs. Due to uncertainty $w \in W$, a set. Let there be n such (x_i, y_i) vector-pairs, forming two $n \times n$ matrices $X = (x_1, \dots, x_n)$, $Y = (y_1, \dots, y_n)$ with the x_i -vector the i^{th} column of X , etc, and $y_j = wx_j$; $j = 1, \dots, n$. It is assumed that the n x_j are an independent set, as are the n y_j . Let the matrix P of transfer functions be defined by $\hat{Y} = \hat{P}\hat{X}$, where \hat{Y} is the matrix of Laplace transforms of the elements of Y , etc. The P matrix is denoted as the LTIE (linear time invariant equivalent) of the mio nonlinear plant w , with respect to the n -vector Y set of outputs. A different X, Y set gives in general a different P , when w is nonlinear. Repeat the process over a set V of n -vectors, to obtain a set of LTIE plants. Repeat over the elements of $W = \{w\}$, to obtain an overall set $P = \{P\}$ of LTIE plants. This set P is the LTIE of the set W , with respect of the set of n -vectors $V = \{Y\}$ (or the set $X = \{X\}$).

5.1.1 The barrel analogy

The following analogy may be helpful in comprehending the LTIE idea. Imagine a barrel $V = \{y\}$ of all the desired n -output vectors the nonlinear plant is supposed to deliver over its life. Also there is a barrel $W = \{w\}$ of all possible $n \times n$ nonlinear plants, due to the parameter uncertainty. We create by the above technique, a barrel $P = \{P\}$ of $n \times n$ linear time invariant plants, which has therefore the following property. Suppose one picks any w_i from the W barrel and any y_j vector from the V barrel. Then there is a n -vector x_{ij} of inputs, such that $y_j = w_i x_{ij}$. Then in the P barrel, there is guaranteed to be a P_{ij} , such that $y_j = P_{ij} x_{ij}$. Thus, the P barrel is equivalent to the W barrel, with respect to the V barrel.

The vital point is that the designer can forget about W . If he makes a proper linear time invariant design for the P barrel, then this same design is guaranteed to work for the W barrel. By a proper design for the P barrel, it is meant that the actual plant output is a member of the desired output set V , no matter which P in P is used as the plant. Thus, the $n \times n$ nonlinear uncertainty design problem has been converted to a $n \times n$ linear time invariant uncertainty problem. It is important to include in V a good sampling of all the desired nonlinear plant output vectors, because the linear design is guaranteed to work only for the P set which is generated in the above manner by the W, V sets, i.e. P is a function of V as well as of W .

5.2 The Nonlinear Plant

Because of the nonlinear coupling between them, the 2×2 vertical translation (α) mode of Chapter 3 and the 3×3 lateral translation (β_2) mode of Ch. 4 were combined into a single 5×5 nonlinear plant:

Control inputs: Elevons δ_e , flaps δ_f , canards δ_c , rudder δ_r , ailerons δ_a .

Plant outputs: Vertical velocity v_z , pitch angle θ , lateral velocity v_y , yaw angle ψ , roll angle ϕ .

Command inputs and performance tolerances: There are command-d simultaneously

vertical velocity of 25 ft./sec. and lateral velocity of 60 ft./sec., with

tolerances on these outputs as in Chs. 3,4. The other tolerances are:

pitch angle $\theta \leq 0.165$, yaw $\psi \leq 1.0$, roll $\phi \leq 2$, all in degrees.

Nonlinear Equation of Motion

$$\begin{aligned}\dot{p} &= \frac{I_y - I_z}{I_x} q \cdot r + \frac{I_{xz}}{I_x} \dot{r} + \frac{I_{xz}}{I_x} p q + \frac{M_x}{I_x} \\ \dot{q} &= \frac{I_z - I_x}{I_y} p \cdot r + \frac{I_{xz}}{I_y} r^2 - \frac{I_{xz}}{I_y} p^2 + \frac{M_y}{I_y} \\ \dot{r} &= \frac{I_x - I_y}{I_z} q \cdot p + \frac{I_{xz}}{I_z} \dot{p} - \frac{I_{xz}}{I_z} q \cdot r + \frac{M_z}{I_z}\end{aligned}\tag{5.1a-c}$$

$$\begin{aligned}\dot{u} &= v \cdot r - w \cdot q + \frac{F_x}{m} \\ \dot{v} &= w \cdot p - u \cdot r + \frac{F_y}{m} \\ w &= u \cdot q - r \cdot p + \frac{F_z}{m}\end{aligned}\tag{5.2a-c}$$

$$M_x = \frac{1}{2} \rho V^2 S b [C_{\ell} + C_{\ell \delta r} \delta_r + C_{\ell \delta a} \delta_a + C_{\ell \delta c} \delta_c + \frac{b}{2V} (C_{\ell r} \cdot r + C_{\ell p} \cdot p)]$$

$$M_y = \frac{1}{2} \rho V^2 S c [C_{m \delta e} \delta_e + C_{m \delta f} \delta_f + C_m + \frac{c}{2V} (C_{mq} q)] \quad (5.3a-c)$$

$$M_z = \frac{1}{2} \rho V^2 S b [C_{n \delta a} \delta_a + C_{n \delta r} \delta_r + C_{n \delta c} \delta_c + C_n + \frac{b}{2V} (C_{nr} r + C_{np} p)]$$

$$F_x = -mg \sin \theta + \frac{1}{2} \rho V^2 S [C_{x \delta e} \delta_e + C_{x \delta f} \delta_f + C_x] \quad (5.4a-i)$$

$$F_y = mg \cos \theta \sin \phi + \frac{1}{2} \rho V^2 S [C_{y \delta r} \delta_r + C_{y \delta a} \delta_a + C_{y \delta c} \delta_c + C_y + \frac{b}{2V} (C_{yr} r + C_{yp} p)]$$

$$F_z = mg \cos \theta \cos \phi + \frac{1}{2} \rho V^2 S [C_{z \delta e} \delta_e + C_{z \delta f} \delta_f + C_z + \frac{c}{2V} (C_{zq} q)]$$

$$A_n = \frac{F_z}{m}; \quad v_z = \int_0^t A_n dt; \quad A_y = \frac{F_y}{m}; \quad v_y = \int_0^t A_y dt$$

$$\dot{\phi} = p + q \tan \theta \sin \phi + r \tan \theta \cos \phi, \quad \phi = \int \dot{\phi} dt$$

$$\dot{\theta} = q \cos \phi - r \sin \phi, \quad \theta = \int \dot{\theta} dt + \theta_0 \quad (5.5a-f)$$

$$\dot{\psi} = r \left(\frac{\cos \phi}{\cos \theta} \right) + q \left(\frac{\sin \phi}{\cos \theta} \right), \quad \psi = \int \dot{\psi} dt$$

V = Total velocity

α_0 = Trim AOA ($\theta_0 = \alpha_0$)

$u_0 = V \cos \alpha_0, w_0 = V \sin \alpha_0$

(5.6a-e)

$u = \int \dot{u} dt + u_0, v = \int \dot{v} dt, w = \int \dot{w} dt + w_0$

$\alpha = \tan^{-1} \frac{w}{u}, \beta = \sin^{-1} \frac{v}{V}$

Strictly the aerodynamic coefficients C_{ij} are functions of α and β . However, here they are so restricted in magnitude by the specifications that they are effectively constants. The nonlinearities are due to the multiplication, etc, of state variables in the above equations (5.1-5.5).

5.3 The Nonlinear Plant Input-Output Sets

Formally, the LTIE P set is obtained by picking any y vector, solving for $x = w^{-1}y$ and repeating over V and W . This is one way, which was used in [4]. Another way is to simulate the nonlinear plant and try to drive it in such a way as to produce the kind of y vectors required by the specifications. This is normally very difficult, but in this problem we already have the linear designs of Chs. 3,4. So the same f,g elements were used as compensations around the 5×5 nonlinear plant, the entire system simulated on the digital computer and subjected to the inputs listed in the specifications. It was hoped that the nonlinear 5×5 plant outputs would not differ very greatly from those achieved separately in the linear 2×2 and 3×3 designs. If they did so differ, one could experiment with other command inputs and hopefully find some which would result in the desired output vectors. It was an experiment worth trying.

The results achieved were very interesting, because they were closely similar to those achieved in the two separate linear designs. This is seen by comparing the two. Figs. 5.1 a,b (nonlinear results) should be compared with δ_f , δ_e curves respectively, in Fig. 3.13 (p. 165), Figs. 5.2a,b with the θ , v_z curves of Fig. 3.13. Each of these gives the results for the five cases listed in Ch. 3. It is seen that case by case the curves are very similar. Figs. 5.3a-c present the nonlinear results for v, ψ, ϕ (cases 1-5), to be compared with the linear results in Fig. 4.12, p. 183 for the same variables; Figs. 5.4a-c (nonlinear, cases 6-10) with the linear results of Fig. 4.12, p. 184; Figs. 5.5a-b for δ_c , δ_r , δ_a (nonlinear, cases 1-5) with Fig. 4.12 (p. 185) linear results; Figs. 5.6a-c (nonlinear, cases 2-10) with Fig. 4.12 (p. 186) linear results. It is seen that case by case, the results are very similar for both the control inputs and the plant outputs. This proves that the LTIE of the 5x5 nonlinear plant (combined lateral and longitudinal) for the above cases, and for this class of plant outputs is essentially that used in the two separate, decoupled linear problems of Chapters 3,4. Hence straightforward application of our technique to the resulting 5x5 LTIE problem would undoubtedly result in the same f,g compensation functions obtained in the two separate 2x2, 3x3 designs. In fact our nonlinear simulation with these compensations has already been done. There is no need for any more work. Figs. 5.1-5.6 are indeed the simulation results.

The above results suggest that at least in mio flight control problems, it is worth doing first a design based on linearized models, before embarking on one based on the more accurate nonlinear model. The compensations resulting from the linear design may then be tried for the nonlinear

plant. Comparison of the results with the linear system, indicates how serious are the nonlinearities. In the above example, the results would undoubtedly be significantly different if the x, z ranges were much larger, such that the C_{ij} are then in the strongly nonlinear ranges of these variables.

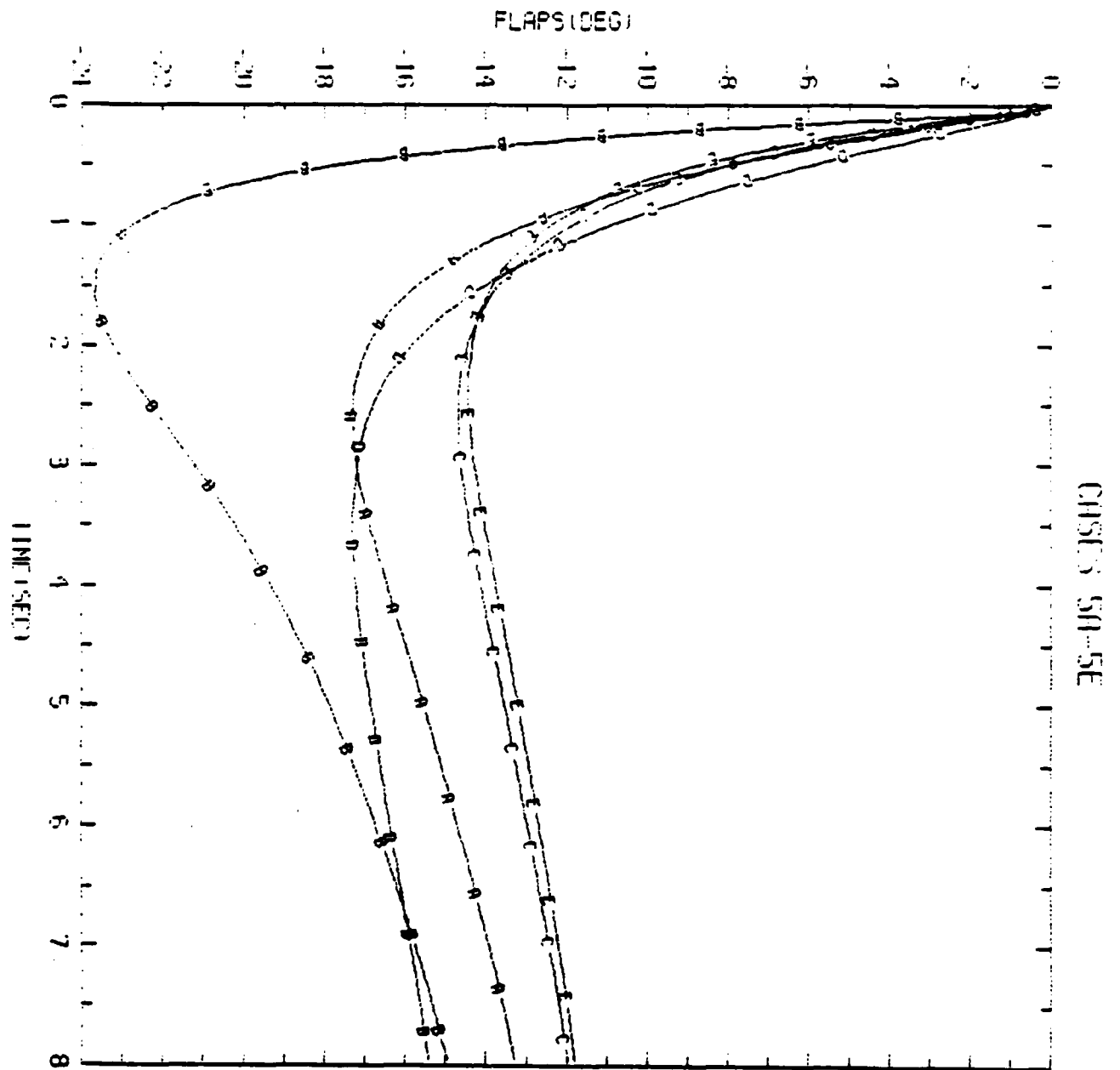


Fig. 5.1a Flap (δ_f) input (cf Fig. 3.13)

Cases: A-5, B-4, C-1, D-3, E-2

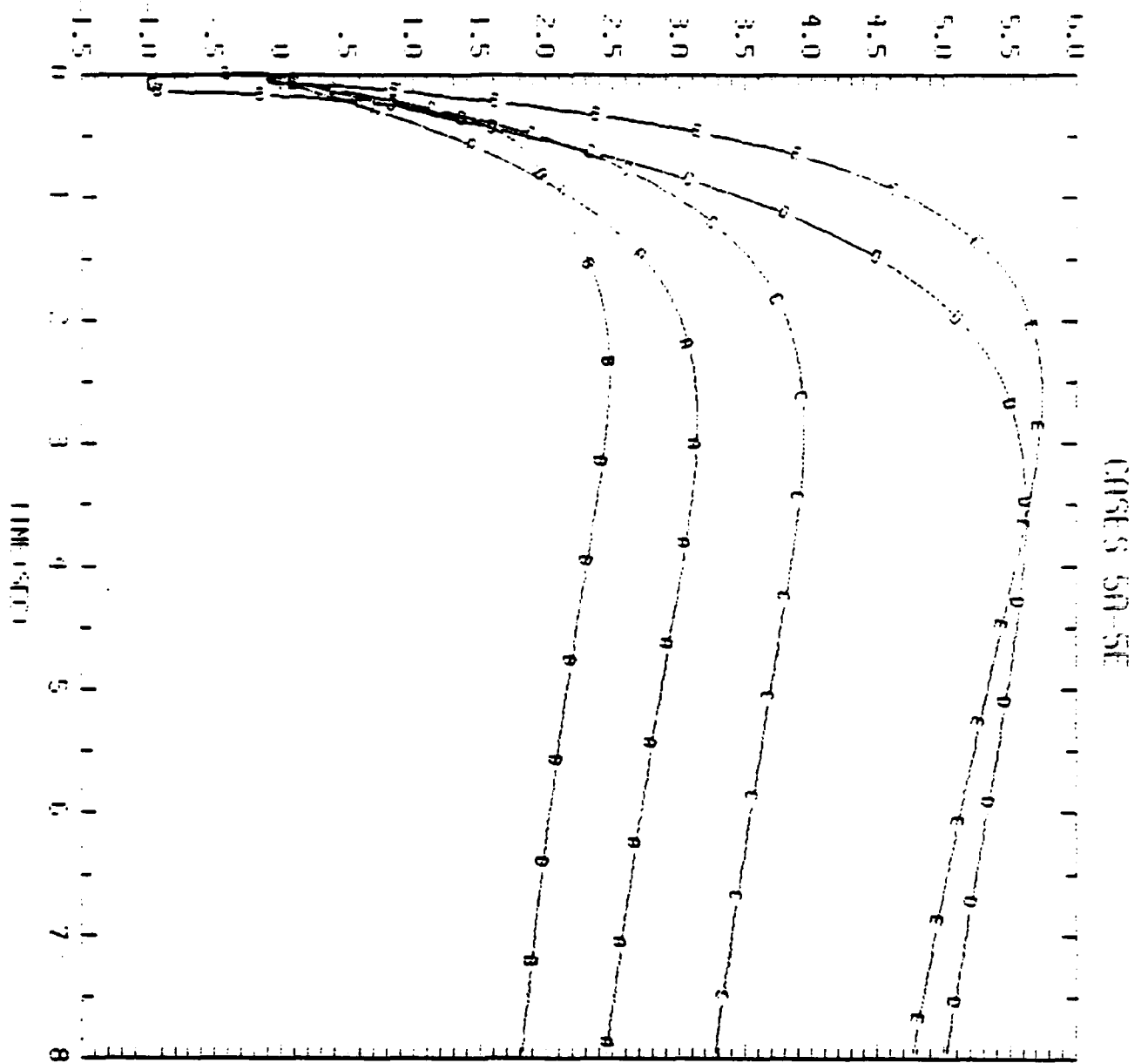


Fig. 5.1b Elevon (δ_e) input (cf Fig. 3.13)

Cases: A-1, B-4, C-2, D-5, E-3

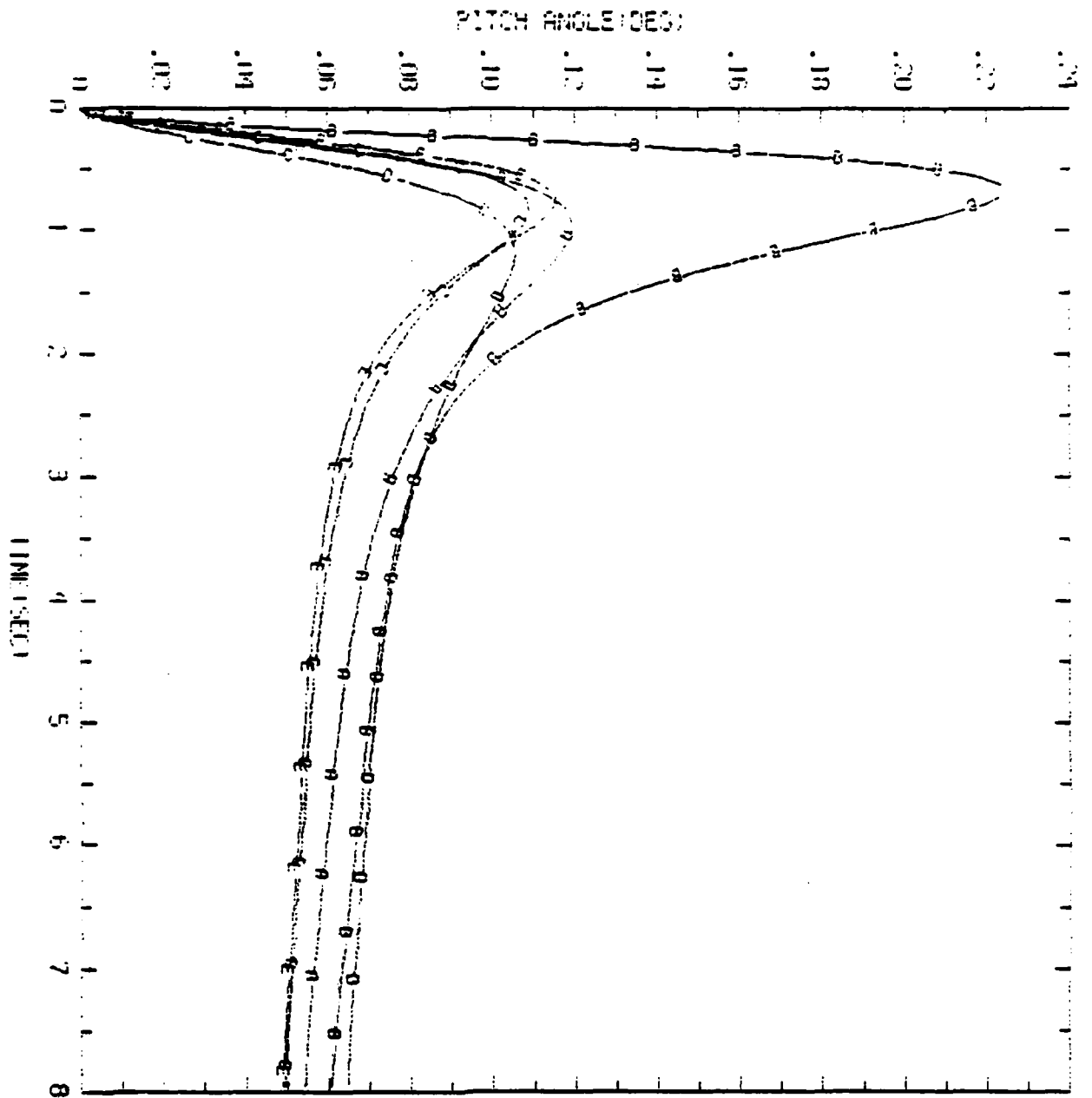


Fig. 5.2a Pitch (θ) output (cf Fig. 3.13)

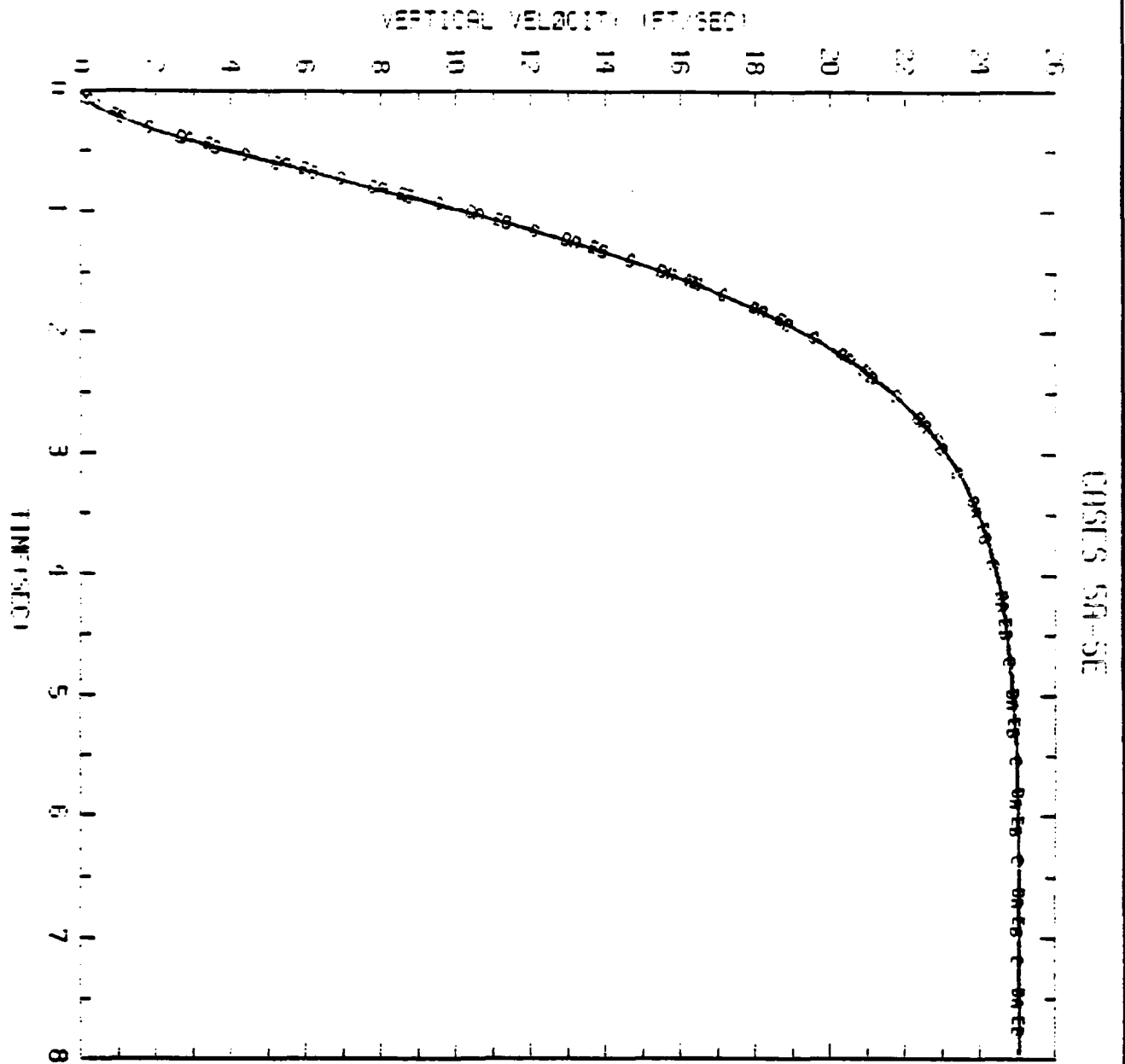


Fig. 5.2b Vertical verlocity (v_z) output (cf Fig. 3.13)

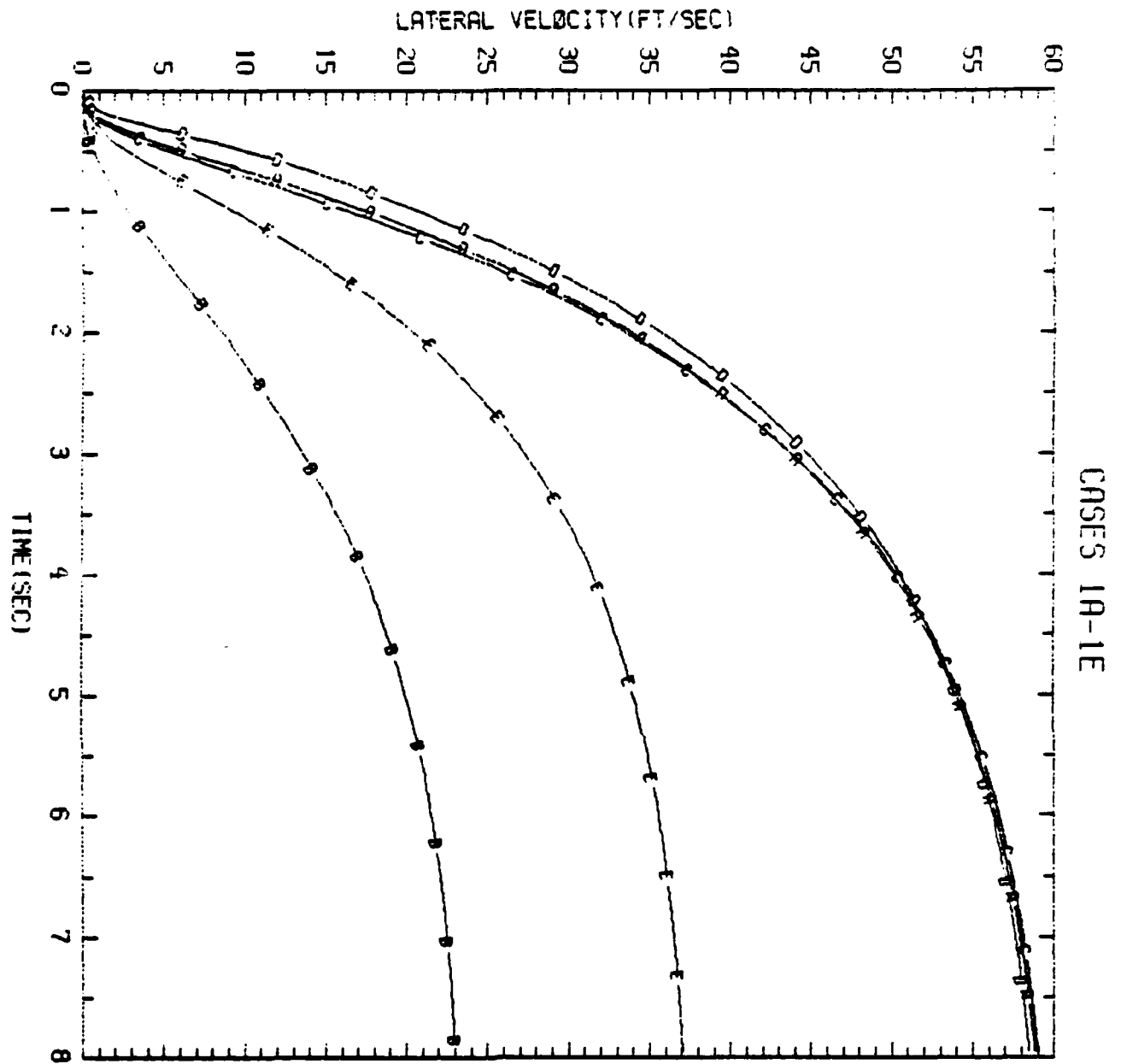


Fig. 5.3a Lateral velocity (v) (cf Fig. 4.12)
Cases: A-1, B-4, C-2, D-3, E-5

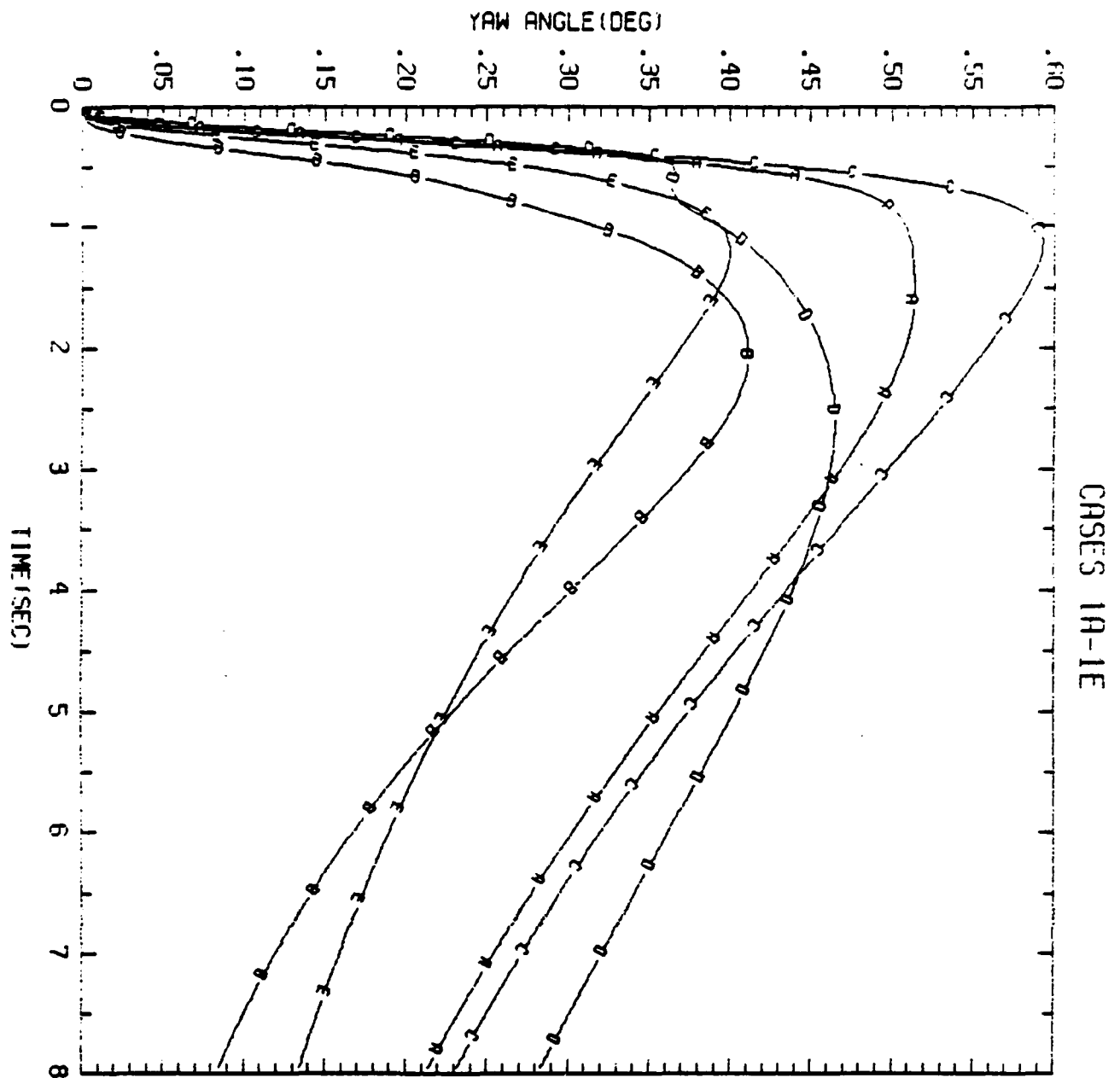


Fig. 5.3b Yaw angle (ψ) (cf Fig. 4.12)

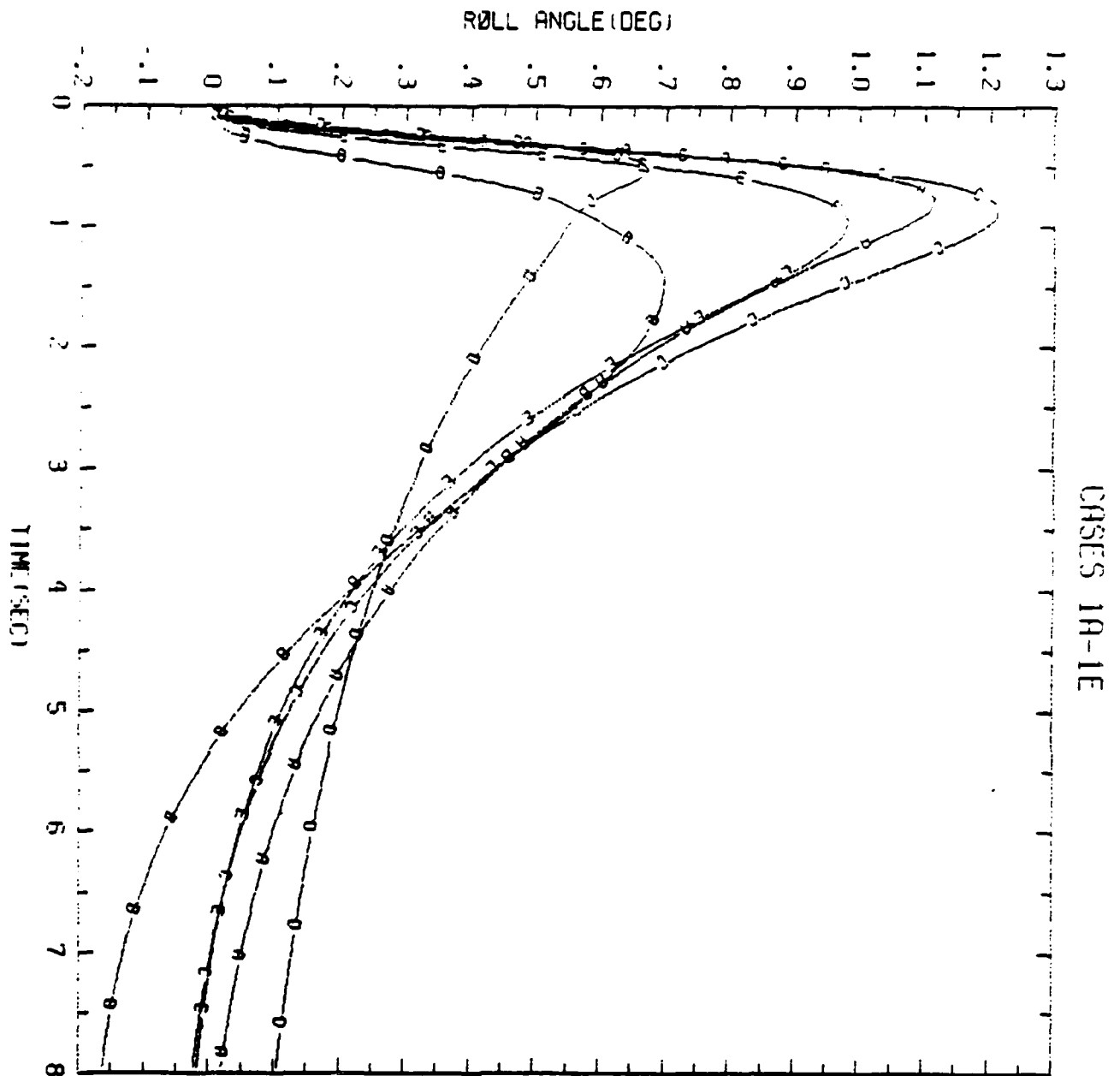


Fig. 5.3c Roll angle (ϕ) (cf Fig. 4.12)

LATERAL VELOCITY (FT/SEC)

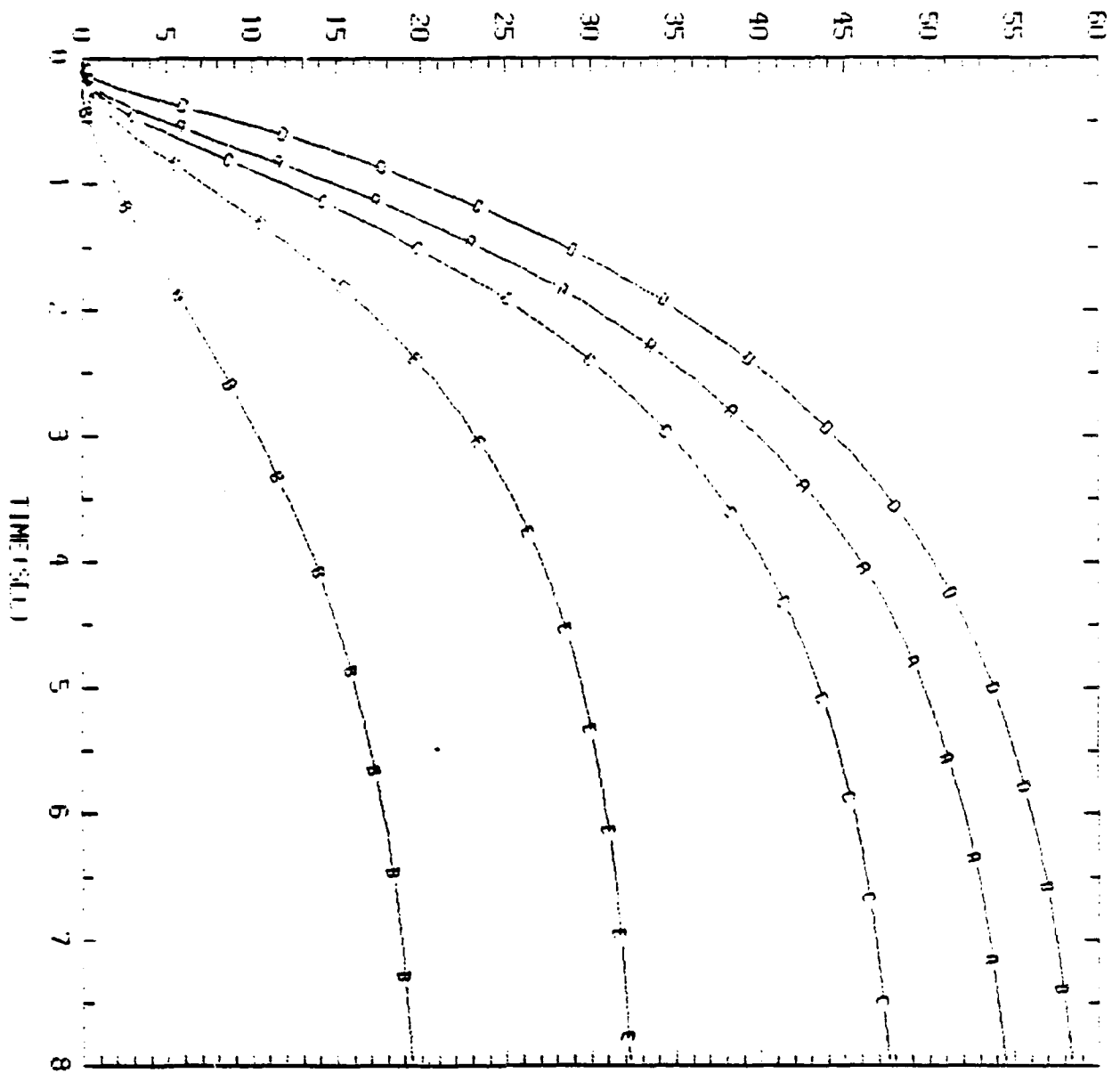
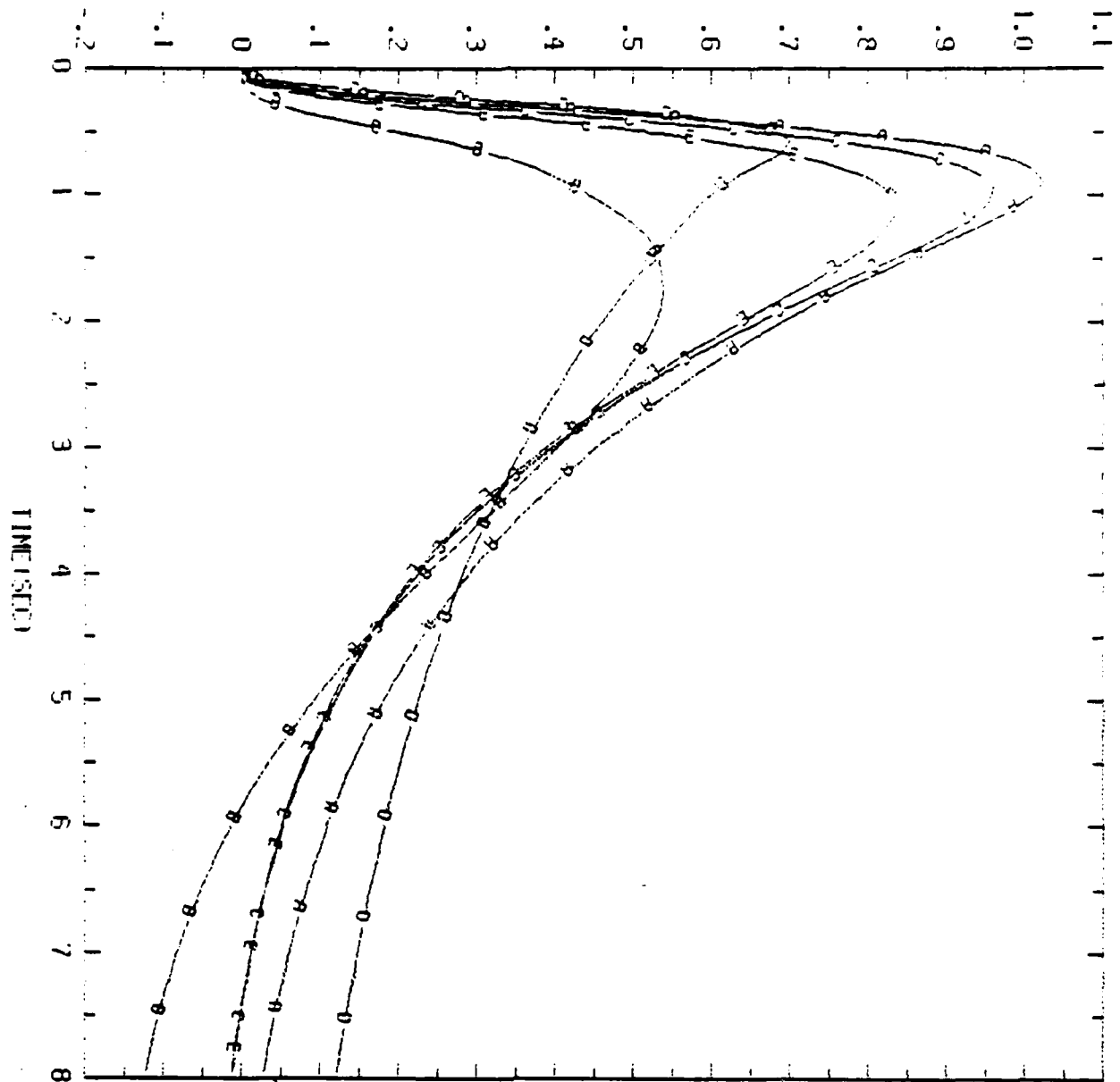


Fig. 5.4, Lateral velocity (cf Fig. 4.12)
Cases: A-4, B-9, C-7, D-8, E-10



CASES 20-2E

Fig. 5.4b Roll angle (cf Fig. 4.12)

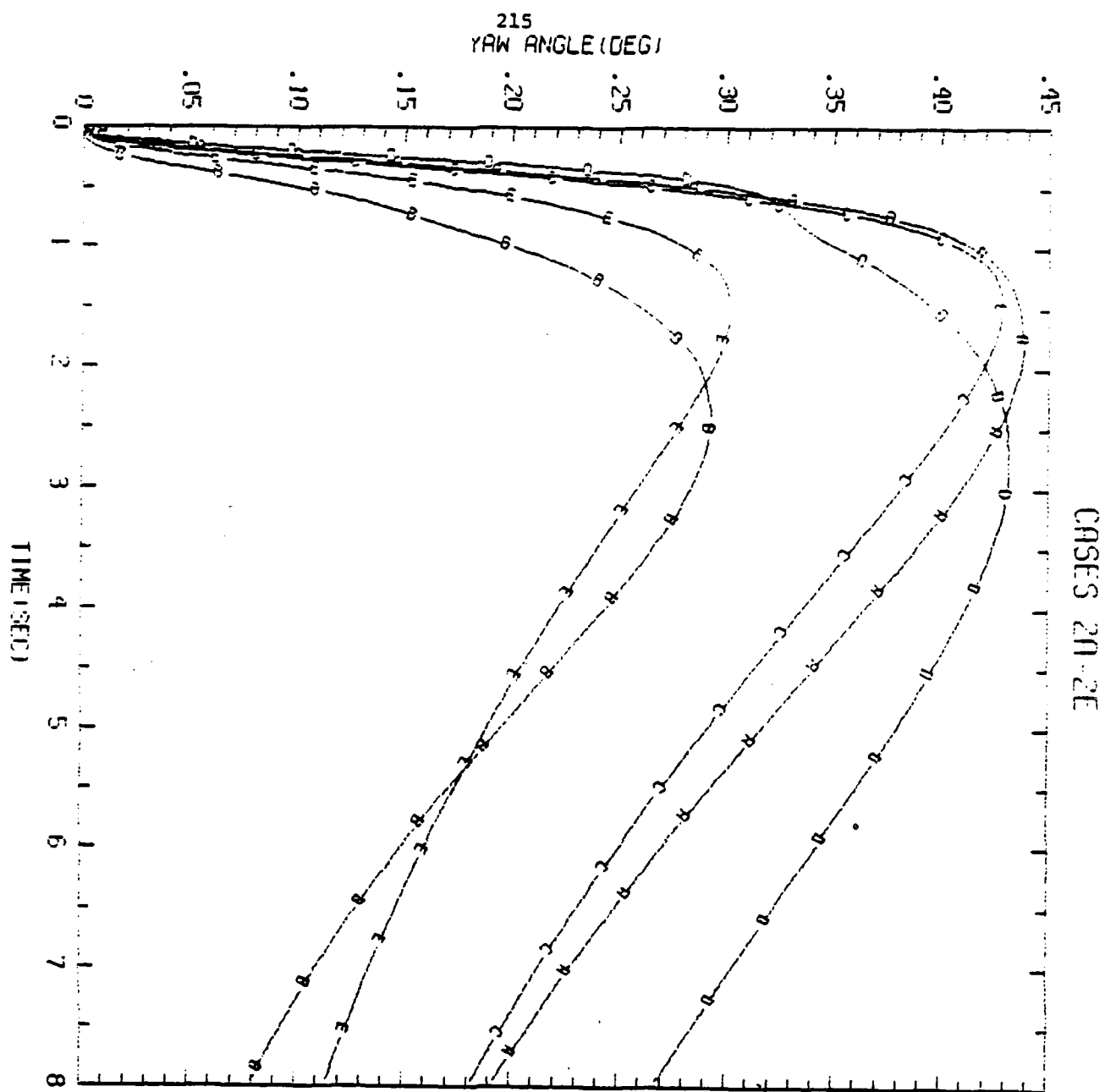


Fig. 5.4c Yaw angle (cf Fig. 4.12)

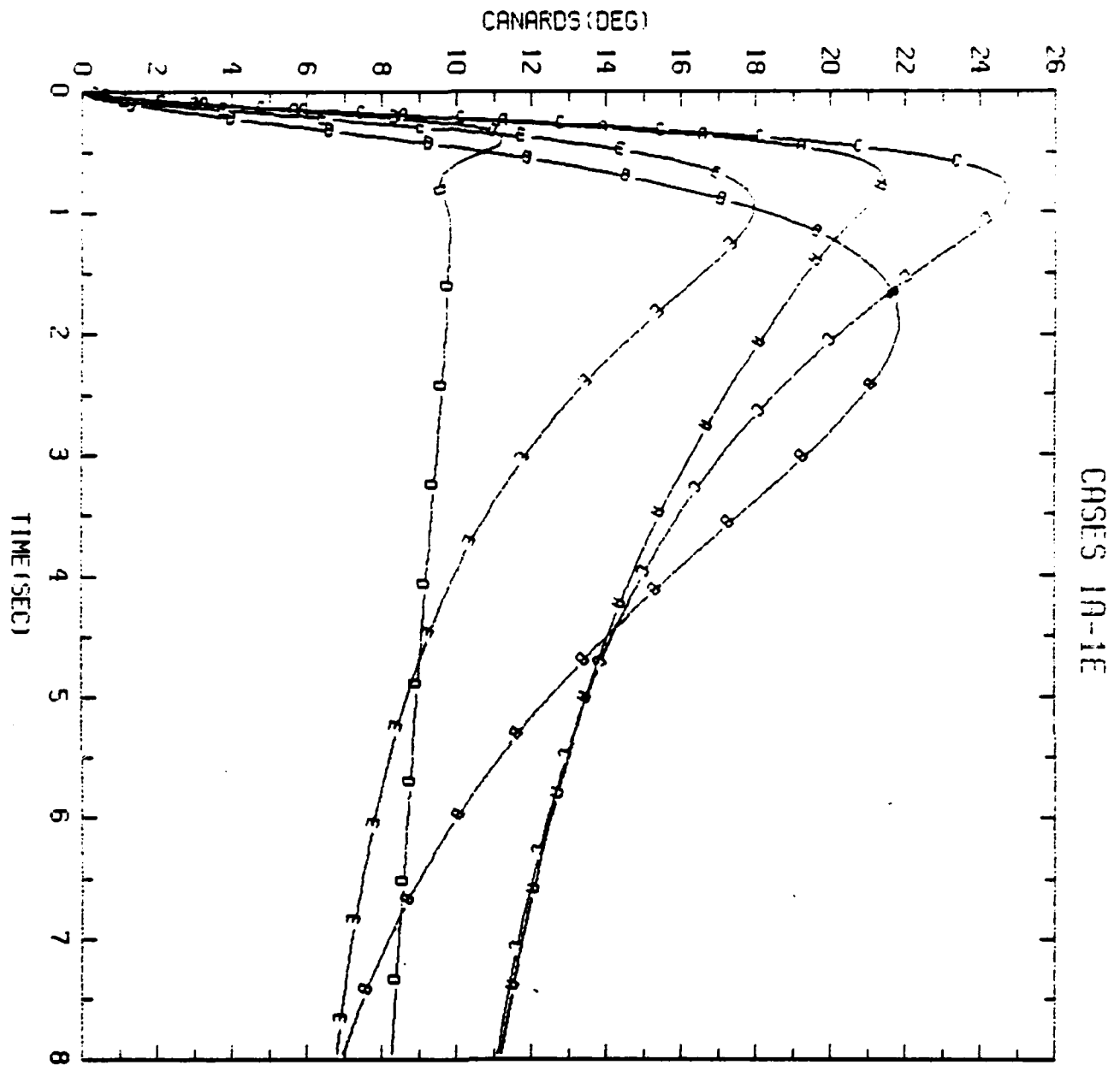


Fig. 5.5a Canard input (δ_c), (cf Fig. 4.12)

Cases: A-1, B-4, C-2, D-3, E-5.

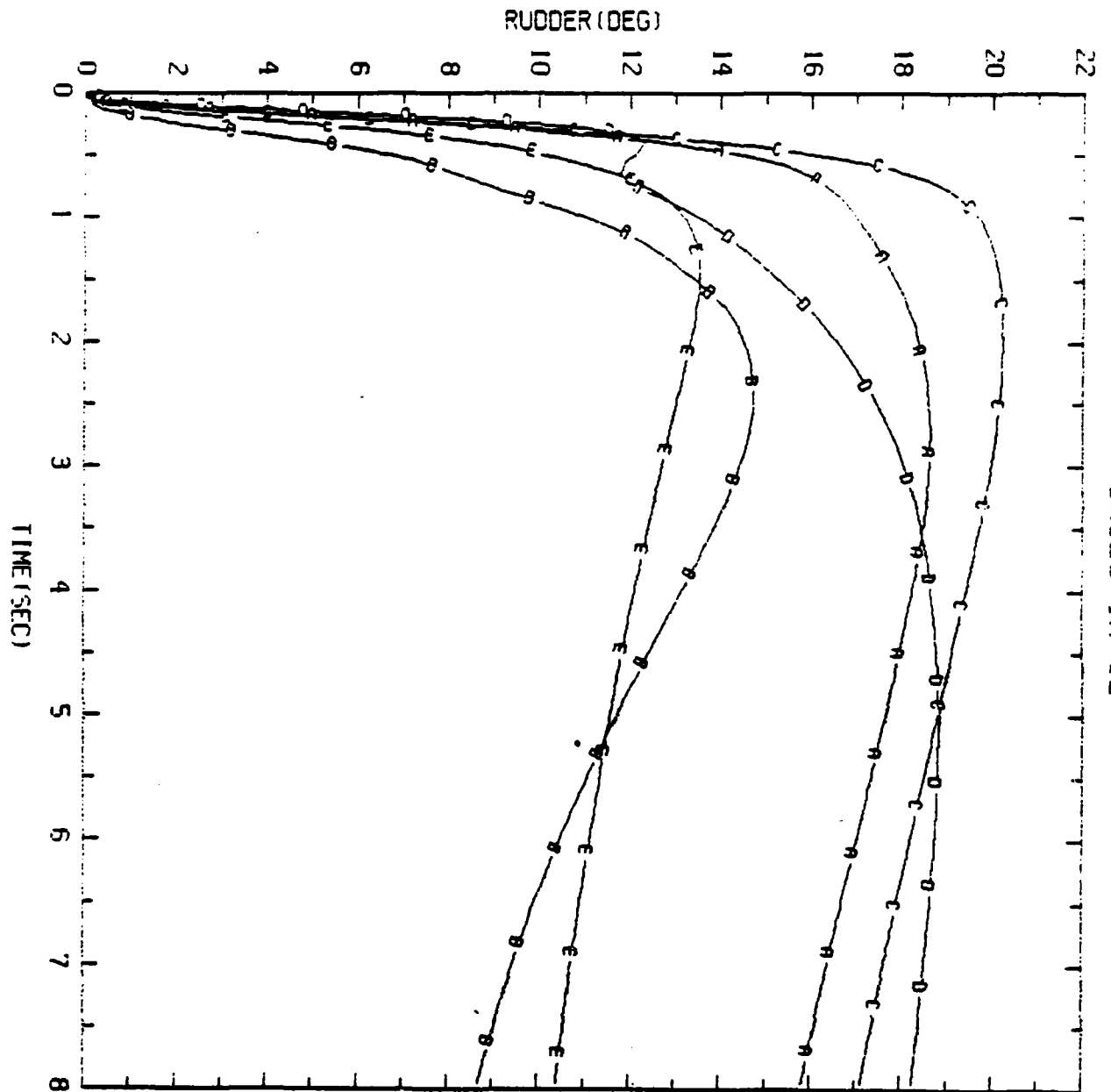


Fig. 5.5b Rudder in δ_r (cf Fig. 4.12)

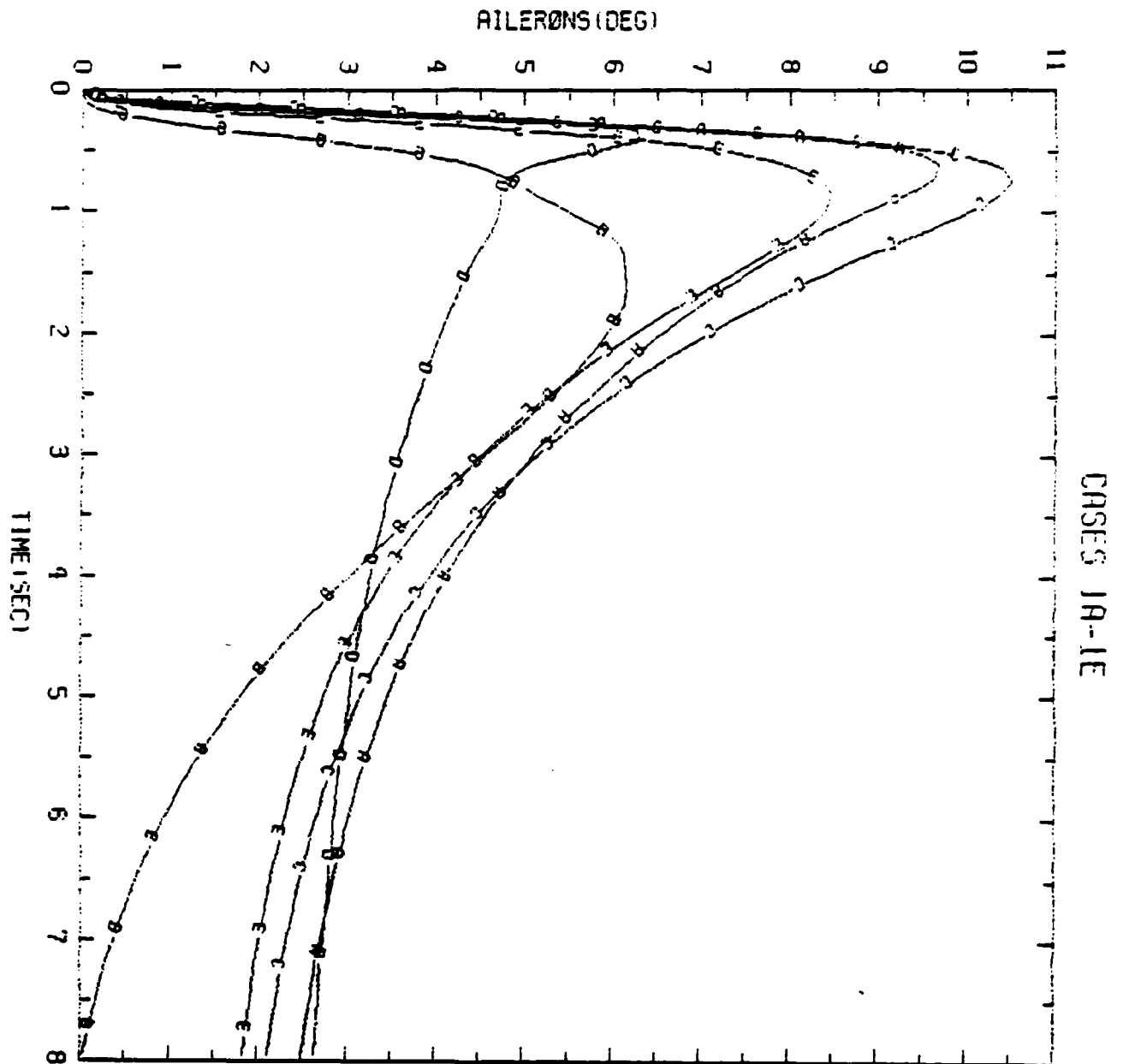
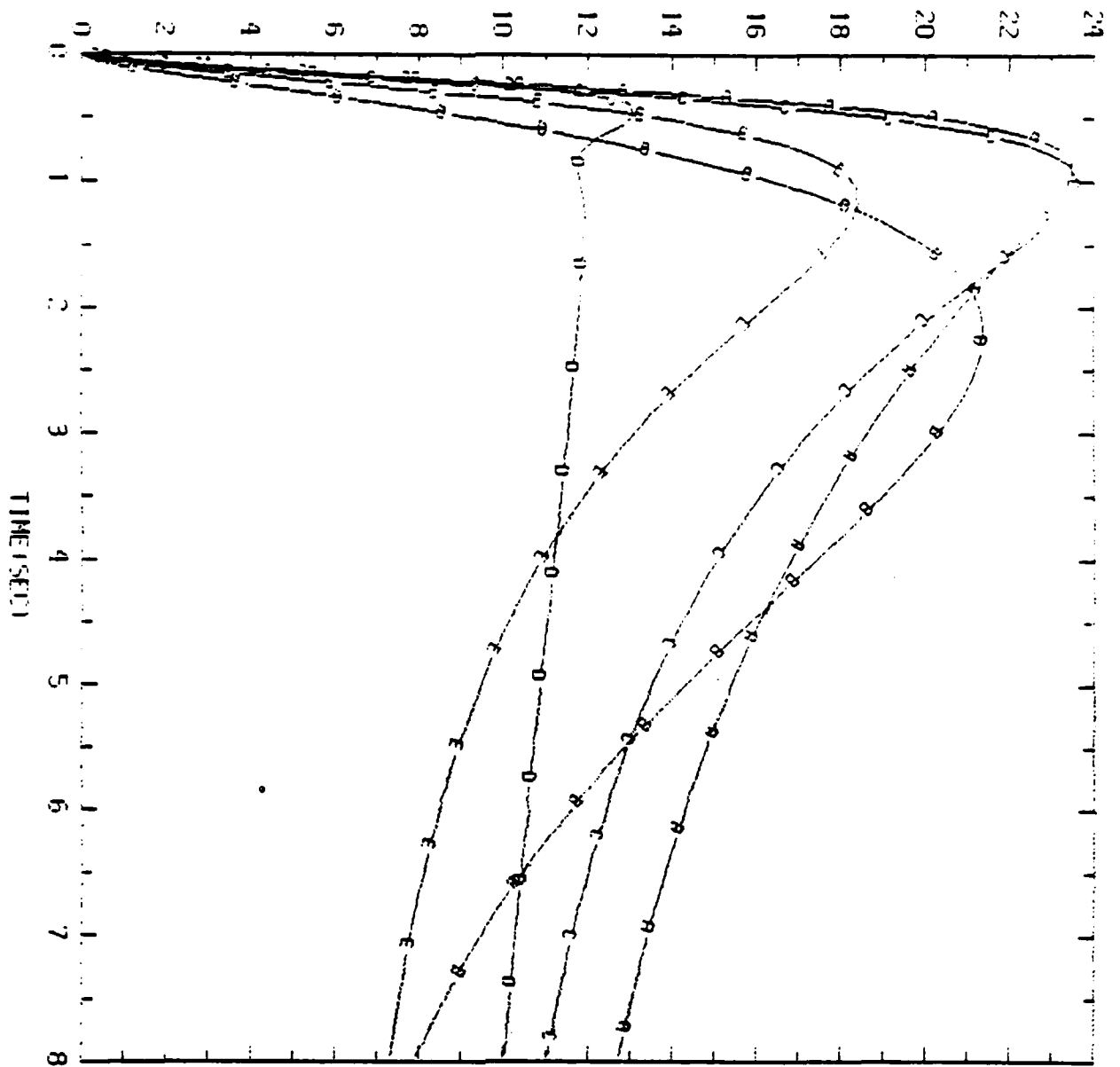


Fig. 5.5c Aileron input (δ_a) (cf Fig. 4.12)



CASES 20-2E

Figure 5.6a

Canard input (cf Fig. 4.12)

Cases: A-6, B-9, C-7, D-8, E-10

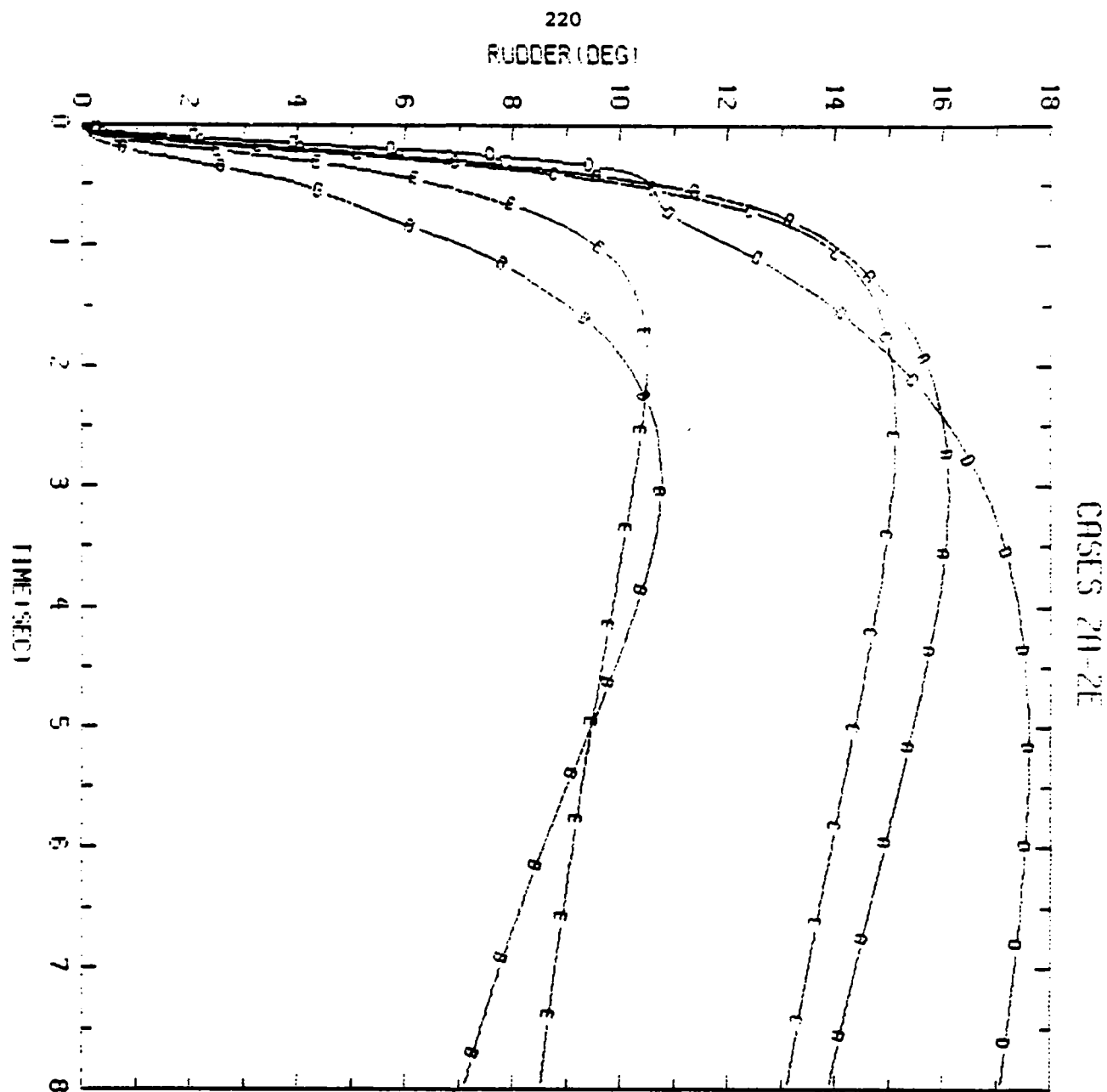


Fig. 5.6b Rudder input (cf Fig. 4.12)

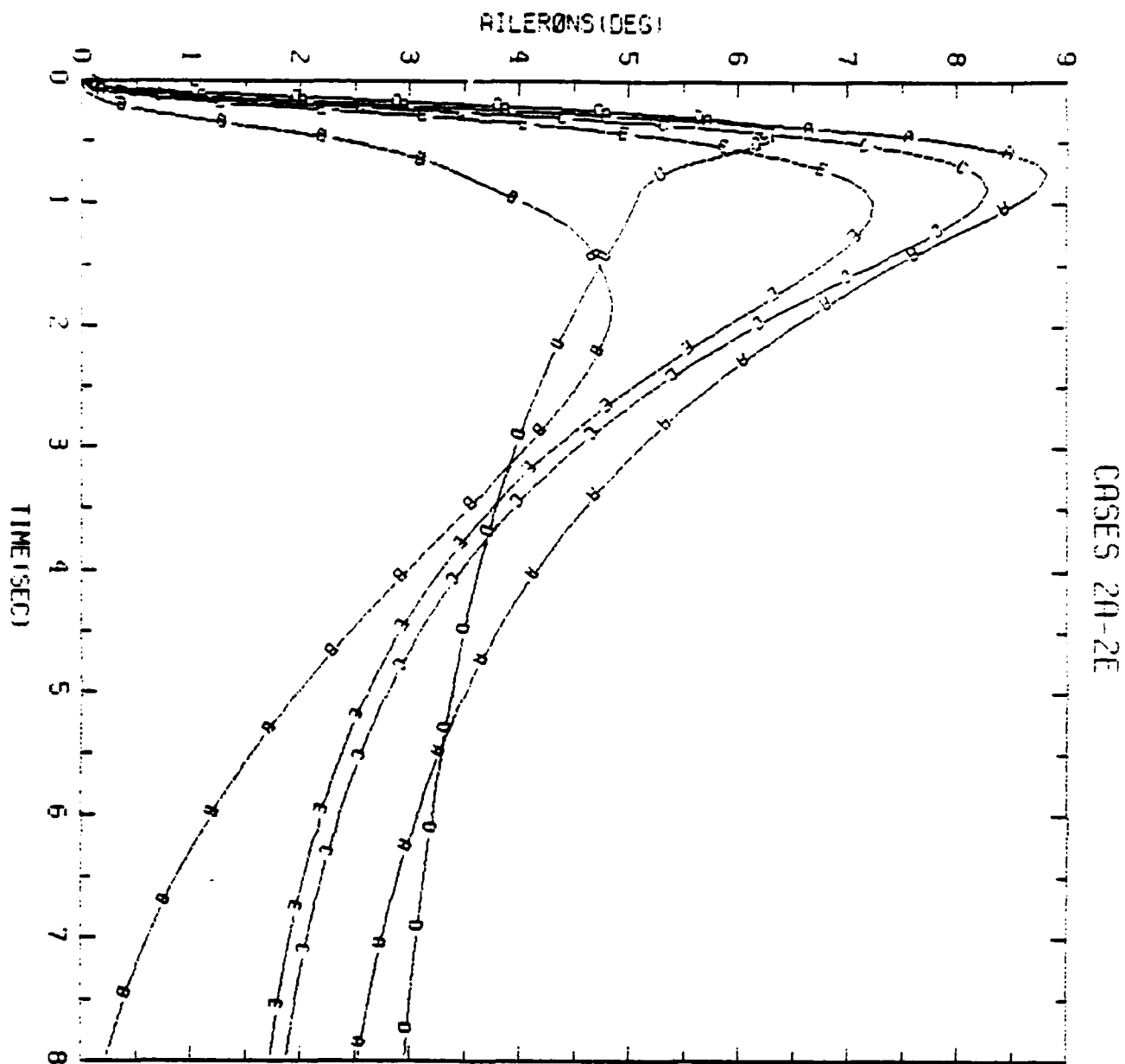


Fig. 5.6c Aileron input (cf Fig. 4.12)

CHAPTER 6

FUSELAGE YAW POINTING MODE (δ_1)

In this mode the control surfaces and the plant outputs are the same as in Chapter 2 (Direct Side Force Mode), so the same plant equations apply, except for the numbering (see 6.2).

6.1 SpecificationsPart I 2x2 System

Ninety degrees roll (ϕ) is commanded and the sideslip (β) is to be maintained as small as possible with $\pm 2^\circ$ as extremes. Time to roll 90° is to be as small as possible (0.75 sec if possible) with little or no overshoot. After steady state has been achieved, a sinusoidal roll is commanded as in fig. 6.1-a tentatively up to 13.5° amplitude and period bounds .5 to 2.5 sec ($.8 \pi$ to 4π rps). The roll output is to be within the tolerances given in fig. 6.1-b where ϕ_c is the commanded roll, i.e. error $< 15^\circ$. The two control inputs are the ailerons and the rudder; the canard input is not used.

Part II 3x3 System

Repeat part I with sideslip step command added after steady state has been achieved, as in fig. 6.1-c. The resulting side-force is to be less than 0.2 g and the canard is now used. The sideslip output is to be within the tolerances given in fig. 6.1d.

6.1.1 Compatibility of Specifications with
Inherent Capabilities

The control input numbering is (1) δ_a -aileron, (2) δ_r -rudder, (3) δ_c -canards. The outputs are (1) ϕ -roll angle, (2) β -sideslips, (3) A_y -sideforce.

Part 1: For the roll step response, the transfer model $T_{11} = [(s/\omega_n)^2 + 1.6(s/\omega_n) + 1]$ was used with damping factor $\zeta = .8$ to achieve small overshoot; $\omega_n = 5$ in order to achieve final value crossing at $t = .75$, and $\omega_n = 8$ was tentatively tried as an upper bound on $T_{11}(j\omega)$. Consider the resulting δ_a due to sinusoidal commanded roll (ϕ_{ss}). From $\delta = P^{-1}Y$, $Y = (\phi, \beta, A_y)'$, $P^{-1} = [P_{ij}]$, $\delta_a = P_{11}\phi + P_{12}\beta + P_{13}A_y$, and it is found that at $\omega = 12.5, 13.5^\circ$ commanded sinusoid amplitude, and the assigned tolerances of 6.1, $\delta_a \approx P_{11}\phi$, with $|\phi(j 12.5)| = (13.5^\circ) |T_{11}(j 12.5)|$. This calculation gives a range of 27° minimum (case 4) to 190° maximum (case 2) for δ_a , both exceeding the ailerons limit value. A similar calculation of $\dot{\delta}_a$ gives a range of 364 deg/sec (Case 4) to 2500°/sec (Case 2), both far exceeding the ailerons rate limit.

The inverse calculation can be made: at 13.5° amplitude command, given $|\delta_a|_{\max} = 20^\circ$, $|\dot{\delta}_a|_{\max} = 56^\circ/\text{sec}$, and $\omega_n = 8$ for the second order $T_{11}(s)$ model, it is found that rate saturation would occur at $\omega = 3$ (Case 3) and position saturation at $\omega = 9$. For case 4, rate limit as low as $\omega = 2$, position at $\omega = 3$. The conclusion is that $\omega_n = 8$ is beyond the system capability for 13.5° sinusoidal input. In the meantime we use $\omega_n = 5, 8$ as the bounds on $T_{11}(j\omega)$, but only for step input. Since the sinusoidal roll command input generally is from another source, it is possible to use a separate prefilter for the sinusoidal signals.

6.1.2 Specifications on T_{1j}

Those on T_{11} were given above. For T_{12} , roll due to sideslip step command $\leq 2^\circ$ dominates, giving $|T_{12}| \leq 2/5 = 0.4$. For T_{22} (β response due to β command), the following transfer function models were found suitable.

$$\text{Upper bound } b_{22}: \left\{ \left(\frac{s}{5} + 1 \right)^2 \left(\frac{s}{13} + 1 \right) \left(\frac{s}{80} + 1 \right) \right\}^{-1}$$

$$\text{Lower bound } a_{22}: \left\{ \left(\frac{s}{2.5} + 1 \right)^2 \left(\frac{s}{10} + 1 \right) \left(\frac{s}{80} + 1 \right) \right\}^{-1}$$

$$T_{21} = 8/\phi_c \leq 2/90 = 0.022 \text{ dominates giving } b_{21}. \quad T_{32} = A_y/\phi_c = (0.15)$$

(32)(57.3)/5 gives $b_{32} = 55 \text{ ft/sec/deg.}$ while $T_{31} = A_y/\phi_c = (.05)(32)(57.3)/13.5$ gives $b_{31} = 6.8 \text{ ft/sec/deg.}$

6.2 Design

The detailed design steps are the same as in the other modes, and there is therefore no need to repeat them here. They are somewhat more complicated because (a) the same compensations are wanted for both the 2x2 system and the 3x3 system, and (b) both step and sinusoidal inputs must be considered. Due to the former, the most severe bounds on G_1 and G_2 (emanating from the 2x2 and 3x3 problems) must be used. As for the second, it has already been noted that the sinusoidal response tolerances were not compatible with the system saturation levels and the step response tolerances, so the approach was to design the loops (G_i , $i=1-3$) to satisfy the step response tolerances, and then find separate prefilters for the sinusoidal commands such that saturation resulted only for an extreme flight condition. The precise design details are not given, because the design technique is the same as has already been greatly detailed in previous chapters, especially Chapter 2. However, the templates, bounds etc and the compensation transfer functions are presented.

6.2.1 Design graphs

The frequency domain bounds on $|T_{11}(j\omega)|$, $|T_{22}(j\omega)|$ are shown in Figs. 6.2a,b. Templates of Q_{11} (2x2) are shown in Fig. 6.3a, Q_{11} (3x3) in Fig. 6.3b, Q_{22} (3x3) in Fig. 6.3c, Q_{33} (3x3) in Fig. 6.3d. Nichols chart bounds on and sketches of $L_{i0}(j\omega)$ are shown in Fig. 6.4 a-c for $i = 1$ to 3 (case 9 is nominal).

6.2.2 Compensation functions

The compensation functions are:

$$g_1 = -0.5 (.8s+1)/(100,0.6)$$

$$g_2 = 14 (.25s+1)/(120,0.5)$$

$$g_3 = 0.14 (150,1200,250)/(30)(1200,0.5)(500)$$

$$f_1 (\text{step}) = 1/(6,0.8)(1200,0.5)(500)$$

$$f_1 (\text{sinusoidal}) = (4.34)(4.34)/(4.34,.707)(4.34,.707)(12.5)$$

$$f_2 (\text{step}) = 1.4/(5)(5)(13)(80)$$

$$f_2 (\text{sinusoid}) = f_1 (\text{sinusoid})$$

(A,B) indicates a complex pair $[(s/\omega_n)^2 + (2\zeta s/\omega_n) + 1]$ with $A = \omega_n$, $B = \zeta$;

(E) indicates a factor $[(s/E)+1]$. The first number is the value of the transfer function at $s = 0$

6.2.3 Simulation Results

In Figs. 6.5-7, the system is 2x2 for the roll command ϕ_c of 90° at $t=0$. At $t=1.8$ sec. there is a sideslip β_c of 5° , and the system is 3x3. The roll responses are shown in Fig. 6.5a, sideslip in 6.5b, sideforce in 6.5c. The results are very good, except that in 6.5a, the response time is not the desired 0.75 sec. But this is because the system is physically incapable of such fast response. This is seen in Fig. 6.6a, 6.7a where the ailerons limit in rate in most cases and in amplitude in two extreme cases. The rates are shown in Figs. 6.7a-c.

In Figs. 6.8-6.10, the system is 3x3. A step roll command is given at $t=0$ and a sinusoidal roll command with amplitude of 15° and frequency 12.5 rps is given at $t=1.8$ sec. The three responses are shown in Figs. 6.8a-c. The control surface time histories are shown in Figs. 6.9a-c and their rates in 6.10a-c. From Fig. 6.8a, 6.9a it is seen that the best possible response is being achieved, because of the ailerons amplitude and rate limiting.

Figs. 6.11-6.13 are similar to Figs. 6.8-10, i.e. the system is 3x3, there is a step roll command of 90° at $t=0$ and a sinusoidal command at $t=1.8$, of 15° amplitude. But now the frequency is the lower bound one of 4 rps, with much better roll sinusoidal response as seen in Fig. 6.11a (note that saturations of δ_a, δ_a occur in the extreme cases - Figs. 6.12a, 6.13a). The actuator responses are shown in Figs. 6.12a-c, their rates in Figs. 6.13a-c.

Figs. 6.14-6.16 are the responses in the 3x3 system design due to a 2.5° sideslip command β_c at $t=0$, followed by a sideslip sinusoidal command at $t=1$ of 1.5° (see Fig. 6.1c) amplitude, frequency 15 rps; 6.14a-c: ϕ, β, A_y ; 6.14d-f: ailerons, rudder, canard; 6.14g-i: rates of these control surfaces. In the next group, Figs. 6.15a-i, the command is again sideslip, step of 2.5° at $t=0$, sinusoid at $t=1$ of 1.5° amplitude, but now the frequency is 4 rps.

In all of the above the interactive specifications are excellently satisfied. The responses to commands which do not satisfy the desired tolerances are due to the physical inability to do so, i.e. the response specifications are not reasonable in view of the ailerons amplitude and rate limits.

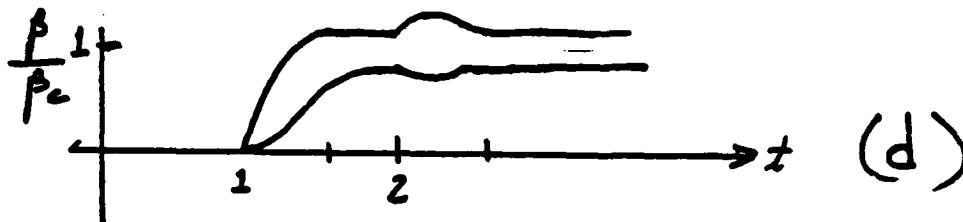
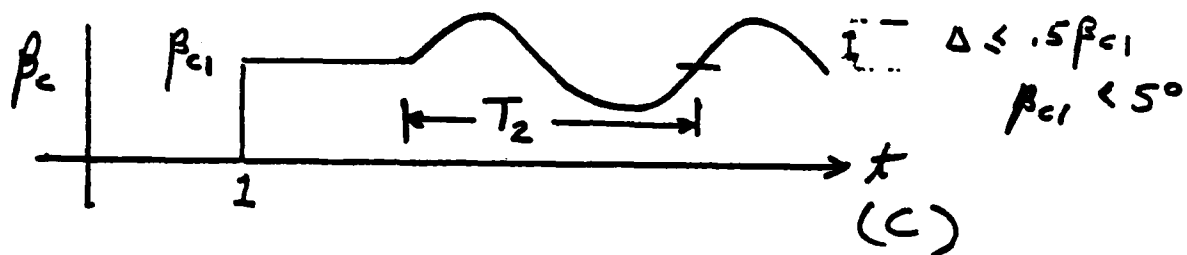
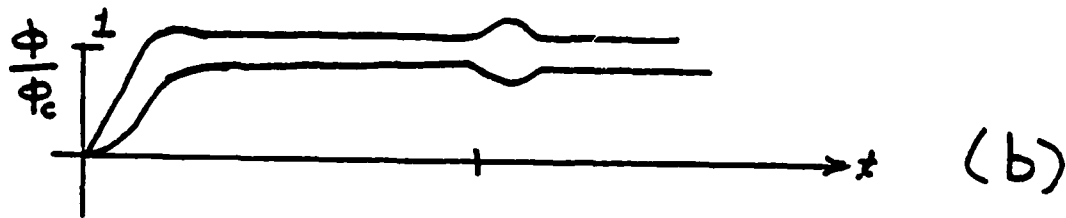
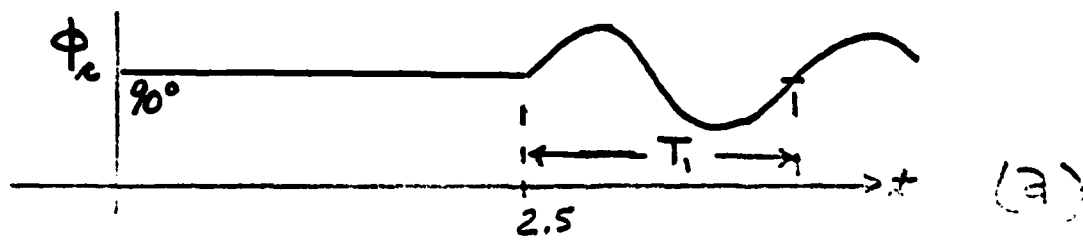


Figure 6.1a,b Specifications 2x2 system.

Figure 6.1c,d Specifications 3x3 system.

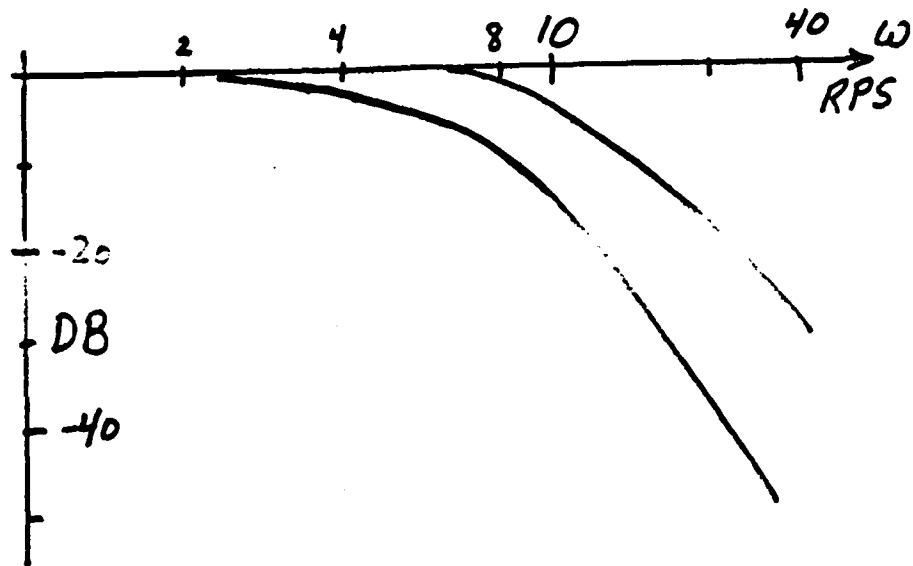


Figure 6.2a Tolerances on $|T_{11}(j\omega)|$

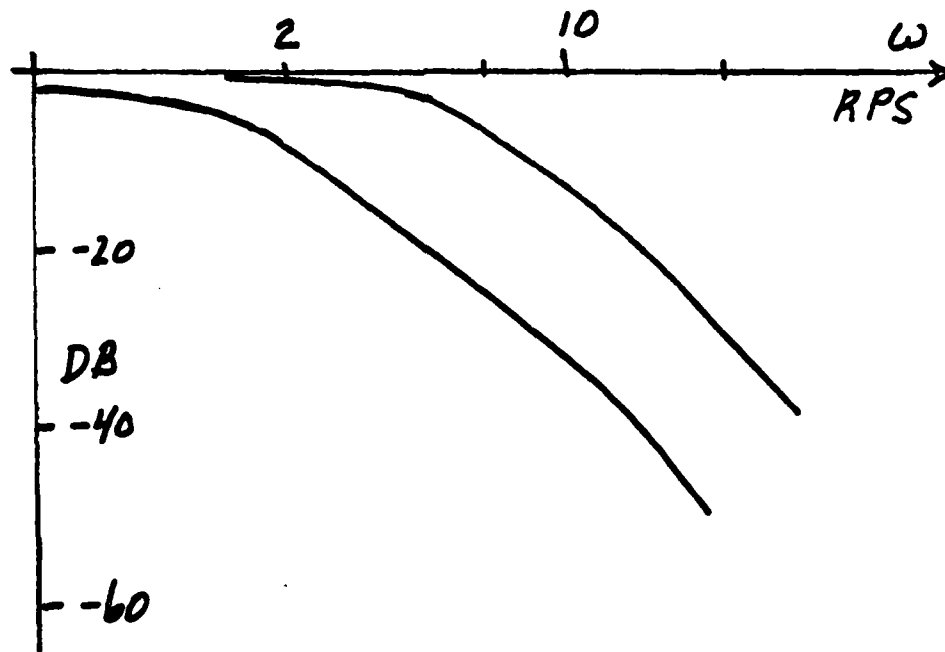
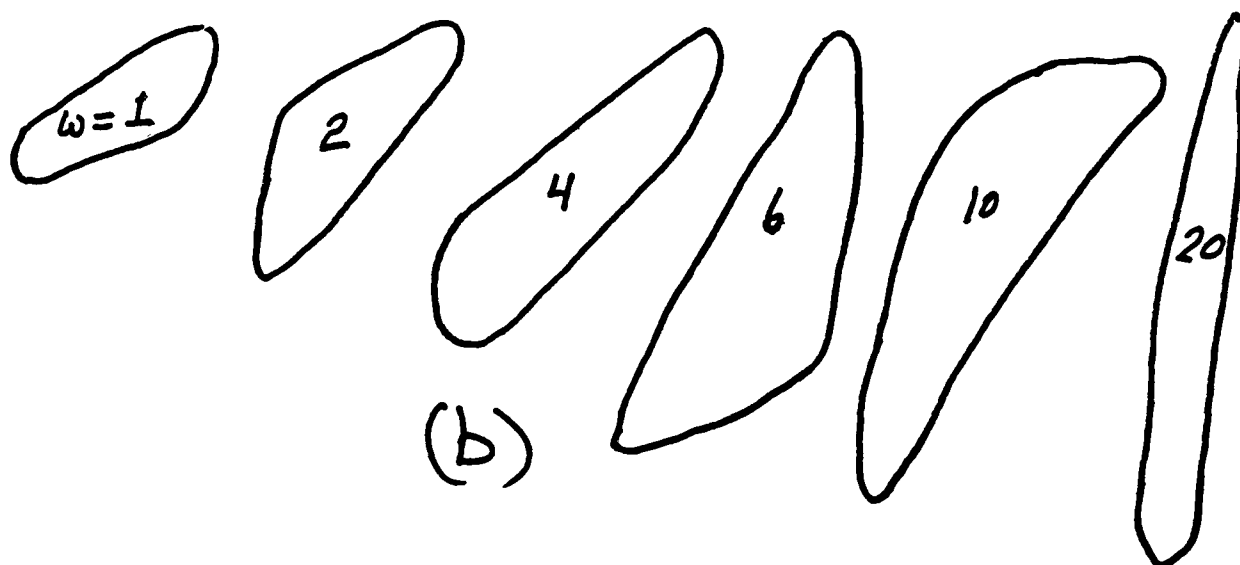
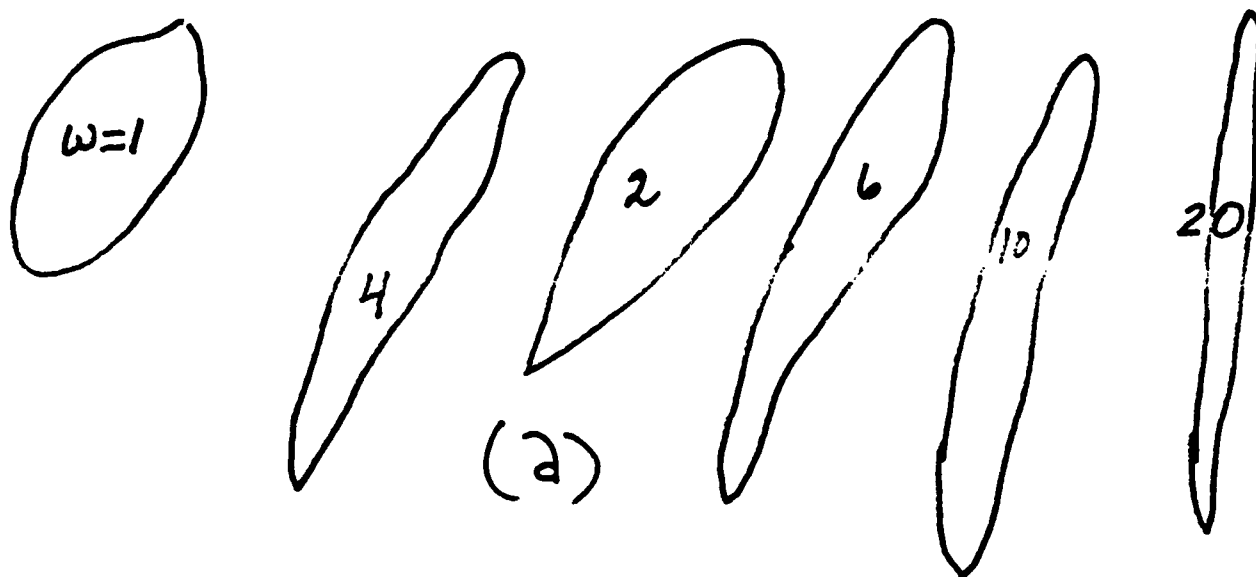


Figure 6.2b Tolerances on $|T_{22}(j\omega)|$



Figures 6.3a,b Plant templates (a) $Q_{11}(2 \times 2)$, (b) $Q_{11}(3 \times 3)$.

$\omega=1$

230

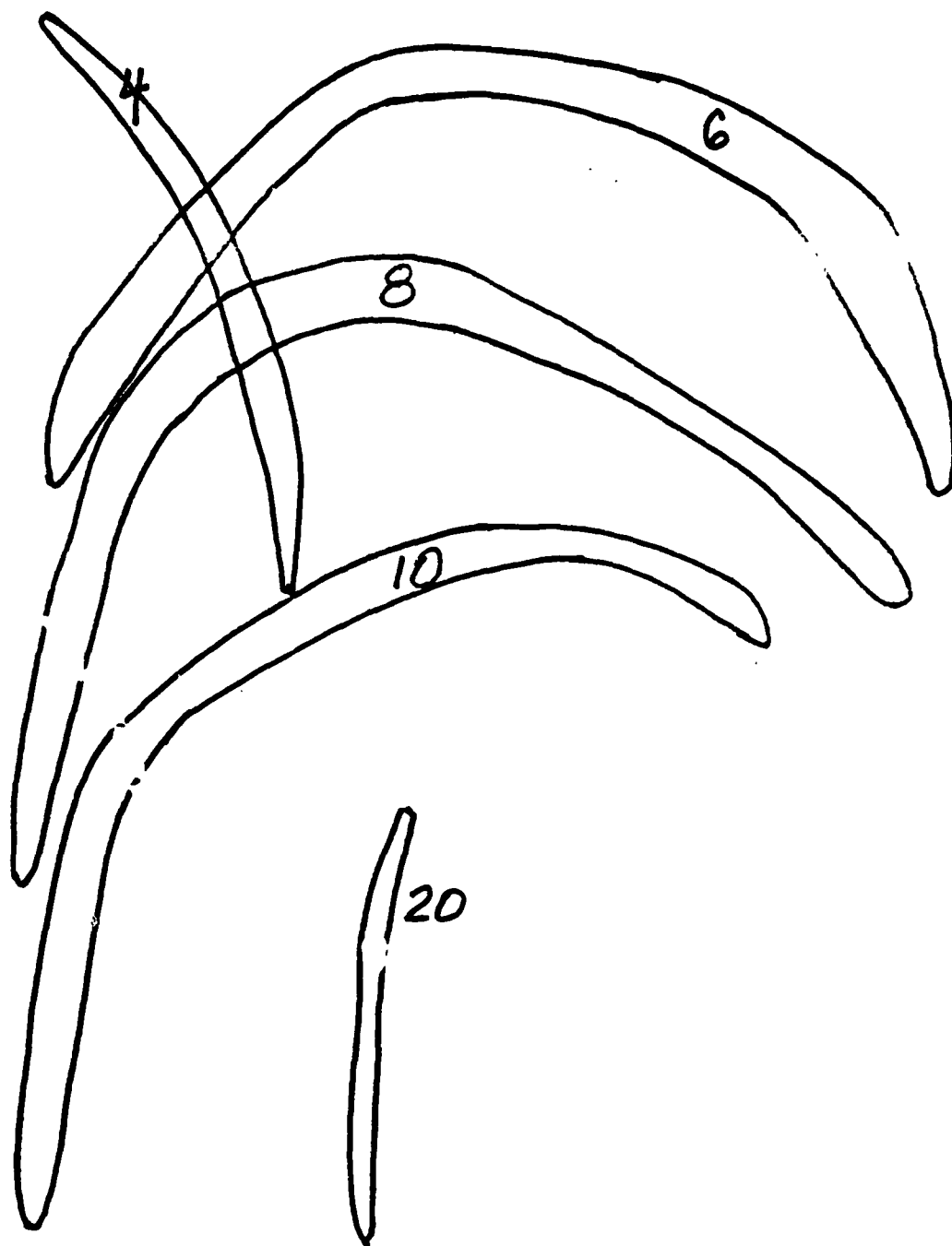


Figure 6.3c $Q_{22}(3 \times 3)$ templates.

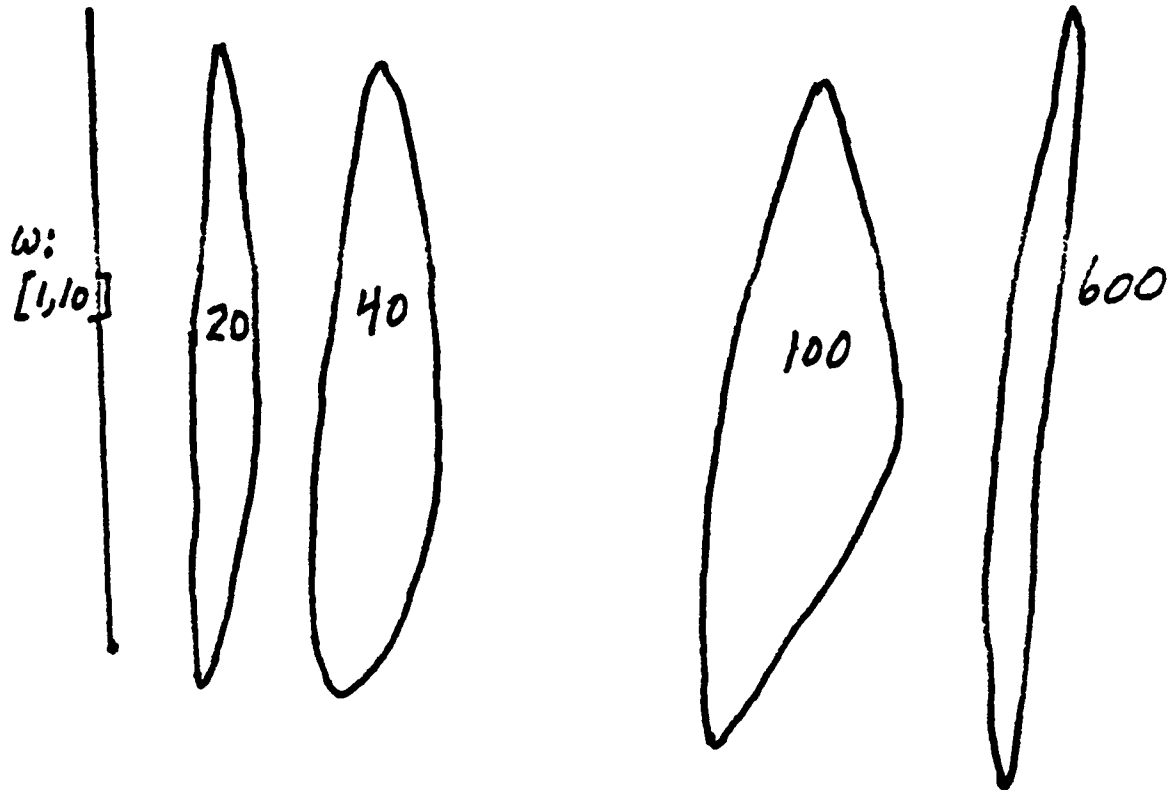


Figure 6.3d $Q_{33}(3 \times 3)$ templates.

232a

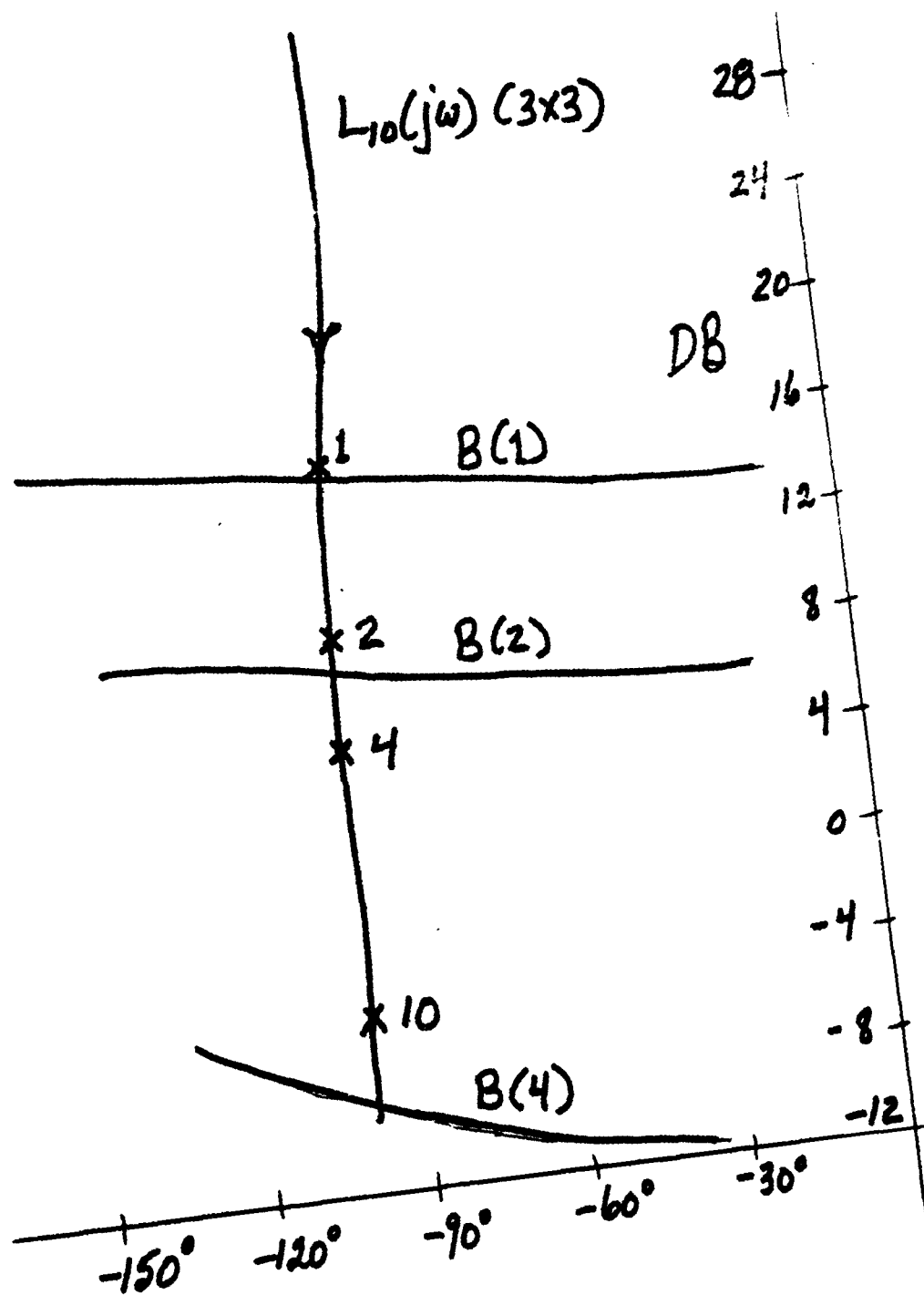


Figure 6.4a Bounds on L_{10} , 3×3 , and $L_{10}^{(3 \times 3)}$.

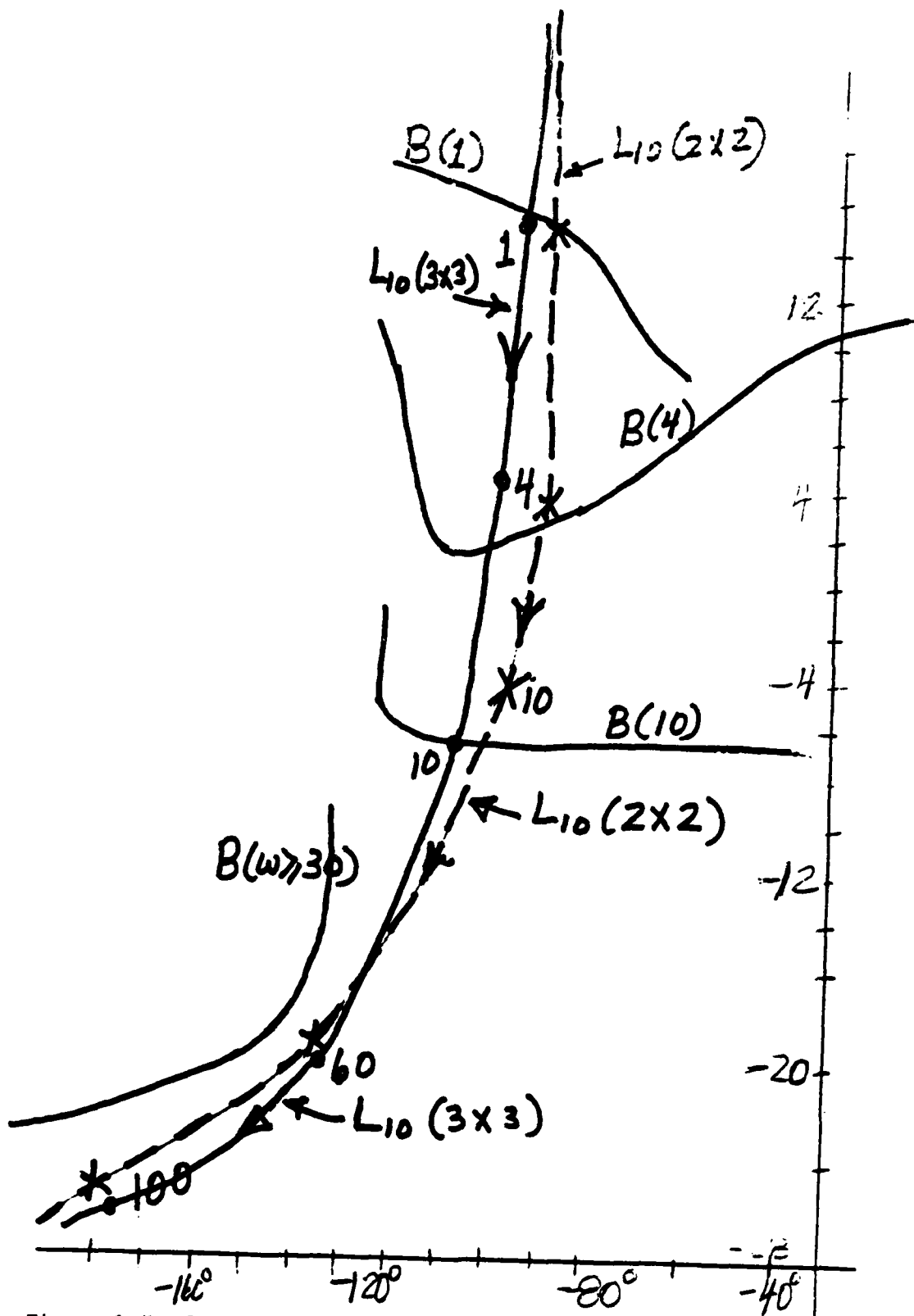


Figure 6.4b Bounds on L_{10} , 2×2 ; $L_{10}(2 \times 2)$ and $L_{10}(3 \times 3)$. G_1 dictated by 2×2 bounds.

BOUNDS ON G_2 — 3×3 ; — 2×2

$$G_2 = 14 \frac{(.25\omega + 1)}{[(\frac{\omega}{120})^2 + \frac{\omega}{120} + 1]}$$

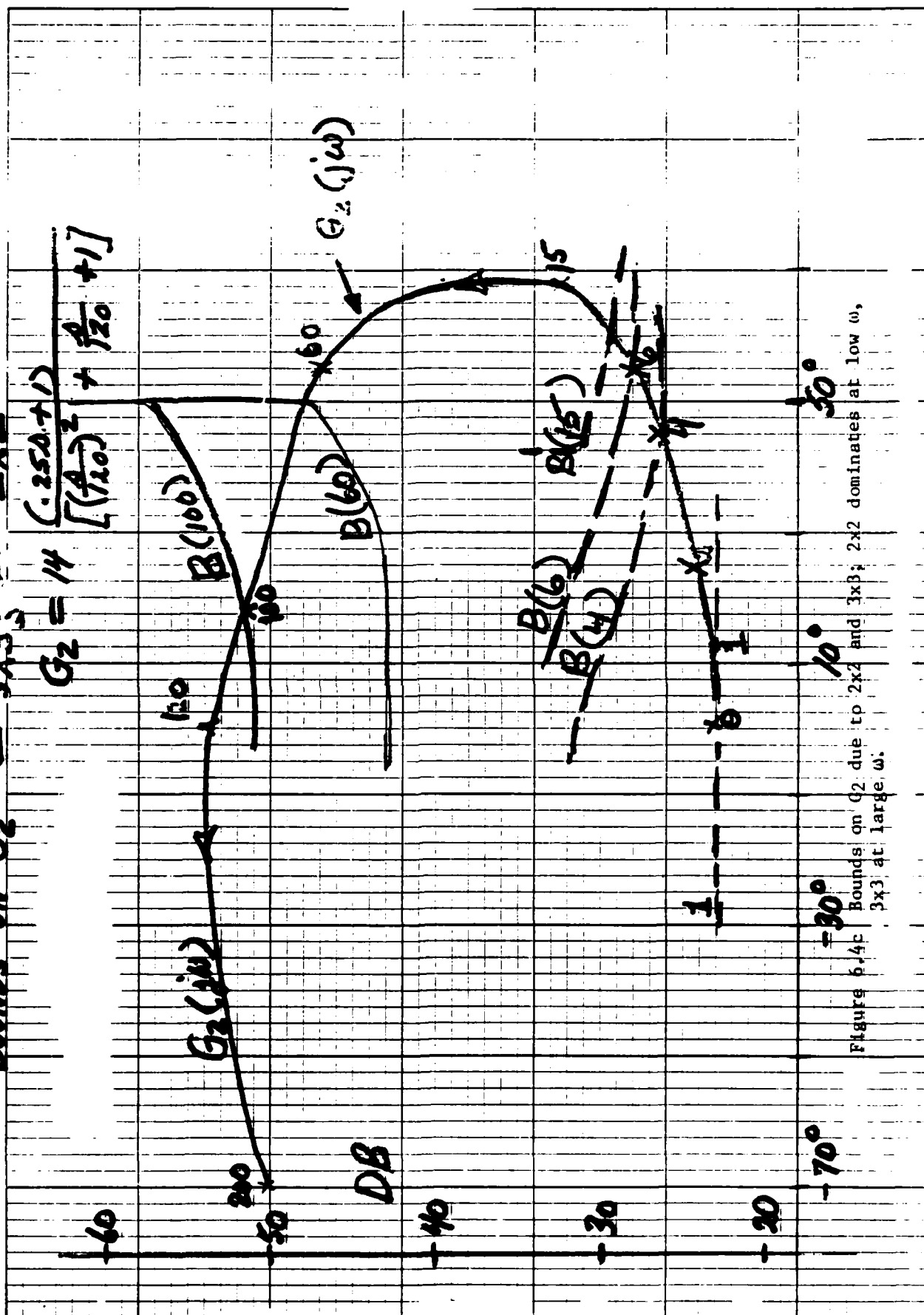


Figure 6.4c Bounds on G_2 due to 2×2 and 3×3 ; 2×2 dominates at low ω , 3×3 at large ω .

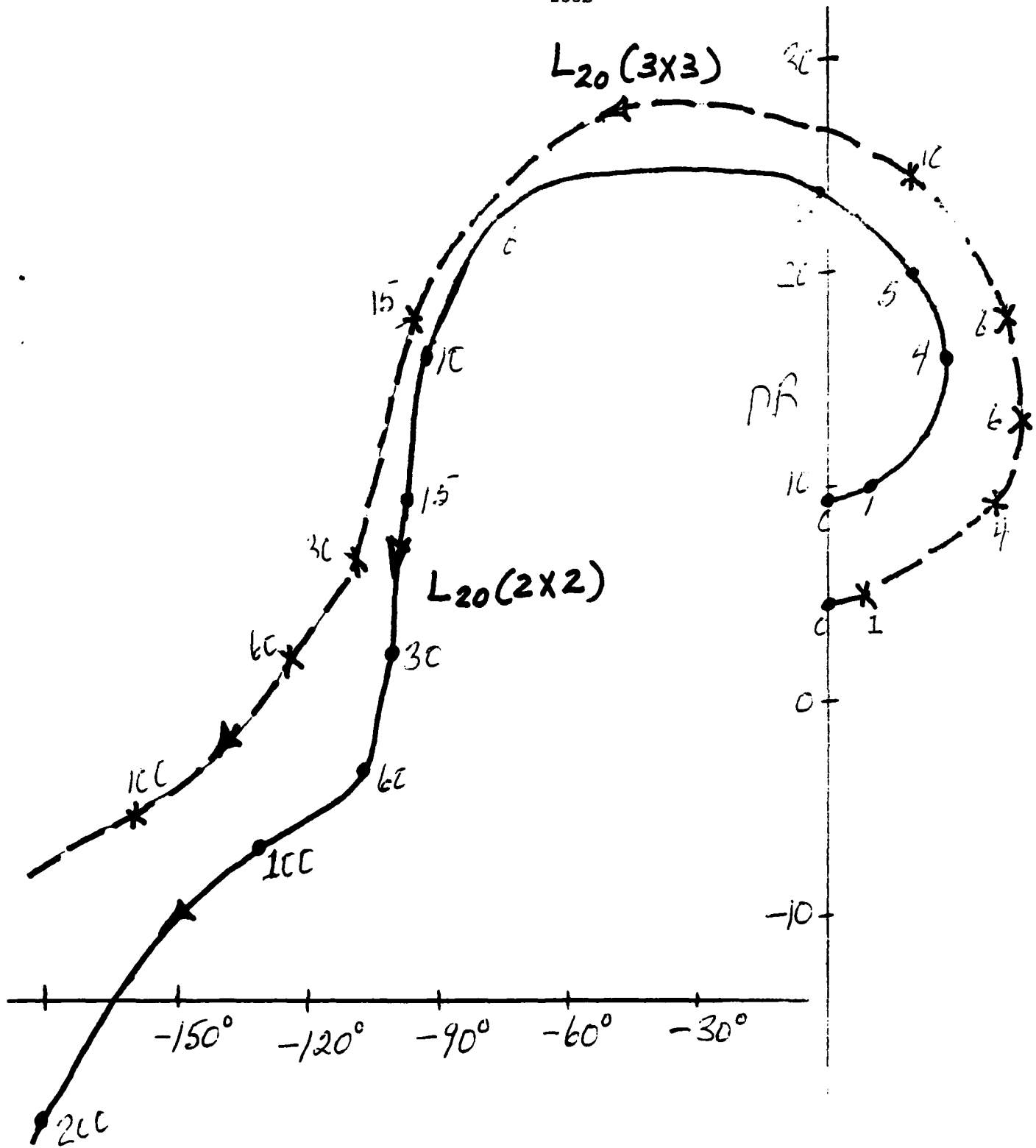


Figure 6.4d $L_{20}(2 \times 2)$ and $L_{20}(3 \times 3)$.

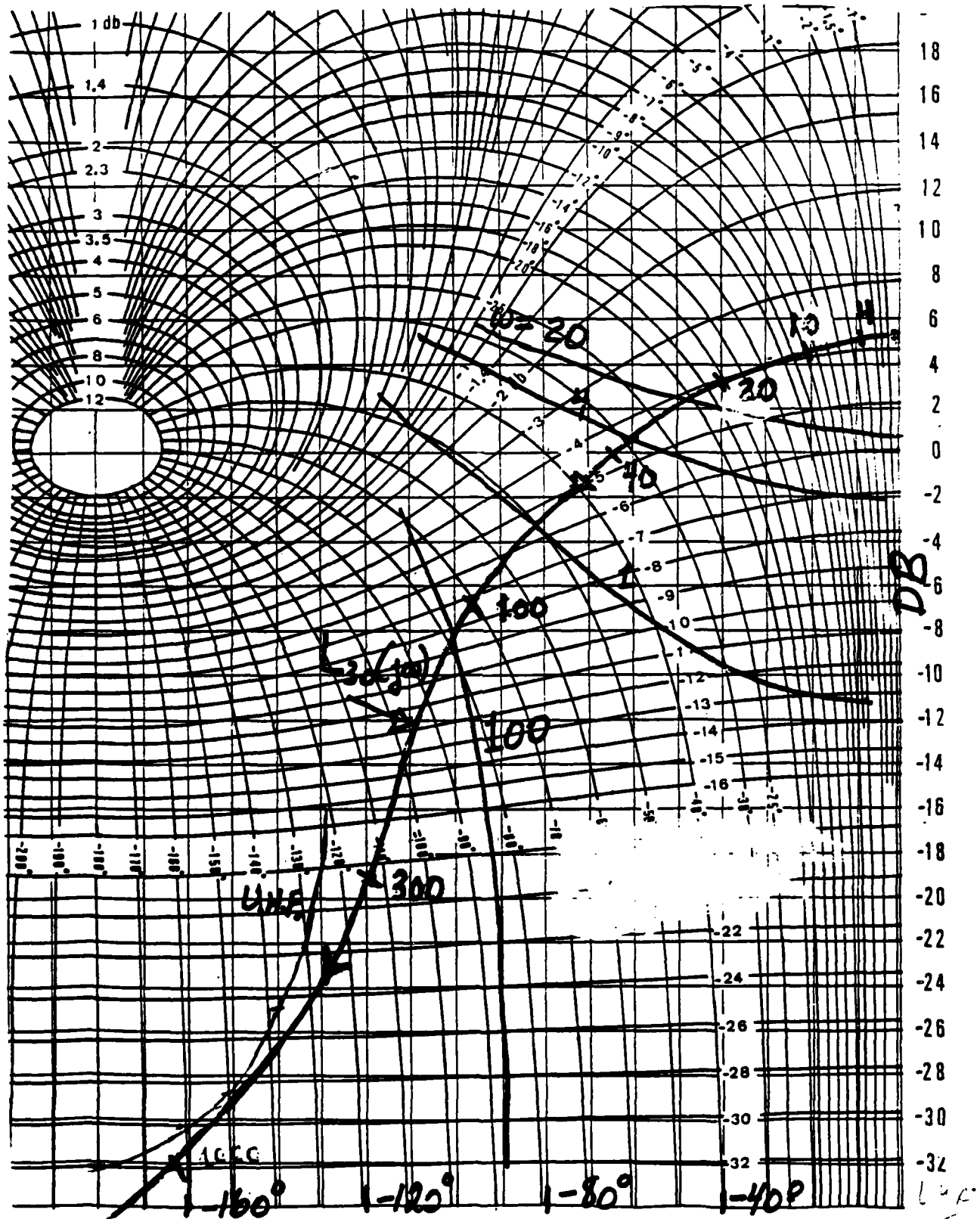
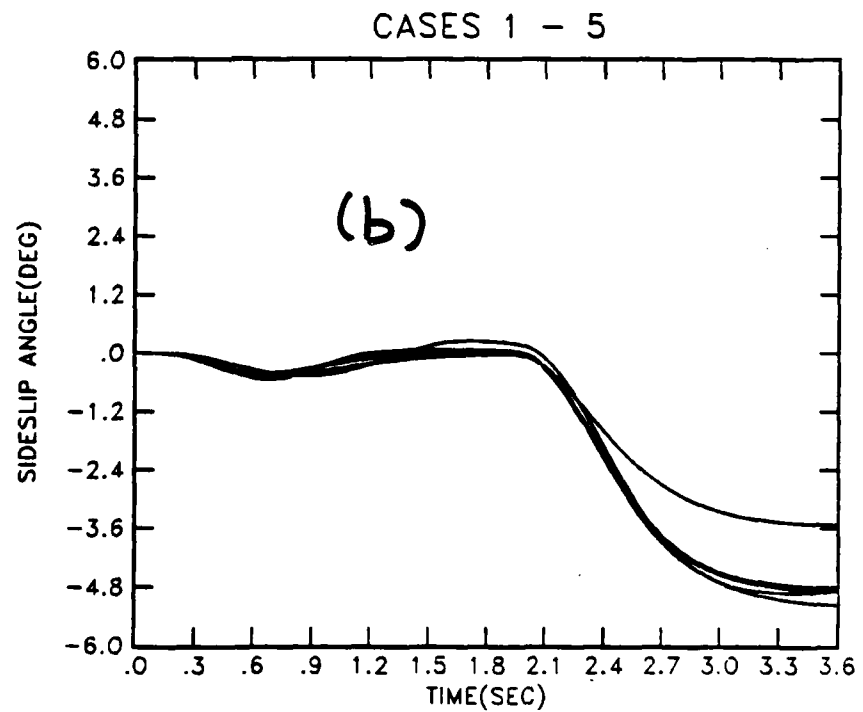
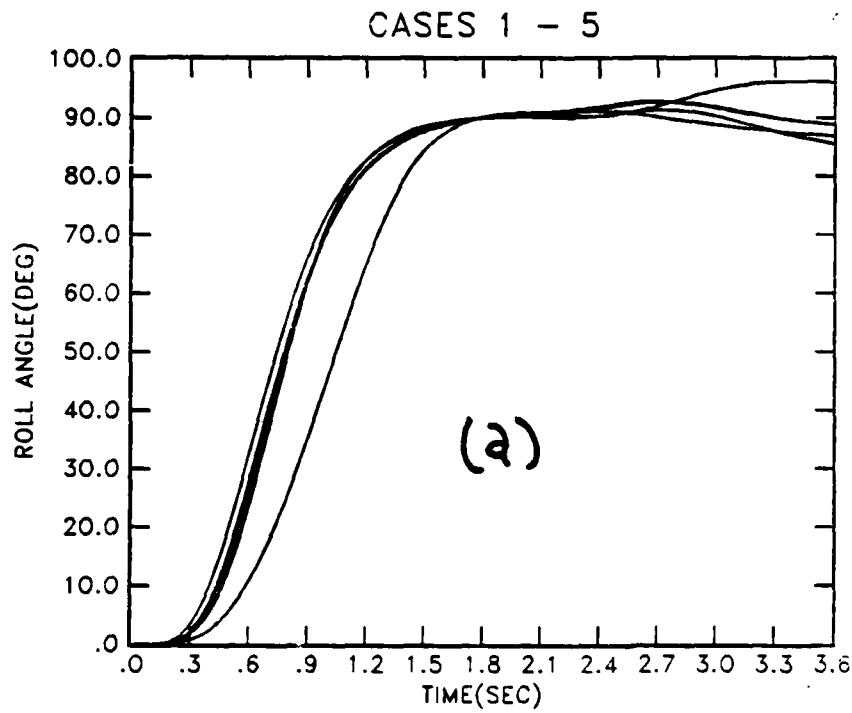


Figure 6.4e Bounds on $L_{30}(j\omega)$; $L_{30}(j\omega)$.



Figures 6.5a,b Roll and sideslip responses ($\phi_c = 90^\circ$ at $t=0$,
 2×2 , $\beta_c = 5^\circ$ at $t=1.8$, 3×3).

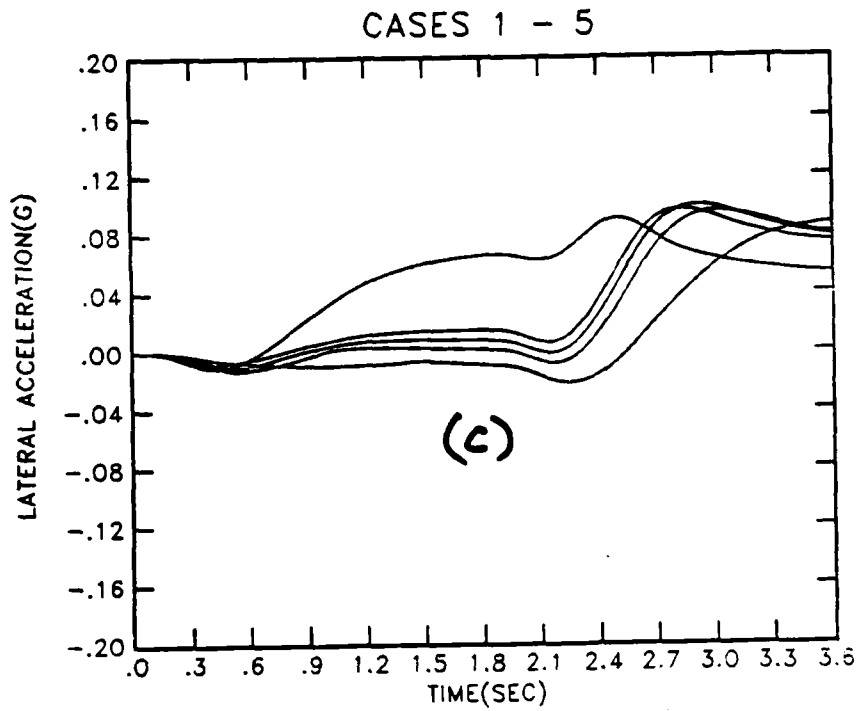
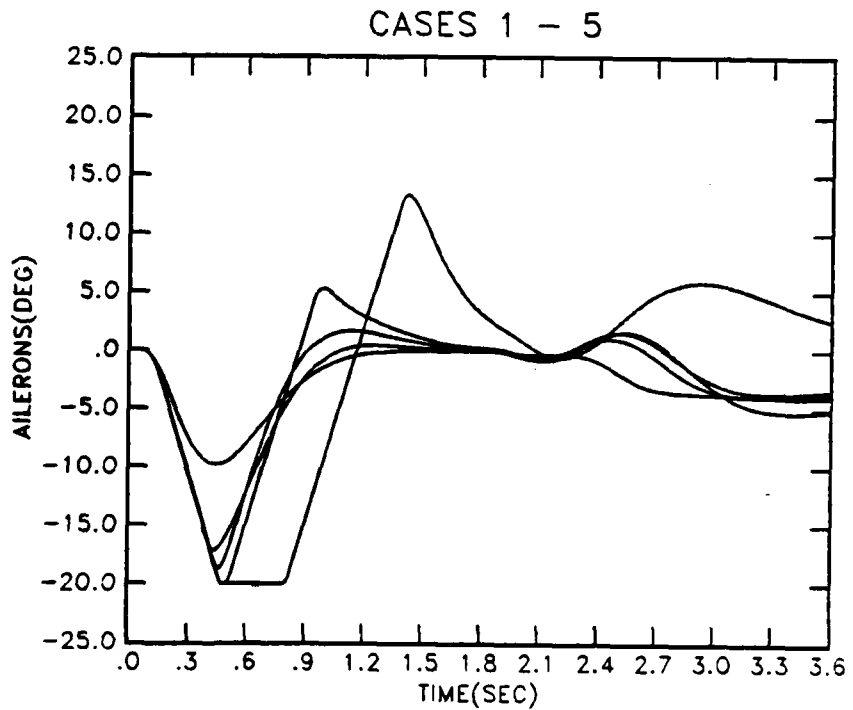


Fig. 6.5c Lateral acceleration response ($\phi_c = 90^\circ$, $t=0$; $\beta_c = 5^\circ$, $t=1.8$).

Figure 6.6a Aileron response ($\phi_c = 90^\circ$, $t=0$; $\beta_c = 5^\circ$, $t=1.8$).



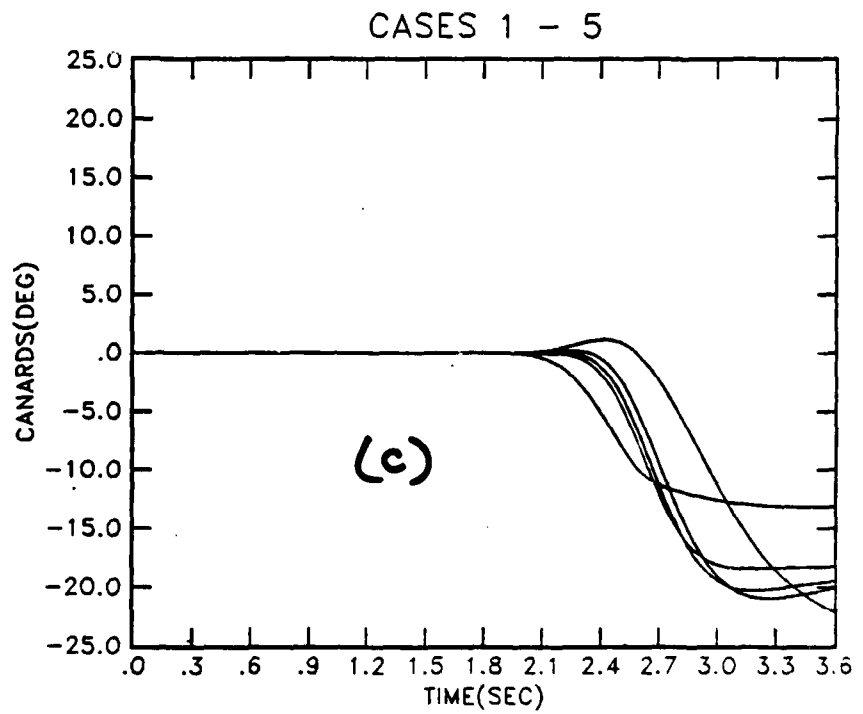
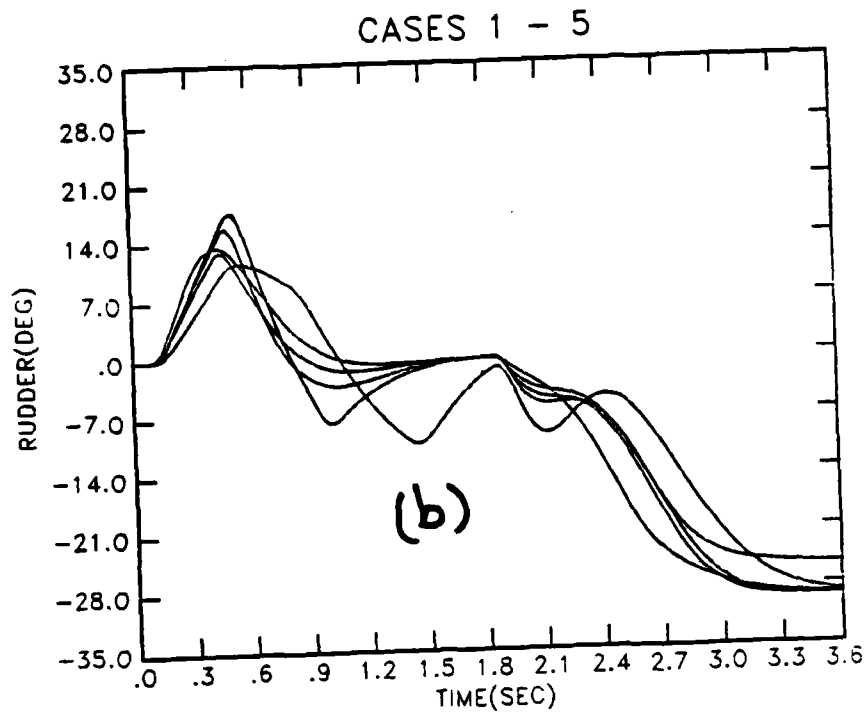
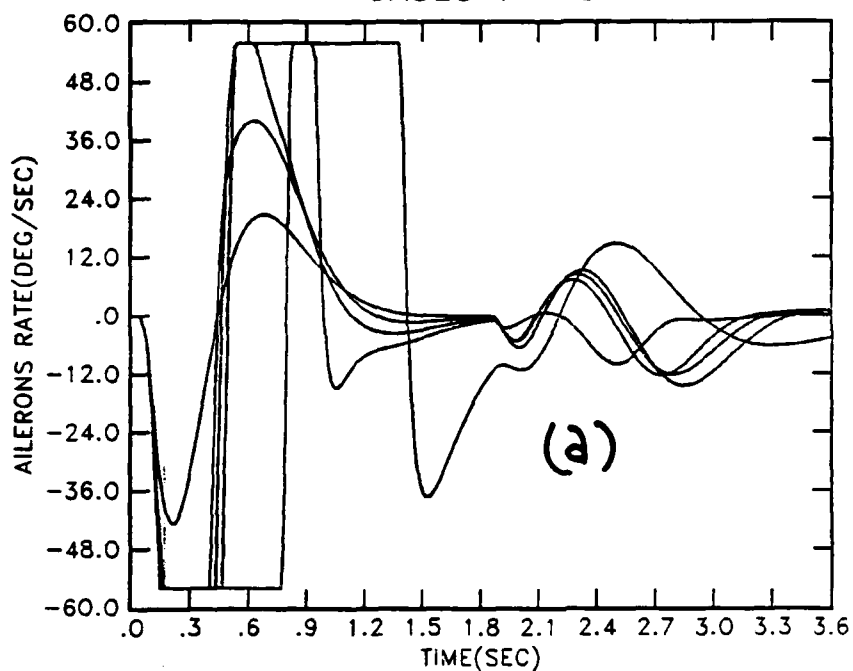


Figure 6.6b,c Rudder and canard responses ($\phi_c = 90^\circ$, $t=0$; $\beta_c = 5^\circ$, $t=1.8$).

CASES 1 - 5



CASES 1 - 5

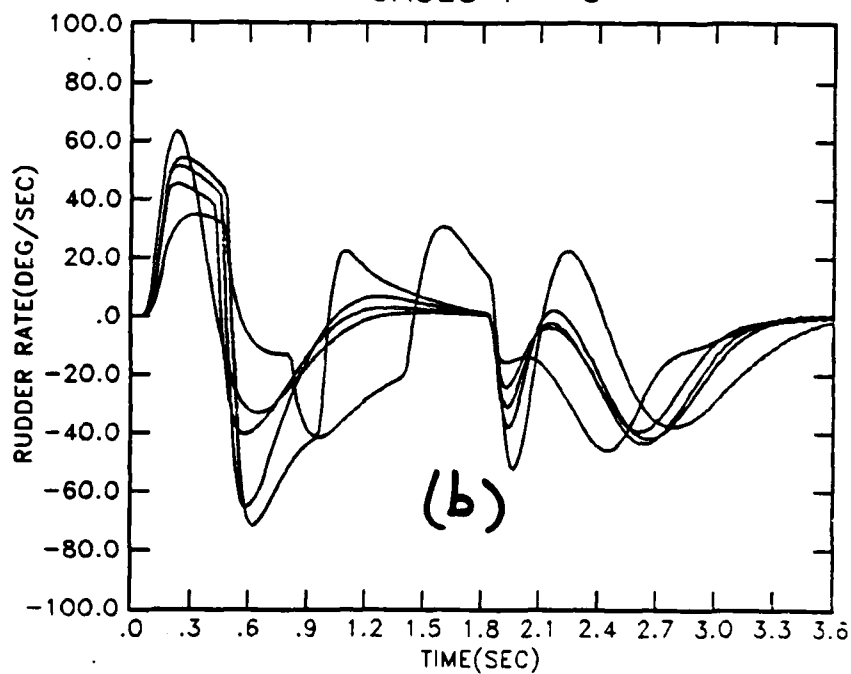
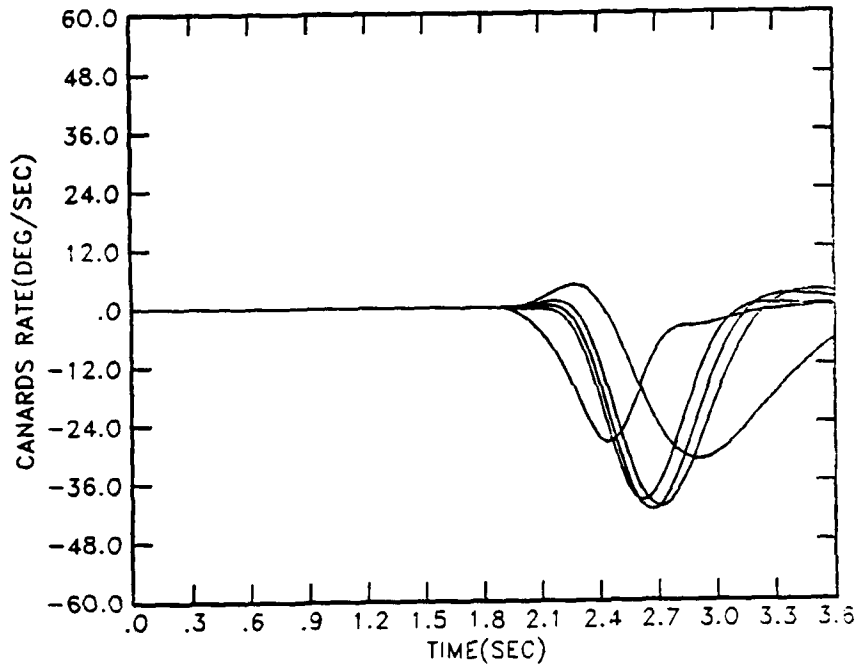


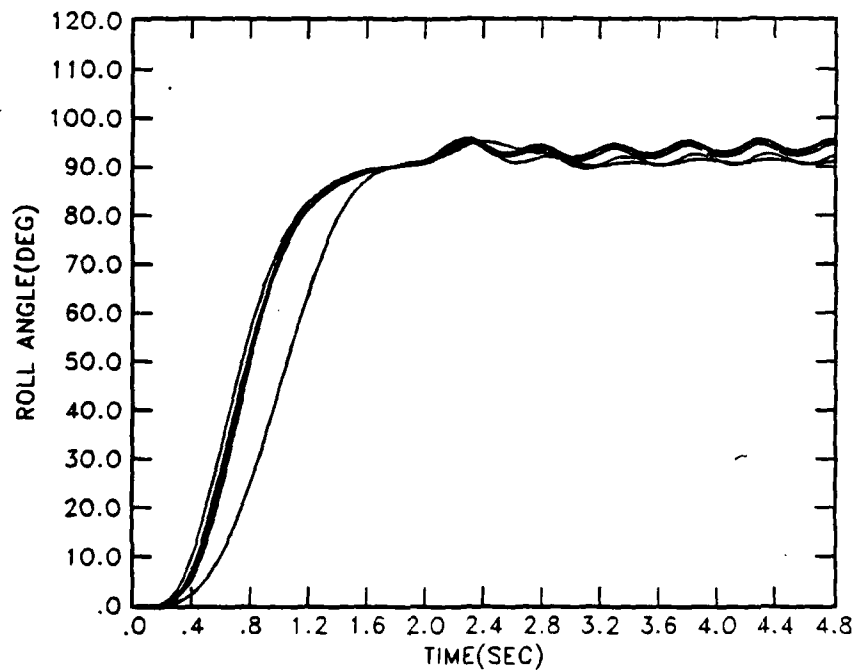
Figure 6.7a,b Aileron and rudder rates ($\phi_c = 90^\circ$, $t=0$; $\delta_c = 5^\circ$, $t=1.8$).

CASES 1 - 5



CASES 1 - 5

Figure 6.8a
 $(\phi_c = 90^\circ, t=0; t=1.8,$
 sinusoid $\omega = 12.5$ rps,
 amplitude 15°).



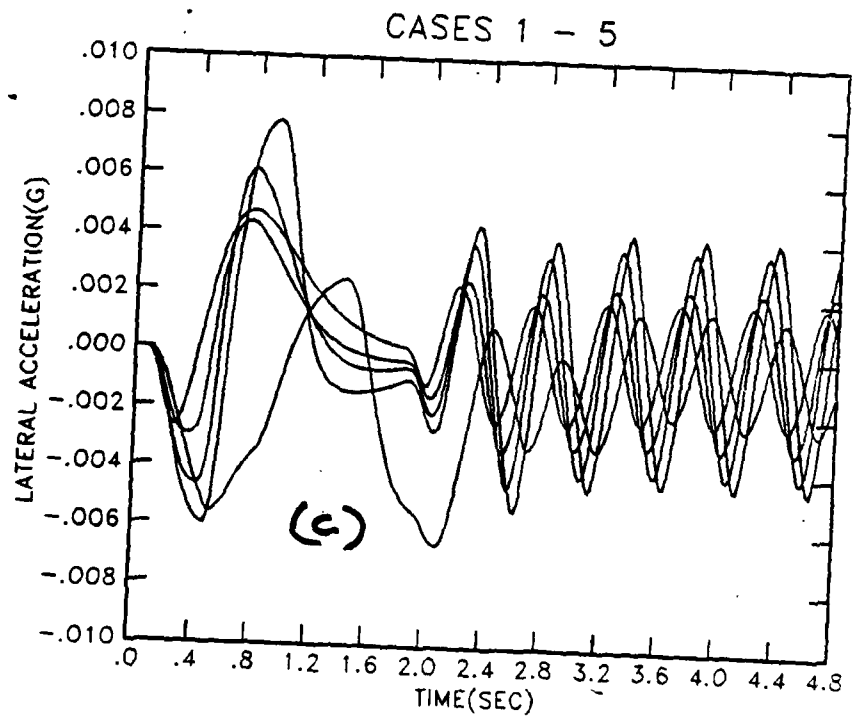
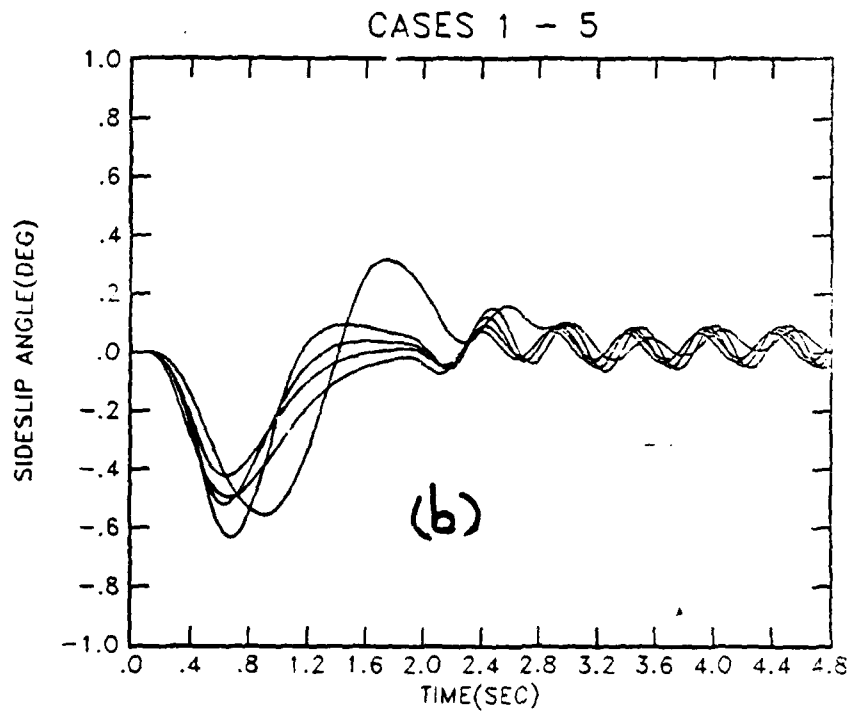


Figure 6.8b,c Sideslip and lateral acceleration, 3x3 ($\phi_c = 90^\circ$, $t=0$;
 $t=1.8$, sinusoid $\omega = 12.5$ rps, amplitude 15°).

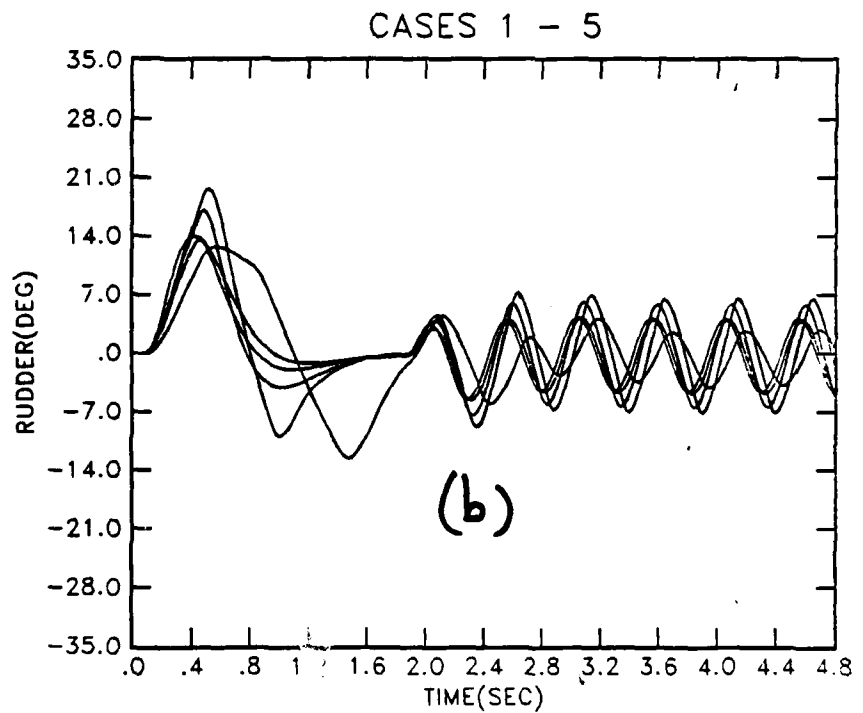
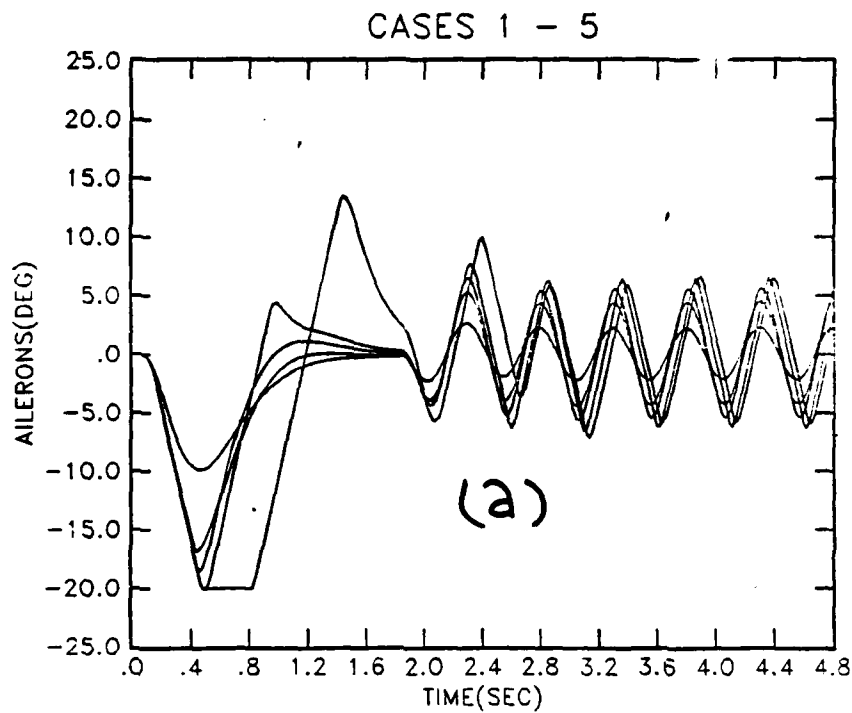


Figure 6.9a,b Aileron and rudder responses, 3x3 ($\phi_c = 90^\circ$, $t=0$; $t=1.8$, sinusoid $\omega = 12.5$ rps, amplitude 15°)

CASES 1 - 5

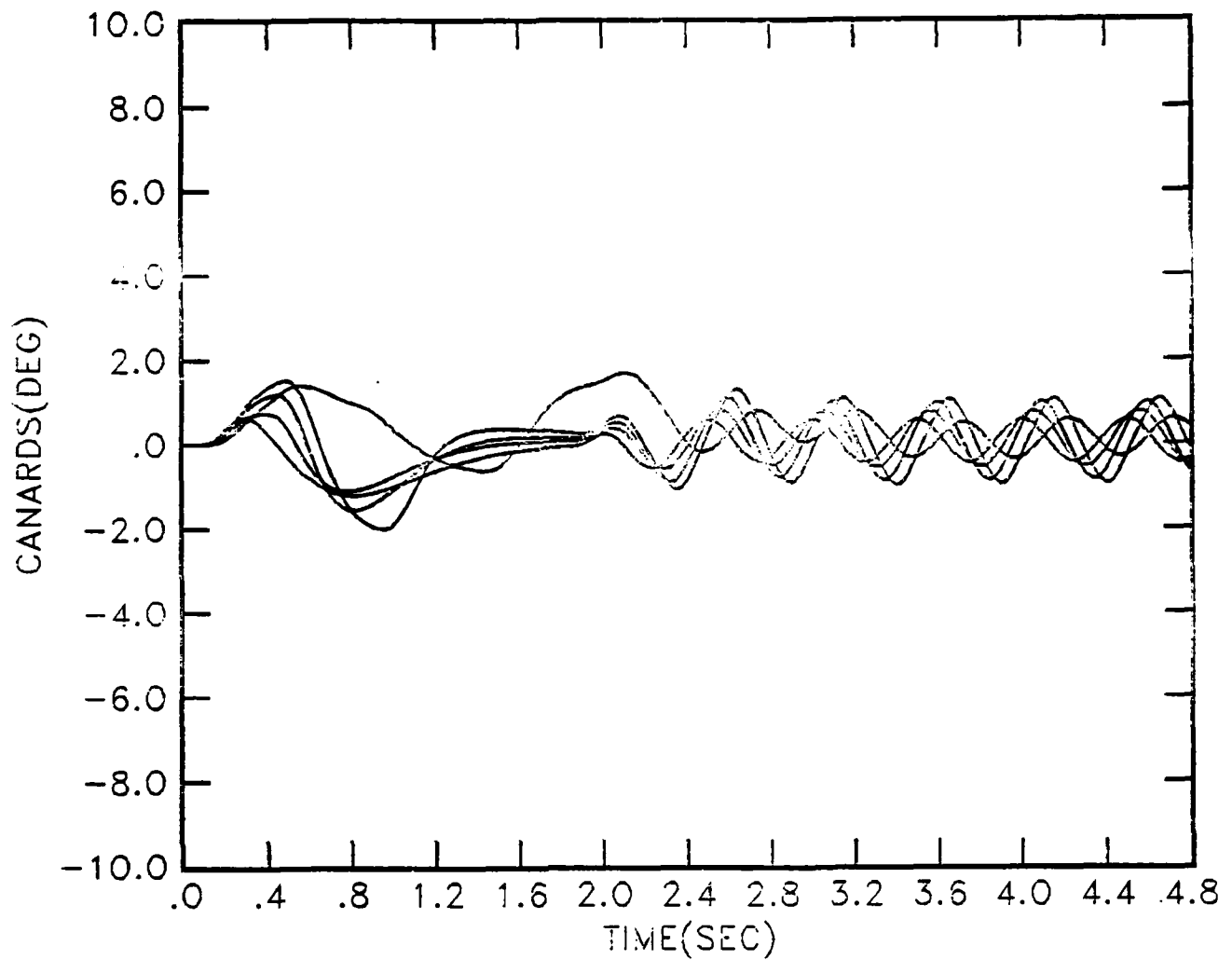


Figure 6.9c Canard response 3x3 ($\phi_c = 90^\circ$, $t=0$; $t=1.8$, sinusoid $\omega = 17.5$ rps, amplitude 15°)

CASES 1 - 5

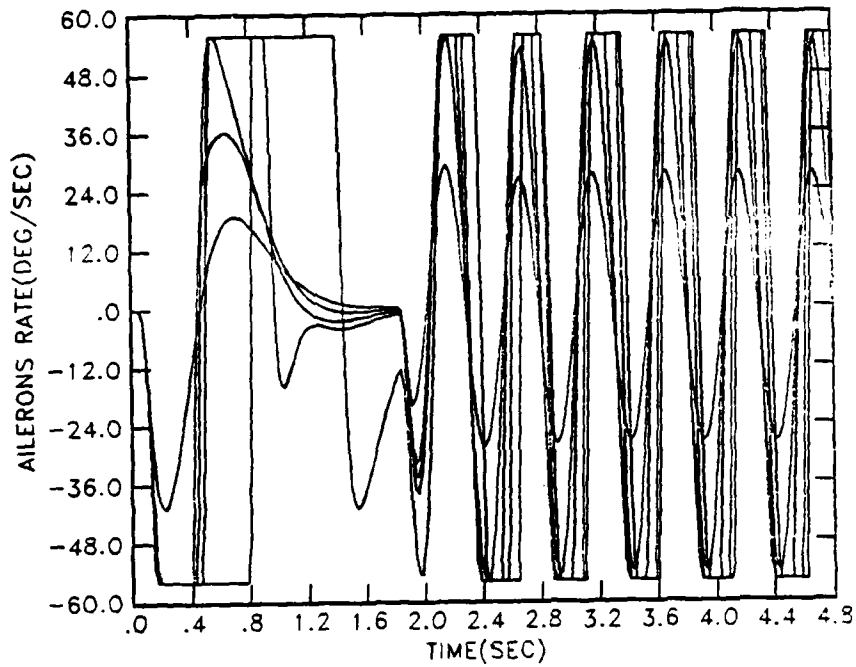
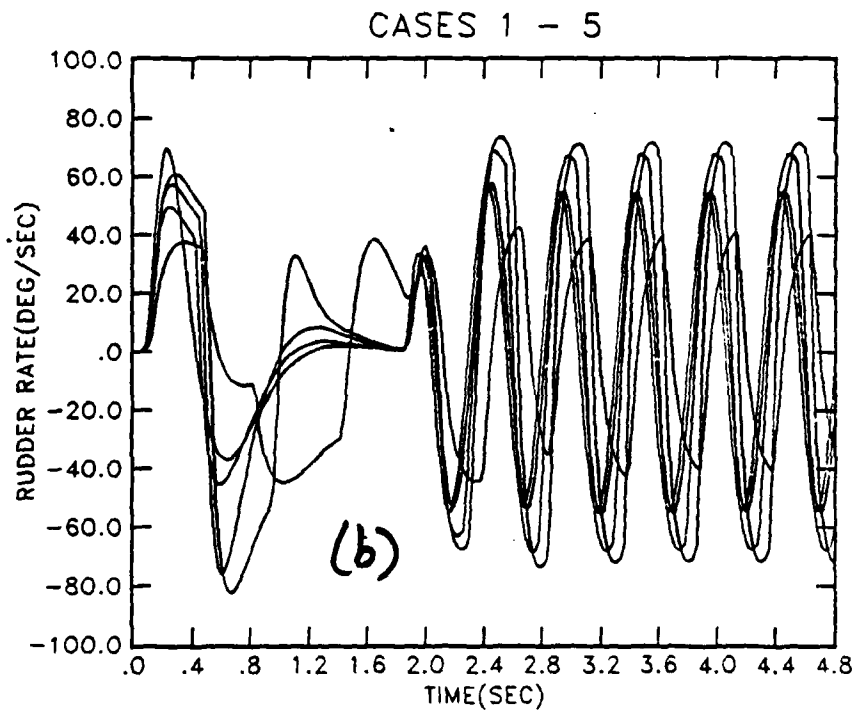


Figure 6.10a,b Aileron and
rudder rates, 3x3 ($\phi_c = 90^\circ$,
 $t=0$; $t=1.8$, sinusoid
 $\omega = 12.5$ rps, amplitude 15°)



CASES 1 - 5

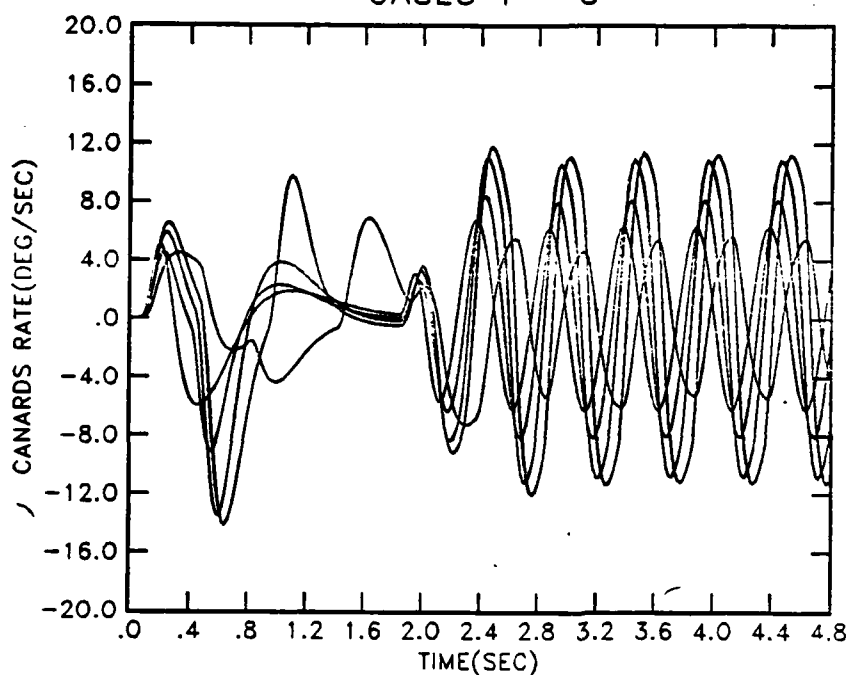


Figure 6.10c Canard rate, 3x3

($\phi_c = 90^\circ$, $t=0$; $t=1.8$,
sinusoid $\omega = 12.5$ rps,
amplitude 15°)

CASES 1 - 5

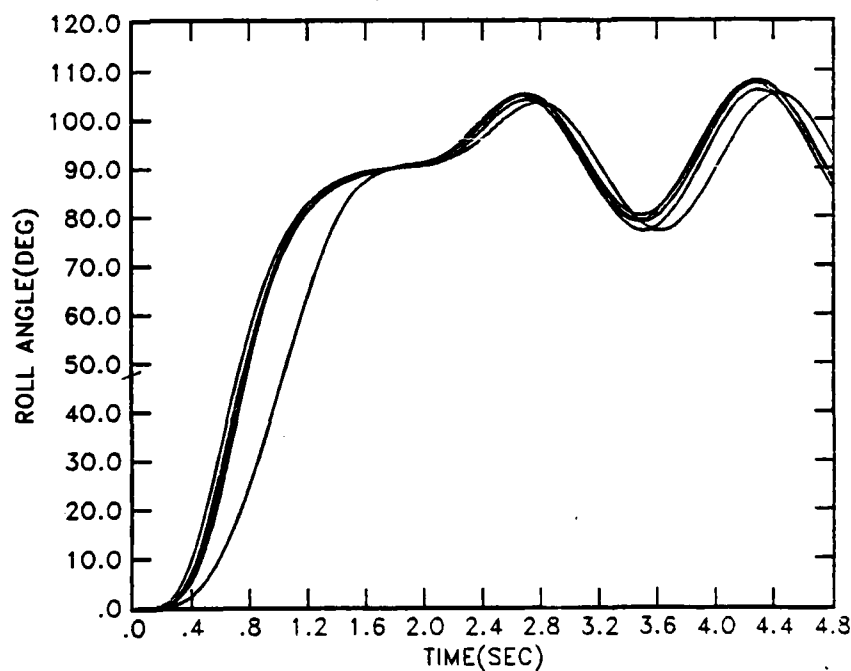


Figure 6.11a

Roll response 3x3
($\phi_c = 90^\circ$, $t=0$, $t=1.8$,
sinusoid $\omega = 4$ rps,
amplitude 15°)

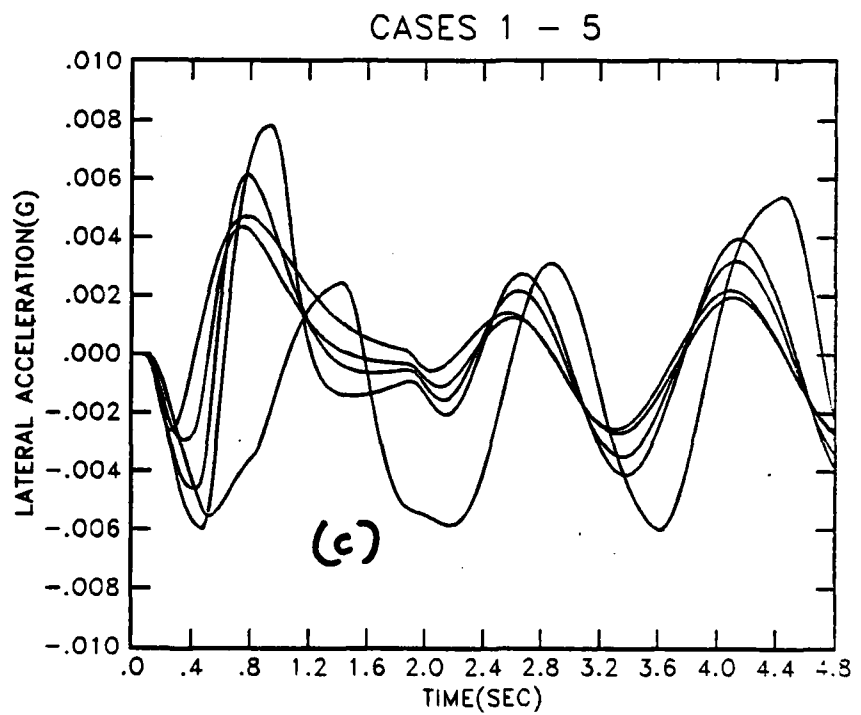
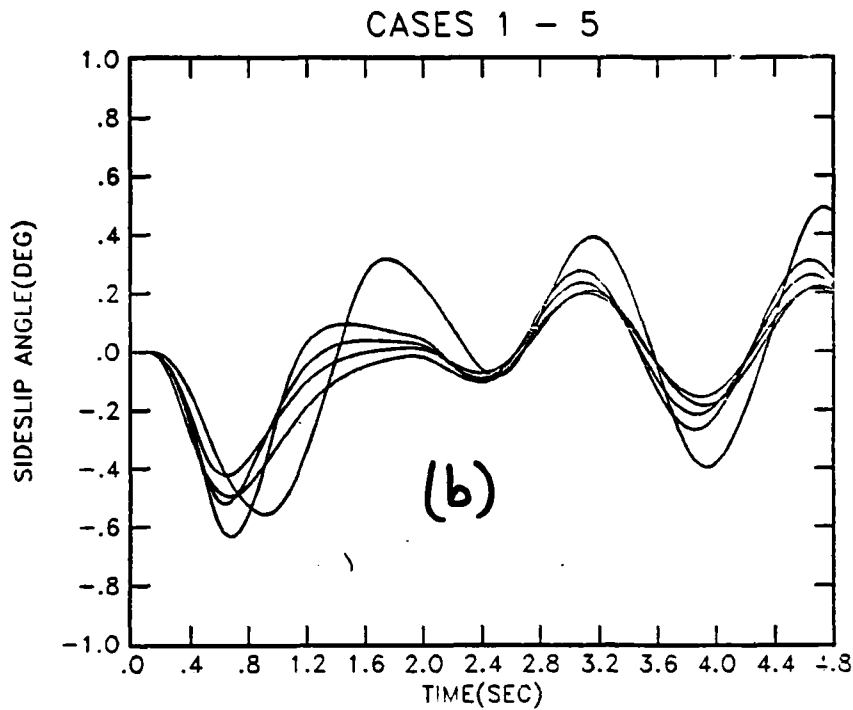


Figure 6.11b,c Sideslip and lateral acceleration responses ($\phi_c = 90^\circ$, $t=0$;
 $t=1.8$, sinusoid $\omega = 4$ rps, amplitude 15°).

CASES 1 - 5

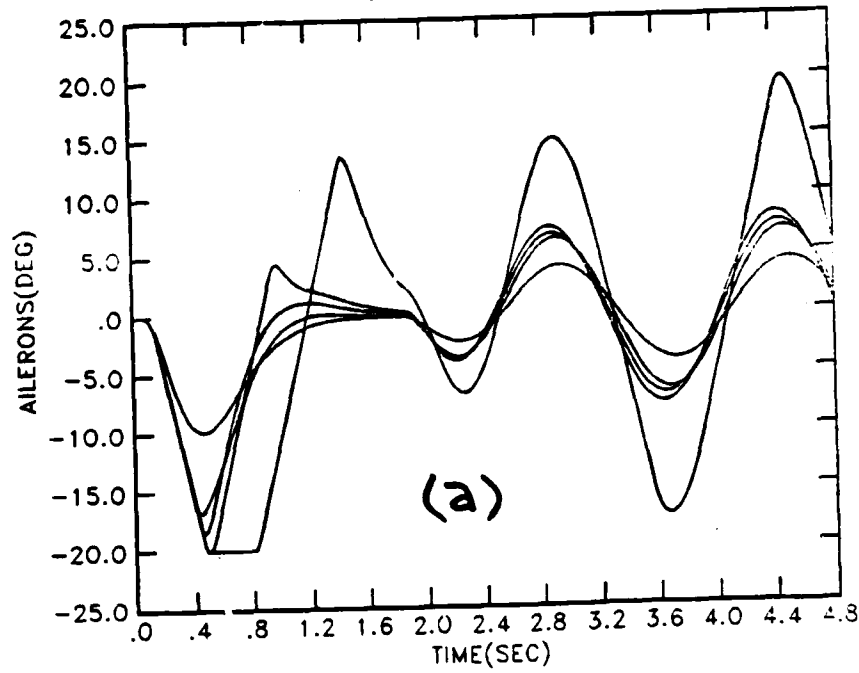
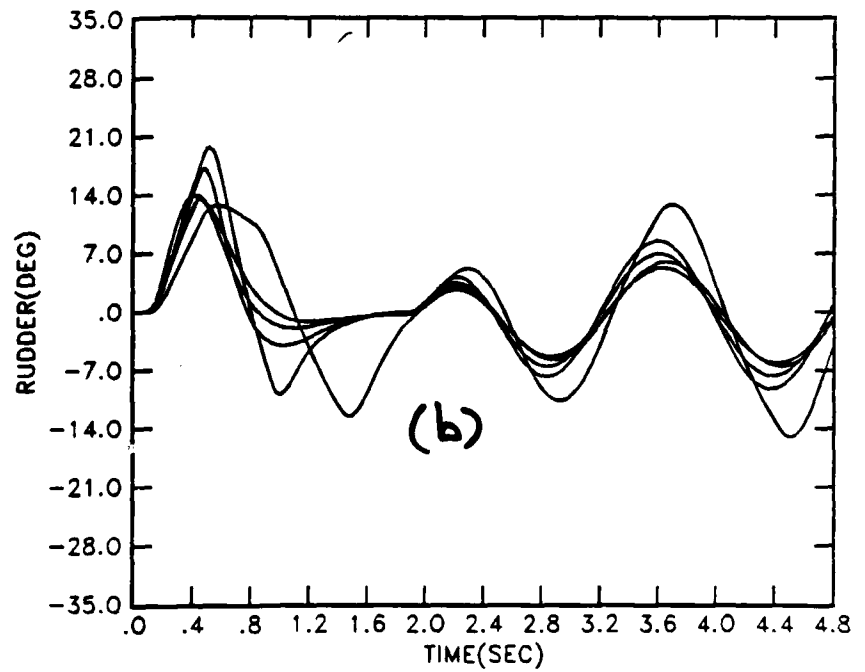


Figure 6.12a,b Aileron and
rudder responses 3x3
($\phi_c = 90^\circ$, $t=0$, $t=1.8$,
sinusoid $\omega = 4$ rps,
amplitude 15°).

CASES 1 - 5



CASES 1 - 5

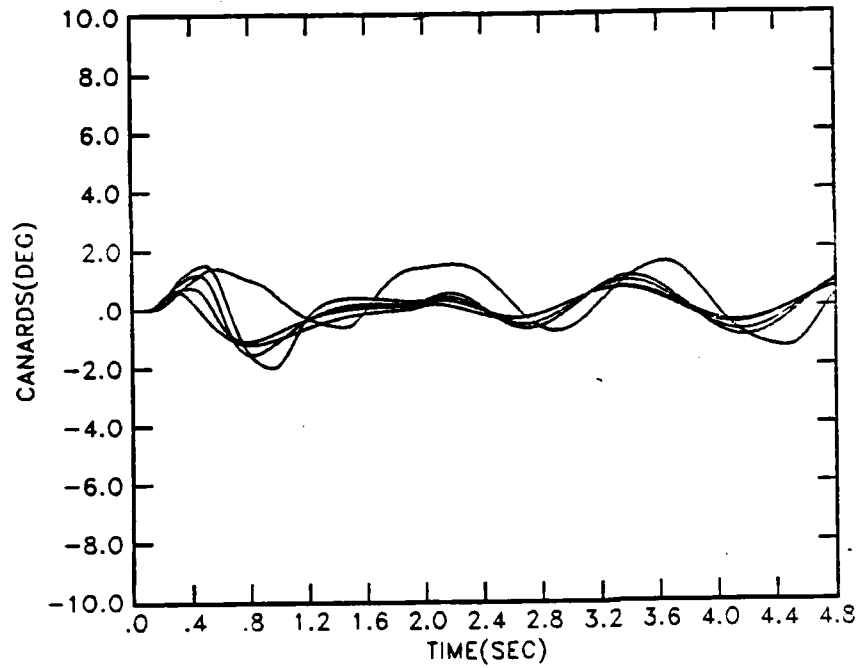


Figure 6.12c Canard response 3x3

($\phi_c = 90^\circ$, $t=0$, $t=1.8$,
 sinusoid $\omega = 4$ rps,
 amplitude 15°)

CASES 1 - 5

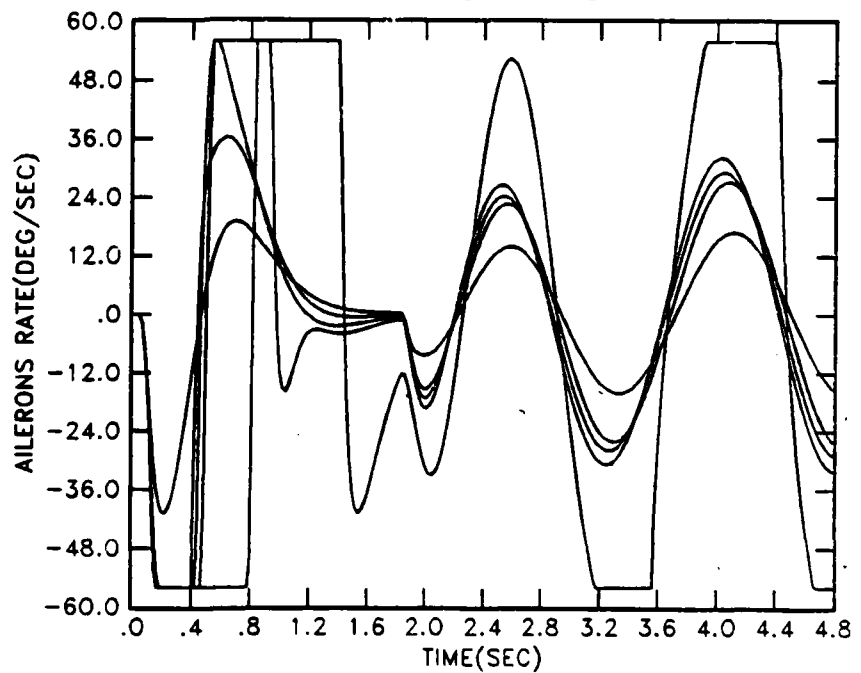


Figure 6.13a

Aileron rate 3x3
 (3x3 ($\phi_c = 90^\circ$, $t=0$,
 $t=1.8$, sinusoid
 $\omega = 4$ rps,
 amplitude 15°)

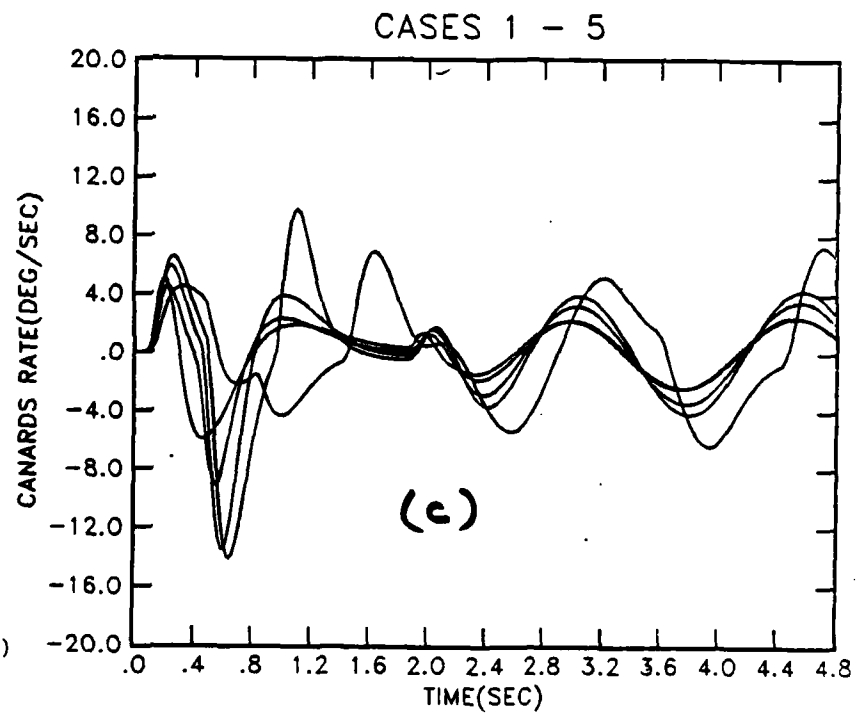
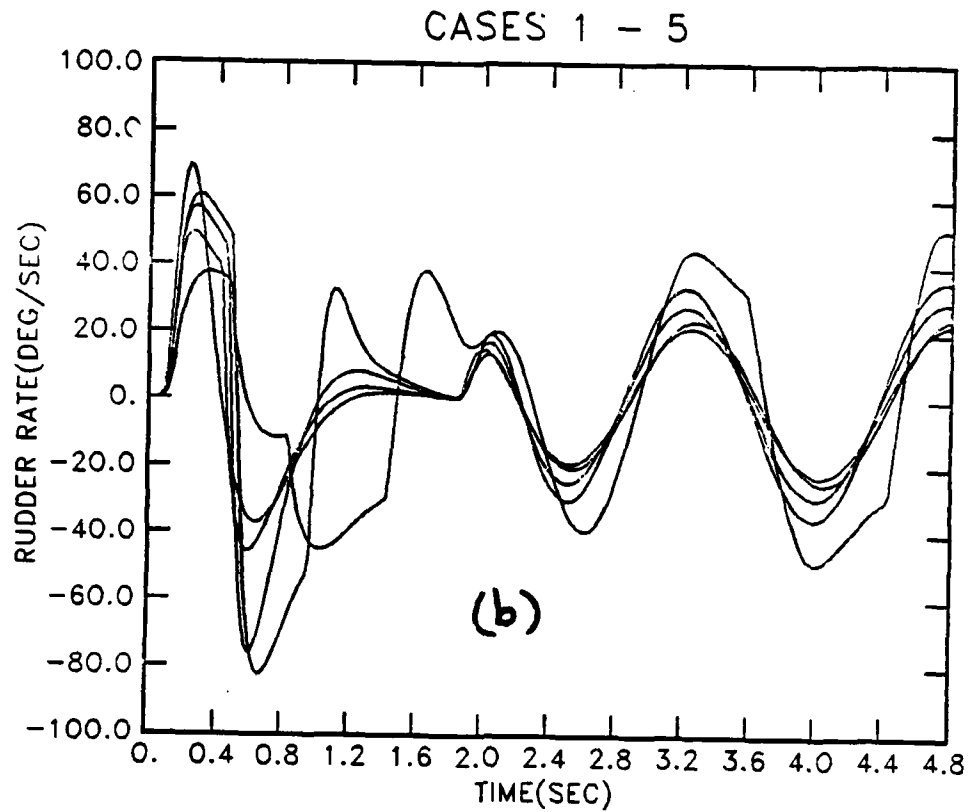


Figure 6.13b,c Rudder and
canard rates 3x3 ($\phi_c = 90^\circ$,
 $t=0$, $t=1.8$, sinusoid
 $\omega = 4$ rps, amplitude 15°)

249
CASES 1 - 5

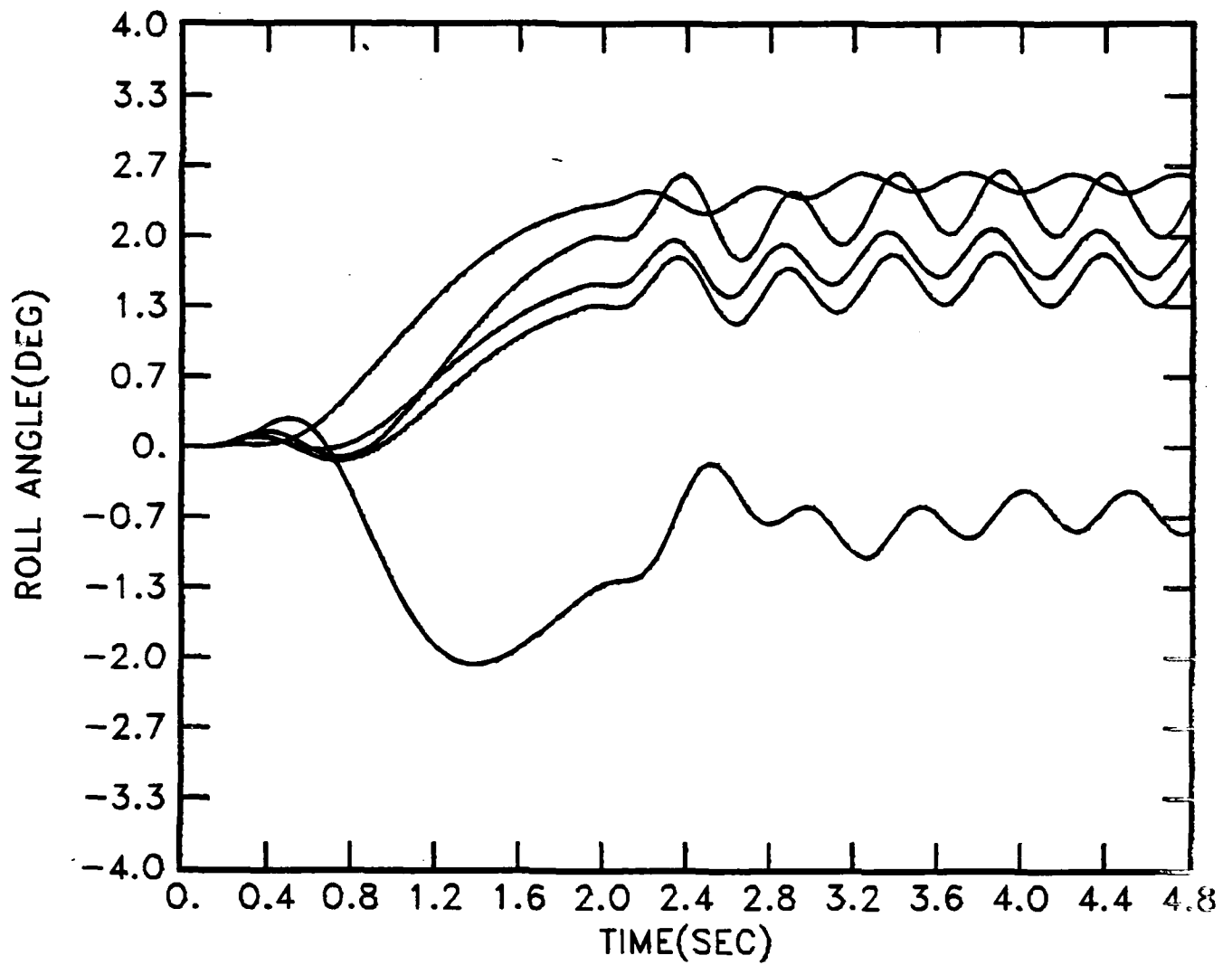


Figure 6.14a Roll

Figure 6.14 a-i Responses due to slideslip command β_c : 2.5° step at $t=0$,
sinusoid at $t=1.0$, amplitude 1.5° , frequency 12.5 rps.

CASES 1 - 5

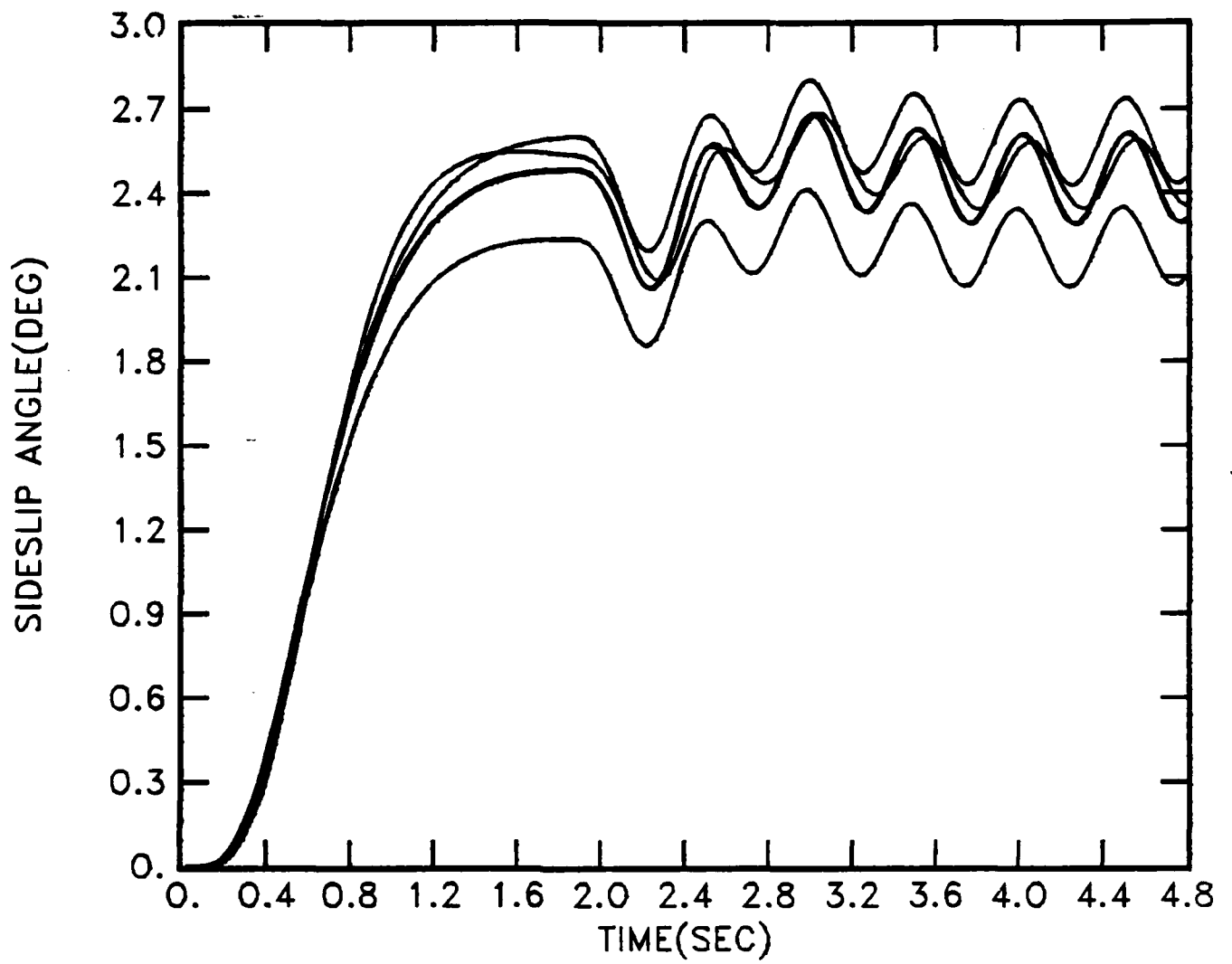


Figure 6.14b Sideslip

251
CASES 1 - 5

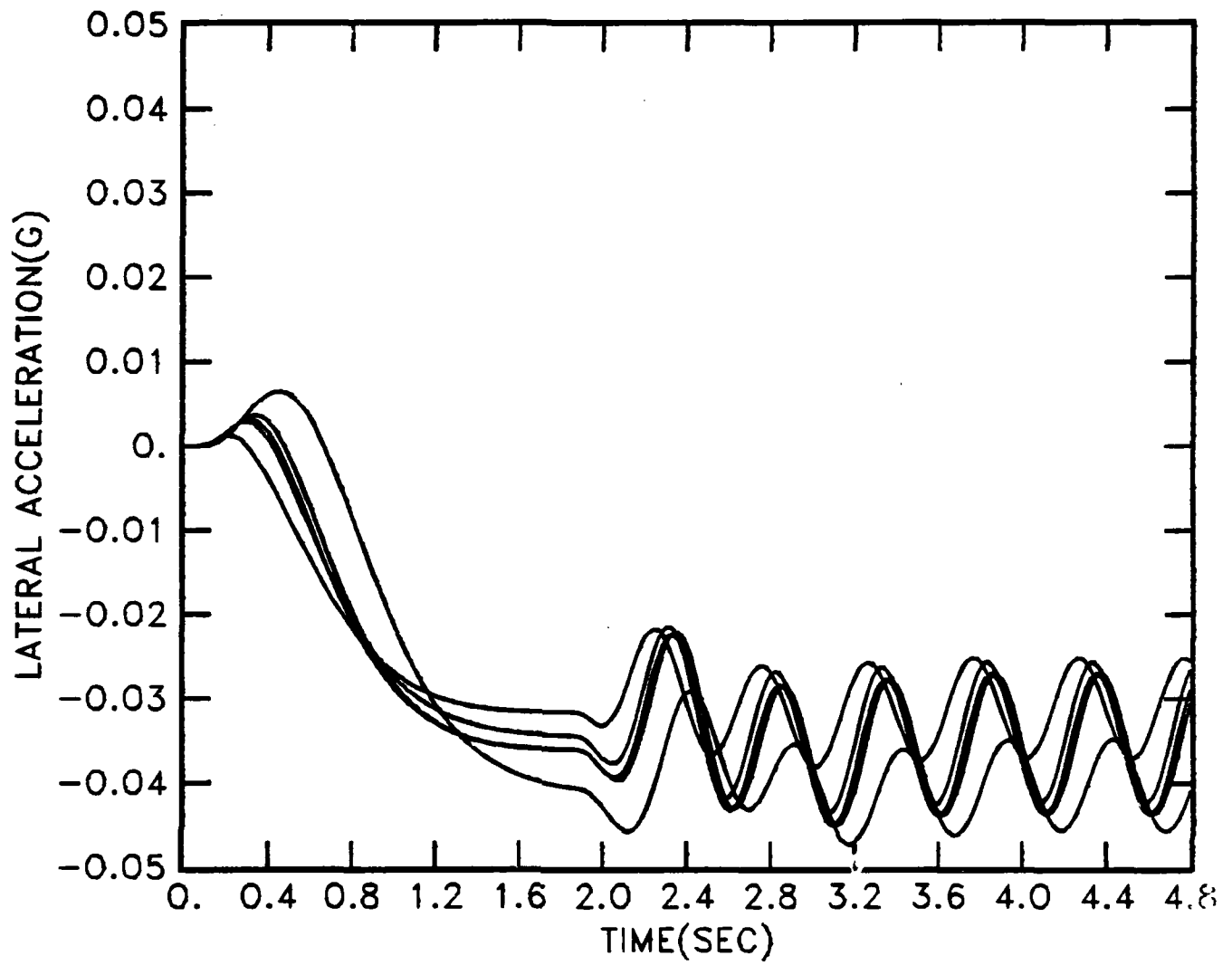


Figure 6.14c Acceleration

CASES 1 - 5

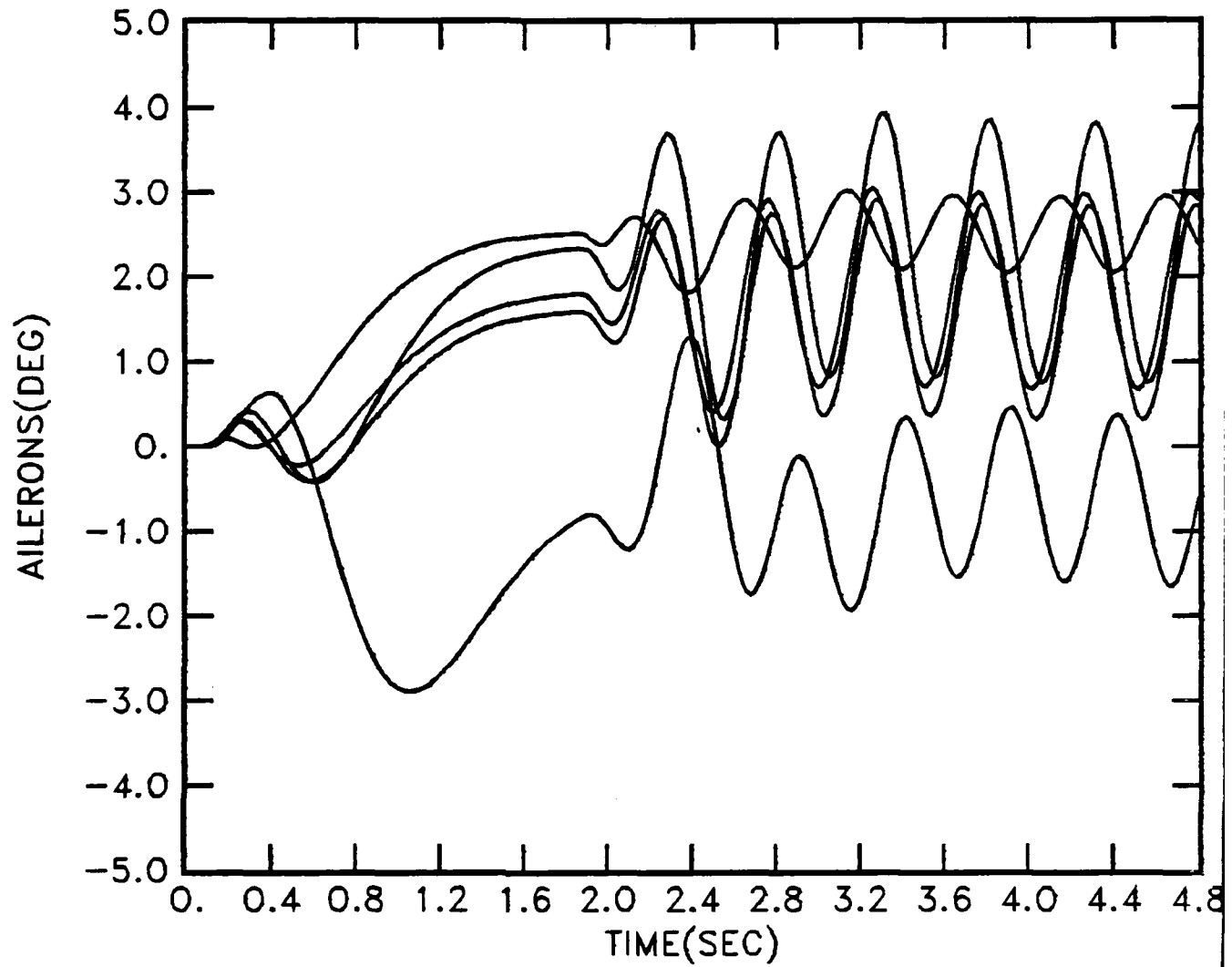


Figure 6.14d Ailerons

CASES 1 - 5

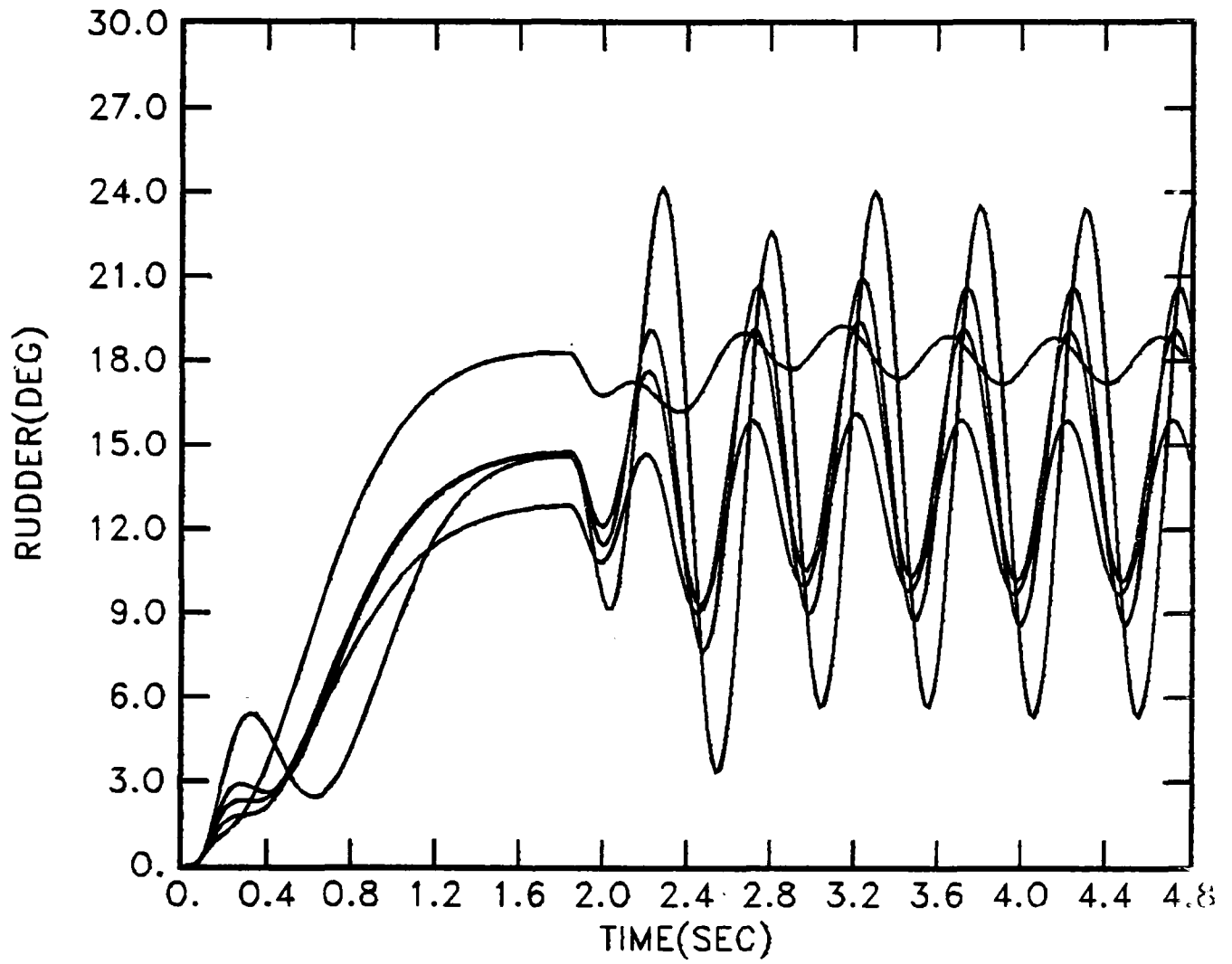


Figure 6.14e Rudder

CASES 1 - 5

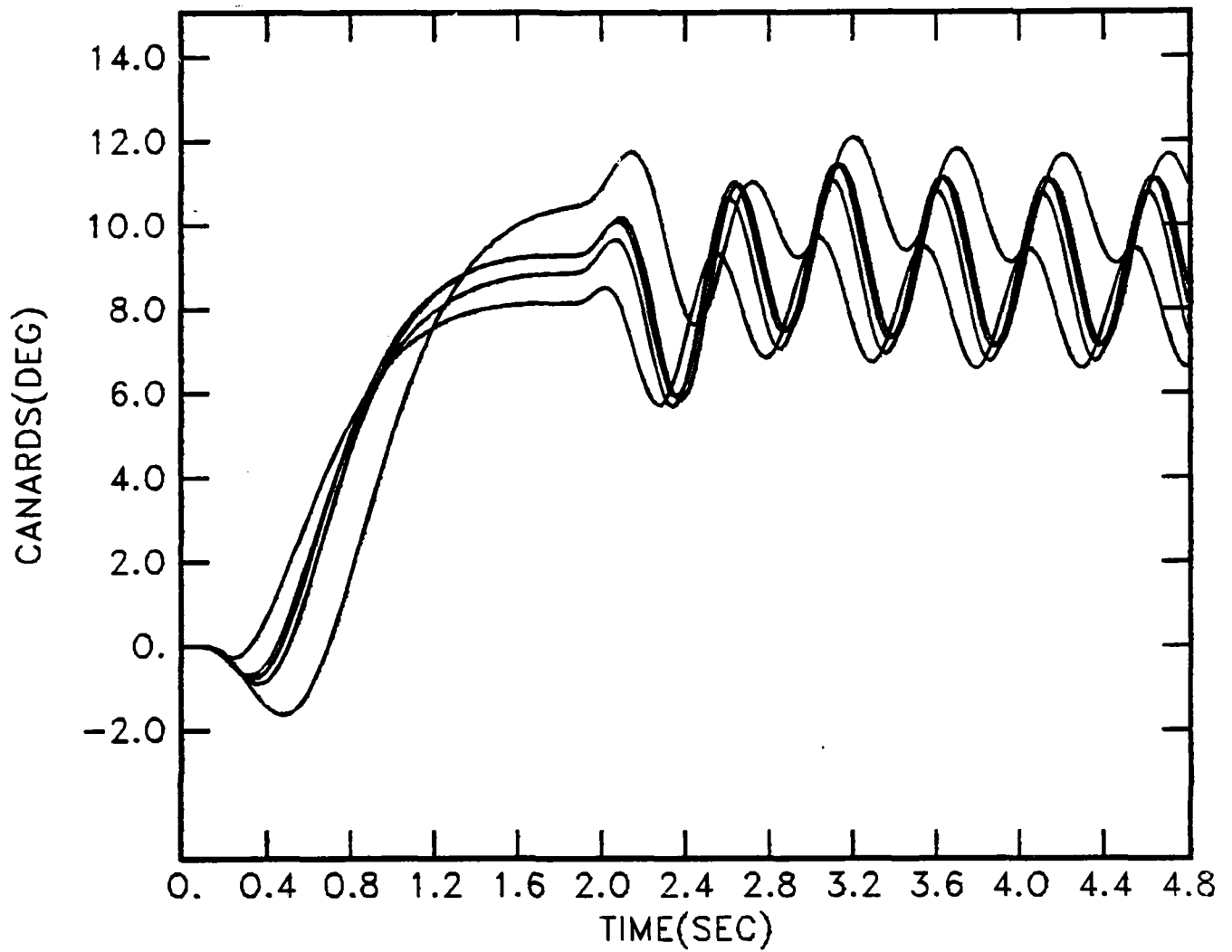


Figure 6.14f Canards

CASES 1 - 5

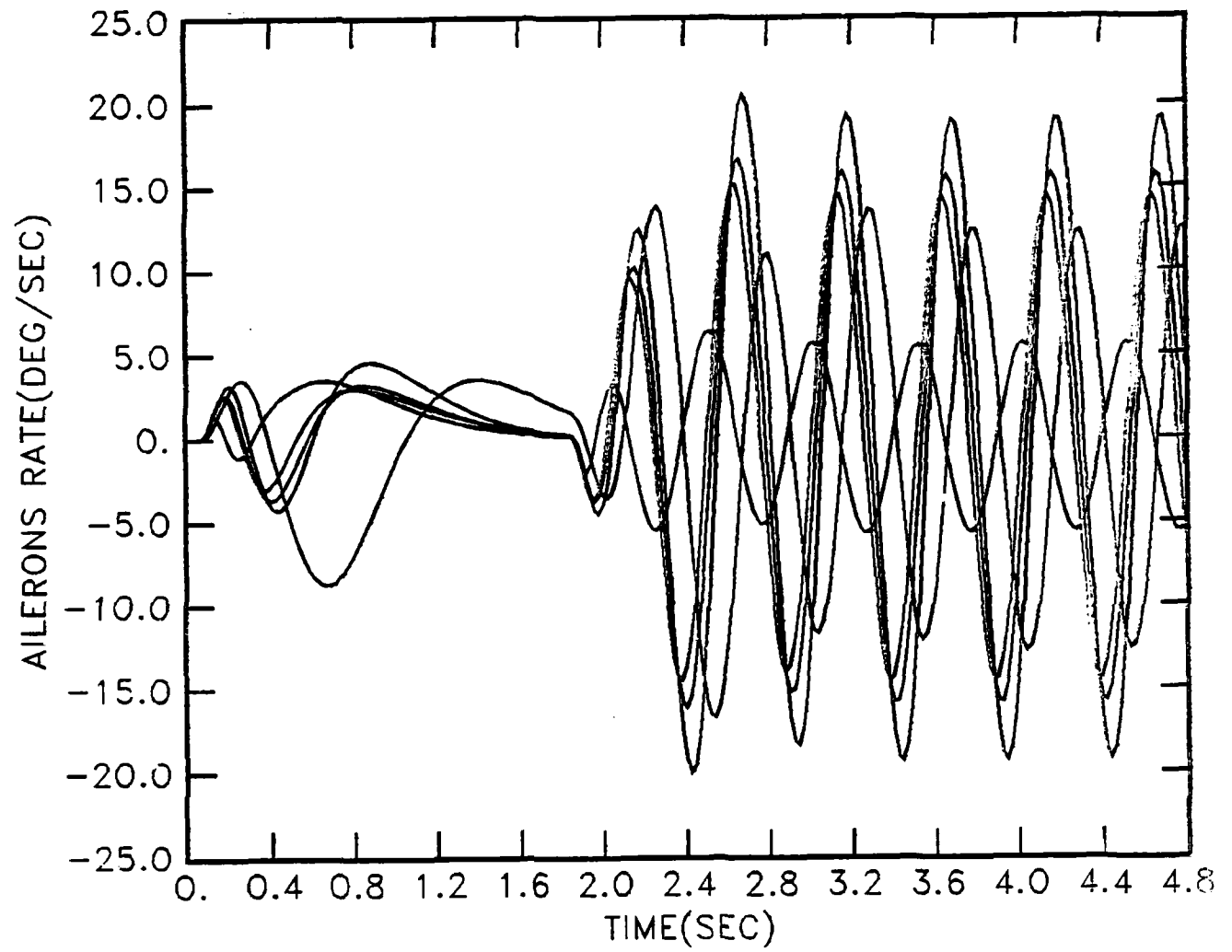


Figure 6.14g Aileron rate.

CASES 1 - 5

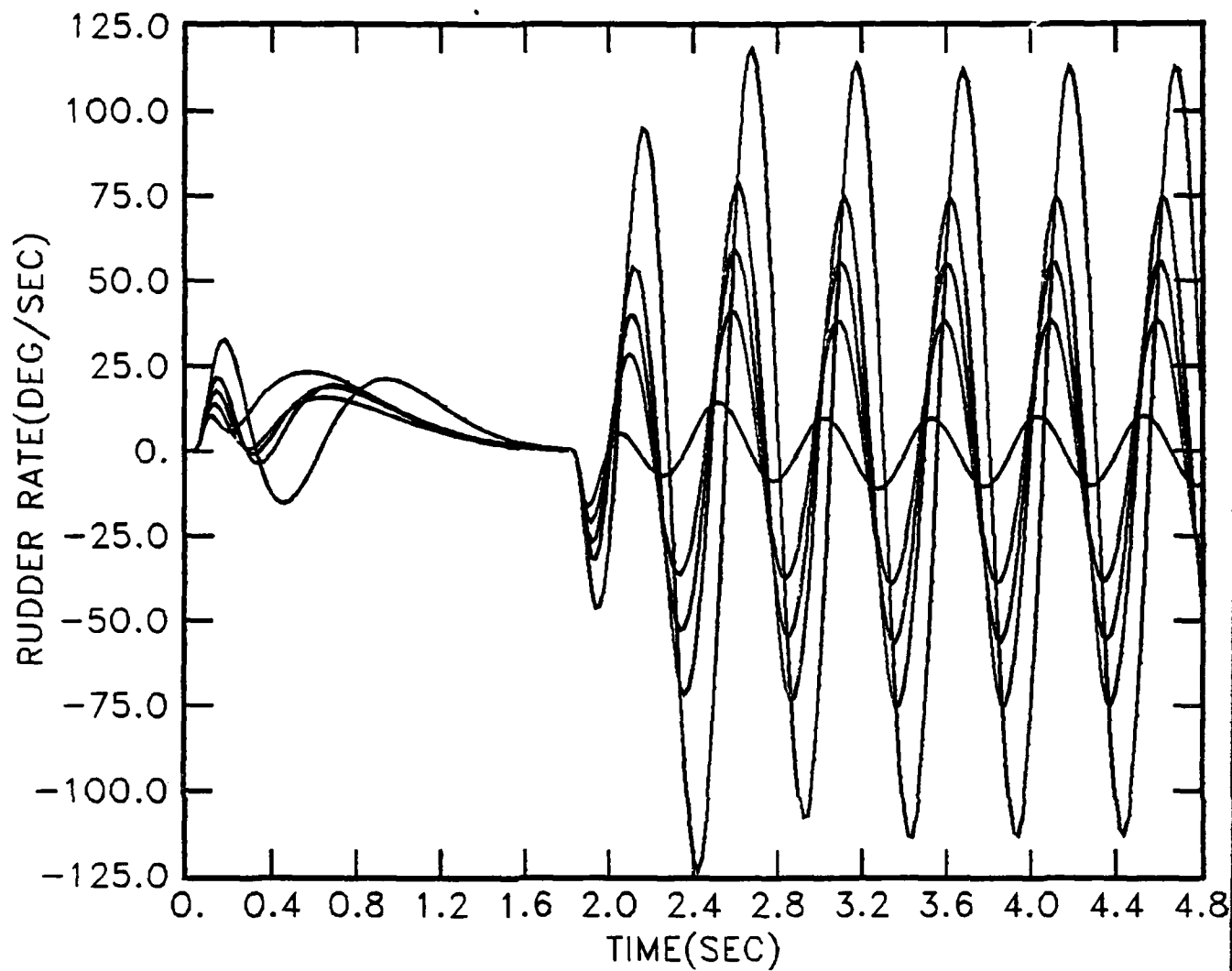


Figure 6.14h Rudder rate.

CASES 1 - 5

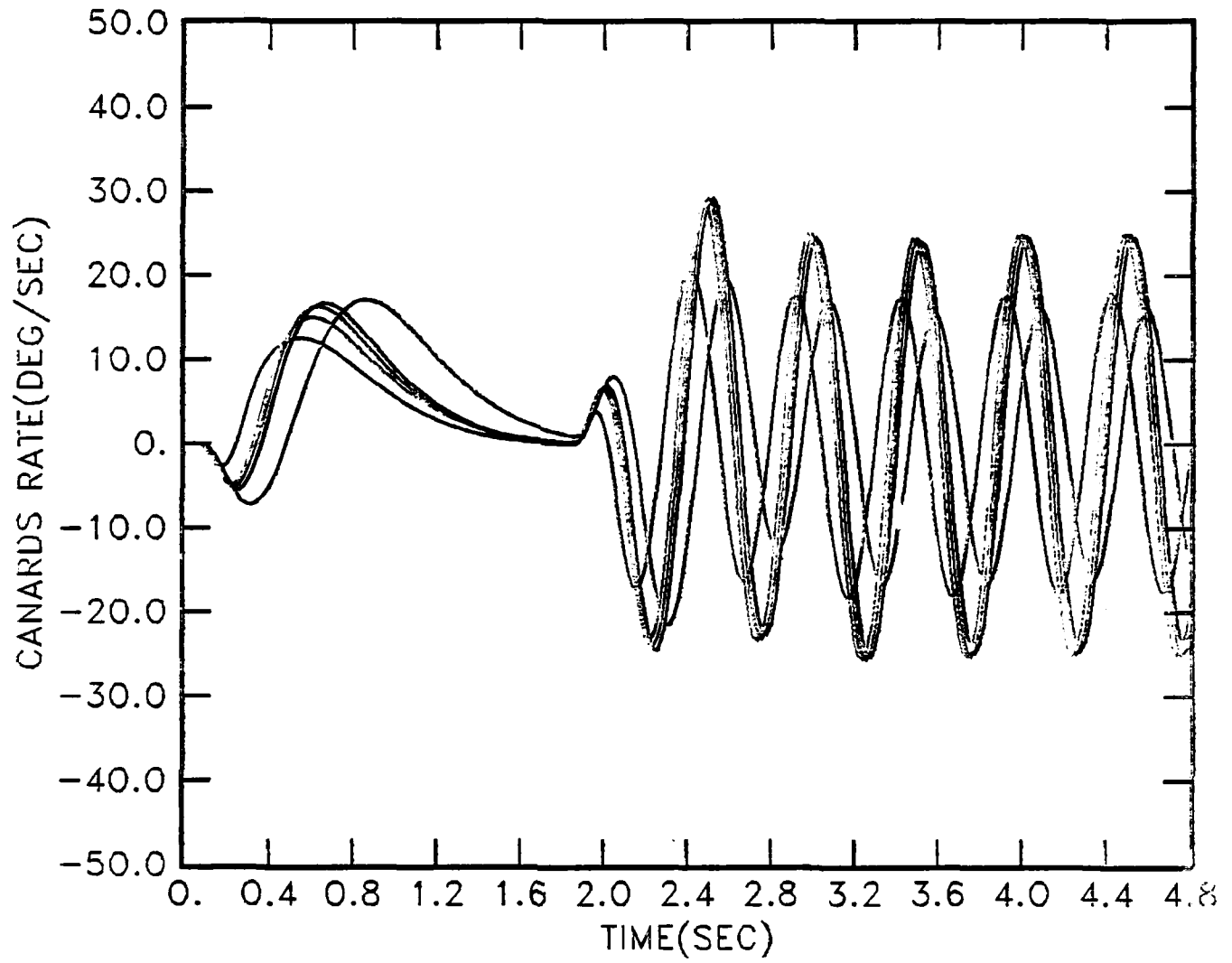


Figure 6.14i Canard rate

CASES 1 - 5

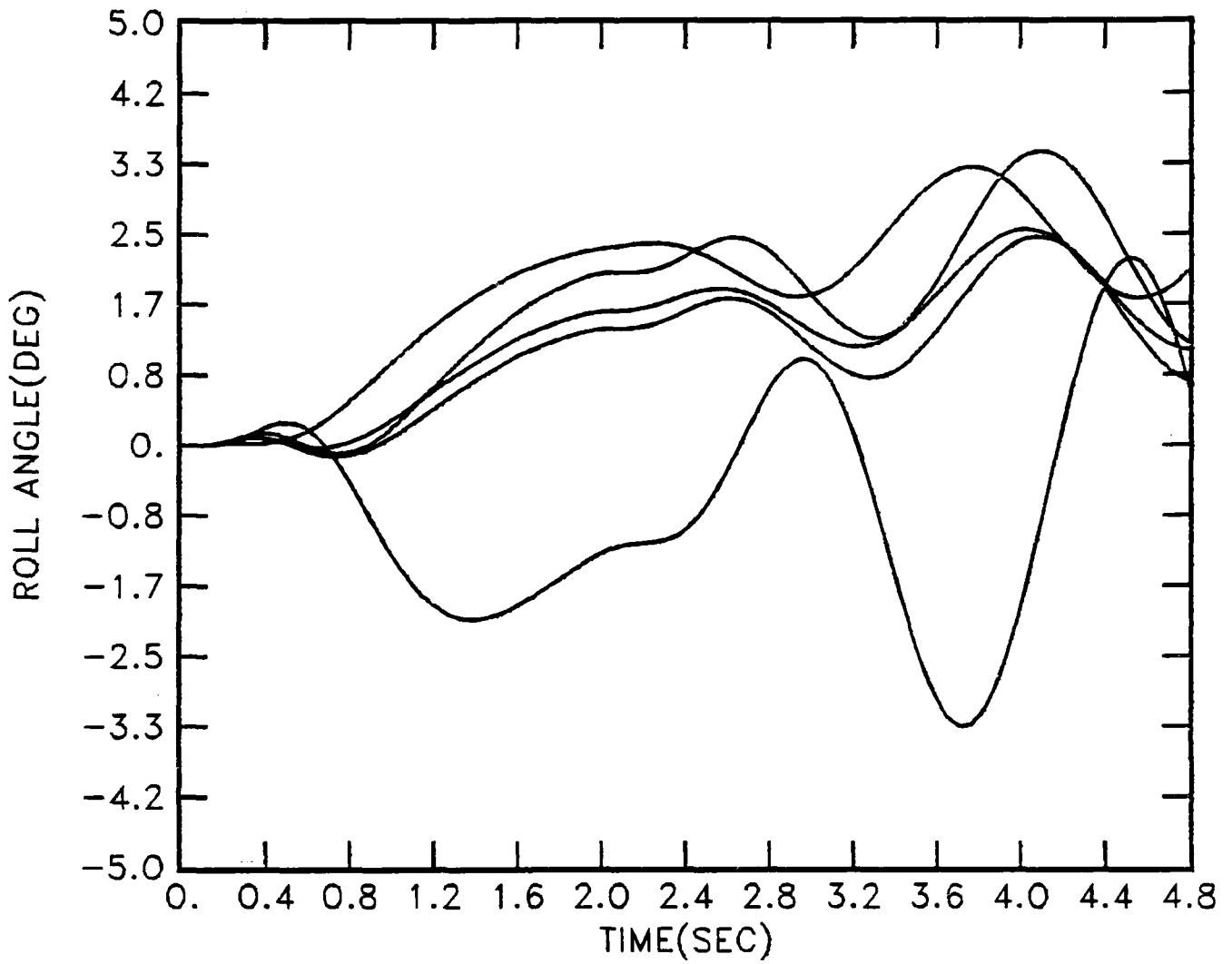


Figure 6.15a Roll

Figure 6.15a-i Responses due to sideslip command δ ; 2.5° step at $t=0$,
sinusoid at $t=1.0$, amplitude 1.5° , frequency 4 rps.

CASES 1 - 5

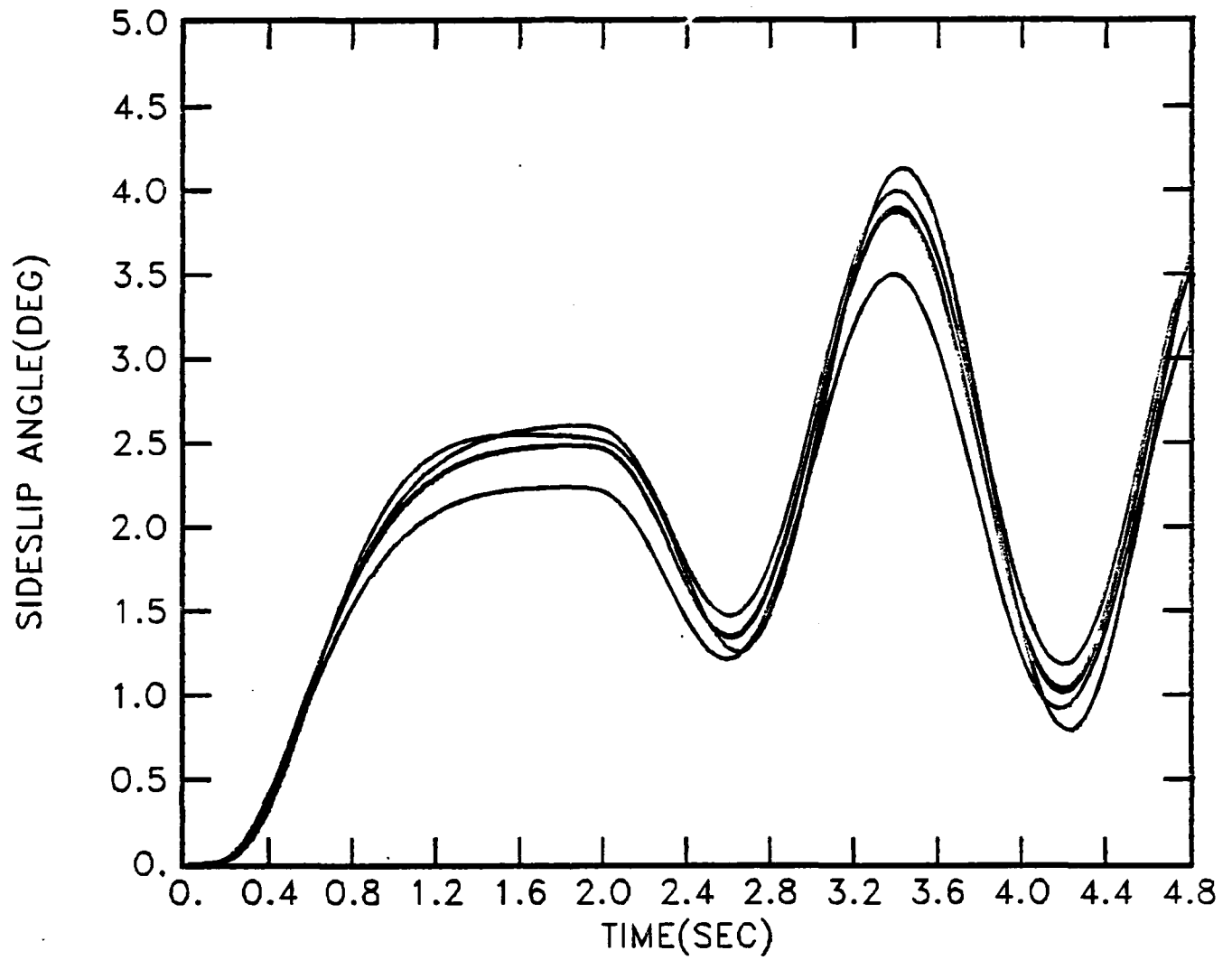


Figure 6.15b Sideslip.

CASES 1 - 5

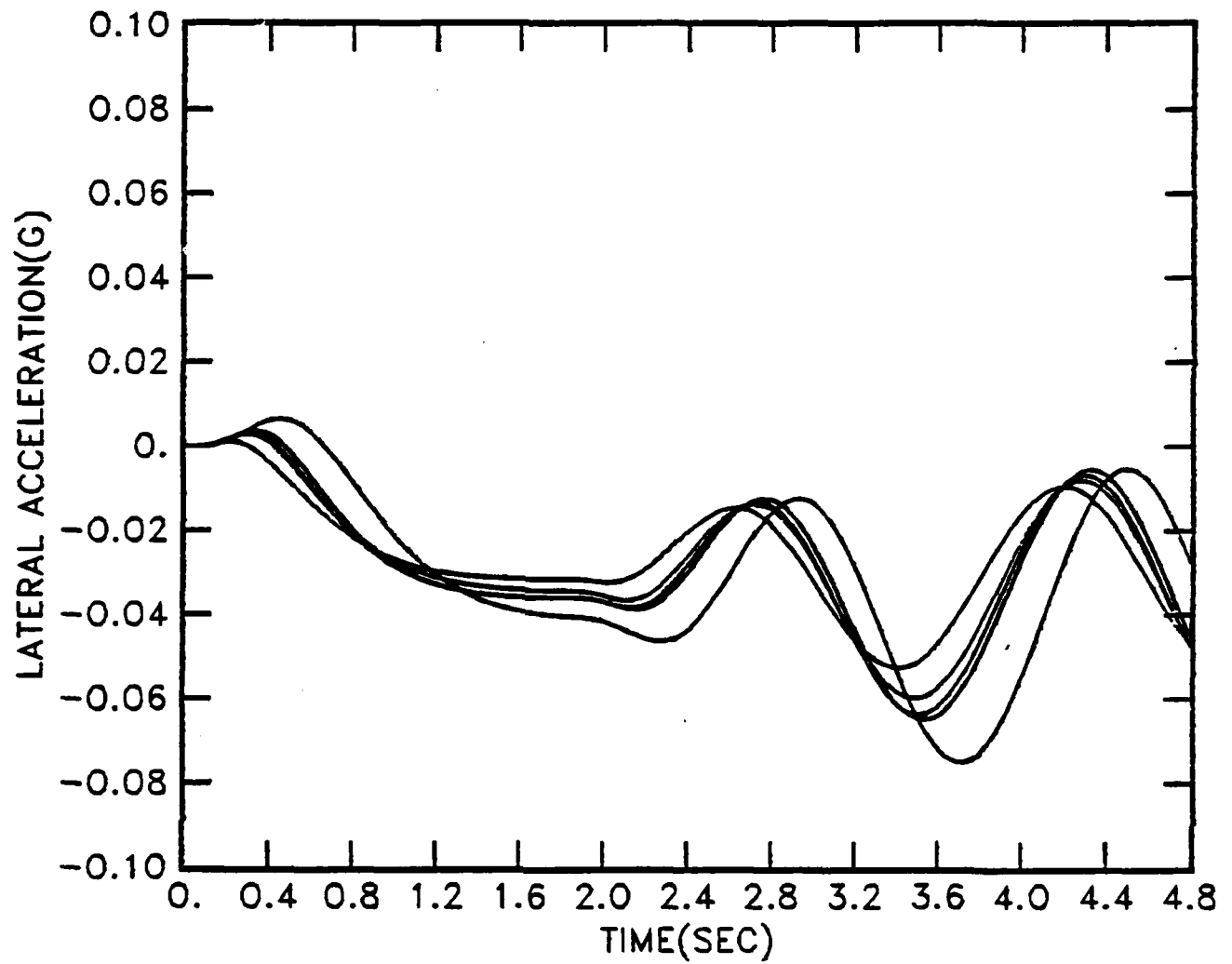


Figure 6.15c

CASES 1 - 5

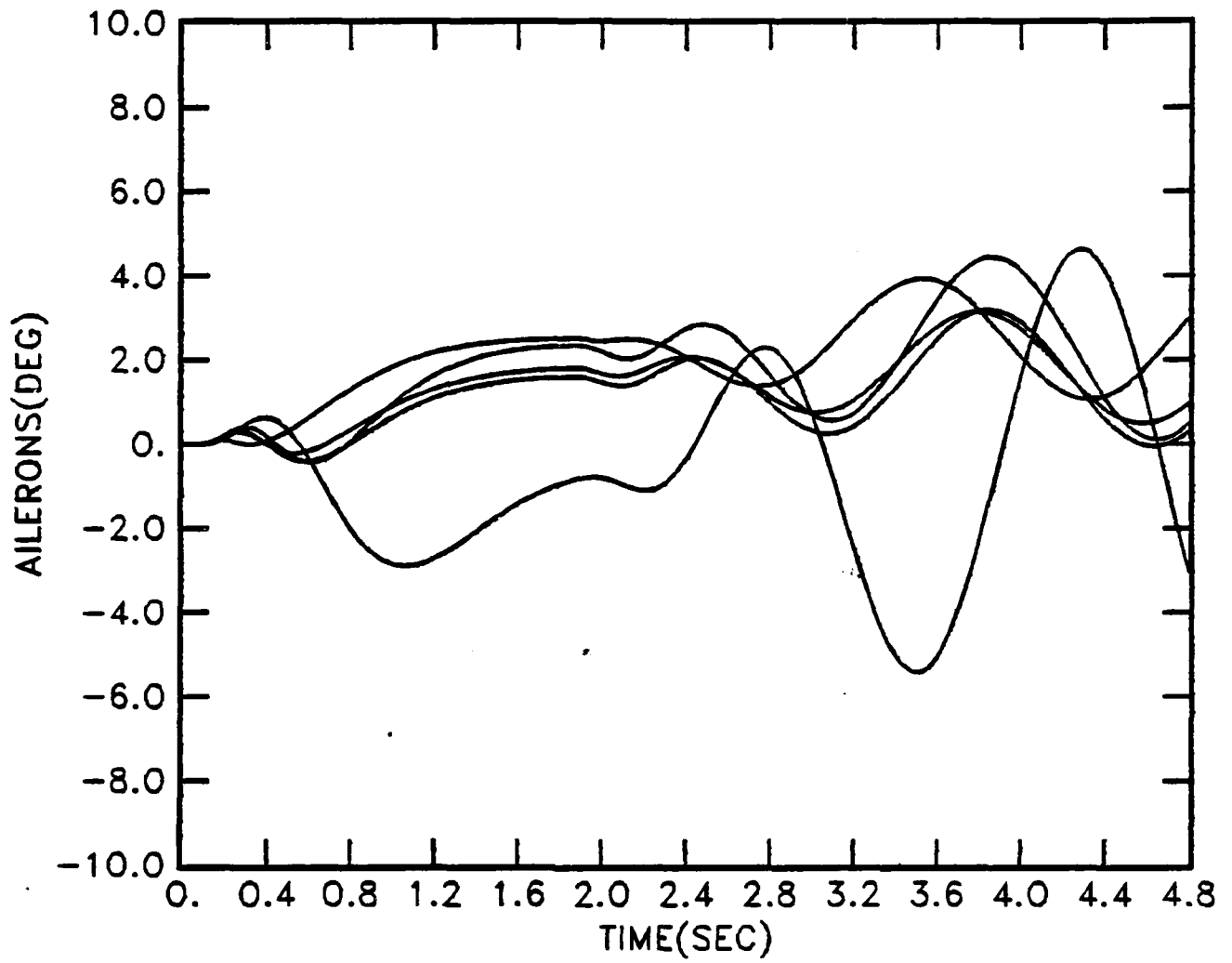


Figure 6.15d

CASES 1 - 5

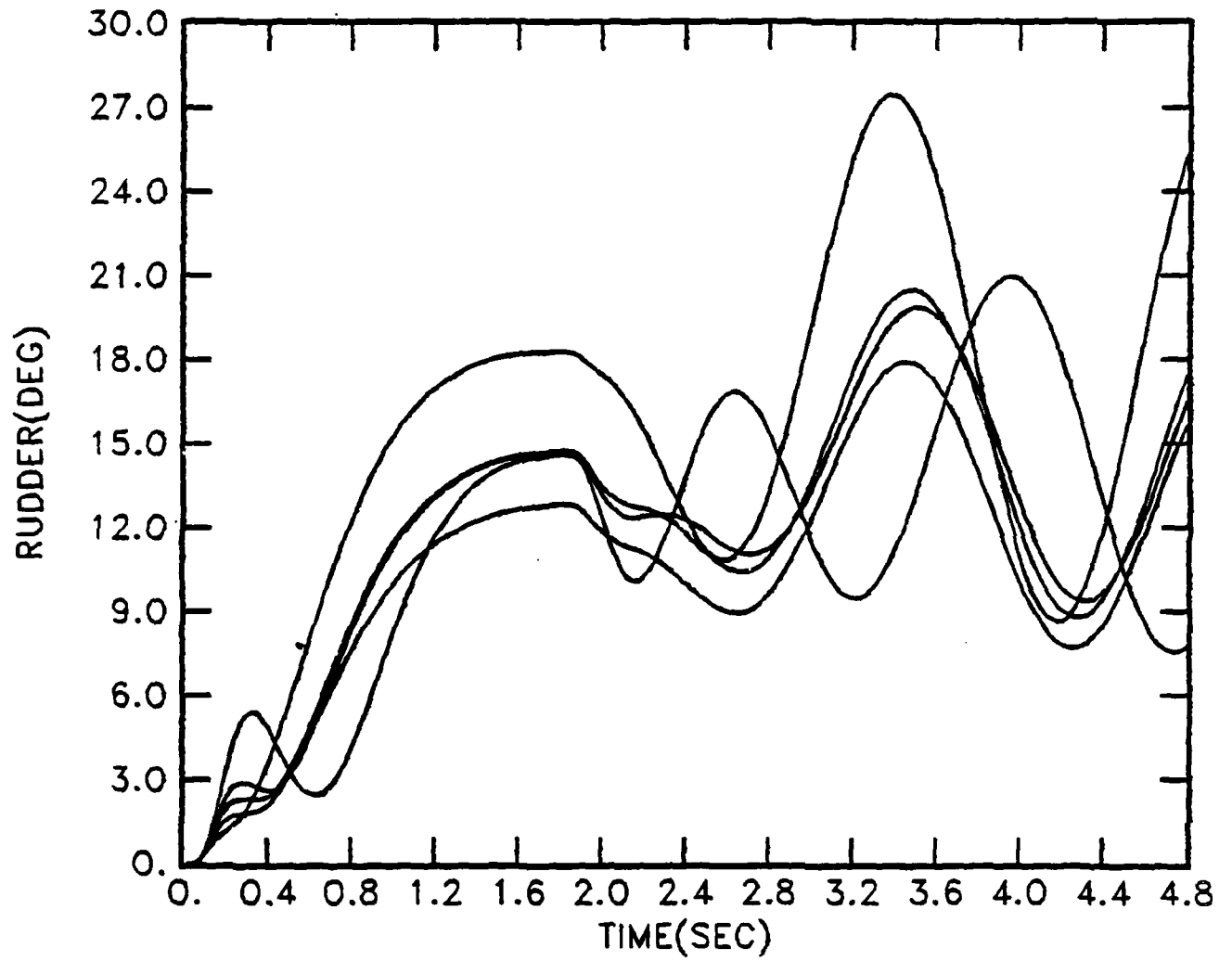


Figure 6.15a

CASES 1 - 5

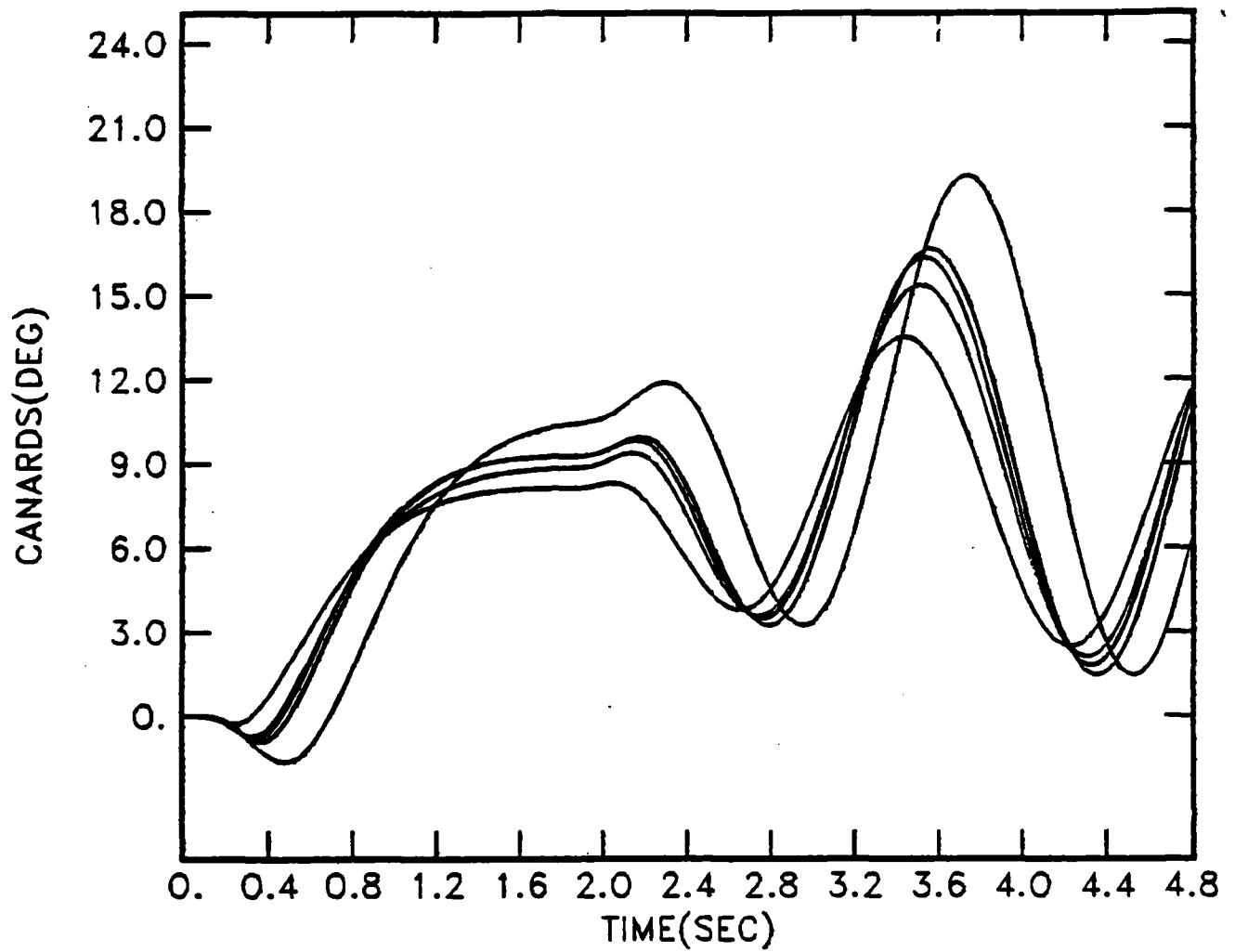


Figure 6.15f

CASES 1 - 5

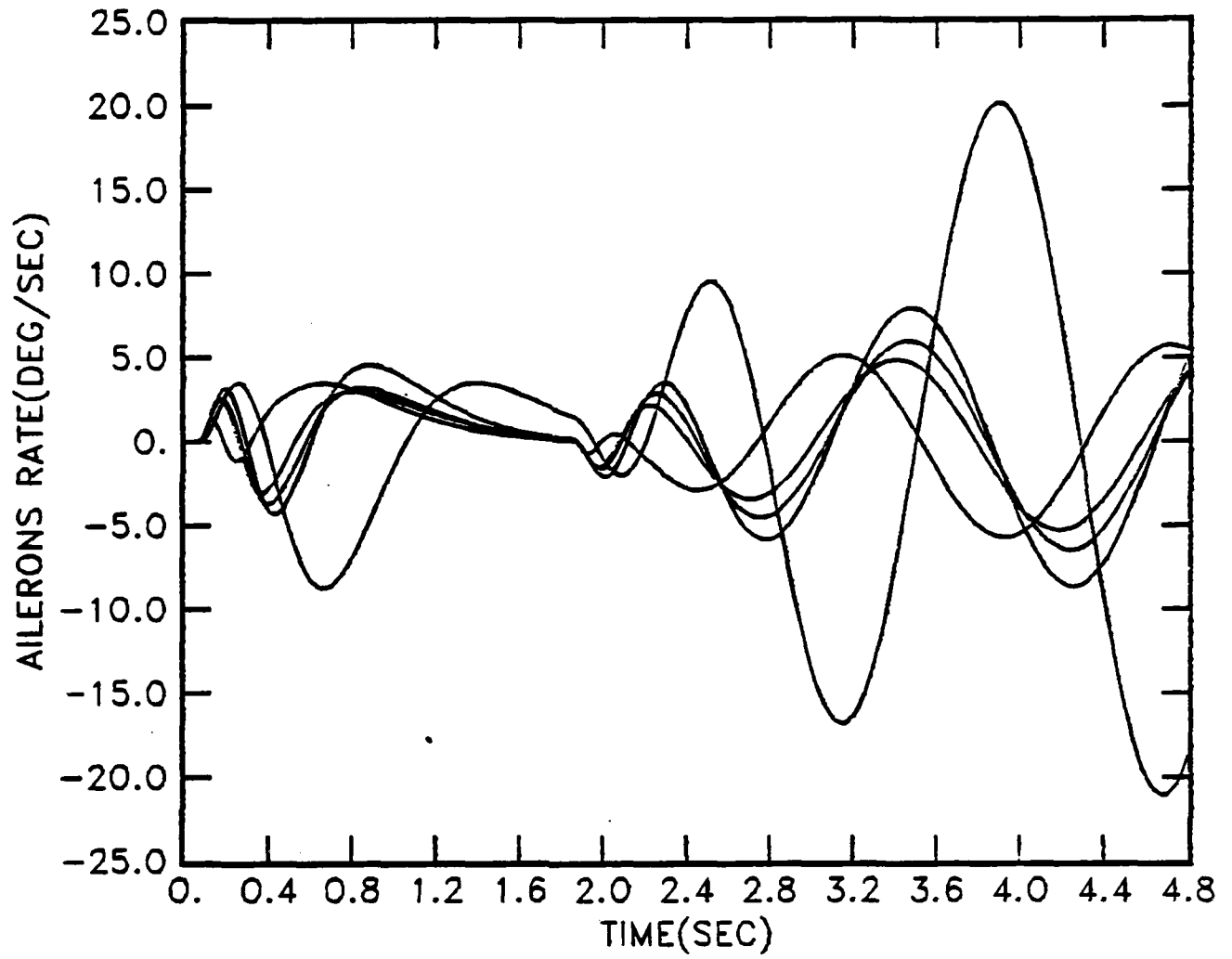


Figure 6.15g Aileron rate

CASES 1 - 5

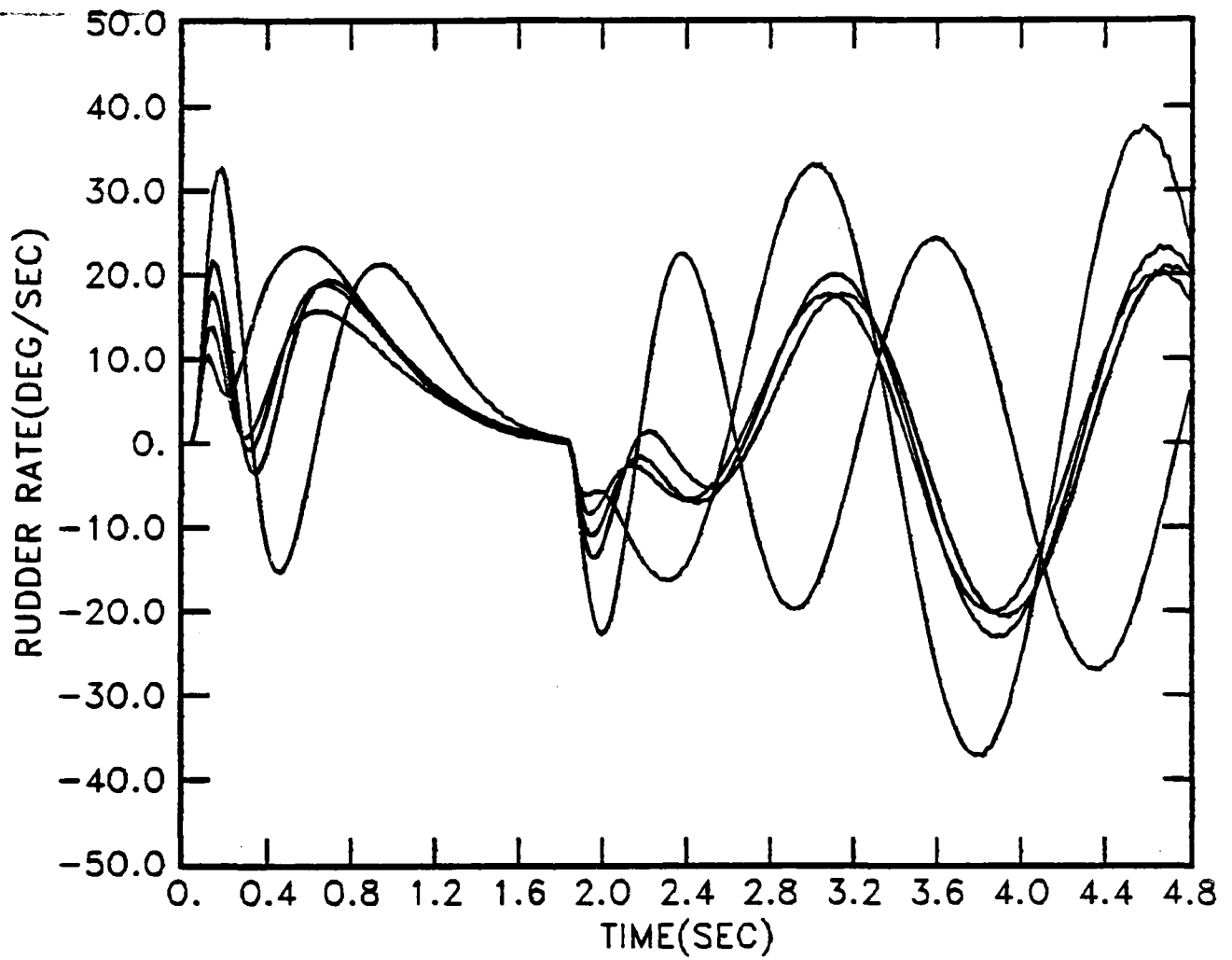


Figure 6.15h Rudder rate

CASES 1 - 5

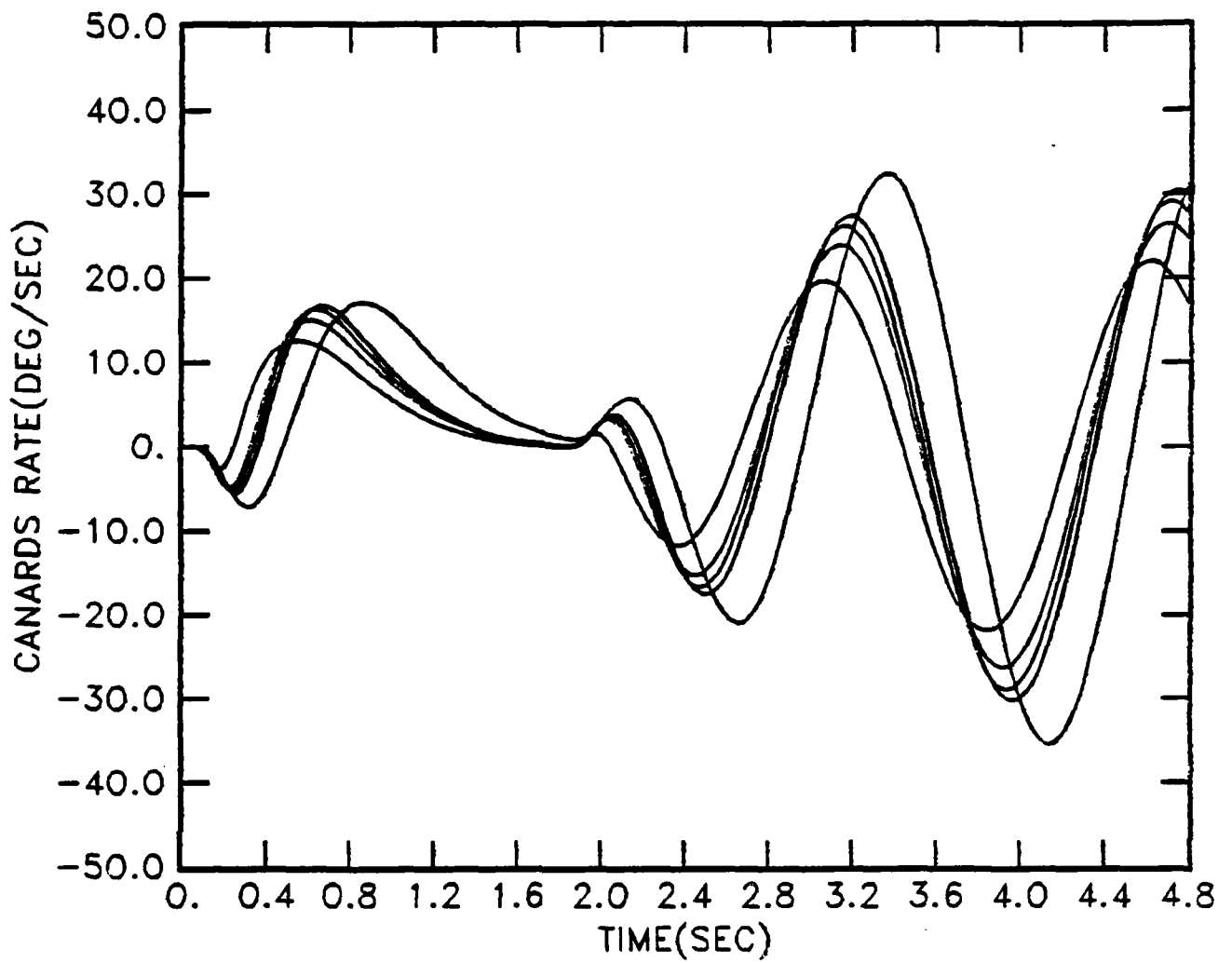


Figure 6.15i Canard rate

Chapter 7DISCUSSION AND CONCLUSIONS

The outstanding feature of the design procedure presented in Chapter 1, is its conversion of the multiple input-output (MIO) design problem with uncertainty, into a number of single input-output (SIO) single loop design problems with uncertainty and disturbances. For a large problem class, it is guaranteed that the designs which satisfy the SIO problems, are also satisfactory for the original MIO problems. To use this method, it is very helpful to assign apriori performance tolerances on the system, to be achieved despite the parameter uncertainty. These can be tentative tolerances, changed in the course of the design because of the transparency of the design technique, which clearly reveals the trade-off between the severity of the tolerances and the price paid in loop gain and bandwidth.

Heretofore this design procedure was successfully applied to academically contrived problems [1-3,6]. They all had very large parameter uncertainty, and the most complex involved a 3x3 plant [2] with a range of plant instability, and some nonminimum-phase elements. In its closed-loop performance specifications, some off-diagonal channels were specified to be "basically noninteracting", while some others were to have significant interaction.

The aircraft problems treated in this report are the first practical real-life ones to be handled (at least by the authors) by this new technique, which revealed its flexibility in several ways. A high-frequency condition (Sec. 1.3.1) existed for this technique, which while not absolutely necessary, was still extremely useful to simplify the design. This high-frequency condition was not satisfied in Chapter 2. A method was found for overcoming this obstacle and which, in fact, significantly improved the technique. This method was explained

in Sec. 1.3.1 and thereafter used successfully in the design of each mode (Chapters 2-4). It is a good example of the importance of application to real problems, by the academic researcher. (See Appendix)

Also, "scheduling" is a well-known, long-standing very useful technique in flight control for economizing on the feedback loop bandwidths. Therefore, the authors considered it important to see how it could be incorporated in a simple manner, within the design technique. This was treated in Sec. 2.8 and it was seen that the technique goes well with scheduling, because it reveals the frequency ranges in which scheduling is most useful, and those in which it is of lesser usefulness.

An area which deserves more theoretical treatment and practical experience involves the use of nondiagonal compensation. This was considered and applied to some extent in Sec. 2.9, but insufficiently. This topic definitely requires more research.

There is considerable interest now in digital realization of compensation networks. A digital compensator always contributes effectively a right half-plane zero in its transfer function, with its accompanying phase lag, which is not good in feedback design. The larger the sampling rate, the smaller this phase lag. The technique lends itself very easily to finding the smallest sampling rates commensurate with specific performance degradations, thus permitting the designer to make intelligent trade-offs. The minimum sampling rate needed for the feedback properties of the system (parameter uncertainty, disturbance attenuation), need not be the same sampling rate needed for its filter properties, i.e. the command inputs may not need to be sampled anywhere as often as the feedback sensors. And some of the sensors may not need to be sampled as often as some others. The feedback technique reveals this information very readily.

AD-A135 738

MULTIVARIABLE FLIGHTCONTROL DESIGN WITH UNCERTAIN
PARAMETERS(U) WEIZMANN INST OF SCIENCE REHOVOTH
(ISRAEL) DEPT OF APPLIED MA I HOROWITZ ET AL SEP 82

4/4

UNCLASSIFIED

AFWAL-TR-83-3036 AFOSR-80-0213

F/G 1/3

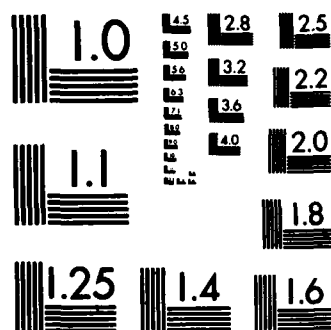
NL

END

FILED

1-84

DTIC



MICROCOPY RESOLUTION TEST CHART
NATIONAL BUREAU OF STANDARDS-1963-A

Finally, it is worth emphasizing that the authors for the most part have hardly any experience in flight control design. They are specialists in feedback theory. Yet the synthesis technique permitted them to zero in relatively quickly and in a systematic manner, onto the vital design conflicts and trade-offs. This is the purpose of a scientific theory - to enable a non-specialist in the specific application to get to the heart of the matter, without the need for a long apprenticeship. But it is important for the theorists to relatively early apply their theory to realistic problems. In this case we were confronted with a situation which wreaked some havoc with our theory (see p. 13, and Appendix), which forced us to a significant advance in the theory.

REFERENCES

1. I. Horowitz, Quantitative Synthesis of Uncertain Multiple Input-Output Feedback Systems, Int. J. Control, 30, 1979, 81-106.
2. I. Horowitz and C. Loecher, Design of 3x3 Multivariable Feedback System with Large Parameter Uncertainty, Int. J. Control, 33, 1981, 677-699.
3. I. Horowitz and M. Sidi, Practical Design of Multivariable Feedback Systems with Large Plant Uncertainty, Int. J. System Science, 11, 1980, 851-875.
4. I. Horowitz and M. Breiner, Quantitative Synthesis of Feedback Systems with Uncertain Nonlinear Multivariable Plants, Int. J. System Sci., 12, 1981, 539-563.
5. H. H. Rosenbrock, Computer-Aided Control System Design, 1974, Academic Press, N.Y.

APPENDIX 1

IMPROVED DESIGN TECHNIQUE FOR UNCERTAIN
MULTIPLE INPUT-OUTPUT FEEDBACK SYSTEMS

Isaac Horowitz*

ABSTRACT

This paper presents a synthesis technique for linear time invariant $n \times n$ multiple input-output (mio) feedback systems with constrained "plant" P , and output feedback. Due to uncertainty, P is known only to be a member of a set $P = \{P\}$. It is required for all $P \in P$, the n^2 system transfer functions t_{uv} be members of specified sets of acceptable outputs. A_{uv} ; $u, v = 1, \dots, n$. The problem is rigorously converted into a number of single input-output (sio) uncertainty problems, whose solutions are guaranteed to solve the original mio problem. The technique has several advantages over a previous one, which also converted the mio system to equivalent sio systems: (1) Fixed point theory is not needed to rigorously justify the theory. The justification is very simple. (2) There is significantly less overdesign inherent in the method. (3) If arbitrary small sensitivity is desired over arbitrary large bandwidth, then the set P must satisfy certain constraints as $s \rightarrow \infty$. It is shown that these constraints are inherent in all linear time invariant compensation techniques. In the old technique, these constraints were always present, even in non-arbitrarily small sensitivity specifications.

*Cohen Professor of Applied Mathematics, Weizmann Institute of Science, Rehovot, Israel and Dept. of Electrical Engineering, University of Colorado, Boulder.

This research was supported in part by the National Science Foundation, Grant ECS-8101958 at University of Colorado and by the Air Force Office of Scientific Research, Grant 80-0213 at Weizmann Institute of Science.

ABBREVIATIONS

Adj	adjoint
a.l.	arbitrarily large
a.s.	arbitrarily small
BW	bandwidth
lhp	left half plane
lti	linear time invariant
mio	multiple input-output
mp	minimum-phase
rhp	right half-plane
sio	single input-output

IMPROVED DESIGN TECHNIQUE FOR UNCERTAIN MULTIPLE INPUT-OUTPUT FEEDBACK SYSTEMS

1. INTRODUCTION

A number of synthesis techniques have recently appeared for linear time invariant (lti) $n \times m$ multiple input-output (mio) feedback systems with significant plant uncertainty (Horowitz 1979, Cruz et al, 1981, Doyle and Stein 1981, Postlethwaite et al 1981, Lehtomaki et al 1981, Safanov et al 1981, Davison and Ferguson 1981, Zames and Bensoussan 1982). Most of these are based on the singular value approach, and do not readily permit detailed control over the individual n^2 closed-loop responses, nor trade-off between the loop bandwidths. The method of (Horowitz 1979) does permit such detailed control. It is also quite transparent in revealing the price paid for the benefits of feedback, in terms of the various loop transmission bandwidths, and permitting trade-off between them. It has been applied successfully to a number of highly uncertain mio problems (Horowitz and Sidi 1980, Horowitz and Loecher 1981), including the YF16CCV 3x3 flight control system (Horowitz et al 1981).

The method is based on fixed point theory and replaces the uncertain $n \times m$ mio system by a number of single input-output (sio) uncertain systems, whose solutions are guaranteed to solve the original mio problem. However, there is some overdesign inherent in the method. This paper presents several refinements of the method, with reduced overdesign, and retaining the sio equivalence approach. One of these does not require fixed point theory for its derivation, only simple matrix manipulation. Also, constraints on the mio plant are derived which permit this design method to achieve arbitrarily small (a.s.) sensitivity over arbitrarily large (a.l.) bandwidth. It is shown that these constraints are inherent in every lti design technique.

2. THE 2x2 SYSTEM

The general $n \times n$ system is defined in Fig. 1, with the matrices: plant $P = [p_{ij}]$, compensations $G = [g_i]$ diagonal, \mathcal{P} all $n \times n$ matrices of transfer functions. Preliminary quasi-diagonalization of the plant may be desirable, which is here absorbed in P . This is discussed in Sec. 6. Hence diagonal G does not necessarily mean diagonal compensation inside the loop in Fig. 1. Due to uncertainty, $P \in \mathcal{P}$ a defined set. Tolerances of the form

$$a_{uv}(\omega) \leq |t_{uv}(j\omega)| \leq b_{uv}(\omega), \quad \forall P \in \mathcal{P} \quad (1a)$$

have been assigned on the magnitudes of the elements of the closed loop system transfer function matrix $T = [t_{uv}(j\omega)]$. Such tolerances suffice for minimum-phase (mp) elements (Horowitz 1979) and determine sets of acceptable $t_{uv}(j\omega)$ denoted by

$$A_{uv}(j\omega) = \{A_{uv}(j\omega)\} = \text{set of acceptable } t_{uv}(j\omega). \quad (1b)$$

Often one wants some or all nondiagonal elements of T to be small $\forall P \in \mathcal{P}$. For such elements, denoted as "basically noninteracting", $a_{uv} = 0$, and their f_{uv} are also made zero (Horowitz and Sidi 1980).

In the new technique, the design equations (for the 2x2 mio system) for t_{11} , t_{12} (or alternatively t_{21} , t_{22}) are identical to Eqn (4a,b) in (Horowitz 1979). They are derived from the matrix equation $T = (I + PG)^{-1} PGF$ of Fig. 1, by manipulating it into $(P^{-1} + G) T = GF$, letting $P^{-1} = [P_{ij}] = [1/Q_{ij}] = V_d + V_n$ with V_d , V_n the diagonal and nondiagonal parts (the diagonal elements of V_n are zero and vice-versa for V_d), giving $T = (V_d + G)^{-1} (GF - V_n T)$ which is used to define (potential) fixed-point mappings.

$$t_{uv} = \frac{(g_u f_{uv} + d_{uv}) Q_{uu}}{1 + g_u Q_{uu}}, \quad d_{uv} = - \sum_{i \neq u} P_{ui} t_{iv} \quad (2a,b)$$

(4a,b Horowitz 1979)

So the design equations used here for t_{1i} are:

$$\phi_{1i} = \frac{f_{1i} L_1 + d_{1i} Q_{11}}{1 + L_1}, \quad L_1 = g_1 Q_{1i}, \quad (3a-d)$$

$$d_{1i} = \frac{-t_{2i}}{Q_{12}}, \quad t_{2i} \in A_{2i} \text{ of (1b); } P^{-1} = [P_{ij}] = [1/Q_{ij}]$$

The objective is to choose $f_{11}(s)$, $f_{12}(s)$, $g_1(s)$ such that the $\phi_{1i}(s)$ have no right half-plane (rhp) poles, and satisfy the tolerances (1) on $|t_{1i}(j\omega)|$, $\forall P \in P$ and $\forall t_{2i} \in A_{2i}$ appearing in d_{1i} . These are precisely the sio design problems of Fig. 2a.

When t_{1i} is substituted for ϕ_{1i} in (3a), the resulting equations are exact. Hence, if indeed $\phi_{1i} \in A_{1i}$ for all t_{2i} (of d_{1i}) $\in A_{2i}$, $P \in P$, then the design objectives for t_{1i} have been achieved by the f_{11} , f_{12} , g_1 but only if actually $t_{2i} \in A_{2i}$. A systematic design procedure for choosing f_{11} , f_{12} , g_1 for the above purpose, has been detailed with examples in (Horowitz and Sidi 1980, Horowitz and Loecher 1981). A 2x2 nonlinear uncertain plant example is given in (Horowitz and Breiner 1981).

The final step, in the 2x2 system, is to choose f_{21} , f_{22} , g_2 to ensure that the $t_{2v}(s)$ have no rhp poles and that $t_{2v} \in A_{2v}$, $\forall P \in P$. In (Horowitz 1979) the design equations are again (2a,b) with $u = 2$ and the d_{2v} containing t_{1v} . Instead, here, there are used equations independent of the t_{1v} , by simply finding t_{2i} from $T = (I + PG)^{-1} PGF$:

$$t_{2i} = \frac{f_{2i} L_{2e} + d_{2i}}{1 + L_{2e}}, \quad L_{2e} = g_2 Q_{22e} = \frac{g_2 Q_{22} (1 + L_1)}{1 - \gamma_{12} + L_1} = \frac{g_2 f_{22} (1 + L_1)}{1 + g_1 P_{11}}$$

$$\gamma_{ij} = \frac{P_{ij} P_{ji}}{P_{ii} P_{jj}}, \quad (4a-e)$$

$$d_{2i} = \frac{g_1 f_{1i} P_{21} (1 - \gamma_{12})}{1 - \gamma_{12} + L_1}, \quad P = [P_{ij}]$$

with the sio structures of Fig. 2b. This design is done after Fig. 2a has been completed by means of (3a-d), so that L_1 , f_{11} , f_{12} are known. It is then necessary to find g_2 , f_{21} , f_{22} so that in Fig. 2b the outputs t_{21} , t_{22} are stable and satisfy the tolerances (1) on $|t_{21}|$, $|t_{22}|$ respectively, which are single-loop problems similar to Fig. 2a, except that only the uncertainty $P \in \mathcal{P}$ need be considered, as the d_{21} in (4a-e) are not functions of the elements of A_{uv} , which they are in (3a-d). At each step, design execution is that of single input-output (sio) single loop systems--which is what makes this design procedure so tractable.

Summarizing, the theoretical justification of the above design procedure is as follows: The design specifications (1) are satisfied for t_{2v} of Fig. 2b, by proper choice of the f_{2v} , g_2 for the given f_{1v} , g_1 . So the design is satisfactory for t_{21} , t_{22} because (4a,b) are exactly the expressions for t_{21} , t_{22} , (even if the specs. for t_{12} , t_{11} are not satisfied). Now Figs. 2a have been designed (via Eqs. 3a-d), so that ϕ_{11} , ϕ_{12} are stable and satisfy the specs. on t_{11} , t_{12} $\forall P \in \mathcal{P}$, if the t_{2i} appearing in d_{1i} are in A_{2i} (which they are). And the equations for ϕ_{11} , ϕ_{12} correspond precisely to those for t_{11} , t_{12} . Thus, no fixed point theory is needed to rigorously justify this design procedure, although the idea and approach were motivated by the fixed point method in (Horowitz 1979). There, the design equations for t_{21} , t_{22} are of the same form as Eqs. (3a-d) with the d_{2i} functions of t_{1i} , so fixed point theory is required to justify the method.

2.1 Reduced Overdesign

Figs. 2a are the same as in (Horowitz 1979) in which t_{21} , t_{22} appear in the disturbance d_{11} , d_{12} . There is inherent overdesign in Fig. 2a, because in reality there is correlation between the t_{21} , t_{22} and the Q_{uv} of P^{-1} . This correlation is not being exploited. The uncertainties in $t_{21} \in A_{21}$, $t_{22} \in A_{22}$ are assumed independent of $P \in P$ in Figs. 2a (see Horowitz and Loecher 1981 for discussion how to reduce this overdesign.) But such overdesign does not exist in Fig. 2b because d_{21} , d_{22} are not functions of the elements of any A_{uv} . In (Horowitz 1979) the design for t_{21} , t_{22} involved overdesign precisely as in Figs. 2a. The above procedure can, of course, be reversed with ϕ_{21} , ϕ_{22} using Eqs. (2a,b) with $u = 2$, and t_{11} , t_{12} using Eqs. (4a-e) by exchanging numbers 1,2.

3. 3x3 DESIGN EQUATIONS

Nine design equations may be defined in a manner similar to (3,4) of Sec. 2. Let ϕ_{1v} , $v = 1-3$, be the same as in (Horowitz 1979, Eqs. 4a,b which are Eqs. (2a,b) here):

$$\phi_{1v} = \frac{f_{1v}L_1 + d_{1v}Q_{11}}{1 + L_1}, \quad L_1 = g_1Q_{11}, \quad d_{1v} = -\sum_{i \neq 1} p_{1i}t_{iv} \quad (5a-c)$$

giving six problems. L_1 and the three f_{1v} are chosen so that ϕ_{1v} are stable and satisfy the tolerances (1) for all $t_{iv} \in A_{iv}$ appearing in d_{1v} and all $P \in P$ - see (Horowitz and Loecher 1981) for procedure and detailed design example. The equations for ϕ_{2v} are obtained from Eq. 2 setting $u = 2$ in which t_{1v} and t_{3v} appear, but the t_{1v} are here replaced by the ϕ_{1v} of (5), giving for $v = 1-3$, in the notation of Eqs. (3,4):

$$\phi_{2v} = \frac{f_{2v} L_{2e} + d_{2v}}{1 + L_{2e}} \quad (6a-c)$$

$$L_{2e} = \frac{g_2 Q_{22}}{1 - \frac{\gamma_{12}}{1+L_1}}$$

$$d_{2v} = \frac{L_{2e}}{g_2} \left\{ t_{3v} \left[\frac{P_{21} P_{13}}{P_{11} (1+L_1)} - P_{23} \right] - \frac{f_{1v} L_1 P_{21}}{1 + L_1} \right\}$$

again sio problems. L_1 and the f_{1v} are known from the designs of (5). Here, the f_{2v} and L_{2e} are chosen so that ϕ_{2v} are stable for all $t_{3v} \in A_{3v}$ appearing in d_{2v} and, of course, for all $P \in P$. Although the forms for d_{2v} and L_{2e} in (6) are different from those in (5), (5a,6a) are otherwise identical in form, so the design techniques for both are basically the same, as detailed in (Horowitz and Loecher 1981).

Finally, sio design equations for t_{3v} are gotten by finding t_{3v} from $T = (I + PG)^{-1} PGF$, or from Eq. (2) for $u = 3$ and eliminating t_{1i} , t_{2i} by means of Eqs. (5,6):

$$t_{3i} = \frac{f_{3i} L_{3e} + d_{3i}}{1 + L_{3e}}, \quad L_{3e} = \frac{L_3 \zeta}{\zeta - \Lambda}, \quad L_3 = Q_{33} g_3$$

$$\zeta = (1+L_1)(1+L_2) - \gamma_{12}$$

$$\Lambda = \gamma_{23}(1+L_1) + \gamma_{13}(1+L_2) - (\gamma_{12}\mu_2 + \gamma_{13}\mu_3) \quad (7a-j)$$

$$\mu_2 = \frac{P_{23} P_{31}}{P_{21} P_{33}}, \quad \mu_3 = \frac{P_{32} P_{21}}{P_{31} P_{22}}$$

$$d_{3i} = \frac{f_{1i} L_1 Q_{33} \eta_1 + f_{2i} L_2 Q_{33} \eta_2}{\zeta - \Lambda}$$

$$\eta_1 = Q_{22} P_{21} P_{32} - P_{31}(1 + L_2)$$

$$\eta_2 = Q_{11} P_{12} P_{31} - P_{32}(1 + L_1)$$

Since L_1, L_2, f_{1v}, f_{2v} are known, the only unknowns in the above are the f_{3i} and g_3 . Eqs. (7a-j) constitute single-loop uncertainty problems, for which the technique and examples of the references (Horowitz, etc.) apply, i.e. they are chosen so that the t_{3i} are stable and satisfy the tolerances in (1). Note, again, that at each step, design execution is that of single-loop systems.

The justification of the above design approach is the same as of the 2x2 case: Suppose the nine f_{uv} and three g_i in (7a-j) are such that the t_{3i} are stable and their tolerances are satisfied, which is so by definition here. Now the design based on (6a-c) guarantees that the t_{2i} tolerances are satisfied, providing the t_{3i} appearing in d_{2i} are $\in A_{3i}$ - which is the case here. Hence, the t_{2i} tolerances are also satisfied. Finally, the design based on (5a-c) guarantees that the t_{1i} tolerances are satisfied, providing that the t_{2i}, t_{3i} , appearing in d_{1v} are $\in A_{2i}, A_{3i}$ respectively, which has been established. In the above, there is some overdesign in (5a-c) because the $t_{iv} \in A_{iv}$, ($i = 2,3$), ($v = 1,2,3$) appear as disturbances uncorrelated to the plant uncertainty. In (6a-d) there is less overdesign because only the t_{3v} so appear, while there is no such overdesign in (7a-j). Of course, the order can be changed and equations of the form (5a-c) used for the second or third channel, etc.

4. nxn SYSTEM, $n > 3$

The procedure for generating the design equations for nxn mio systems with $n > 3$, should be clear from the above. One uses for any channel (say the first) design equations in which all the t_{iv} ($i \neq 1$) appear as disturbances. Denote these as Eqs. A. These equations can be derived or obtained from (Horowitz 1979, Eqs. (4a,b) with $u = 1$). For the next

chosen channel (say the second), one starts with Eqs. (4a,b) of (Horowitz 1979) with $u = 2$, but eliminates all the t_{1v} by means of Eqs. A above. Denote the resulting design equations as Eqs. B. For the next chosen channel (say the third), start again with Eqs. (4a,b) $u = 3$, but eliminate all the t_{1v} , t_{2v} by means of Eqs. A, B above. The process continues until the end, and the theoretical justification is the same as given above for $n = 2, 3$.

Mixtures of the technique in (Horowitz 1979) and the one described above, may also be used. For example, for the 3x3 system, Eq. 2 may be used for both channels 1,2 and (7a-j) for channel 3. The theoretical justification is now as follows: Design for channel 3 is correct by definition, but fixed point theory, precisely as in (Horowitz 1979) is used to justify the designs for channels (1,2): The two sets of design equations for t_{1v} , t_{2v} are taken as the mappings on the acceptable sets A_{uv} and the third set of mappings is simply $\phi_{3v} = a_{3v} \in A_{3v}$. The nine f_{uv} , three g_u have been chosen so that these mappings map A_{uv} into themselves, etc., so a fixed point exists, etc., as in (Horowitz 1979). For larger n , it is clear that a larger variety of mixtures is possible, giving the designer useful flexibility. However, he must understand the sio design theory used in the design execution, which reveals the cost of feedback and the available tradeoffs among the loops, in order to be able to exploit this flexibility to its fullest extent. A detailed 3x3 example based on fixed point theory is given in (Horowitz and Loecher 1981).

5. CONDITIONS FOR EXISTENCE OF A SOLUTION

This section considers the conditions required for the applicability of the above design technique. Also, it considers the inherent, irreducible conditions applicable for lti compensations in general, and compares the two sets of conditions. This is done for "arbitrarily small (a.s.) sensitivity" defined as achievement of a.s. sensitivity of the t_{uv} over arbitrarily large (a.l.) bandwidth. Such "a.s. sensitivity" also achieves a.l. attenuation over a.l. bandwidth, of external disturbances acting on the plant. This problem has also been studied in an abstract setting by (Zames and Bensoussan 1982).

In Fig. 2a, it is required that $\phi_{11} \in A_{11}$, $\phi_{12} \in A_{12}$, for all $P \in P$, $t_{21} \in A_{21}$, and $t_{22} \in A_{22}$. In the general n case, the disturbance component in, for example, ϕ_{11} is

$$T_{d_{11}} = \frac{d_{1v} Q_{11}}{1 + g_1 Q_{11}} = \sum_{i \neq 1} t_{iv} \frac{(\text{Adj } P)_{1i} / (\text{Adj } P)_{11}}{1 + g_1 \frac{\det P}{(\text{Adj } P)_{11}}}$$

Right half-plane (Rhp) poles of $(\text{Adj } P)_{1i}$ are normally cancelled by similar poles in $\det P$, since $(\text{Adj } P)_{1i}$ is a term in expansion of $\det P$. Rhp zeros of $(\text{Adj } P)_{11}$ are, of course, normally cancelled by similar ones in the denominator. There may be exceptional cases when in $\det P$, for example, a rhp pole of $(\text{Adj } P)_{1i}$ is cancelled by an identical zero of p_{1i} and does not appear in the other terms of $\det P$. Such cases are excluded.

5.1 Conditions for "a.s. sensitivity" in single-loop design

In Eqs. (3), it is seen that a.s. tolerances over a.l. bandwidth (i.e. "a.s. sensitivity") for t_{11} , t_{12} are achievable if $L_1 = g_1 Q_{11}$ can be made a.l. over a.l. bandwidth. Indeed this is at least theoretically possible, if Q_{11} satisfies certain constraints. These have been detailed in (Horowitz 1979, Appendix 1), so are only qualitatively described here by means of Fig. 3.

Fig. 3 is the extended logarithmic complex plane (Nichols chart). Since P ranges over \mathcal{P} , the set $\{L_1 = g_1 Q_{11}(j\omega)\}$ is not a single complex number (at any fixed ω) in the Nichols chart but a region, denoted as $T_p(L(j\omega))$, the template of L_1 , which is the same as $T_p(Q_{11}(j\omega))$ but translated horizontally by $20 \log |g_1(j\omega)|$ db and vertically by $\text{Arg } g_1(j\omega)$ degrees, because $L_1 = g_1 Q_{11}$. In a design with significant plant uncertainty $T_p(L_1(j\omega))$ must lie relatively high up, above the zero db line as shown in Fig. 3 for ω_1 . This is so over the important ω range of t_{11} , t_{12} (their bandwidths generally), in order to achieve the desired sensitivity reduction. Such large values for $T_p(L_1(j\omega))$ can be maintained theoretically for any finite ω range, if Q_{11} is m.p. For those ω for which $T_p(L_1(j\omega))$ is so located, the uncertainty in the magnitude and phase of $Q_{11}(j\omega)$ (i.e. the area of $T_p(Q_{11}(j\omega))$), can be arbitrarily large. (Note, however, that in order to maintain $T_p(L_1(j\omega))$ above the zero db line, any zeros of $Q_{11}(j\omega)$ on the $j\omega$ axis must be known and finite in number in order for $g_1(s)$ to be assigned poles there. (Obviously, transcendental compensation can be used for special countable cases.) If the range of such $j\omega$ axis zeros is uncertain, then the specifications(1) must be modified to permit such zeros of t_{1i} .)

Sooner or later $L_1(j\omega)$ must decrease and $\rightarrow 0$ as $\omega \rightarrow \infty$. Stability over the range of P requires that $T_p(L_1(j\omega))$ move downward in between the vertical lines V_1, V_2 without the points $\dots 0_{-1} 0_1 0_2, \dots$ lying in any $T_p(L_1(j\omega))$. This appears to allow $(360 - 2\theta_m)$ degrees phase width for $T_p Q_{11}(j\omega)$, with θ_m phase margin. However $\angle L_1(j\omega)$ must be negative on the average, in order for $|L_1(j\omega)|$ to decrease. So in practice only $(180 - \theta_m)$ phase width is tolerable in this range. As ω increases and the $T_p(L_1(j\omega))$ descend lower on the chart below the zero db line, clearly their width may increase again, but it is essential that the points $\dots 0_1, 0_2, \dots$ never be a part of any $T_p(L_1(j\omega))$. Unstable Q_{11} are included in the above discussion and don't require separate treatment. It follows from the above that the manageable uncertainties depend on the assigned t_{uv} tolerances, but two important constraints are stated here for the case of "a.s. sensitivity."

(5.1a) $Q_{11} = \det P / \text{Adj. } P)_{11}$ must be mp.

(5.1b) Suppose $\exists \omega_h, \epsilon$ for all $\omega > \omega_h$, the width of $T_p(Q_{11}(j\omega))$ exceeds $(180 - \theta_m)$, θ_m a desired phase margin, then it is impossible to achieve a.s. tolerances for $\omega > \omega_h$. This prevents "a.s. sensitivity" if $Q_{uu} = k\pi(s+z_i)/\pi(s+p_j)$, with the k uncertainty including a sign change which is independent of the signs of the z_i, p_j . Also excluded is a factor $(1+Ts)$ in the numerator or denominator of Q_{uu} , with the uncertainty in T including a sign change which is independent of other parameters.

5.2 Application of 5.1 to New Design Technique

The above constraints therefore apply to the $Q_{uu} = \det P / (\text{Adj } P)_{uu}$ of the first channel u , used in the new design technique of Secs. 2, 3. So

from (5.1a), Q_{uu} must be m.p. $\forall P \in P$ (rhp poles are tolerable), for "a.s. sensitivity" design. Suppose $P = [p_{uv}]$ has each $p_{uv} \rightarrow k_{uv}/s^e$ as $s \rightarrow \infty$.

For $n = 2$

$$Q_{uu} = \frac{P_{11}P_{22} - P_{12}P_{21}}{P_{vv}} \rightarrow \frac{k_{11}k_{22} - k_{12}k_{21}}{k_{vv}s^e}, \quad (8)$$

Let $K = [k_{uv}]$, so (5.1b) states that there may be no change in the sign of $\det K/k_{vv}$ as P ranges over P . In this paper it is assumed that all $k_{uv} > 0$ for all $P \in P$, so (5.1b) gives $k_{11}k_{22} > k_{12}k_{21} \forall P \in P$, or vice versa. To remove the ambiguity it is also assumed that the plant terminals are numbered so that for at least one $P \in P$, $k_{11}k_{22} > k_{12}k_{21}$, so (5.1b) gives the constraint

$$k_{11}k_{22} > k_{12}k_{21} \quad \forall P \in P \quad (9)$$

This is a diagonal dominance condition as $s \rightarrow \infty$. (Zames and Bensoussan) have defined a diagonal dominance condition as $s \rightarrow \infty$, in more abstract form.

The above applies to the first channel, say no. 1, for which (3) is used. Eqs. (4) are used for the second channel. The mp condition of (5.1a) therefore applies to $Q_{22}(1+L_1)$, most of which is not new because mp $(1+L_1)$, $\det P$ are already required. As for (5.1b), there are two extremes. "A.s. sensitivity" can be achieved by L_1 bandwidth \gg that of L_2 (denoted by $BW(L_1) \gg BW(L_2)$), and then (4b) implies (5.1b) applies to Q_{22} . It can also be achieved by the opposite strong inequality, and then (5.1b) applies to P_{22} . For the condition assumed with Eqs. 8,9) of no sign changes in the k_{uv} , the results are the same. It may also be so in the general case but this would require consideration of simultaneous sign changes among the k_{uv} , which is not done here.

n=3. Application of (5.1) to the first channel makes it applicable to Q_{11} . Application to the second (eqs. 6) gives the same results as to the second in $n=2$ above, because L_{2e} has the same form in both (compare 4b, 6b). If "a.s. sensitivity" is achieved (as it may be) by $BW(L_1) \gg BW(L_2) \gg BW(L_3)$, the result is that (5.1) apply to Q_{11} , Q_{22} , Q_{33} . If the opposite is done, in the notation of (3.7), they apply to $Q_{11} \frac{Q_{22}}{1 - \gamma_{12}}$,

$$\frac{Q_{33}(1 - \gamma_{12})}{1 - (\gamma_{12} + \gamma_{23} + \gamma_{13}) + (\gamma_{12}\mu_2 + \gamma_{13}\mu_3)}$$

It has not been ascertained whether these two sets of constraints are identical. However Sec. 5.3 shows that (5.1) must always apply to each Q_{uu} , $u = 1$ to n . Constraints for $n > 3$ may be similarly developed.

5.3 Inherent Constraints

It is important to determine whether the above constraints are due to the specific design technique, or are inherent in the problem itself. For this purpose examine (4a) for t_{22} . How can "a.s. sensitivity" of t_{22} be achieved despite large uncertainty in P ? Clearly by large L_{2e} , the usual feedback method. Large L_{2e} is achieved by large $g_2 Q_{22}$, because large L_1 (needed likewise for small t_{11} sensitivity) gives $L_{2e} = g_2 Q_{22} = L_2$. The latter also attenuates d_{22} , which may not be small because of g_1 in its numerator. This same principle applies to all t_{uv} , and is basically the same as that derived from examination of (3), i.e. there is need for a.l. L_2 , L_1 over a.l. bandwidth in order to achieve "a.s. sensitivity." But do the constraints of Sec. 5.1, in particular (5.1a,b) apply to Q_{22} and Q_{11} ?

This is indeed so, and proven by (3a) and its analog for t_{2i} (by interchanging 1,2), by simply asking whether stable t_{11} is possible if $1 + L_1$ has rhp zeros? For if not, and since a.l. L_1 over a.l. bandwidth is needed, it follows that L_1 (and L_2) must satisfy constraints (5.1). Suppose $(1 + L_1)$ has rhp zeros. These are rhp poles of t_{11} , unless in (3a for $i = 1$) the numerator of t_{11} has these same zeros. Suppose it has them, and there is a small change in f_{21} . Since F is outside the feedback loops, system stability is unaffected. The zeros of $1 + g_1 Q_{11}$ in (3a) are thereby unaffected, so neither should the zeros of the numerator of (3a for $i = 1$). The term $f_{11} g_1 Q_{11}$ is unaffected, but t_{21} is affected--see (4) with $i = 1$. Hence, the hypothesis $(1 + L_1)$ has rhp zeros is untenable, so (5.1) applies to Q_{11} (and Q_{22}).

Comparing these results with Sec. 5.2, the conclusion is that "a.s. sensitivity" may be achieved by the new design technique, with plant constraints which are inherent and irreducible, i.e. not more severe than inherently necessary. This is achieved by letting $BW(L_1) \gg BW(L_2) \gg BW(L_3)$, wherein the only constraints are (5.1) applicable to Q_{11} , Q_{22} , Q_{33} , which have been shown to be inherent. This is associated with the following design order: first L_1 (Eqs. 5), second L_2 (6), third L_3 (7). The design procedure is facilitated by such inequalities, because then in (6b), $L_{2e} + L_2 = g_2 Q_{22}$ over its important design range, and $L_{3e} + L_3 = g_3 Q_{33}$. If other factors are equal ($\bar{T}_p(Q_{uu})$, tolerances on t_{ui} , $i = 1-3$ for each u), there is a natural tendency for this order of the inequalities because of the inherent greater overdesign of L_1 , lesser of L_2 and least of L_3 (recall Secs. 2.1, and last paragraph in Sec. 3.).

However, the above is rather of theoretical, academic interest, because it applies only for "a.s. sensitivity," defined at the beginning of Sec. 5. Thus it applies if one is given a plant with specific uncertainty range and is challenged to achieve a.s. performance tolerances over a.l. bandwidths. However, given a plant set P and sets of tolerances A_{uv} ($u, v = n$), it is conceivable that the latter are not achievable by the new technique, but are inherently achievable. The reason (e.g. for $n = 2$) is that in Eq. (2), the demand on L_1 to achieve the desired sensitivity reduction, may be greater than is inherently needed, because of the overdesign, discussed in Sec. 2.1, and is therefore unachievable, because of the nature of P , say it has some non-mp elements. Thus, a specific problem may be incompatible with (5.1) only due to this overdesign. There may exist as yet undiscovered better methods with reduced demand on L_1 , which renders them compatible with (5.1). From Sec. 2.1, it is clear that the best method will be achieved with Eqs. (3) by maximum use of the correlation which exists between the P uncertainty and the $t_{2i} \in A_{2i}$ in (3a-d). A suggestion for this purpose has been given in (Horowitz and Loecher 1981). One subdivides the plant set into subsets P_i which are correlated with subsets A_{uvi} of A_{uv} . Eqs. (3) (similarly 5,6) are now applied to these pairs P_i, A_{uvi} separately for each i . This approach has not as yet been attempted in any numerical problem.

It is worth noting that constraints of the diagonal dominance type as $s \rightarrow \infty$, appear in the design technique of (Horowitz 1979). However, they are always present there, even if "a.s. sensitivity" is not attempted. In the new technique they are in effect only for "a.s. sensitivity." Hence, it is possible that a specific synthesis problem with given A_{uv}, P sets may not be solvable by the older method, but is solvable by the new method. This was the case in (Horowitz et al 1981).

6. NONDIAGONAL G

The constraints on P in Sec. 5 were deduced on the assumption G is diagonal. Are these constraints eased if nondiagonal G is used? To answer this question, let H be a fixed lti pre-compensator matrix inserted ahead of the plant and let $V = PH$ be the new effective plant in the set $V = \{PH, P \in P\}$. The design techniques with diagonal G , are now applied to set V instead of set P . If H is helpful in overcoming some constraint, then it is necessary that the constraint violated by P , is not violated by V . The constraint $\det P$ is mp. $\forall P \in P$ is not eased at all, because $\det V = (\det P) (\det H)$, and obviously cancellation of rhp zeros of $\det P$ by $\det H$ cannot be done for many reasons. The other important constraint involving diagonal dominance as $s \rightarrow \infty$, is also not eased, because it applies to the sign of $\det V$ not changing, as $s \rightarrow \infty$. Thus the constraints on P for "a.s. sensitivity" are not eased by nondiagonal G .

However, H may be very helpful in reducing the amount of feedback needed to achieve specified tolerance sets (1), for a given plant set P , so that a design unachievable by diagonal G (say, because of non-mp P or sensor noise problems) may be achievable via H . For example in Eq. (4a), L_{2e} must handle the uncertainties due to L_{2e} itself and attenuate the effective disturbance set $\{d_{21}\}$. For basically noninteracting tolerances on $t_{uv}(u \neq v)$, f_{uv} is made zero, so only the latter need exist. It may be possible to considerably reduce $|d_{21}|_{\max}$ by means of H , by making $V = PH$ quasidiagonal, even though P has large nondiagonal components.

Off diagonal plant elements appear in all the design equations (2-7) in the 'disturbance' components, so their reduction via H is desirable. How is this systematically done in the case of significant P uncertainty? For $n = 2$,

let the normalized H have 1 for its diagonal elements and $h_{12} = \mu$, $h_{21} = \nu$.

Then $v_{12} = \mu p_{11} + p_{12}$, $v_{21} = p_{21} + \nu p_{22}$. The objective is to minimize over P $\max |v_{12}|, |v_{21}|$ at each ω . Sketches of the sets $\{\frac{p_{12}}{p_{11}}(j\omega)\}$, $\{\frac{p_{22}}{p_{21}}(j\omega)\}$ in the complex plane, are clearly very helpful in choosing $\mu(j\omega)$, $\nu(j\omega)$.

However, one should check the effect on the resulting sets of $v_{11} = p_{11} + \nu p_{12}$, $v_{22} = \mu p_{21} + p_{22}$, because of the obligations on the loop transmissions due to their uncertainties. The final choice depends on the relative importance of the two terms in the numerators of ϕ_{11}, ϕ_{21} in (3,4). (See Horowitz and Loecher 1981 Secs. 3.2,4 for discussion relevant to this topic).

If the elements of P have a rhp pole in common, i.e. $P = P_1/(s-p)$, then one should not try to diagonalize P by means of $PH = \Lambda$ diagonal, because in practice $H = P_a^{-1} \Lambda$ with $P_a^{-1} \neq P^{-1}$ exactly, giving $PH = P P_a^{-1} \Lambda$ with rhp dipoles. Instead, one tries to diagonalize P_1 by means of $P_1 H = \Lambda$, giving $H = P_{1a}^{-1} \Lambda$, and $PH = P_1 P_{1a}^{-1} \Lambda/(s-p)$.

7. CONCLUSIONS

This paper has presented new synthesis techniques for highly uncertain $n \times n$ mlti feedback systems with output feedback, with the following features:

- (a) There is detailed control over the n^2 individual system transfer functions.
- (b) The mlti uncertainty problem is rigorously converted into a number of sio uncertainty problems. Solutions of the latter are guaranteed to be satisfactory for the former. Relatively simple sio, single loop feedback techniques can be used to solve the sio problems.

- (c) For "arbitrary small sensitivity" over arbitrary large bandwidth, the technique in Secs. 2, 3 give constraints on the plant which are inherent and irreducible, i.e. every lti compensation technique has these constraints.
- (d) Part of the constraints (at infinite s) in (c) were always present in the previously developed sio equivalence techniques of (Horowitz 1979), i.e. even if "a.s. sensitivity" was not required. They are present in the new techniques only for a.s. sensitivity. Also, fixed point theory is not required for justification of the new technique.
- (e) The overdesign inherent in the fixed point techniques of (Horowitz 1979), has been reduced but some overdesign is still present.

REFERENCES

- Cruz, J., Jr., Freudenberg, J., and Looze, D., 1981, IEEE Trans. A.C., 26, 66.
- Davison, E., and Ferguson, I., 1981, *ibid.*, 93.
- Doyle, J., and Stein, G., 1981, *ibid.*, 26, 4.
- Horowitz, I., 1979, Int. J. Control, 30, 81.
- Horowitz, I., and Breiner, M., 1981, Int. J. Systems Sci., 12, 539.
- Horowitz, I., and Loecher, C., 1981, Int. J. Control, 33, 677.
- Horowitz, I., and Sidi, M., 1980, Int. J. Systems Sci., 11, 851.
- Horowitz, I., Yaniv, D., Golubev, B., and Neumann, L., 1981, Proc. Naecon Conf., IEEE, p. 1276.
- Lehtomaki, N., Sandell, N. Jr., and Athans, M., 1981, IEEE Trans. A.C., 26, 75.
- Postlethwaite, I., Edmunds, J., and MacFarlane, A., 1981, *ibid.*, 32.
- Safanov, M., Laub, A., and Hartmann, G., 1981, *ibid.*, 47.
- Zames, G. and Bensoussan, D., Multivariable sensitivity reduction by diagonal feedback, to appear in IEEE Trans. Auto. Control.

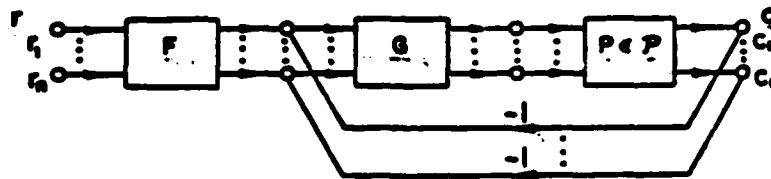


Fig. 1 General nxm system

$$c = Tr, T = (I + PG)^{-1} PGF.$$

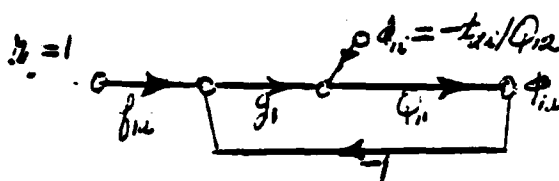


Fig. 2a. Sio structure for t_{11}
($i = 1, 2$), Eq. 3a.

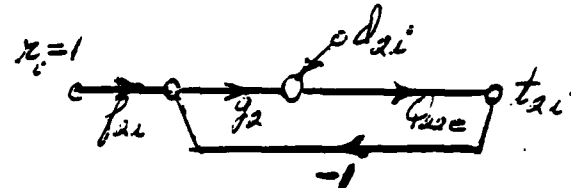


Fig. 2b. Sio structure for t_{21}
($i = 1, 2$), Eq. 4a.

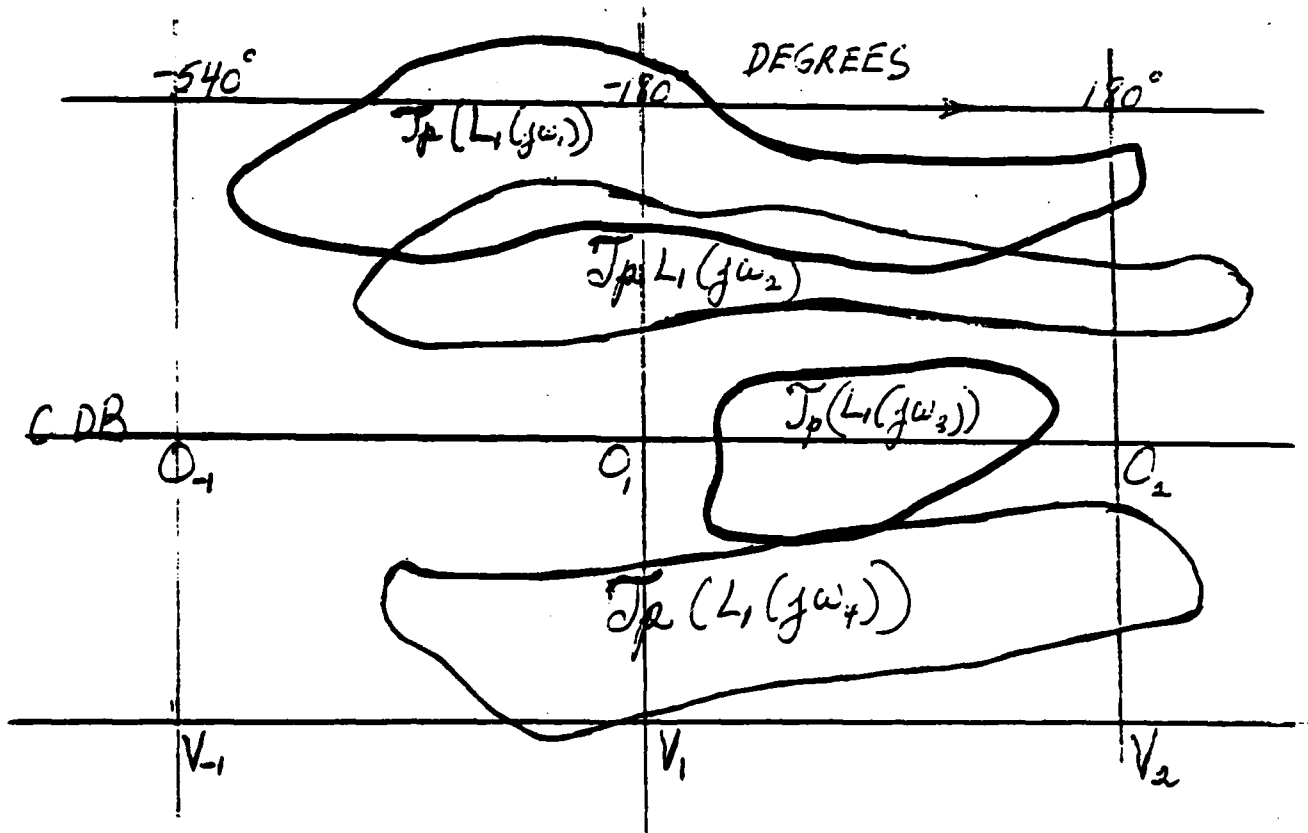


Fig. 3. Templates of $L_1(j\omega)$ on logarithmic complex plane (Nichols chart)

FILM
1-8